IDENTIFICATION AND CHARACTERIZATION OF PANCREATIC BETA-CELL SURVIVAL FACTORS

by

Yu Hsuan Carol Yang

B.Sc., The University of British Columbia, 2008

A THESIS SUBMITTED IN PARTIAL FULFILLMENT OF

THE REQUIREMENTS FOR THE DEGREE OF

DOCTOR OF PHILOSOPHY

in

THE FACULTY OF GRADUATE AND POSTDOCTORAL STUDIES

(Cell and Developmental Biology)

THE UNIVERSITY OF BRITISH COLUMBIA

(Vancouver)

April 2014

Abstract

Programmed β-cell death plays an important role in both type 1 and type 2 diabetes, but analysis of candidate survival factors has yielded a few hormones and growth factors exhibiting modest β-cell protection against various stresses. Most of what is known about the mechanisms of β-cell death comes from single time-point, single parameter measurements of bulk populations of mixed cells, which are inadequate for studying the heterogeneity in death mechanisms. We simultaneously measured the kinetics of six distinct cell death mechanisms by using a caspase-3 sensor and three vital dyes, together with bright-field imaging. This allowed the characterization of the timing and order of molecular events associated with cell death in single β-cells under multiple diabetic stress conditions. Using this approach, we identified several cell death modes where the order of events that typically define apoptosis were not observed. It is becoming increasingly apparent that islets release and respond to more secreted factors than previously thought and systematic analyses of their pro-survival effects can assist in therapeutic developments. Novel putative autocrine/paracrine signalling loops in islets were identified by compiling results from gene expression datasets. Factors best known for their roles in axon guidance, Netrin and Slit families, were further characterized for their pro-survival roles in adult β-cells. With the development of the live-cell imaging-based, high-throughput screening methods capable of identifying factors that modulate β-cell death, we screened the Prestwick library of small molecules and a custom library of endogenous factors. Carbamazepine, a Na^+ channel inhibitor, down-regulated the pro-apoptotic and ER-stress signalling induced by cytotoxic cytokines pointing to Na^+ channels as a novel therapeutic target in diabetes. Whether specific cellular stresses associated with type 1 or type 2 diabetes require specific β-cell survival factors remains unknown. Our comparison of 206 endogenous soluble factors, predicted to act on islet cells, under 5 diabetes-relevant stress conditions revealed unique sets of protective survival factors for each stress and identified a cluster of survival factors that exhibited generalized protective effects. Since diabetes results from a deficiency in functional β-cell mass, these studies are important steps towards developing novel therapies to improve β-cell survival and function.

Preface

A subset of Chapter 1 Section 1.2 has been published in the following book chapter:
Johnson JD, **Yang YH**, Luciani DS (2013) Mechanisms of pancreatic β-cell apoptosis in diabetes and its therapies. *Islets of Langerhans*, ed Islam M (Springer, Heidelberg), pp. 1-17.
I edited the chapter and added a new section, including Figure 1-2, to the 2nd edition of this book chapter detailing the role of non-apoptotic mechanisms of β-cell death.

A version of Chapter 3 has been published in the following article:
Yang YH, Johnson JD (2013) Multi-parameter, single-cell, kinetic analysis reveals multiple modes of cell death in primary pancreatic β-cells. *J Cell Sci.* 126(Pt 18):4286-4295.
I generated the hypothesis, designed and conducted the experiments, analyzed the data, and wrote the manuscript in consultation with my supervisor JD Johnson.

A version of Chapter 4 has been published in the following article:
Yang YH, Vilin YY, Roberge M, Kurata HT, Johnson JD (2014) Multi-parameter screening reveals a role for Na^+ channels in cytokine-induced β-cell death. *Mol Endocrinol.* 28(3):406-417.
I designed and performed the screen for compounds that can protect β-cells from cytokine-induced cell death, conducted all non-electrophysiology follow-up studies to elucidate the mechanism of action of the hits, analyzed the data, and wrote the manuscript in consultation with JD Johnson. YY Vilin, research associate in the laboratory of HT Kurata, performed and analyzed the electrophysiology experiments to characterize voltage gated sodium channels (the data were referenced, but not included in the thesis). M Roberge provided access to the Prestwick library of compounds.

A version of Chapter 5 and Chapter 6 has been published in the following article:
Yang YH, Szabat M, Bragagnini C, Kott K, Helgason CD, Hoffman BG, Johnson JD (2011) Paracrine signalling loops in adult human and mouse pancreatic islets: netrins modulate beta cell apoptosis signalling via dependence receptors. *Diabetologia*. 54(4):828-842.

I compiled the data detailing the expression of soluble factors and receptors in pancreatic islet cells, designed and conducted the experiments characterizing the role of netrin signalling in β-cells, analyzed the data, and wrote the manuscript in consultation with JD Johnson. M Szabat provided access to FACS purified β-cell microarray dataset. C Bragagnini and K Kott were undergraduates who conducted preliminary bioinformatics searches through publicly available datasets. BG Hoffman and CD Helgason provided access to mouse islet Tag-Seq datasets.

A version of Chapter 7 has been published in the following article:

Yang YH, Manning Fox JE, Zhang KL, MacDonald PE, Johnson JD (2013) Intra-islet SLIT-ROBO signalling is required for beta-cell survival and potentiates insulin secretion. *Proc Natl Acad Sci U S A.* 110(41):16480-16485.

I generated the hypothesis, designed and conducted the experiments, analyzed the data, and wrote the manuscript in consultation with JD Johnson. JE Manning Fox, a research associate in the laboratory of PE MacDonald, conducted the cortical F-actin characterization presented in Figure 7-9E. KL Zhang, an undergraduate student in the laboratory of JD Johnson, contributed to some of the replicate experiments in Figure 7-8F under my direct supervision.

Studies in Chapter 8 have not been published as of April 2014, but are being considered for publication:

Yang YH, Johnson JD (2014) High-content parallel comparison of secreted factors identifies protein families that prevent beta-cell death. Submitted April 03, 2014.

I generated the hypothesis, designed and performed the experiments, analyzed the data, and wrote the manuscript in consultation with JD Johnson.

Table of Contents

List of Tables

List of Figures

List of Abbreviations

ADP	adenosine diphosphate
AM	acetoxymethyl
ANOVA	analysis of variance
ATP	adenosine triphosphate
AUC	area under the curve
BrdU	5-bromo-2-deoxyuridine
BSA	bovine serum albumin
Ca^{2+}	calcium
cAMP	cyclic adenosine monophosphate
CBZ	carbamazepine
cDNA	complementary deoxyribonucleic acid
CFP	cyan fluorescent protein
CHOP	CCAAT/enhancer binding protein homologous protein
Ct	threshold cycle
cyto	cytoplasmic
Cyto C	cytochrome C
DMEM	Dulbecco's modified eagle medium
DMSO	dimethyl sulfoxide
DNA	deoxyribonucleic acid
eBFP	enhanced blue fluorescent protein
EDTA	ethylenediaminetetraacetic acid
eGFP	enhanced green fluorescent protein
ELISA	enzyme-linked immunosorbent assay
ER	endoplasmic reticulum
FACS	fluorescence-activated cell sorting
FBS	fetal bovine serum
FRET	fluorescence resonance energy transfer
GPCR	G protein-coupled receptor
h	hour(s)

HEPES	4-(2-hydroxyethyl)-1-piperazineethanesulfonic acid
IFN-γ	interferon gamma
IL-1β	interleukin-1 beta
JNK	c-Jun N-terminal kinase
K^+	potassium
K_{ATP} channel	ATP-sensitive potassium channel
LIDO	lidocaine
min	minute(s)
MIN6	mouse insulinoma β-cell line
mito	mitochondrial
mM	milli
MOMP	mitochondrial outer membrane permeabilization
mRNA	messenger ribonucleic acid
NA	numerical aperture
Na^+	sodium
NAD^+	nicotinamide adenine dinucleotide
Na_v channel	voltage-gated sodium channel
ND	not detected
NF-κB	nuclear factor kappaB
p38 MAPK	p38 mitogen-activated protein kinase
PAR	poly-ADP-ribose
PBS	phosphate buffered saline
PCR	polymerase chain reaction
PercevalHR	Perceval High Range
PI	propidium iodide
RNA	ribonucleic acid
ROS	reactive oxygen species
RPMI	Roswell Park Memorial Institute
RT-PCR	reverse transcription polymerase chain reaction
s	second(s)
SDS-PAGE	sodium dodecyl sulfate polyacrylamide gel electrophoresis

SEM	standard error of the mean
SERCA	sarco(endo)plasmic reticulum calcium ATPase
SF	serum free
siRNA	small interfering ribonucleic acid
tBID	truncated BH3-interacting domain death agonist
Tg	thapsigargin
TNF-α	tumor necrosis factor alpha
TTX	tetrodotoxin
UBC	University of British Columbia
UPR	unfolded protein response
YFP	yellow fluorescent protein

Acknowledgements

I offer my sincere gratitude to the faculty, postdoctoral fellows, research technicians, and graduate students that have influenced my Ph.D. experience and inspired me to continue research. I thank my supervisor Dr. Jim Johnson for his dedication towards providing a stimulating research environment that has trained me to think outside the box and for his endless encouragements towards stepping out of my comfort zone. I thank my graduate advisory committee members Drs. Tim Kieffer, Francis Lynn, and Tim O'Connor for their helpful discussions and critical feedback. Many thanks to our collaborators, Drs. Brad Hoffman, Pat MacDonald, and Harley Kurata, for their contributions to the manuscripts. I am grateful to all the past and present Johnson lab members that have made graduate school a memorable experience. Special thanks to the postdoctoral fellows (Connie, Gareth, Dan, Marta), graduate students (Emilyn, Arya, Tobias, Michelle, Michael, Nicole), and technicians (Betty, Farnaz, Tatyana) for their friendship and support.

I acknowledge the financial support from the NSERC Post Graduate Scholarship and UBC Four Year Fellowship.

To my parents, for their love and support towards my pursuit of higher education. Although a research career can be unpredictable, they still encourage me to follow by dreams.

Dedication

To my parents, for their endless love and support

Chapter 1: Introduction

1.1 Pathophysiology of diabetes: Importance of β-cell death

Over 382 million people worldwide are currently living with diabetes and by 2035 this number is estimated to increase to 592 million people (1). Patients diagnosed with diabetes have an increased risk of developing other complications including cardiovascular disease, neuropathy, and retinopathy. The eventual outcome of these complications can include heart attack, stroke, limb amputation, blindness, and kidney failure. In North America, 1 in 10 adults are affected by diabetes and an estimated 1.5 million deaths worldwide in 2013 are attributed to diabetes and the associated complications (1). The economic burden of treating diabetes is massive with an estimated $16.3 billion in 2013 and a projected increase to $19.6 billion in 2035 in Canada alone (1). Worldwide healthcare cost for diabetes was a staggering $548 billion. Given the costs and reduced quality of life associated with diabetes, research focusing on the cause, prevention, and cure of this disease is essential.

Diabetes is characterized by sustained elevation of fasting blood glucose levels caused in part by an absolute or relative deficiency in functional pancreatic β-cell mass (2, 3). The endocrine pancreas is made up of numerous cell types including β-cells, α-cells, δ-cells, PP cells, and ε-cells that produce and release hormones in a regulated manner. In response to the elevated blood glucose, the β-cells release insulin into the bloodstream, which acts on the peripheral tissues, including liver, muscle, and fat, to stimulate glucose uptake and reduce glucose production. Functional β-cell mass is maintained by a balance between β-cell proliferation, neogenesis, differentiation, and programmed cell death (4, 5). Postnatal development and remodelling of the endocrine pancreas proceeds with a perinatal wave of β-cell death, followed by massive β-cell proliferation (6). While maintenance of β-cell mass in adults involves low rates of β-cell turnover with low levels of β-cell apoptosis, for humans this level is estimated to be ~0.1%, which is compensated for by low levels of β-cell proliferation (7-10). Progressive β-cell death is present in both type 1 and type 2 diabetes (Fig. 1-1). Type 1 diabetes is characterized by the specific autoimmune destruction of pancreatic β-cells by pro-inflammatory cytokines (TNF-α, IL-1β, IFN-γ) released from infiltrating immune cells (2, 11), which leads to an almost complete ablation of β-cell mass (12, 13). Both genetic and environmental factors are thought to regulate the progression of type 1 diabetes. Studies have

implicated β-cell apoptosis as the source of β-cell autoantigens for antigen presenting cells to initiate the activation of β-cell specific T-cells and trigger the insulitis mediated β-cell death (2, 14). Molecular mimics of β-cell antigens introduced through infection or diet have also been proposed (2). Genetic susceptibility to type 1 diabetes is most commonly linked to genes that play roles in the immune system. Mutations in the major histocompatibility complex region containing the human leucocyte antigen genes are believed to regulate the magnitude and specificity of the autoimmune response to β-cell antigens (15, 16). Genotypic variation in the non-coding variable number of tandem repeat region of the insulin gene is also associated with autoimmune diabetes. Reduced number of tandem repeats in this regulatory region results in lower expression of insulin in the thymus, where it may play a role in promoting tolerance through negative selection of insulin-specific T-lymphocytes (17). Although the initial triggers of autoimmune diabetes is not fully understood, the residual β-cell mass in patients suffering from type 1 diabetes may represent a potential source of β-cells that can be expanded by preventing β-cell death due to the ongoing autoimmune attack and by promoting β-cell survival and proliferation (12). Additionally, because the onset of type 1 diabetes may be triggered by the initial apoptosis of β-cells, understanding the mechanisms of β-cell death may eventually allow us to target this destructive pathway to prevent or delay the onset of this disease (2).

The progression of type 2 diabetes is commonly characterized by insulin resistance and initial β-cell compensation, followed by a decrease in insulin secretion due in part to increase β-cell death (9, 11) (Fig. 1-1). Gene-environment interactions dictate the onset of type 2 diabetes. The major environmental component is a sedentary lifestyle, which mediates the development of obesity and hyperlipidemia. In obese individuals, the resulting insulin resistance in metabolic tissues, including liver, fat, and muscle, can often be compensated by the expansion of β-cell mass and increase in β-cell response to the metabolic demand (3, 18). However, failure to compensate for the insulin resistance leads to type 2 diabetes. This failure is partially due to the increase in β-cell death (9, 11). Postmortem studies of pancreatic samples from type 2 diabetic patients revealed on average a 40 to 70% decrease in β-cell mass compared to non-diabetic subjects (9, 19, 20). Nonetheless, it is important to note that a decrease in β-cell mass is not always observed in type 2 diabetic subjects (20). Contributors to the observed β-cell demise that ensues include glucotoxicity, lipotoxicity, ER stress, oxidative stress, inflammation, and amyloid deposition (21-27). Genome wide association studies have also

implicated polymorphisms in numerous genes involved in β-cell development, survival, and function with the susceptibility to type 2 diabetes (28, 29). Thus, enhancing β-cell survival, proliferation, and function may be critical for therapeutic interventions for both type 1 and type 2 diabetes. As a consequence of diabetes, chronic hyperglycemia persists, which has been demonstrated to induce further β-cell apoptosis (30-32). Although, candidate approaches have led to the discovery of endogenous regulators of β-cell survival, the clinical utilization of these regulators remains elusive.

Islet transplantation is a promising, minimally-invasive therapy for type 1 diabetes that was greatly advanced by the Edmonton Protocol (33-35). However, the high level of β-cell death during the isolation, pre-transplant culturing, transplantation procedure, and post-transplant engraftment stages often dictates the success of the transplant and the requirement of islets from multiple donors (33-35). Additionally, transplanted islets are susceptible to the recurrent autoimmune attack, and caspase-3-dependent apoptosis in the transplanted islets can be induced by the same immunosuppressants that are required to prevent graft rejection for successful islet transplantation (33-36). The rate of human β-cell apoptosis in culture can range from 2 to 20%, while proliferation remains absent (37-39). Reducing the level of apoptosis both pre- and post-transplantation will be beneficial to the success of this therapy.

1.2 Mechanisms of β-cell death

Numerous intrinsic and extrinsic signals are required for the maintenance of functional β-cell mass by providing pro-survival and pro-death signals. Mechanistic studies on the initiation and progression of β-cell death can make significant contributions to the prevention and treatment of type 1 diabetes and type 2 diabetes, in addition to improving the success of islet transplantations. There are 3 commonly characterized forms of cell death distinguished by morphological and biochemical features: apoptosis, necrosis, and autophagy (40-42) (Fig. 1-2). Understanding the redundancy and exclusiveness of different mechanisms of cell death has important implications for the detection and therapeutic manipulation of cell death.

Programmed cell death via apoptosis has been well characterized as an important mechanism of β-cell death (2, 11). Apoptosis is a complex mode of cell death characterized by a series of morphological features preceding the loss of plasma membrane integrity, including plasma membrane blebbing, chromatin condensation and fragmentation, rounding up of the

cell, and cellular and nuclear volume reduction (40). Molecular signalling associated with the progression of apoptosis includes caspase-3 activation, phosphatidylserine translocation to the outer leaflet of the plasma membrane, mitochondrial outer membrane permeabilization, and excessive generation of reactive oxygen species (40, 42). Apoptosis can be triggered by two distinct signalling networks that share many regulatory components. Extrinsic apoptosis proceeds when death receptors at the plasma membrane are activated by extracellular ligands, including TNF-α, Fas ligand, and TRAIL (2, 43). Alternatively, initiation of pro-apoptotic signal by dependence receptors, including netrin and nerve growth factor receptors, can occur when the level of their specific trophic ligands is below a critical threshold (44, 45). Following assembly of the death inducing signalling complexes, initiated at the cytoplasmic tails of the death receptors, initiator procaspases-8 or -10 are activated, which in turn activates effector procaspase-3 and -7 to generate active proteases (42, 43). In β-cells, the proteolytic cleavage of effector procaspases can be catalyzed directly by active caspase-8, or in a mitochondrion-dependent manner resulting from cleavage of BH3-interacting domain death agonist (BID) to truncated BID (tBID) (42, 43). Mitochondrial outer membrane permeabilization (MOMP) triggered by tBID results in the loss of mitochondrial transmembrane potential and the release of cytochrome c from the mitochondrial intermembrane space (42, 46). Assembly of the apoptosome, a multimeric complex involving apoptotic protease activating factor 1, cytochrome c, and dATP/ATP, results in the activation of caspase-9, which can subsequently activate caspase-3 and caspase-7 (46).

Intrinsic apoptosis results from exposure to ultraviolet light, cellular stress, and toxins, which can trigger oxidative stress, DNA damage, cytosolic Ca^{2+} overload, and ER stress (42). The cascade of signalling events that follows often involve the activation of pro-apoptotic Bcl-2 family members, BAX and BAK, triggering MOMP prior to the activation of effector caspases (2, 40, 43). Consequently, MOMP dissipates the mitochondrial transmembrane potential, essential for ATP synthesis and various transport activities, releases toxic proteins from the intermembrane space, including cytochrome c, apoptosis-inducing factor (AIF), endonuclease G (ENDOG), and direct IAP-binding protein with low pI (DIABLO), and increases ROS production, as a result of inhibiting the respiratory chain (42, 47). In addition to the loss of metabolic potential and the activation of proteolytic activity mediated by caspases, DNA fragmentation occurs as AIF and ENDOG translocate to the nucleus (42). The

caspase repressing activity of members of the inhibitor of apoptosis protein (IAP) family are further blocked by DIABLO (42). The redundancy of signalling molecules involved in the temporal cascade of events leading to β-cell apoptosis, autophagy, and necrosis has not been well characterized on a single cell level, resulting in the under-appreciation of non-apoptotic forms of cell death.

Autophagy is a catabolic process often favouring cell survival under conditions of nutrient deprivation, hypoxia, ER stress, pathogen infection, and DNA damage (40, 48-50). These conditions are relevant to the initiation and progression of diabetes. Also, in islet transplantation, islet cells are exposed to hypoxia and nutrient deprivation prior to vascularization and engraftment. The formation of double membrane vacuoles that sequesters damaged organelles and harmful cytoplasmic contents, termed autophagosomes, is a defining feature of autophagy, which concludes with the delivery of the contents to the lysosome for degradation and recycling (48, 50). Autophagic cell death is characterized by the lack of chromatin condensation and accumulation of autophagosomes, and does not necessarily implicate autophagy as the cause of cell death (40). Ablation of free fatty acid-induced autophagy leads to a lack of compensatory β-cell hyperplasia and impaired glucose tolerance (51). Diminished maintenance of functional β-cell mass by autophagy may increase the susceptibility to β-cell death under basal and stressed conditions, and consequently affect diabetes initiation and progression (51-53). The mutual inhibition between apoptosis and autophagy further supports the involvement of autophagy in maintaining β-cell health (48, 54).

β-Cell death via necrosis has also been implicated in the pathogenesis of diabetes (55, 56). Necrosis is often defined as cell death lacking the characteristics of apoptosis or autophagy. In addition, key morphological features of necrosis include plasma membrane rupture and swelling of cytoplasmic organelles (40, 57). Although initially believed to be an uncontrolled form of cell death leading to the release of inflammatory cellular contents, there is accumulating evidence supporting the notion that necrotic cell death is regulated by a defined set of signalling events induced by oxidative stress, loss of Ca^{2+} homeostasis, or ischemia (40, 57, 58). In fact, apoptosis and necrosis may share common signalling pathways involving mitochondrial membrane permeabilization through activation of proapoptotic Bcl-2 family members (57, 59). Receptor-interacting protein kinase 1 (RIP1) dependent necrosis is a well characterized mechanism of regulated necrosis that can be activated upon binding of tumor

necrosis factor α (TNFα) to TNF receptor 1 in the absence of caspase-8 activity (42, 60). Consequently, RIP1 is deubiquitinated and associates with RIP3 to activate necrotic cell death. Upon exposure to stress, inhibition of the apoptotic signalling cascade by direct inhibition of caspase activation or depletion of ATP (which is required for caspase activation) can favour necrotic cell death (59, 61, 62). Cells that have entered an apoptotic cascade can undergo secondary necrosis in the absence of phagocytosis by scavenger cells (63) (Fig. 1-2). This suggests that multiple modes of cell death can co-exist within the same cell and they have the potential to substitute for each other. The complex interplay between different modes of cell death further complicates the development of therapeutics for preventing β-cell death.

Understanding the molecular processes behind cell death may reveal novel therapeutic targets. In addition to the complex interplay between apoptosis, necrosis, and autophagy other pathways can also proceed. The diversity of the molecular pathways mediating cell death has led to the characterization of new modalities of cell death that sometimes share similar features resulting from an array of biochemical signalling. Mitotic catastrophe is initiated by aberrant mitosis leading to cell death during mitosis or interphase via apoptosis or necrosis (40). Anoikis is an intrinsic apoptotic response of adherent cells to the detachment from extracellular matrix interactions (42, 64). Parthanatos is a caspase independent cell death pathway involving DNA damage induced by overactivation of poly-ADP-ribose polymerases (PARPs), which can further result in ATP and NAD^+ depletion, PAR accumulation, loss of mitochondrial membrane potential, and subsequently AIF release (65, 66). Pyroptosis is a caspase-1 mediated cell death pathway that exhibits morphological features of apoptosis and/or necrosis. The activation of caspase-1 leads to the mature processing of inflammatory cytokines interleukin-1β (IL-1β) and IL-18 (58). It remains controversial whether these new modalities constitute unique cell death subroutines or whether they represent specific cases of apoptosis and/or necrosis.

1.3 The role of intracellular Ca^{2+} in the maintenance of β-cell health and function

Intracellular Ca^{2+} signalling regulates cell survival and cell death mechanisms. Disruption of Ca^{2+} homeostasis by diabetes related stresses, including cytotoxic cytokines, and prolonged hyperglycemia and hyperlipidemia, can impact β-cell function and induce β-cell death (67-69). Ca^{2+} plays an essential role in the modulation of glucose-stimulated insulin

secretion in β-cells. Upon stimulation, β-cells take up glucose through glucose transporters, metabolize the glucose through glycolysis and the tricarboxylic acid cycle to generate ATP, during which elevation in ER and mitochondrial Ca^{2+} levels and a transient decrease in cytosolic Ca^{2+} levels are observed (70-72). The increase in ATP/ADP ratio stimulates the closing of ATP-sensitive potassium channels (K_{ATP} channel), plasma membrane depolarization, the opening of voltage gated L-type Ca^{2+} channels, and the resulting Ca^{2+} influx triggers insulin release (67). Disruption of glucose-stimulated Ca^{2+} responses can lead to impaired stimulus-secretion coupling and β-cell dysfunction.

Disturbed cellular Ca^{2+} homeostasis is a trigger for β-cell death (73). Basal Ca^{2+} levels are elevated prior to glucose stimulation in β-cells treated with cytokines (67) and blocking the dominant L-type Ca^{2+} channels can prevent cell death induced by TNF-α and IFN-γ (74). The ER is one of the major organelle for intracellular Ca^{2+} storage and signalling. Ca^{2+} is sequestered in the ER when cytosolic levels are high and released from the ER when cytosolic levels are low (70, 75). Activities of the sarco(endo)plasmic reticulum calcium ATPase (SERCA) pumps, inositol triphosphate receptors, and ryanodine receptors regulates the ER Ca^{2+} level. ER protein binding and molecular chaperone activity requires ER Ca^{2+} and depletion of ER Ca^{2+} can result in protein misfolding and induction of ER stress (76, 77). The unfolded protein response (UPR) is the protective mechanism by which cells turn on to alleviate ER stress, triggering increase in expression of ER chaperones, degradation of misfolded protein, and decrease in protein translation (67, 77). In situations of excessive ER stress and prolonged UPR, activation of cell death cascades are mediated by c-Jun N-terminal kinase (JNK), p38 mitogen-activated protein kinase (p38 MAPK), nuclear factor kappaB (NFκB), Bcl-2 family members, and CCAAT/enhancer binding protein homologous protein (CHOP) (77). The mitochondria is another organelle where disruption of Ca^{2+} signalling can lead to β-cell dysfunction (67, 78). Increases in cytosolic Ca^{2+} also increase mitochondrial Ca^{2+}, which if overloaded can trigger mitochondrial mediated cell death pathways involving loss of mitochondrial membrane potential and increase ROS production (78). The depletion of ER Ca^{2+} stores can consequently trigger accumulation in mitochondrial Ca^{2+}, opening of the mitochondrial permeability transition pore, release of cytochrome c, and activation of the apoptotic cascade (78). Mitochondrial Ca^{2+} uniporters, sodium-calcium exchangers, and permeability transition pore, along with membrane potential regulates Ca^{2+} handling in the

mitochondria (78, 79). Ca^{2+} homeostasis in the mitochondrial matrix is required for the activity of metabolic enzymes, including pyruvate, α-ketoglutarate, and isocitrate dehydrogenases, involved in cellular respiration and the generation of ATP (78). Consequently, insulin secretion from β-cells is also modulated by mitochondrial Ca^{2+} (72). Persistent pathological disruption of intracellular Ca^{2+} levels and mobilization can influence β-cell function and trigger cell death.

1.4 Approaches for defining the cell death molecular pathways

The signalling cascades dictating the different modalities of cell death are neither isolated nor mutually exclusive (40, 42). Multiple pro-survival and pro-death pathways can often be activated under stress conditions, and the crosstalk between these pathways complicates the interpretation of the modality controlling the eventual death of the cells. Cell death pathways are often defined by the use of specific chemical inhibitors or gene knockout/mutation studies. Instead of blocking cell death, inhibiting one pathway can often expose an alternative pathway of cell death. In addition, many of the proteins involved in cell death pathways have multiple functions. For instance, cytochrome c is essential for electron transfer in the mitochondrial respiratory chain and can activate the apoptosome when released to the cytosol. RIP1 mediates both apoptotic and necrotic cell death, but is also involved in NF-κB pro-survival signalling. Caution must be taken when interpreting results from biochemical studies of whole cell populations.

Given that β-cell death can be driven by multiple cell death modalities, it is important to characterize both the extent of cell death and modulation of associated pathways under various stress conditions when developing therapeutics to circumvent β-cell death. Distinct morphological and biochemical characteristics have been utilized to distinguish between different cell death pathways. Traditionally, the use of single time point bulk population analysis has provided biochemical insights into the molecular pathways that are activated or repressed prior to cell death. Including terminal deoxynucleotidyl transferase-mediated dUTP nick-end labelling (TUNEL) assays for the detection of DNA fragmentation, luciferase-based detection of ATP changes, immunoblotting for specific signalling cascades, and RT-PCR quantification of changes in gene expression. Single parameter analysis of cell death cannot accurately determine the modalities of cell death because several processes overlap in multiple modalities and can also manifest in settings unrelated to cell death. While single endpoint

techniques cannot be used to assess the temporal dynamics between commonly occurring processes used to differentiate between different modes.

Time-lapse video microscopy allows for single cell characterization, which reduces complications associated with interpreting whole cell population data. With the development of vital dyes and novel biosensors for measuring activation of signalling cascades, microscopy has surpassed its well-known use for static single time point morphological characterizations. Exclusion dyes like propidium iodide, which can only cross compromised plasma membranes, are commonly used to label dead cells in both flow cytometry and imaging based assays (80). Selective labelling of living cells is also possible with fluorogenic esterase substrates, like calcein acetoxymethylester, since membrane-impermeant fluorescent products are generated through hydrolysis of the substrates by intracellular esterases. Nuclear morphology and cell numbers can be assessed with fluorescent chromatin dyes, like Hoechst 33342, or histone 2B fluorescent fusion proteins, like H2B-GFP. Quantification of cellular ATP levels allows for an indirect assessment of cell viability and combined with the use of other markers can provide useful information on the mechanism of cell death. The fluorescent biosensors for ATP/ADP ratio, Perceval and PercevalHR (81, 82), and total ATP levels, ATeam (83), display several advantages over luciferase based assays, including non-invasive real-time measurements, single cell resolution, and capability for multichannel imaging. Activation of initiator and executioner caspases is often associated with apoptotic cell death. However, caspase activity has also been demonstrated to elicit non-lethal signalling functions (84). Nonetheless, monitoring the transient caspase activation in conjunction with other parameters is still fundamental in apoptosis detection.

Direct real-time assessment of caspase activity can be accomplished with the use to fluorescence resonance energy transfer (FRET) biosensors or fluorogenic substrates displaying caspase sensitive cleavage sites (85, 86). Indirectly, caspase activation can be monitored by visualizing the characteristic cellular consequences, including plasma membrane blebbing due to the cleavage of RHO-associated coiled-coil containing protein kinase 1 (ROCK1) and changes in plasma membrane morphology due to the cleavage of pannexin 1. Phosphatidylserine translocation from the inner to the outer leaflet of the plasma membrane is triggered by the activation of phospholipid scrambalase 1 that perturbs the plasma membrane asymmetry, and is an early event in apoptosis (87). Externalization of phosphatidylserine can

be monitored with the binding of fluorescently labelled annexinV to non-permeabilized cells. The ability to simultaneously track in single cells specific morphological events, signalling modulations, protein translocations, and changes in metabolic status has advanced our detection of the true extent of apoptotic cell death. A major caveat of *in vitro* single cell analysis approach is the disruption of cell-cell interactions. Therefore, the relevance of *in vitro* cell death mechanisms must be validated for their pathophysiological significance with *in vivo* studies.

Mitochondrial membrane permeabilization is a critical event in apoptotic cell death and the resulting consequences can be monitored. Several dyes can monitor the loss of mitochondrial transmembrane potential including rhodamine 123, tetramethylrhodamine methyl ester (TMRM), and tetramethylrhodamine ethyl ester (TMRE). These dyes accumulate in the mitochondria in proportion to the mitochondrial transmembrane potential, but they can interfere with mitochondrial respiration. Reactive oxygen species (ROS) generation can also be detected with dihydroethidium, a fluorescent probe that display a red shift in its emission upon oxidation, and other commercially available fluorescent indicators. Alternatively, ROS-induced DNA damage can be monitored with the nuclear relocalization of the GFP fusion protein of 8-oxoguanine DNA glycosylase (OGG1), a DNA repair enzyme, to nuclear speckles (88). The use of fluorescently tagged mitochondrial intermembrane space proteins, like GFP-tagged cytochrome c, allows for the monitoring of their cytoplasmic translocation (89). Another feature of mitochondrial dysfunction is the associated morphological changes, which can be monitored with mitochondrial matrix targeted fluorescent proteins, albeit changes can occur independently of cell death from mitochondrial fission and fusion dynamics (90).

Homeostatic regulation of intracellular Ca^{2+} is crucial for maintaining cell function and health (91). Tracking changes in Ca^{2+} levels in response to cytotoxic conditions can help decipher the mechanism of cell death. Cytosolic changes in Ca^{2+} levels can be tracked with small molecule fluorescent indicators and genetically encoded biosensors (92). Membrane permeable acetoxymethyl (AM) ester derivatives of the small molecule Ca^{2+} indicators (for example, Fura-2-AM) become sequestered in the cell upon cleavage by intracellular esterases, and ratiometric imaging allows for detection of rapid intracellular Ca^{2+} transients with high signal-to-noise ratio (92). Although very convenient for short term imaging (for hours), extended imaging (for days) in specific subcellular compartments requires the use of

genetically encoded biosensors. Signal sequences can target the biosensors to defined subcellular locations, including the ER, mitochondria, Golgi, and plasma membrane (92). Both ratiometric FRET-based sensors and intensiometric single fluorescent protein-based sensors (including, GCaMPs and GECOs) utilize the Ca^{2+} responsive element CaM and a CaM binding peptide to elicit conformational changes resulting in increase in FRET efficiency or fluorescence intensities of the chromophores, respectively (92-94). Chromophores that display Ca^{2+} dependent shifts in emission spectra (GEM-GECO) or excitation spectra (GEX-GECO) have allowed for ratiometric imaging (94). With a variety of Ca^{2+} indicators that are spectrally distinct and can be spatially targeted, we can study the Ca^{2+} signalling dynamics in different organelles and/or in conjunction with other signalling molecules.

Indications of autophagic cell death can be detected with static methods of quantifying autophagosome formation, including electron microscopy based quantification of autophagosomes, immunoblotting for lipidated microtubule-associated protein 1 light chain 3 (LC3), and immunofluorescence imaging for punctate LC3 pattern. However, these techniques cannot distinguish between the cause of autophagosome accumulation, whether it be due to increase in autophagy initiation or decrease in autophagic flux, associated with decrease in autophagolysosome formation and degradation. Distinguishing between the two can be achieved through monitoring of autophagosome formation and its fusion with lysosome with tandem monomeric mRFP-GFP-tagged LC3 (95). Upon fusion of the autophagosome with lysosome, the acidic environment quenches GFP fluorescence while mRFP fluorescence is retained, allowing for the detection of progression through autophagy. Monitoring autophagy in combination with spectrally and spatially distinguishable indicators of apoptotic cell death is crucial in determining the mechanism of death.

Necrosis, whether it be regulated or not, also has markers related to the loss of plasma membrane permeability. The passive release of a non-histone chromatin-binding protein, high mobility group 1 (HMGB1), into the extracellular space can be monitored in cell culture supernatants or with fluorescent protein-tagged HMGB1 (96). Peptidylprolyl isomerase A release (PPIA) in the early stages of regulated necrosis can also be monitored (97). The characteristic oncosis that occurs can be tracked over time. Although necrosis has been associated with mitochondrial membrane permeabilization and RIP1 activation, the lack of consensus on the biochemical changes defining necrosis has resulted in the routine

identification of necrosis by the absence of apoptotic or autophagic features (40). With the advancements in cellular imaging and palette of genetically encoded biosensors, underlying molecular mechanisms that dictates the morphological features can be simultaneously detected.

1.5 Discovery of β-cell survival factors through candidate approaches

The loss of functional β-cell mass is a critical event in the pathogenesis of diabetes and high levels of β-cell death severely limits the success of islet transplantation. Development of methods for improving β-cell survival as diabetes therapies can be achieved through advanced understanding of the mechanisms behind the initiation and progression of β-cell death. The effects of a number of candidate growth factors on islet cell survival and proliferation have been studied. A list of these growth factors including glucagon-like peptide 1 (GLP-1), fibroblast growth factor (FGF), transforming growth factor beta (TGF-β), hepatocyte growth factor (HGF), insulin-like growth factor (IGF), betacellulin, growth hormone, and lactogens (98-100). Pro-survival effects of candidate growth factors observed *in vitro* and with *in vivo* mouse models suggests that our goal of preventing β-cell death caused by autoimmune attack, transplantation stresses, and other stresses associated with diabetes can be attained by harnessing islet cell survival factor signalling pathways activated by locally secreted factors or circulating factors. GLP-1, for example, has been shown to activate the anti-apoptotic transcription factor Pdx1 through a calcium dependent signalling pathway, and increase proliferation and decrease apoptosis of pancreatic β-cells (101-103). Although evidence suggests that there is an increase in islet transplant success when GLP-1 expression is locally induced, the clinical application of GLP-1 as an effective stimulator of β-cell mass, proliferation, and survival is unknown (104, 105). Overall, elucidating the effects of candidate growth factors has provided an introduction to understanding β-cell survival and proliferation. However, an unbiased screen beyond characterizing candidate growth factors, where all the secreted factors are tested as potential hits is necessary to discover any factors that have been overlooked.

The activation or mimicking of local autocrine and/or paracrine survival factor signalling present within the islets would be the most ideal scenario for diabetes therapies. The localized microenvironment of endogenous autocrine/paracrine signalling factors often eliminates their

effects on peripheral tissues through local action, and prevents over-stimulation through self-limiting feedback. Insulin, for example, has been shown to be a potent and self-limiting islet survival factor and physiological dosage of insulin may increase β-cell proliferation (38). Although insulin could potentially be used to preserve functional islet mass *in vitro* prior to transplantation, its metabolic effects limit its use as a pro-survival agent *in vivo.* Thus, the search for other potent survival factors not involved in the regulation of metabolic pathways is needed. Several growth factors critical for pancreatic development can be found in the literature; however, their functions in adult islets are currently unknown. Nonetheless, we cannot overlook the promising effects of distally secreted endocrine factors, like GIP and GLP-1, acting to promote β-cell survival and function.

1.6 Hypothesis and objectives

Efforts towards the discovery of novel therapeutics for the maintenance of β-cell survival and function through the use of high-throughput screening have led to the discovery of interesting hits (106, 107). However, high-throughput screens are often bioluminescence based end-point assays that are limited by one-dimensional readouts, lack of information on cell health, and lack of temporal resolution. High-content imaging, on the other hand, allows for detailed cellular morphological analysis, but is often time-consuming. Advancements in computational image analysis software, microscope automation, and robotic liquid handling has provided the tools required for multiple parameter, high-content, high-throughput screening platforms.

The goal of this project was to identify and characterize endogenous factors that can significantly improve survival of adult human and mouse β-cells upon exposure to stressed environments associated with diabetes. As a result, we may be able to harness these signals to promote β-cell survival initially in islets cultured prior to transplantation and eventually in individuals suffering from diabetes. We used multiple fluorescent probes to define the different modes of cell death that occur under different stress conditions. Elucidating the context-dependent distribution of various mechanisms of cell death may determine the success of targeted therapeutic interventions to control β-cell death. It is conceivable that therapies for promoting β-cell survival may require inhibition of all forms of cell death through targeted inhibition of upstream events or combinatorial therapies. Through the use of multi-parameter,

high-content, 96-well and 384-well imaging platforms, we have simultaneously compared different small molecules and soluble factors for their efficacy on β-cell survival. The specific aims in the thesis are designed to test the following overall hypothesis: novel factors that promote adult β-cell survival will be identified through multi-parameter, high-content, high-throughput imaging, and their pro-survival signalling mechanisms will be validated.

The results presented in Chapter 3 detail the characterization of the timing and order of molecular events associated with the progression of β-cell death under multiple diabetic stress conditions. Chapter 4 describes the use of a multiple parameter, live-cell imaging-based screening method of the Prestwick library for identifying small molecules that block β-cell death in response to cytotoxic cytokines. Follow-up studies validating the protective effects of a sodium channel inhibitor, carbamazepine, and defining potential mechanism of action are also presented in Chapter 4. Chapter 5 reports the bioinformatic analyses of autocrine/paracrine signalling loops in adult human and rodent islets and highlights the importance of unbiased approaches for the discovery of novel islet growth factors. From our list of potential growth factors we found a group of molecules known to provide axonal guidance cues during neuronal development. Given the similarities between neuronal and endocrine pancreas development, we first took a candidate approach and characterized netrin and Slit-Robo pro-survival signalling in β-cells, which are presented in Chapters 6 and 7, respectively. In Chapter 8, the systematic comparison of the protective effects of 206 soluble factors was conducted under 5 diabetes-related stress conditions. The multi-parameter, high-content imaging assay revealed unique sets of protective factors specific to each stress and a cluster of general protective factors. Because the loss of functional β-cell mass results in diabetes, the studies presented in this thesis are important steps towards developing novel therapies to improve β-cell survival.

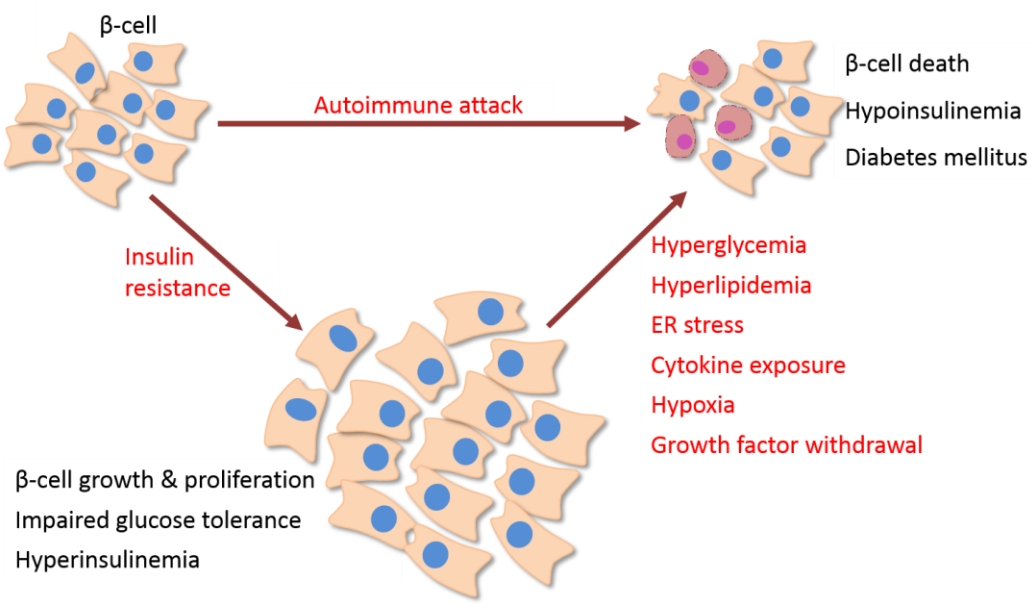

Figure 1-1. Schematic of the progression towards β-cell death in diabetes.
Type 1 diabetes is caused by the specific autoimmune destruction of β-cells. Type 2 diabetes progresses through an initial insulin resistance and β-cell mass compensation phase, followed by eventual β-cell death due to exposure to multiple stresses including hyperglycemia, hyperlipidemia, ER stress, and hypoxia.

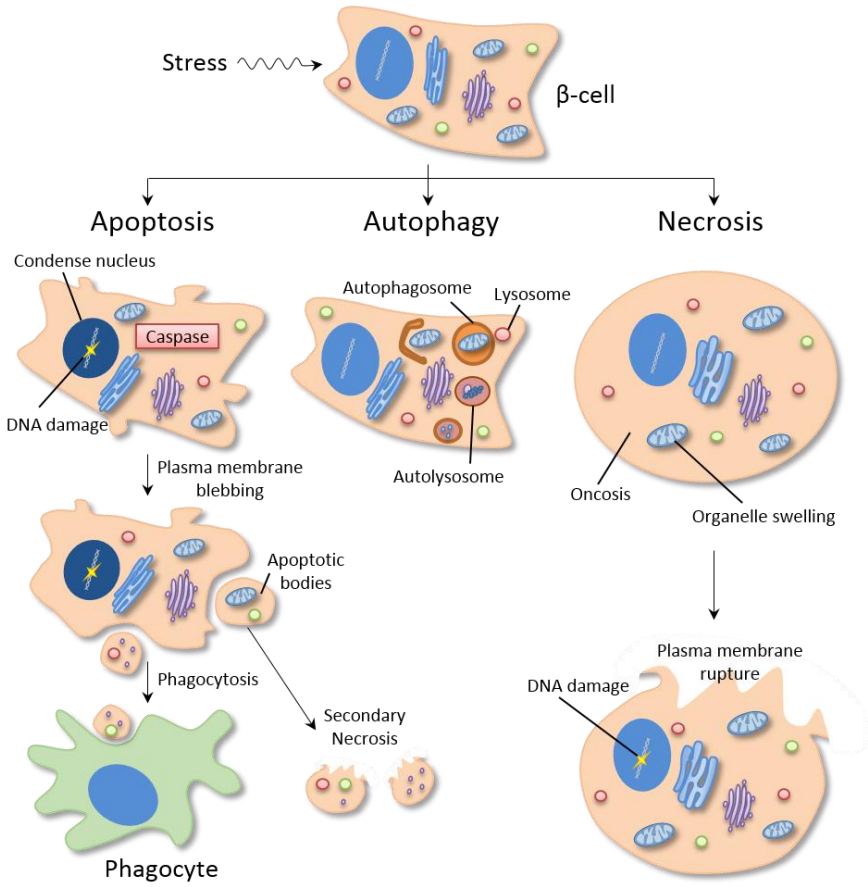

Figure 1-2. Schematic of common β-cell death pathways.
Prolonged exposure to stress conditions, including cytokine exposure hyperglycemia, hyperlipidemia, oxidative stress, and ER stress, can lead to β-cell death. Apoptosis, autophagy-mediated, and necrosis are the most well characterized modes of cell death.

Chapter 2: Materials and methods

2.1 Reagents

Chemicals were from Sigma (St Louis, MO, USA) unless specified otherwise. Netrin-1 rabbit monoclonal antibody was from Calbiochem (La Jolla, CA, USA). Polyclonal antibodies to Netrin-4 (rabbit), Neogenin (goat), UNC5A (goat), and UNC5C (goat) were from Santa Cruz (Santa Cruz, CA, USA). Rabbit polyclonal antibodies to SLIT1 and ROBO2 were from Sigma. Polyclonal antibodies to SLIT2 (rabbit) and ROBO1 (goat) were from Santa Cruz. Purchased antibodies included rabbit polyclonal SLIT3 and guinea pig polyclonal insulin from Millipore (Billerica, MA, USA), mouse monoclonal glucagon from Sigma, and mouse monoclonal β-actin from Novus (Littleton, CO, USA). Rabbit polyclonal antibodies to phospho-Akt (Ser473), phospho-Akt (Thr308), Akt, Erk1/2, phospho-Ask1 (Thr845), ASK1, phospho-JNK (Thr183/Tyr185), JNK, caspase-12, cleaved caspase-7, mouse monoclonal antibody phospho-Erk1/2 (Thr202/Tyr204), and rabbit monoclonal antibody cleaved caspase-3 were from Cell Signaling Technology (Danvers, MA, USA). Mouse monoclonal CHOP antibody was from Thermo (Rockford, IL, USA). A list of antibody dilutions can be found in Table 2-1. Draq5 nuclear stain was from Biostatus (Leicestershire, UK). Validated biologically active recombinant mouse Netrin-1, Netrin-4, SLIT1, SLIT2, and SLIT3 and recombinant human TNF-α, IL-1β, and IFN-γ were from R&D Systems (Minneapolis, MN, USA). A complete table of all recombinant proteins and manufacturer information can be found in Table 2-2.

2.2 Primary islet and cell line culture

Pancreatic islets were isolated from both male and female C57BL/6J mice (Jax, Bar Harbor, MA, USA) using collagenase and filtration. Unless otherwise indicated, 15- to 20-week-old male and female mice were used in the studies. Mouse housing guidelines and experimental procedures were approved by the University of British Columbia Animal Care Committee. Human islets (>80% purity estimated by dithizone staining) and pancreata were provided by Dr. Garth Warnock, collected via protocols approved by the University of British Columbia Institutional Advisory Board. Donors were men or women aged 23 to 56 years. None of the donors were known to have diabetes. The islets were further hand-picked using a

brightfield microscope. Islets were cultured overnight (37°C, 5% CO_2) in RPMI1640 medium (Invitrogen, Burlington, ON, Canada) with 5 mM glucose (Sigma), 100 units/ml penicillin, 100 µg/ml streptomycin (Invitrogen) and 10% vol/vol FBS (Invitrogen) as described in more detail elsewhere (108, 109). MIN6 and HEK293T cells were cultured in Dulbecco's modified eagle's medium (Invitrogen) containing 22.2 mM glucose, 100 units/ml penicillin, 100 µg/ml streptomycin and 10% vol/vol FBS as described (109, 110).

2.3 Analyses of islet secretions

To measure the dynamics of insulin secretion, mouse islets were perifused (37) and hormone secretion was measured using a rat insulin radioimmunoassay kit (Millipore). Briefly, 150 size-matched islets were collected, suspended with Cytodex microcarrier beads (Sigma), and placed into 300 µl perifusion chambers. The islets were perifused at 350 µl/min in Krebs-Ringer's solution containing 5 g/L BSA and the following (in mM): 4.8 KCl, 2.5 $CaCl_2$, 1.2 $MgSO_4$, 1.2 KH_2PO_4, 5 $NaHCO_3$, 10 HEPES, 129 NaCl and 3 glucose. Fractions were collected every 5 min and stored at -20°C.

Netrin-1 secretion was measured from 100 hand-picked human islets by ELISA (Enzo, Farmingdale, NY, USA) following perifusion. ELISA kits used for quantification of SLIT1, SLIT2, and SLIT3 secretion from mouse islets were from Uscn Life Science Inc (Wuhan, Hubei, PRC). Supernatants from 150 mouse islets were collected following 2 h incubation in Krebs-Ringer's solution containing 3 mM or 15 mM glucose. Protease inhibitors (Roche) were immediately added to avoid protein degradation.

2.4 Gene expression analyses

Total RNA was isolated from human and mouse primary islet and MIN6 cells using Trizol followed by cleanup with RNeasy kit or directly with RNeasy Mini or Micro kits (Qiagen, Mississauga, ON, Canada). Reverse transcription (qScript cDNA SuperMix; Quanta Biosciences, Gaithersburg, MD, USA or SuperScript III; Invitrogen) was used to generate cDNA. For RT-PCR, PCR amplification was carried out using 1 cycle of 94°C for 2min, 35 cycles of 94°C for 30s, 57°C for 30s, 72°C for 45s, and 1 cycle of 72°C for 5 min. Primers were purchased from Integrated DNA Technologies (Coralville, IA, USA) (109). TaqMan quantitative RT-PCR was conducted using probes from Applied Biosystems (Streetsville, ON,

Canada) or Integrated DNA Technologies and PerfeCTa qPCR SuperMix (Quanta) on a StepOnePlus device (Applied Biosystems, Streetsville, ON, Canada). Relative gene expression changes were analysed by $2^{-\Delta C_t}$ or $2^{-\Delta\Delta C_t}$ methods as indicated in the figure legends. Unless specified otherwise, *Hprt1* or *Ppia* were used as reference genes.

2.5 siRNA mediated gene knock-down

MIN6 and mouse islet cells dispersed with 0.01% trypsin-EDTA (Invitrogen) were transfected with a combination of Silencer Select siRNA (Ambion, Burlington, ON, Canada) targeting *Slit1*, *Slit2* and *Slit3*. Cells transfected with scramble siRNA (Ambion) was used as negative control. Neon transfection (Invitrogen) with 100 nM of each siRNA for MIN6 and 200 nM for dispersed mouse islet cells was used. For MIN6 cells, the electroporation settings were 1200 V, 20 ms, and 2 pulses. For dispersed islet cells, the electroporation settings were 1000 V, 30 ms, and 2 pulses. Cells were analyzed by quantitative RT-PCR and immunoblotting at least 48 h following transfection.

2.6 Immunofluorescence imaging

MIN6 and dispersed islet cells were fixed in 4% wt/vol paraformaldehyde (10 min) and permeabilized using 0.1% vol/vol Triton X-100 (10 min). Antigen retrieval was conducted on de-paraffinized pancreas sections by boiling for 15 min in sodium citrate buffer (10 mM $Na_3C_6H_5O_7$, 0.05% vol/vol Tween-20, pH 6.0). Normal goat serum (10% vol/vol) was used for blocking. Primary antibodies (Table 2-1) were incubated overnight at 4°C. AMCA- (1:200, Jackson ImmunoResearch, West Grove, PA, USA), and AlexaFluor-488-, -555-, and -647-conjugated secondary antibodies (1:400; Invitrogen) were incubated for 1 h at 20°C, prior to mounting in Vectashield (Vector Laboratories, Burlington, ON, Canada). Cells were imaged using an inverted microscope equipped with 0.75 NA 20× and 1.45 NA 100× objectives. For cell death assays, MIN6 and dispersed islet cells were seeded into 96-well plates and stained with 0.05 µg/ml Hoechst 33342 (Invitrogen), 0.5 µg/ml propidium iodide (Sigma) and AlexaFluor647-conjugated annexinV (1:500 unless otherwise indicated; Invitrogen) (76). Following treatments, cells were imaged with ImageXpress^{MICRO} (Molecular Devices, Silicon Valley, CA, USA) every 1 or 2 h at 37°C and 5% CO_2 (109). For proliferation analysis (38), MIN6 cells were seeded into 96-well plates, 10 µM bromodeoxyuridine (BrdU) was

supplemented to the media following 2 hours of treatment. Cells were stained with BrdU Labeling Kit (Roche, Laval, QC, Canada) then imaged using ImageXpress Micro (Molecular Devices, Silicon Valley, CA, USA).

2.7 Immunoblotting

MIN6 and islet cells were lysed with cell lysis buffer (Cell Signaling) containing protease inhibitors (Calbiochem). Lysates were sonicated for 20 s then centrifuged for 10 min at 10,000 *g*. Protein concentrations were determined using a bicinchoninic acid assay (Thermo, Rockford, IL, US). Proteins were separated on 8 or 12% wt/vol SDS-PAGE gels and transferred to polyvinylidene fluoride membranes. After blocking (0.2% wt/vol I-block, 0.1% vol/vol Tween-20 PBS), membranes were probed with primary antibodies (Table 2-1), followed by horseradish peroxidase-conjugated secondary antibodies (1:3000; Cell Signaling). Immunodetection was performed using enhanced chemiluminescence (Thermo). PathScan intracellular signaling array was used for islet lysates with low protein yield, following the manufacture's protocol (Cell Signaling).

2.8 Live cell imaging of second messengers

Dispersed mouse islet cells and MIN6 cells were transfected with D3cpv, D1ER or 4mtD3cpv CFP-YFP-FRET based biosensors for the detection of cytosolic, endoplasmic reticulum, or mitochondrial Ca^{2+} (76, 92, 93, 111). Cells were transfected using the Neon system (Invitrogen) and imaged 48 h later. Alternatively, cytosolic Ca^{2+} was imaged using cells loaded with Fura-2-AM (Invitrogen). Dispersed mouse islet cells seeded onto glass coverslips were loaded with 5 μM of Fura-2-AM for 30 min at 37°C. For short term (less than 2 hours) Ca^{2+} imaging, cells were incubated in Ringer's solution containing (in mM): 5.5 KCl, 2 $CaCl_2$, 1 $MgCl_2$, 20 HEPES, 134 NaCl and 3 glucose. Solutions were maintained at 37°C and cells were imaged using an inverted microscope at 5 or 10 s intervals (Zeiss 200m; Intelligent Imaging Innovations, Denver, CO, USA) operated by Slidebook 5.0 software (Intelligent Imaging Innovations). CFP excitation and emission was controlled by 430/25nm and 470/30nm filters, respectively. Conformational change of the FRET probe upon exposure to elevated Ca^{2+} levels leads to increase in FRET between CFP and YFP. FRET with YFP was measured using a 535/30nm filter and normalized to CFP emission intensity. Long term Ca^{2+}

changes were imaged with ImageXpress^{MICRO} systems at 1 or 20 min intervals under 37°C and 5% CO_2 conditions in RPMI medium. CFP excitation and emission was controlled by 438/24nm and 483/32nm filters, respectively. FRET with YFP was measured using a 542/27nm filter and normalized to CFP emission intensity.

For live cell imaging of cAMP, MIN6 cells seeded onto glass coverslips were transfected with the AKAR2 FRET probe (112) and imaged 48 h later. For cAMP imaging, cells were incubated in Ringer's solution containing (in mM): 5.5 KCl, 2 $CaCl_2$, 1 $MgCl_2$, 20 HEPES, 141 NaCl, and 3 glucose. Solutions were maintained at 37°C and cells were imaged using Zeiss 200m inverted microscope operated by Slidebook 5.0.

2.9 Reporter for detecting caspase-3/7 activation in β-cells

To allow for multiplexing, the miCy-DEVD-mKO FRET probe from A. Miyawaki (85) was changed to eBFP2-DEVD-eGFP FRET sensor for detection of caspase-3/7 activation. Generating the triple reporter construct involved insertion of the new caspase-3/7 sensor downstream of the *Ins1* promoter in replacement of the eGFP cassette from the published lentiviral *Ins1*/*Pdx1* dual reporter construct (110). The eBFP2-DEVD-eGFP FRET sensor was cloned downstream of the *Ins1* promoter with flanking NheI and KpnI restriction sites. Following restriction digest of the published dual reporter with NheI/KpnI restriction enzymes, the *Ins1* promoter-eGFP cassette was excised. Ligation of the remaining construct with the *Ins1* promoter-eBFP2-DEVD-eGFP FRET cassette produced the triple reporter construct.

Lentiviral particles were prepared as described (110, 113). Briefly, HEK293T cells at 60% confluence were transfected with CPRΔEnv, pCI-VSVG and FIV-pTiger-triple reporter constructs using FuGENE6 (Roche) under serum free and antibiotics free conditions. 48 and 72 h following transfection, viral particles were collected from the culture media and concentrated by centrifugation at 50,000 x g. The viral pellet was resuspended in tris-NaCl-EDTA buffer and stored at -80°C. Concentrated virus was titered in MIN6 cells infected with a serial dilution of the virus particles in 96-well plates and imaged for reporter gene expression on ImageXpress^{MICRO} (Molecular Devices, Sunnyvale, CA, USA) 48 h following infection.

2.10 Multi-parameter time-lapse cell death assay

For cell death assays, MIN6 and dispersed islet cells were seeded into 96-well plates and infected with lentiviral particles carrying the triple reporter construct at MOI of 5. Cell death experiments were conducted 48 h following lentiviral infection. Cells were stained with 50 ng/ml Hoechst 33342 (Invitrogen), 0.5 µg/ml propidium iodide (PI: Sigma) and 3:500 dilution of annexinV-conjugated to AlexaFluor647 (Invitrogen). Following treatments, cells were imaged with ImageXpress^{MICRO} (Molecular Devices) every 5-15 min at 37°C and 5% CO_2. Treatments included 5 and 20 mM glucose containing RPMI media supplemented with 10% vol/vol FBS, a cytokine cocktail (25 ng/ml TNF-α, 10 ng/ml IL-1β, 10ng/ml IFN-γ: R&D Systems, Minneapolis, MN, USA) and/or 1 µM thapsigargin. Serum free conditions were used to mimic nutrient deprivation. Hoechst and eBFP2 excitation and emission was controlled by 386/23nm and 445/20nm filters, respectively. PI and mRFP excitation and emission was controlled by 562/40nm and 624/40nm filters, respectively. Spatial restriction of PI fluorescence in the nucleus allowed for analysis of PI signal independent of cytoplasmic mRFP. AlexaFluor647 excitation and emission was controlled by 628/40nm and 692/40nm filters, respectively. eGFP excitation and emission was controlled by 472/30nm and 520/35nm filters, respectively. The FRET probe is cleaved upon activation of caspase-3/7 leading to the loss of FRET between eBFP2 and eGFP. FRET with eGFP was measured using a 520/35nm filter and normalized to eBFP2 emission intensity. Time-lapse images of single cells were analyzed using MetaXpress Software (Molecular Devices).

2.11 Multi-parameter cell death screening platform

MIN6 cells expressing the eBFP2-DEVD-eGFP FRET sensor for detection of caspase-3/7 activation were seeded into 96-well plates at 20,000 cells/well. MIN6 cells were stained with 50 ng/ml Hoechst 33342 (Invitrogen), 0.5 µg/ml propidium iodide (PI: Sigma) and 3:500 dilution of AnnexinV-conjugated to AlexaFluor647 (Invitrogen). Cells were treated with test drugs in the presence of 22.2 mM glucose containing DMEM media supplemented with 10% vol/vol FBS and a cytokine cocktail (25 ng/ml TNF-α, 10 ng/ml IL-1β, 10 ng/ml IFN-γ: R&D Systems, Minneapolis, MN, USA). We employed the Prestwick Library of 1120 drugs, which includes a diverse array of chemicals, including off-patent drugs (www.prestwickchemical.com). Compounds were pinned into the 96-well round bottom plates

(Corning) at ~15 µM using a 0.7 mm diameter 96-pin tool equipped onto a Biorobotics Biogrid II robot. Final compound concentrations of ~8.5 µM were attained when treatments were added to the cells at 1:2 dilution. Following 30 h treatments, cells were imaged with ImageXpress^{MICRO} (Molecular Devices, Sunnyvale, CA, USA) at 37°C and 5% CO_2. The excitation and emission filter sets used are described above. Time-lapse images for the secondary screens were captured every 2 h and analyzed using MetaXpress Software (Molecular Devices).

Mouse islets were dispersed and seeded into 384-well plates at 4000 cells/well. 48 hours following seeding, cells were washed 4 times with serum free RPMI medium, and stained with 60 ng/ml Hoechst 33342 (Invitrogen), 0.6 µg/ml propidium iodide (PI: Sigma), and 1:400 dilution of annexinV-conjugated to AlexaFluor647 (Invitrogen) for 1 hour prior to imaging of basal cell death with ImageXpress^{MICRO} at 37°C and 5% CO_2 (114). Following treatments, cells were imaged at 3 hour intervals for 60 hr. Treatments included 5 and 20 mM glucose serum free RPMI medium supplemented with a cytokine cocktail (25 ng/ml TNF-α, 10 ng/ml IL-1β, 10ng/ml IFN-γ: R&D Systems, Minneapolis, MN, USA), 1 µM thapsigargin, and/or 1.5 mM palmitate (complexed to BSA at 6:1 molar ratio)(114, 115). Serum free conditions were used to mimic nutrient deprivation and eliminate any potential synergistic effects with unknown factors in the serum. Serum free conditions were achieved through sequential washing of the cells with serum free RPMI medium. 10% vol/vol FBS was used as positive control for unstressed cells. Factors were transferred with Perkin Elmer Janus liquid handler (Waltham, Massachusetts, USA). To achieve a 10 nM final concentration, aliquots of 3 µl of each factor at 300 nM were pinned into 384-well plates and stored at -80°C. On the day of screening, factors were thawed and 12 µl of the stress treatment medium was added to each well, yielding 60 nM of each factor. Following imaging of the serum starved cells, 10 µl of each treatment was transferred into each well using the onboard ImageXpress^{MICRO} robotics, resulting in the final concentration of 10 nM. Hoechst excitation and emission was controlled by 377/50nm and 447/60nm filters, respectively. PI excitation and emission was controlled by 543/22nm and 593/40nm filters, respectively. AlexaFluor647 excitation and emission was controlled by 628/40nm and 692/40nm filters, respectively. Time-lapse images of single cells were analyzed using MetaXpress Software (Molecular Devices). Media were collected 72 hours following

treatments and insulin in the media was assayed by radioimmunoassay (Rat insulin RIA kit, Millipore, Billerica, MA, USA).

2.12 Data analysis

Following image analysis using MetaXpress software (Molecular Devices), the level of cell loss was calculated relative to the amount of viable cells present in the time point prior to the treatments. The level of PI+ and AnnexinV+PI- cells were calculated relative to the total cell count in each time point. The accumulation of cell loss, PI+ cells, and AnnexinV+PI- cells was extracted from the area under the curve between 0-24 hours and 24-48 hours. Z-score values were determined for each individual screen based on (x – median)/MAD, where MAD represents the median absolute deviation. Data are expressed as mean ± SEM unless otherwise indicated.

2.13 Bioinformatics and database mining

Secreted factors and receptors expressed in mouse or human islet cells were identified through bioinformatic database mining. Human islet genes were also confirmed in the Massively Parallel Signature Sequencing (MPSS) data set of Kutlu *et al* (116). A mouse islet Tag-seq library was analyzed for RefSeq accessions with tag counts >5 as described (109, 117, 118). Briefly, DNaseI treated total RNA isolated from hand-picked islets were used for Tag-seq libraries, sequenced to a depth of 7,481,000 tags. Tags with a count of ≤5 were considered as not expressed. 7098 unique RefSeqs were identified. 4810 RefSeq transcripts were expressed (109). The transcriptomes of human and mouse FACS purified β-cells (110) were also analyzed by microarray (109). Dispersed mouse or human islet cells were stably infected with reporter lentivirus for detecting *Pdx1* and *Ins1* promoter activities. RNA was isolated from FACS purified $Pdx1^{+}/Ins^{+}$ cells, cRNA was generated, labelled, and hybridized to MouseWG-6 v2.0 Expression BeadChip (Illumina, San Diego, CA, USA) or HumanWG-6 v3.0 Expression BeadChip (Illumina) for mouse or human samples, respectively. The Gene Expression Analysis Module in BeadStudio 3.3 software (Illumina) was used for background correction and normalization. A particular probe set with a detection p-value <0.05 was considered "detected" (*i.e.* significantly expressed). Gene expression was confirmed using T1Dbase (119). Interactions between the ligands and receptors were found via PubMed.

2.14 Statistics

Data are expressed as mean ± SEM unless otherwise indicated. Results were considered statistically significant when $p < 0.05$ using Student's t test when comparing between 2 groups or one-way ANOVA with Tukey-Kramer post-hoc test when comparing between 3 or more groups (GraphPad Prism; GraphPad, La Jolla, CA, USA).

Table 2-1. List of primary antibodies.

Antibody	Manufacturer	Source*	Dilution	
			Immunoblotting	Immunostaining
p-p38 MAPK (Thr180/Tyr182)	Cell Signaling	R	1:1000	-
p38 MAPK	Cell Signaling	R	1:1000	-
p-AKT (Ser473)	Cell Signaling	R	1:1000	-
p-AKT (Thr308)	Cell Signaling	R	1:1000	-
AKT	Cell Signaling	R	1:1000	-
p-ASK1 (Thr845)	Cell Signaling	R	1:1000	-
ASK1	Cell Signaling	R	1:1000	-
p-BAD (Ser112)	Cell Signaling	R	1:1000	-
BAD	Cell Signaling	R	1:1000	-
Beta-actin	Novus Biologicals	M	1:10 000	-
Cleaved Caspase-3	Cell Signaling	R	1:1000	-
Cleaved Caspase-7	Cell Signaling	R	1:1000	-
Caspase-12	Cell Signaling	R	1:1000	-
CHOP	ThermoFisher	M	1:1000	-
p-ERK1/2 (Thr202/Tyr204)	Cell Signaling	M	1:1000	-
ERK1/2	Cell Signaling	R	1:1000	-
p-JNK (Thr183/Tyr185)	Cell Signaling	M	1:1000	-
JNK	Cell Signaling	R	1:1000	-
Glucagon	Sigma	M	-	1:1000
Insulin	Millipore	GP	-	1:1000
Netrin-1	Calbiochem	R	1:500	1:50
Netrin-4	Santa Cruz	R	1:200	1:25
Neogenin	Santa Cruz	G	1:200	1:25
ROBO1	Santa Cruz	G	1:200	1:25
ROBO2	Sigma	R	1:500	1:100
SLIT1	Sigma	R	1:1000	1:50
SLIT2	Santa Cruz	R	1:200	1:25
SLIT3	Millipore	R	1:1000	1:50
UNC5A	Santa Cruz	G	1:200	1:25
UNC5C	Santa Cruz	G	1:200	1:25

***** Antibody source: rabbit (R), mouse (M), guinea pig (GP), goat (G)

Table 2-2. List of recombinant proteins and peptides.

Gene Symbol	Protein/Peptide Name	Manufacturer*	Source**
ACRP30	adiponectin (NS0 cells-derived)	R&D Systems	H
ACRP30	adiponectin (Hi-5 insect cells-derived)	Peprotech	H
ADM	adrenomedullin 52	Sigma	H
AGT	angiotensinogen, Angiothesin II	Sigma	H
ANG1	angiopoietin 1	Peprotech	H
ANGPT2	angiopoietin 2	R&D Systems	H
ANGPT4	angiopoietin 4	R&D Systems	H
ANGPTL3	angiopoietin-like 3	R&D Systems	H
ANGPTL4	angiopoietin-like 4	R&D Systems	H
AVP	arginine vasopressin	Tocris	H
BDNF	brain-derived neurotrophic factor	Peprotech	H
BMP1	bone morphogenetic protein 1	R&D Systems	H
BMP10	bone morphogenetic protein 10	R&D Systems	H
BMP15	bone morphogenetic protein 15 (GDF9B)	R&D Systems	H
BMP2	bone morphogenetic protein 2	Peprotech	H
BMP4	bone morphogenetic protein 4	Peprotech	H
BMP5	bone morphogenetic protein 5	R&D Systems	H
BMP6	bone morphogenetic protein 6	Peprotech	H
BMP7	bone morphogenetic protein 7 (osteogenic protein 1)	Peprotech	H
BTC	betacellulin	Peprotech	H
CALCA	calcitonin-related polypeptide alpha	Sigma	H
CARTPT	cocaine and amphetamine regulated transcript peptide (55-102)	Sigma	H
CCK	cholecystokinin (CCK Octapeptide)	Tocris	H
CCL11	chemokine (C-C motif) ligand 11 (eotaxin)	Peprotech	H
CCL16	chemokine (C-C motif) ligand 16 (LEC)	Peprotech	H
CCL17	chemokine (C-C motif) ligand 17 (TARC)	Peprotech	H
CCL19	chemokine (C-C motif) ligand 19 (MIP-3 beta)	Peprotech	H
CCL2	chemokine (C-C motif) ligand 2 (MCP-1)	Peprotech	H
CCL20	chemokine (C-C motif) ligand 20 (MIP-3 alpha)	Peprotech	H
CCL25	chemokine (C-C motif) ligand 25 (TECK)	Peprotech	H
CCL26	chemokine (C-C motif) ligand 26 (Eotaxin-3)	Peprotech	H

Gene Symbol	Protein/Peptide Name	Manufacturer*	Source**
CCL27	chemokine (C-C motif) ligand 27 (CTACK)	Peprotech	H
CCL4	chemokine (C-C motif) ligand 4 (MIP-1 beta)	Peprotech	H
CCL5	chemokine (C-C motif) ligand 5 (RANTES)	Peprotech	H
CCL7	chemokine (C-C motif) ligand 7 (MCP-3)	Peprotech	H
CD55	decay accelerating factor (DAF)	R&D Systems	H
CFC1	cripto, FRL-1, cryptic family 1 (cryptic)	R&D Systems	H
CHGA	pancreastatin (37-52)	Sigma	H
CHGA	WE 14 (324-337)	Sigma	H
CHGA	catestatin	Sigma	H
COPA	xenin-8	Tocris	H
CRH	corticotropin releasing hormone	Sigma	H
CSF1	colony stimulating factor 1 (M-CSF)	Peprotech	H
CSF2	colony stimulating factor 2 (GM-CSF)	Peprotech	H
CSH1	placental lactogen	R&D Systems	H
CX3CL1	chemokine (C-X3-C motif) ligand 1 (Fractalkine)	Peprotech	H
CXCL1	chemokine (C-X-C motif) ligand 1 (GRO alpha)	Peprotech	H
CXCL10	chemokine (C-X-C motif) ligand 10 (IP-10)	Peprotech	H
CXCL11	chemokine (C-X-C motif) ligand 11 (I-TAC)	Peprotech	H
CXCL12	chemokine (C-X-C motif) ligand 12 (SDF-1 alpha)	Peprotech	H
CXCL13	chemokine (C-X-C motif) ligand 13 (BCA-1)	Peprotech	H
CXCL14	chemokine (C-X-C motif) ligand 14 (BRAK)	Peprotech	H
CXCL16	chemokine (C-X-C motif) ligand 16	Peprotech	H
CXCL2	chemokine (C-X-C motif) ligand 2 (GRO beta)	Peprotech	H
CXCL3	chemokine (C-X-C motif) ligand 3 (GRO gamma)	Peprotech	H
CXCL6	chemokine (C-X-C motif) ligand 6 (GCP-2)	Peprotech	H
DLL1	delta-like 1 (Drosophila)	Peprotech	H
EDN3	endothelin 3	Sigma	H
EFNA1	ephrin-A1	R&D Systems	M
EFNA4	ephrin-A4	R&D Systems	H
EFNA5	ephrin-A5	R&D Systems	H
EFNB1	ephrin-B1	R&D Systems	M
EFNB2	ephrin-B2	R&D Systems	M
EFNB3	ephrin-B3	Sigma	H

Gene Symbol	Protein/Peptide Name	Manufacturer*	Source**
EGF	epidermal growth factor	Peprotech	H
estrogen	estrogen (estradiol, alpha)	Tocris	H
FGF1	fibroblast growth factor 1 (acidic)	Peprotech	H
FGF12	fibroblast growth factor 12	R&D Systems	H
FGF17	fibroblast growth factor 17	Peprotech	H
FGF18	fibroblast growth factor 18	Peprotech	H
FGF2	fibroblast growth factor 2 (basic)	Peprotech	H
FGF21	fibroblast growth factor 21	Peprotech	H
FGF23	fibroblast growth factor 23	Peprotech	H
FGF3	fibroblast growth factor 3	R&D Systems	H
FGF5	fibroblast growth factor 5	Peprotech	H
FGF7	fibroblast growth factor 7 (keratinocyte growth factor)	Peprotech	H
FGF9	fibroblast growth factor 9 (glia-activating factor)	Peprotech	H
FLT3LG	fms-related tyrosine kinase 3 ligand	Peprotech	H
FRZB	frizzled-related protein (sFRP-3)	R&D Systems	H
GAL	galanin (1-30)	Tocris	H
GAST	gastrin	Sigma	H
GCG	glucagon	Sigma	H
GCG	oxyntomodulin (OXM)	Tocris	H
GCG	glucagon-like peptide 1 (GLP-1)	Peprotech	H
GCG	glucagon-like peptide 2 (GLP-2)	Tocris	H
GDF11	growth differentiation factor 11 (BMP11)	Peprotech	H
GDF15	growth differentiation factor 15	Peprotech	H
GDNF	glial cell line-derived neurotrophic factor	Peprotech	H
GHRL	ghrelin	Tocris	H
GIP	gastric inhibitory polypeptide	Tocris	H
GRN	progranulin	R&D Systems	H
GRP	gastrin-releasing peptide	Tocris	H
HBEGF	heparin-binding EGF-like growth factor	Peprotech	H
HGF	hepatocyte growth factor (scatter factor)	Peprotech	H
IAPP	islet amyloid polypeptide (amylin)	Tocris	H
IFNG	interferon gamma	Peprotech	H
IGF1	insulin like growth factor-1	R&D systems	H

Gene Symbol	Protein/Peptide Name	Manufacturer*	Source**
IGF2	insulin-like growth factor 2 (somatomedin A)	Peprotech	H
IHH	Indian hedgehog homolog (Drosophila)	R&D Systems	M
IL10	interleukin 10	Peprotech	H
IL11	interleukin 11	Peprotech	H
IL13	interleukin 13	Peprotech	H
IL15	interleukin 15	Peprotech	H
IL17	interleukin 17	Peprotech	H
IL18	interleukin 18 (interferon-gamma-inducing factor)	R&D Systems	H
IL1alpha	interleukin 1alpha	Peprotech	H
IL1beta	interleukin 1beta	Peprotech	H
IL22	interleukin 22	Peprotech	H
IL25	interleukin 25 (IL-17E)	Peprotech	H
IL27	interleukin 27 (IL-17D)	Peprotech	H
IL32	interleukin 32 (IL-32 gamma)	R&D Systems	H
IL33	interleukin 33	Peprotech	H
IL4	interleukin 4	Peprotech	H
IL6	interleukin 6	Peprotech	H
IL7	interleukin 7	Peprotech	H
IL8	interleukin 8 (CXCL8)	Peprotech	H
INHA	inhibin, alpha (Inhibin-Like Peptide, human)	Sigma	H
INHBA	inhibin, beta 1 Activin A (Activin A)	Peprotech	H
INS	insulin	Sigma	H
JAG2	jagged 2	R&D Systems	H
KNG1	bradykinin	Tocris	H
LEP	leptin	Peprotech	H
LTB	lymphotoxin alpha2/beta1	R&D Systems	H
MCH	melanin-concentrating hormone	Tocris	H
MDK	midkine (neurite growth-promoting factor 2)	Peprotech	H
MIF	macrophage migration inhibitory factor	R&D Systems	H
NGF	nerve growth factor (beta polypeptide)	Peprotech	H
NLGN1	neuroligin 1	R&D Systems	R
NLGN2	neuroligin 2	R&D Systems	H
NLGN4	neuroligin 4	R&D Systems	H

Gene Symbol	Protein/Peptide Name	Manufacturer*	Source**
NMB	neuromedin B	Tocris	H
NP	natriuretic peptide (atrial natriuretic factor 1-28)	Tocris	R
NPW	neuropeptide W-23	Tocris	H
NPY	neuropeptide Y	Sigma	H
NTF3	neurotrophin-3 (NT-3, NGF2)	Peprotech	H
NTF4	neurotrophin-4/5 (NT-4/NT-5)	Peprotech	H
NTN1	netrin 1	R&D Systems	M
NTN4	netrin 4	R&D Systems	H
NTN4	netrin 4	R&D Systems	M
NTNG1	netrin G1-a	R&D Systems	M
OLFM1	olfactomedin 1 (noelin-1)	R&D Systems	H
OSM	oncostatin M	Peprotech	H
PACAP	pituitary adenylate cyclase activating polypeptide (1-38)	Tocris	H
PDGFA	platelet-derived growth factor alpha polypeptide	Peprotech	H
PF4	platelet factor 4 (chemokine (C-X-C motif) ligand 4)	Peprotech	H
PGF	placental growth factor (PIGF)	Peprotech	H
PNOC	[Phe1-ψ(CH2-NH)-Gly2]-Nociceptin Fragment 1-13 amide	Sigma	H
POMC	α-melanocyte stimulating hormone (α-MSH)	Sigma	H
POMC	β-melanocyte stimulating hormone (β-MSH)	Sigma	H
POMC	γ-melanocyte stimulating hormone (γ-MSH)	Sigma	H
POMC	adrenocorticotropic hormone (ACTH)	Sigma	H
POMC	Met-enkephalin (M-ENK)	Tocris	H
POMC	β-endorphin	Sigma	H
PPY	pancreatic polypeptide	Sigma	H
PRL	prolactin	Peprotech	H
PYDN	dynorphinB	Tocris	H
PYDN	dynorphinA	Tocris	H
PYY	peptide YY	Sigma	H
REG3A	regenerating islet-derived 3 alpha	R&D Systems	M
SAA1	serum amyloid A1 (Apo-SAA1)	Peprotech	H
SCG2	secretogranin II (chromogranin C, secretoneurin)	Sigma	M
SCT	secretin	Tocris	H
SEMA3A	semaphorin 3A	R&D Systems	H

Gene Symbol	Protein/Peptide Name	Manufacturer*	Source**
SEMA3C	semaphorin 3C	R&D Systems	H
SEMA3E	semaphorin 3E	R&D Systems	H
SEMA4A	semaphorin 4A	R&D Systems	H
SEMA4G	semaphorin 4G	R&D Systems	H
SEMA5A	semaphorin 5A	R&D Systems	H
SEMA6A	semaphorin 6A	R&D Systems	H
SHH	sonic hedgehog	Peprotech	H
SLIT1	slit homolog 1 (Drosophila)	R&D Systems	H
SLIT2	slit homolog 2 (Drosophila)	Peprotech	H
SLIT2	slit homolog 2 (Drosophila)	R&D Systems	M
SLIT3	slit homolog 3 (Drosophila)	R&D Systems	H
SST	somatostatin-14	Tocris	H
TAC1	tachykinin, precursor 1 (α-neurokinin fragment 4-10)	Sigma	H
TFF1	trefoil factor 1	Peprotech	H
TFF2	trefoil factor 2 (spasmolytic protein 1)	Peprotech	H
TFF3	trefoil factor 3 (intestinal)	Peprotech	H
TGFA	transforming growth factor, alpha	Peprotech	H
TGFB1	transforming growth factor, beta 1	Peprotech	H
TGFB2	transforming growth factor, beta 2	Peprotech	H
TGFB3	transforming growth factor, beta 3	Peprotech	H
TNFSF10	tumor necrosis factor superfamily, member 10 (TRAIL)	Peprotech	H
TNFSF13B	tumor necrosis factor superfamily, member 13b (BAFF)	Peprotech	H
TNFSF14	tumor necrosis factor superfamily, member 14 (LIGHT)	Peprotech	H
TNFSF15	tumor necrosis factor (ligand) superfamily, member 15	Peprotech	H
TNFSF4	tumor necrosis factor (ligand) superfamily, member 4	Peprotech	H
TNFSF9	tumor necrosis factor (ligand) superfamily, member 9	Peprotech	H
UCN	urocortin	Sigma	H
UCN2	urocortin 2	Sigma	H
UCN3	urocortin 3	Sigma	H
VEGF	vascular endothelial growth factor	Peprotech	H
VEGFB	vascular endothelial growth factor B	Peprotech	H
VEGFC	vascular endothelial growth factor C	Peprotech	H
VGF	TLQP-21	Tocris	H

Gene Symbol	Protein/Peptide Name	Manufacturer*	Source**
VIP	vasoactive intestinal peptide	Sigma	H
WNT1	wingless-type MMTV integration site family, member 1	Peprotech	H
WNT11	wingless-type MMTV integration site family, member 11	R&D Systems	H
WNT3A	wingless-type MMTV integration site family, member 3A	Peprotech	H
WNT4	wingless-type MMTV integration site family, member 4	R&D Systems	H
WNT5A	wingless-type MMTV integration site family, member 5A	R&D Systems	H
WNT5B	wingless-type MMTV integration site family, member 5B	R&D Systems	H
WNT7A	wingless-type MMTV integration site family, member 7A	Peprotech	H
WNT9B	wingless-type MMTV integration site family, member 9B	R&D Systems	H
	serotonin (5-HT)	Tocris	H
	dopamine	Tocris	H

***** Manufacturers: R&D Systems (Minneapolis, MN, USA), Peprotech (Rocky Hill, NJ, USA), Sigma (St Louis, MO, USA), Tocris (Avonmouth, Bristol, UK)

****** Source: human (H), mouse (M), rat (R)

Chapter 3: Multi-parameter, single-cell, kinetic analysis reveals multiple modes of cell death in primary pancreatic β-cells

3.1 Introduction

The loss of β-cell mass plays a crucial role in the pathophysiological onset and progression of diabetes. Numerous intrinsic and extrinsic signals are required for the maintenance of functional β-cell mass by providing pro-survival and pro-death signals. Apoptosis, necrosis, and autophagic cell death are the three commonly characterized forms of cell death (40, 41). Each modality is distinguished by a set of morphological features and the underlying biochemical changes. The detection and therapeutic manipulation of cell death for the treatment of diabetes requires comprehensive knowledge of the redundancy and exclusivity of different mechanisms of cell death. However, the interpretation of the different modes of β-cell death is often misled by the use of single parameter, end-point measurements in heterogeneous whole cell populations. Guidelines provided for the interpretation of different modes of cell death require multiple readouts, but these guidelines are often overlooked and are rarely examined simultaneously in living cells (40, 41, 120).

Here, we report a novel 6-parameter live-cell imaging approach that enables single-cell analysis of multiple cell death mechanisms and applied this approach to the study of primary and transformed pancreatic β-cells exposed to multiple distinct stresses. Our results illustrate the heterogeneity in cell death kinetics and demonstrate that the majority of primary β-cells die via mechanisms that are distinct from strictly defined apoptosis. These observations have implications for therapeutic efforts to block β-cell death.

3.2 Results

3.2.1 Detection of apoptotic and non-apoptotic forms of β-cell death

The potential for multiple modes of cell death within the β-cell population complicates the development of therapeutics. Our attempt to determine the predominant modes of cell death began with the development of a multiple-parameter live cell assay for the detection of different phases of cell death. With the use of vital dyes and a caspase-3 activity reporter expressed under the control of the *Ins1* promoter (Fig. 3-1A,B), we were able to track the onset of specific events during the progression of cell death and classify the mode of cell death for

individual β-cells. Culturing cells in a low concentration of Hoechst 33342 (0.05 μg/ml) allowed for the detection of nuclear condensation. Importantly, we employed a concentration of Hoechst 33342 that does not have significant effects on cell survival when compared to cells that were not exposed to the nuclear dye (Fig. 3-1C). AlexaFluor647-conjugated annexinV allowed for the detection of phosphatidylserine translocation from the inner leaflet to the outer leaflet of the plasma membrane, an early event in the classical apoptotic cascade (121, 122). The dilution of AlexaFluor647-conjugated annexinV employed also did not induce significant levels of cell death (Fig. 3-1D). The detection of late phase cell death was monitored with propidium iodide (PI) incorporation, which marks the irreversible compromise of the plasma membrane. Cells were transduced with lentiviral particles carrying EBFP2-GFP caspase-3 FRET sensor expressed under the control of the *Ins1* promoter, as well as mRFP driven by the *Pdx1* promoter (Fig. 3-1B). The temporal tracking of caspase-3 activation (decrease in FRET), plasma membrane blebbing (brightfield imaging), nuclear condensation, annexinV incorporation, PI incorporation, and changes in *Ins1* or *Pdx1* promoter activities can be observed in a representative MIN6 cell treated with cytokines (Fig. 3-1E). Due to interference in the red channel and the weak activation of the *Pdx1* promoter in primary cells, we were unable to simultaneously monitor *Pdx1* promoter activity and PI incorporation in primary β-cells. Nevertheless, these results clearly demonstrate that multiple molecular events in programmed cell death can be distinguished at the single-cell level.

We next sought to determine the length of time required for each cell death mechanism and the relative order in which they occur at the single cell level. When the time of onset of plasma membrane blebbing, caspase-3 activation, PI incorporation and nuclear condensation were assessed relative to annexinV incorporation, 3D dot plots of individual cell analysis allowed for the identification of different modes of cell death (Fig. 3-2A,B). Cells that underwent classical apoptosis were defined as undergoing plasma membrane blebbing, caspase-3 activation, nuclear condensation and annexinV incorporation prior to PI incorporation. Cells that underwent 'partial-apoptosis' displayed PI incorporation simultaneously with one or more of the other events. Cells lacking all apoptotic features prior to PI incorporation were considered necrotic. Individual primary mouse β-cells undergoing different types of cell death were categorized (Fig. 3-3A-D). Of the apoptotic cells analyzed, plasma membrane blebbing always occurred first, followed by nuclear condensation and

caspase-3 activation. AnnexinV incorporation occurred last before PI incorporation in all apoptotic cells (Fig. 3-3A). Complete loss of GFP was used as an indication of protein loss, which was often coincident with PI incorporation. Caspase-3 activation is often associated with apoptosis (40). Two types of distinct 'partial-apoptotic' cell death involving caspase-3 activation were found (Fig. 3-3B,C). The first form of partial apoptosis displayed plasma membrane blebbing and caspase-3 activation with a lack of nuclear condensation (Fig. 3-3B). The second form of partial apoptosis displayed nuclear condensation, caspase-3 activation and prolonged period of oncosis with a lack of plasma membrane blebbing (Fig. 3-3C). We also identified a small number of cells undergoing necrotic cell death, which lacked any of the apoptotic cell death features including caspase-3 activation (Fig. 3-3D). Collectively, our data suggests that nuclear condensation, caspase-3 activation, and plasma membrane blebbing exist in both apoptotic and partial-apoptotic cell death (Fig. 3-4). AnnexinV incorporation rarely occurred in cells undergoing partial-apoptotic cell death (Fig. 3-4B). Perhaps, cells that were initially undergoing apoptosis were re-routed to other forms of cell death due to the cellular state induced by specific stress conditions.

3.2.2 Temporal progression of cell death events in distinct stress conditions

It is not known whether the time courses of specific cell death events or the temporal relationships between cell death events are dependent on the type of stress. We asked this question by exposing primary β-cells to hyperglycemia, cytokines, ER stress and/or nutrient deprivation, and determining the onset of cell death events relative to annexinV incorporation (Fig. 3-5). Detection of plasma membrane blebbing under all conditions was variable. The delay in the initiation of nuclear condensation and caspase-3 activation following plasma membrane blebbing was dependent on the treatment conditions. Often cells with concurrent annexinV and PI incorporation did not display plasma membrane blebbing, suggesting activation of non-apoptotic pathways. Depending on the treatment conditions, the average length of time between the detection of the first cell death morphological feature and last phase of cell death (loss of membrane integrity) was between 10 to 20 h. Remarkably, some cells initiated cell death up to 2 days prior to the loss of membrane integrity. Significant differences can also be observed between the absolute time of onset of different events for cells treated

under low and high glucose conditions (Fig. 3-6). These data provide evidence of a critical window of time for reversing cell death after it has been initiated.

3.2.3 Primary β-cells predominantly undergo partial-apoptotic cell death

Apoptosis is the main mode of cell death commonly assessed in the β-cell field (2, 11, 30-32, 123, 124), whereas contributions of other modes of cell death are often overlooked. Using our multiple-parameter single cell analysis, we were able to distinguish between apoptotic, partial-apoptotic, and non-apoptotic modes of primary β-cell death, which cannot be disassociated using cell population analyses of cell death (Fig. 3-7A,B). We found changes in the relative proportion of β-cells undergoing cell death displaying all four to none of the apoptotic features assayed under the different stress conditions (Fig. 3-7C). Cells were considered apoptotic if they underwent all four apoptotic morphological/biochemical changes (plasma membrane blebbing, nuclear condensation, caspase-3 activation, and annexinV incorporation) prior to PI incorporation. Using these stringent criteria, we determined that primary mouse β-cells predominately undergo non-apoptotic cell death in low glucose conditions (Fig. 3-7D). Under conditions of ER-stress or serum-withdrawal, no cells were observed to follow the canonical apoptotic pathway. Interestingly, under serum containing conditions, exposure to high glucose or a cytokine cocktail of TNF-α, IL-1β and IFN-γ increased the proportion of primary β-cells undergoing apoptotic cell death. Similarly, high glucose increased the proportion of apoptosis in cells with thapsigargin-induced ER stress from 0% to 16% (Fig. 3-7D). As a control to demonstrate that our multi-parameter assay could detect multiple modes of cell death, including complete classical apoptosis, the same study was conducted using the MIN6 β-cell line, which has been characterized to predominantly undergo apoptotic cell death. Indeed, under the same stress conditions, MIN6 cells predominantly underwent complete classical apoptosis (Fig. 3-7E-H). Together, these data demonstrate that primary mouse β-cells and MIN6 cell line do not undergo classically defined apoptosis to the same extent and glucose controls the mode of programmed cell death exhibited by individual primary β-cells.

3.3 Discussion

Apoptosis is the most well studied mode of β-cell death and it is characterized by a stereotypical order of molecular events. Few, if any studies, have examined whether the apoptotic series of events occurs in single cells. In the present study, we clearly demonstrated that most pancreatic β-cells undergo forms of cell death that differ from strictly defined apoptosis. Our studies began with the elucidation of the complex and variable interplay between cell death mechanisms within single β-cells. The progression of β-cell death events was simultaneously assessed using a live cell assay that detected the temporal induction of plasma membrane blebbing, nuclear condensation, caspase-3 activation, annexinV incorporation, PI incorporation and loss of GFP. We characterized the kinetic interrelationships between cell death events in the context of multiple diabetes associated conditions that can trigger the onset of β-cell death, including prolonged exposure to hyperglycemia, inflammatory cytokines and ER stress (2, 11, 31, 32, 123, 124). While some kinetic features were common to all forms of β-cell death, we also found significant differences in event timing and order between distinct stresses.

The molecular mechanisms and progression of programmed cell death via apoptosis have been characterized, based mostly on whole cell population biochemical and flow cytometry studies, as a series of events preceding the loss of plasma membrane integrity. The widely accepted temporal and mechanistic model of apoptosis posits that plasma membrane blebbing, chromatin condensation and fragmentation, rounding up of the cell, and cellular and nuclear volume reduction all occur prior to the final loss of membrane integrity, which can be imaged by the incorporation of normally membrane impermeant dyes, like propidium iodide, within the nucleus (40). Apoptosis can be triggered by two distinct signalling networks that share many regulatory components. Extrinsic apoptosis proceeds when death receptors at the plasma membrane are activated by extracellular ligands, including TNF-α, Fas ligand and TRAIL (2, 43). Following assembly of the death inducing signalling complexes, initiated at the cytoplasmic tails of the death receptors, initiator procaspases-8 and -10 are activated, which in turn activates effector procaspases-3 and -7 to generate active proteases (43). Intrinsic apoptosis results from exposure to ultraviolet light, cellular stress and toxins. The cascade of signalling events that follows often involves the activation of pro-apoptotic Bcl-2 family members (Bax, Bak, Bad, Bid), triggering mitochondrial outer membrane permeabilization

prior to the activation of caspases (2, 40, 43). Studies by our group and others have also focused on the role of ER and cytosolic Ca^{2+} dynamics in β-cell survival and function upon initiation of the intrinsic apoptotic pathway (76, 111, 125, 126). We have previously noted robust glucose-dependent differences between the mechanisms of β-cell death with respect to the involvement of notch signalling, netrin signalling, carboxypeptidase E, ATP-citrate lyase, Uchl1, and intracellular Ca^{2+} release channels (IP3R, RyR) (37, 76, 109, 115, 123, 125, 127, 128). Consistent with other reports, glucose does indeed modulate β-cell death levels (31, 32, 129, 130). Here, we found differences in the kinetics and mode of the core cell death events between cells treated in low glucose and cells treated in high glucose. To the best of our knowledge, this is the first comprehensive single cell analysis of β-cell death modulation by glucose.

The roles of signalling molecules involved in the temporal cascade of events leading to β-cell apoptosis, autophagy and necrosis have not been well characterized at the level of individual cells, resulting in the under-appreciation of non-apoptotic and pseudo-apoptotic forms of cell death. Notwithstanding, β-cell death via necrosis has also been implicated in the pathogenesis of diabetes (55, 56). Necrosis is often defined as cell death lacking the characteristics of apoptosis or autophagy. In addition, key morphological features of necrosis include plasma membrane rupture and swelling of cytoplasmic organelles (40, 57). Although initially believed to be an uncontrolled form of cell death, there is accumulating evidence supporting the notion that necrotic cell death is regulated by a defined set of signalling events induced by oxidative stress, loss of Ca^{2+} homeostasis, and/or ischemia (40, 57). In the conditions tested, a small fraction of β-cells underwent classical necrosis upon treatment with cytokines under high glucose, characterized by oncosis, plasma membrane rupture and the lack of apoptotic features (including plasma membrane blebbing, nuclear condensation, caspase-3 activation and annexinV incorporation) prior to loss of plasma membrane integrity. Indeed, necrosis mediated β-cell death has been observed upon treatment with IL-1 alone (56). We were also able to identify other forms of partial-apoptotic cell death, which shared some of the apoptotic characteristics (40, 57). The term necroptosis has been used to describe similar atypical apoptosis-like forms of programmed cell death (60, 131). Without characterization of additional mechanisms at the single cell level, we were not able to further classify these cell death modalities or determine their precise molecular mechanisms.

We speculate that apoptosis was initially triggered in some of the cells, but due to the change in cellular environment (e.g. lack of sufficient cellular ATP, loss of Ca^{2+} homeostasis, or ischemia) apoptosis could not proceed to completion. Not surprisingly, apoptosis and necrosis may share common signalling pathways involving mitochondrial membrane permeabilization through activation of proapoptotic Bcl-2 family members (57, 59). When exposed to stress conditions, direct inhibition of caspase activation or depletion of cellular ATP (required for caspase activation) can inhibit apoptotic signalling and favour necrotic cell death suggesting that cell death modalities co-exist within the same cell and have the potential to substitute for each other (59, 61, 62). In our studies of individual β-cells, partial-apoptotic cell death played a major, if not exclusive, role in β-cell death under all the diabetes-related stress conditions tested. Additionally, we were able to determine the relative onset of each cell death feature and quantify their contribution to cells undergoing 'partial apoptosis' by tracing single cells over time. The complex interplay between different modes of cell death further complicates the development of therapeutics for preventing β-cell death.

Therapeutic interventions preventing β-cell death have the potential to treat diabetes. When looking at nuclear condensation or caspase-3 activation alone, our data are consistent with others estimating the apoptosis duration in β-cells to be 2.5 h under unstressed conditions or 90-110 min under stressed conditions, respectively (132, 133). When we define the duration of β-cell death as the length of time between the detection of the first cell death morphological feature and last phase of cell death (loss of membrane integrity), we determined that the cell death duration was usually between 10 to 20 h. In some cells, plasma membrane blebbing was initiated up to 2 days prior to the loss of membrane integrity. Thus, we provided evidence of a critical therapeutic window of time for reversing cell death after it has been initiated. Comprehensive understanding of the different modes of β-cell death and the functional state of β-cells under varying stress conditions will provide mechanistic insight into diabetes initiation and progression.

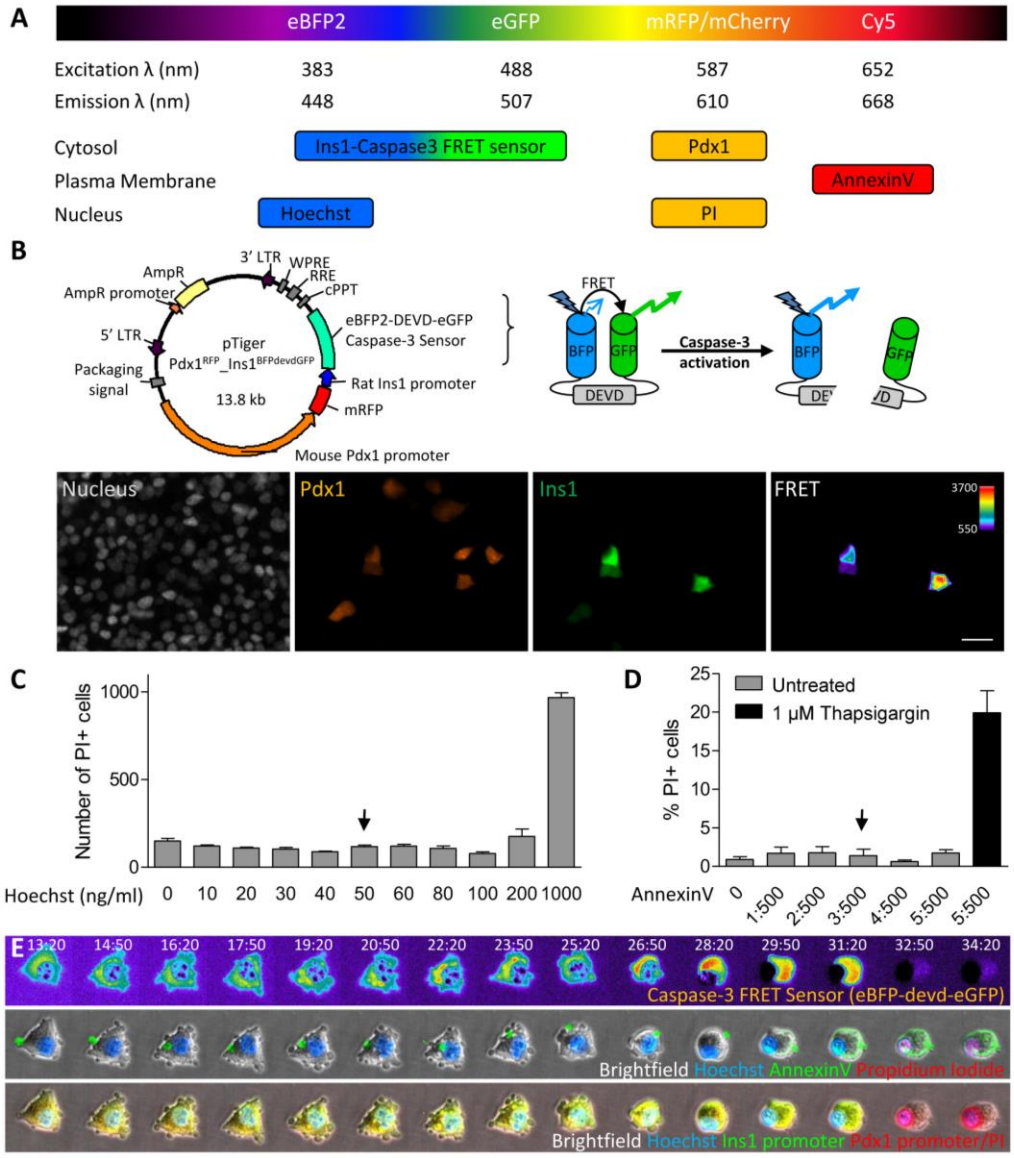

Figure 3-1. Live cell kinetic analyses of cell death in β-cells.
A. Schematic of multi-parameter live cell detection of multiple phases of β-cell death. **B.** Dual reporter lentivirus that reports *Ins1* and *Pdx1* promoter activities and caspase-3 activation (loss of FRET) in living β-cells. **C.** MIN6 cells incubated with 0-1000 ng/mL Hoechst 33342 under 20 mM glucose 10% FBS conditions for 48 hours were stained with 0.5 μg/mL propidium iodide (PI) 30 min prior to imaging. The total number of PI positive cells were analyzed (n = 4-6, mean ± SEM). Arrow represents concentration of Hoechst used in subsequent assays. **D.** MIN6 cells incubated with indicated dilution of annexinV-647 for 48 hours were stained with 50 ng/mL Hoechst and 0.5 μg/mL PI 30 min prior to imaging. The percentage of PI positive cells were analyzed (n = 9, mean ± SEM). Arrow represents dilution of annexinV-647 used in subsequent assays. **E.** MIN6 cells stably expressing RFP under the *Pdx1* promoter and caspase-3 eBFP-devd-eGFP FRET sensor under the *Ins1* promoter were stained with Hoechst, PI, and annexinV-647. The cells were treated with a cytokine cocktail (25 ng/mL TNF-α, 10 ng/mL IL-1β, 10 ng/mL IFN-γ) and imaged every 5 min for 49 hours. Representative single cell images taken 13 hr 20 min following treatment with cytokine cocktail (hr:min, time following treatment with cytokines). The various fluorescent dyes and sensors are spectrally and spatially distinguishable to allow for the detection of different modes of cell death and maturation states.

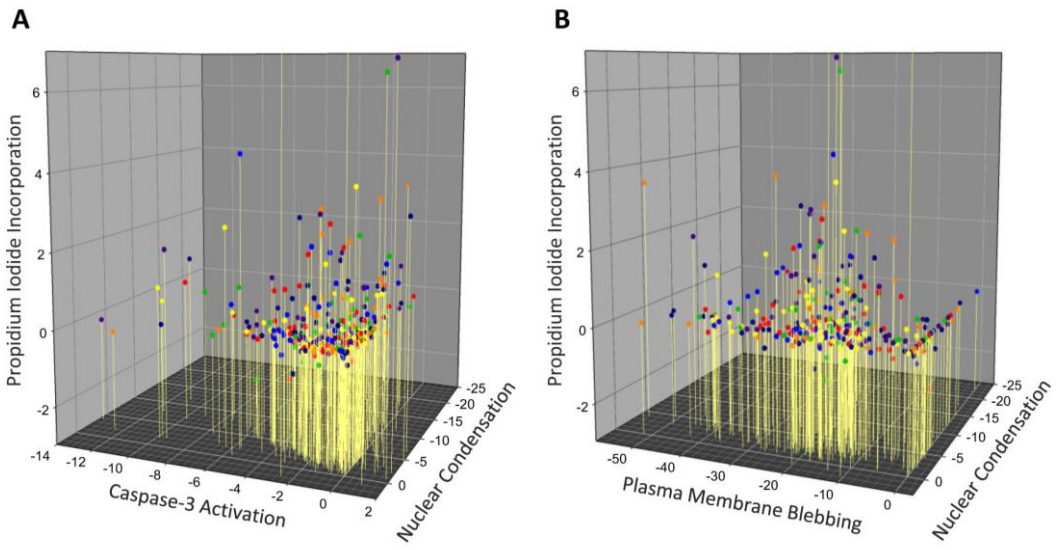

Figure 3-2. Different modalities of β-cell death identified through single cell analysis of cell death morphological features.

A-B. Dispersed mouse islet cells stably expressing the β-cell specific caspase-3 reporter and stained with Hoechst, PI, and annexinV-647 were imaged for 60 hours. Cells were treated in 5 or 20 mM glucose RPMI medium with cytokines (25 ng/ml TNF-α, 10 ng/ml IL-1β, and 10 ng/ml IFN-γ), 1 μM thapsigargin or serum free conditions. β-cells that underwent cell death during the time course were analyzed for the time of onset of plasma membrane blebbing, nuclear condensation, caspase-3 activation, annexinV incorporation, and PI incorporation. 3-dimentional plots of the time of onset of the indicated cell death events relative to the onset of annexinV incorporation for individual primary mouse β-cells (time scales in hours).

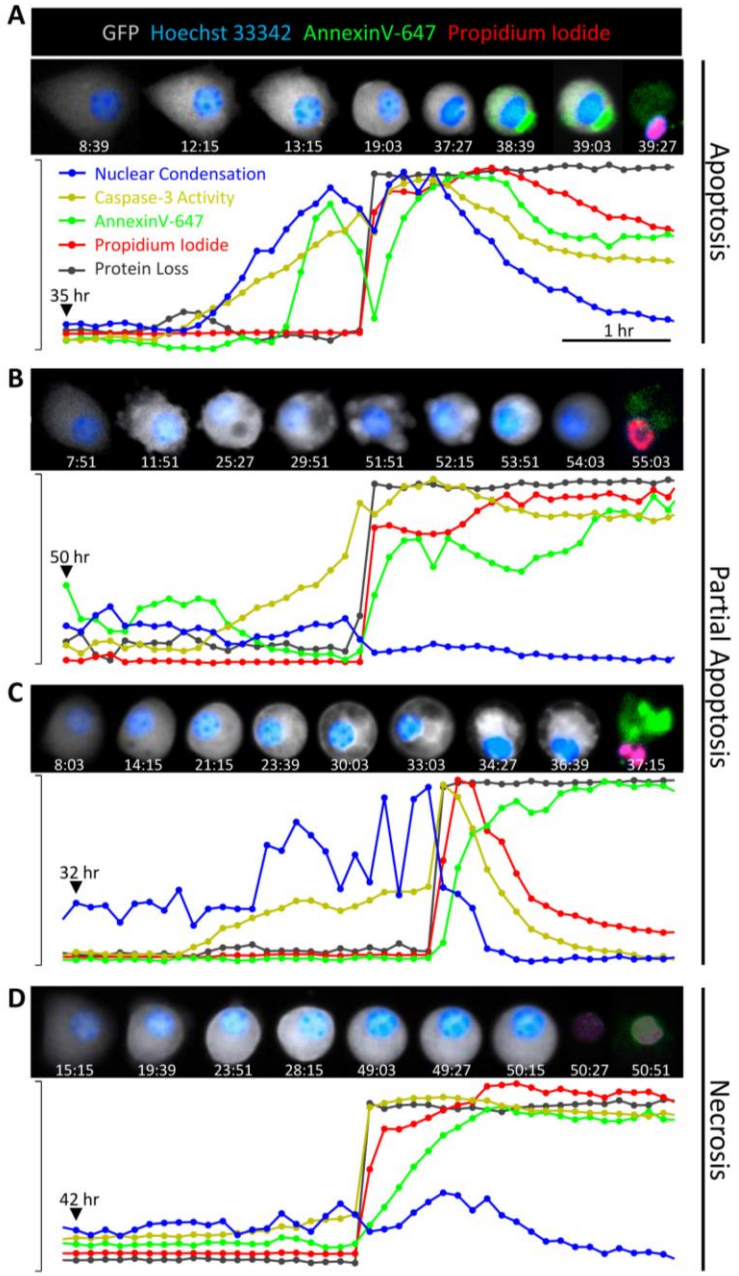

Figure 3-3. Cytokine exposure induced distinct apoptotic and non-apoptotic forms of β-cell death.
A-D. Dispersed mouse islet cells stably expressing the β-cell specific caspase-3 reporter and stained with Hoechst, PI and annexinV-647 were treated with a cytokine cocktail (25 ng/mL TNF-α, 10 ng/mL IL-1β, 10 ng/mL IFN-γ) and imaged. Four distinct types of cell death were identified (**A**: apoptosis, **B-C:** partial-apoptosis, **D**: necrosis). *Top panel:* representative images of single cells throughout the time course (hr:min, time following treatment with cytokines). *Bottom panel:* Measured changes in the indicated features (nuclear condensation, caspase-3 activity, annexinV-647 intensity, propidium iodide intensity, GFP protein loss) were plotted.

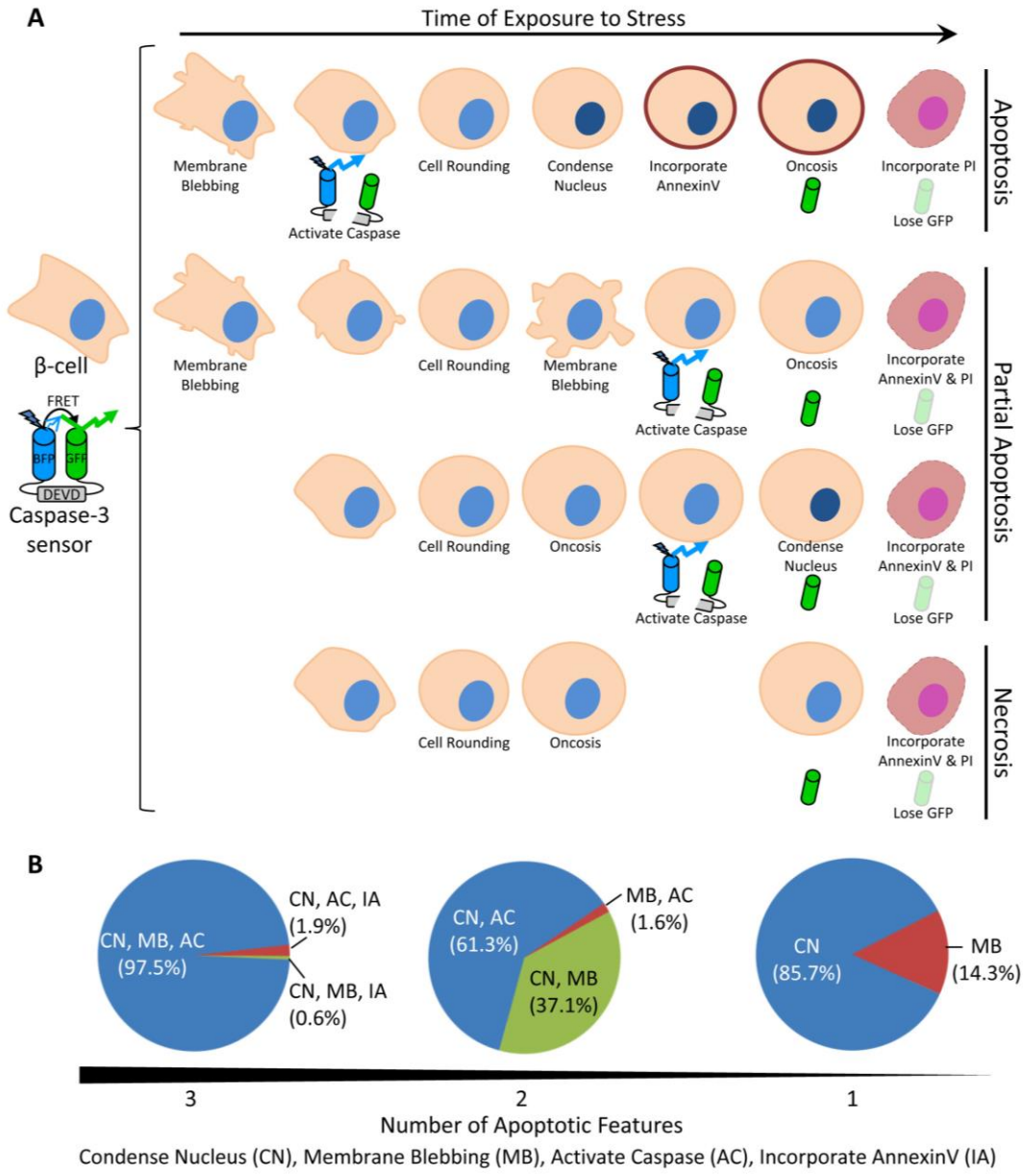

Figure 3-4. Schematic of distinct apoptotic and non-apoptotic forms of β-cell death.
A. Schematic representation of the relative onset of individual events (plasma membrane blebbing, cell rounding, nuclear condensation, caspase-3 activation, annexinV-647 incorporation, oncosis, propidium iodide incorporation, and GFP protein loss). **B.** Proportion of apoptotic features remaining in mouse β-cells undergoing partial apoptotic cell death displaying 1 to 3 of the apoptotic features.

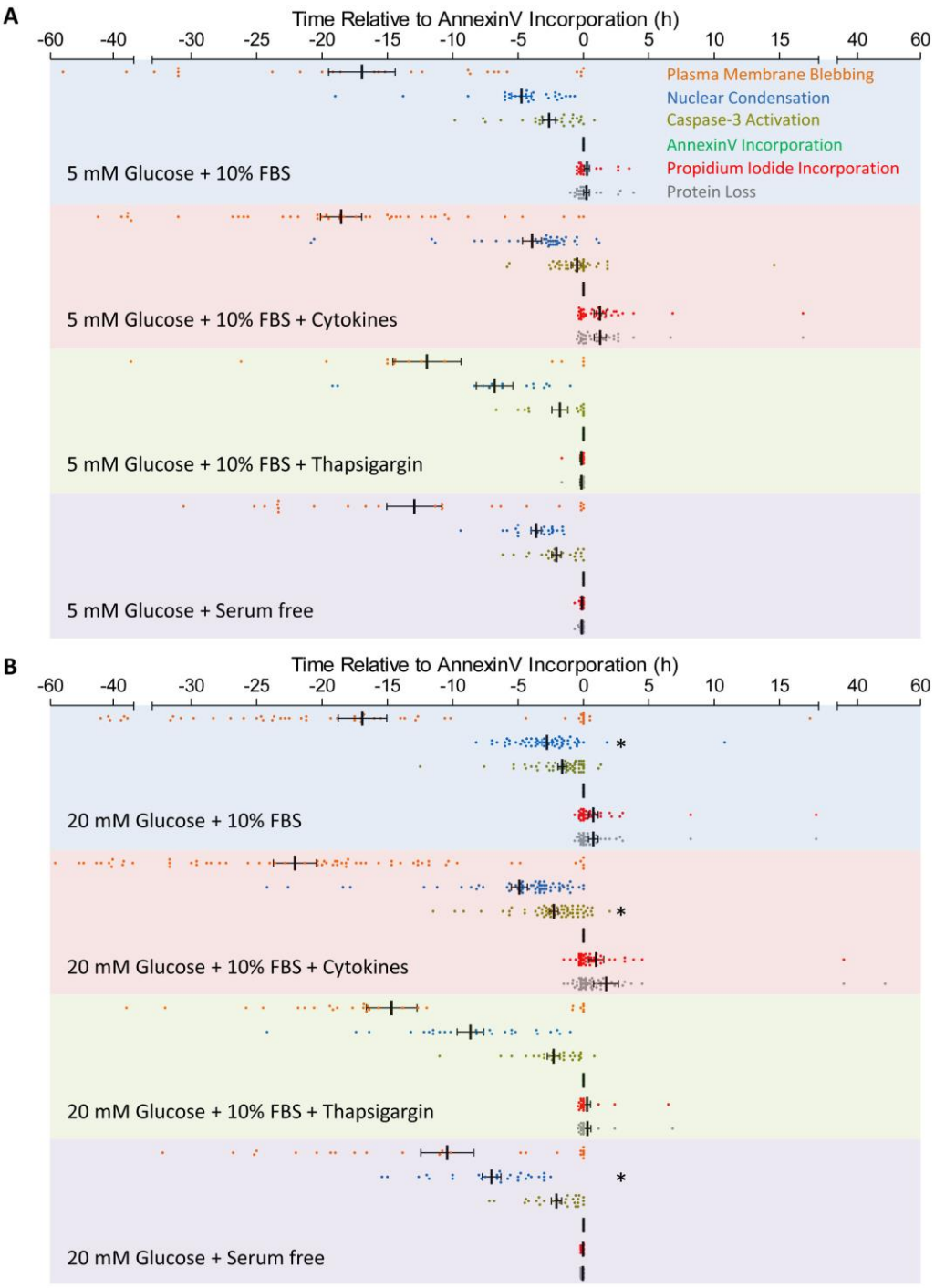

Figure 3-5. Stress treatments influenced the relative timing of cell death molecular events in single mouse β-cells.

A-B. Mouse β-cells carrying a caspase-3 sensor were stained with Hoechst, PI, and annexinV-647. Cells were treated with the indicated treatments under 5 mM **(A)** and 20 mM glucose **(B)** and imaged for 60 hours at 37°C and 5% CO_2. The relative time interval between the onset of annexinV incorporation and plasma membrane blebbing, nuclear condensation, caspase-3 activation, PI incorporation and protein loss were determined (n = 15-63, mean ± SEM, * $p<0.05$ compared to 5 mM glucose).

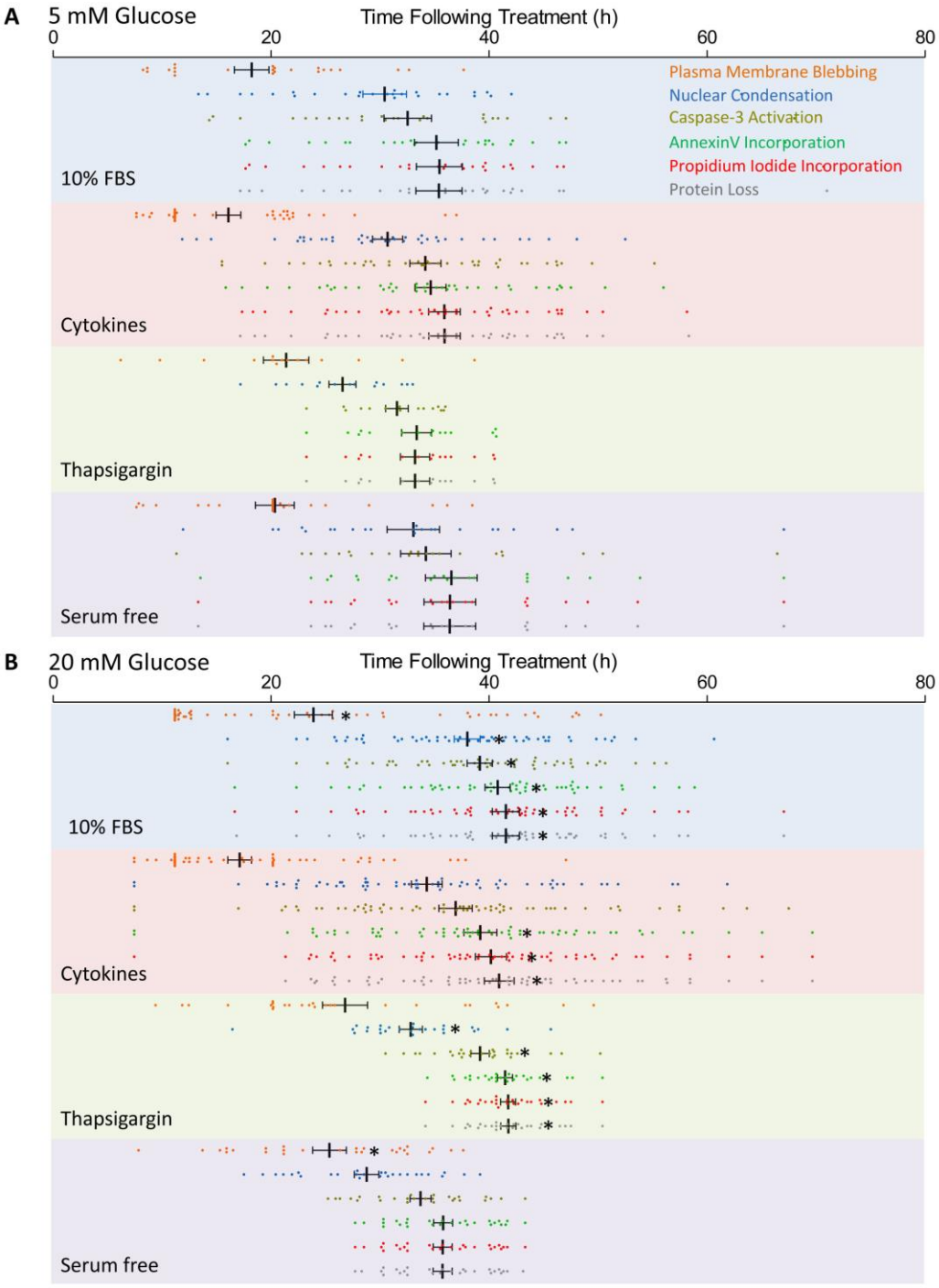

Figure 3-6. Stress treatments influenced the absolute onset of cell death molecular events in single mouse β-cells.

A-B. Mouse β-cells carrying a caspase-3 sensor were stained with Hoechst, PI, and annexinV-647. Cells were treated with the indicated treatments under 5 mM **(A)** and 20 mM glucose **(B)** and imaged for 60 hours at 37°C and 5% CO_2. The absolute time for the onset of plasma membrane blebbing, nuclear condensation, caspase-3 activation, annexinV incorporation, PI incorporation and protein loss were determined (n = 15-63, mean ± SEM, * $p<0.05$ compared to 5 mM glucose).

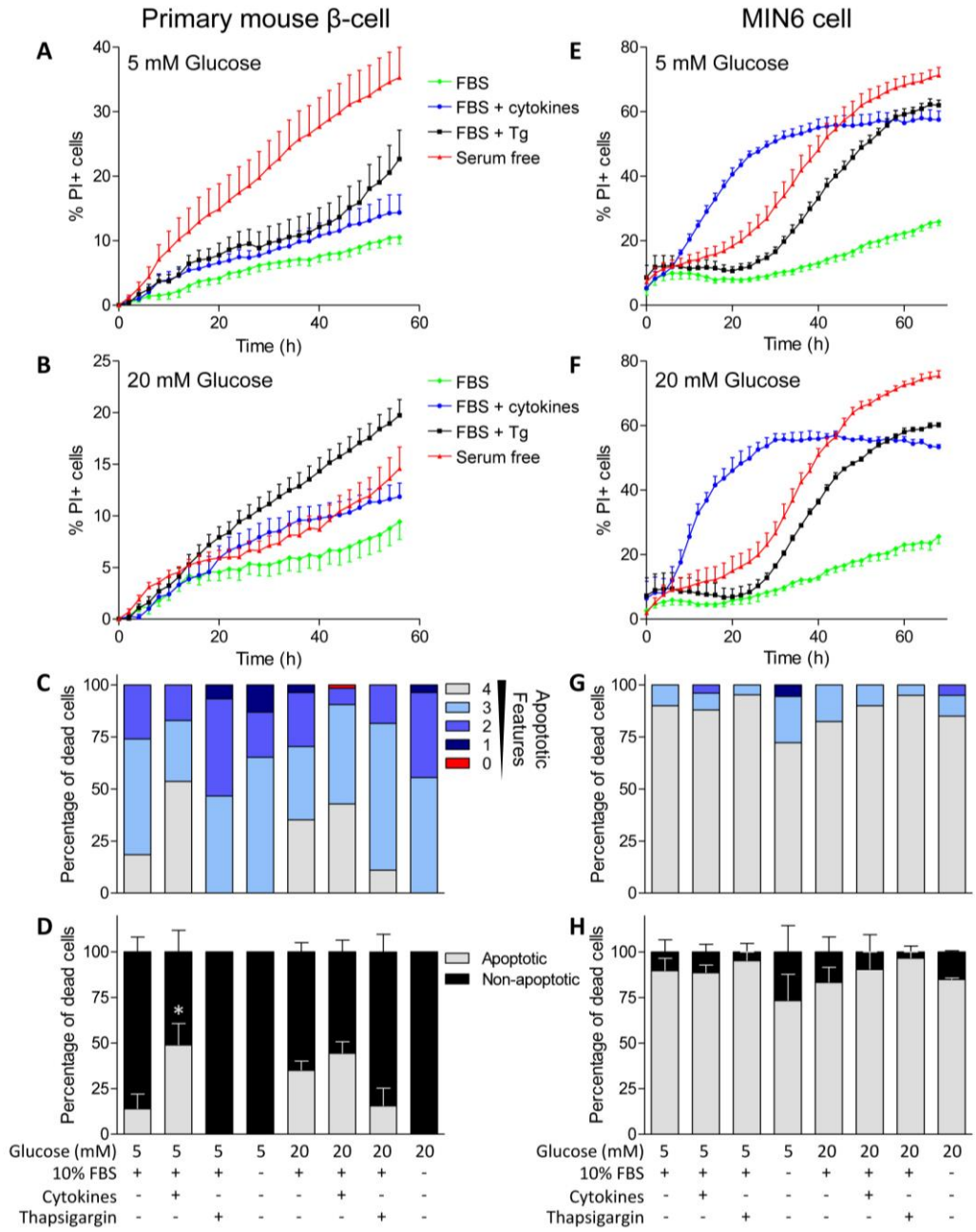

Figure 3-7. The level of different β-cell death modalities is determined by specific stress treatments.
A-H. Primary mouse β-cells or MIN6 cells carrying a caspase-3 sensor were stained with Hoechst, PI, and annexinV-647. Cells were imaged with Molecular Devices ImageXpress^{MICRO} at 37°C and 5% CO_2. Cells were treated in 5 or 20 mM glucose RPMI medium with cytokines (25 ng/ml TNF-α, 10 ng/ml IL-1β, and 10 ng/ml IFN-γ), 1 µM thapsigargin or serum free conditions. **A-B.** Population analysis of islet cell death represented by percentage of PI positive cells (n = 8-30, mean ± SEM). **C.** The proportion of primary β-cells displaying 0 to 4 of the apoptotic features (n = 15-63). **D.** The percentage apoptotic and non-apoptotic (includes partial apoptotic and necrotic cells) cell death within the pool of primary β-cells that died during the time course was determined (n = 3-4, mean ± SEM, * $p<0.05$ compared to serum containing treatment of the same glucose level). **E-F.** Population analysis of MIN6 cell death represented by percentage of PI positive cells (n = 3-11, mean ± SEM). **G.** The proportion of MIN6 cells displaying 0 to 4 of the apoptotic features (n = 17-30). **H.** The percentage apoptotic and non-apoptotic cell death within the pool of MIN6 cells that died during the time course was determined (n = 3-4, mean ± SEM).

Chapter 4: Multi-parameter screening reveals a role for Na^+ channels in cytokine induced β-cell death

4.1 Introduction

Pancreatic β-cell death is pathologically elevated in type 1 diabetes, type 2 diabetes, as well as failing islet transplants. In type 1 diabetes, infiltrating auto-reactive T-cells secrete pro-inflammatory cytokines, such as TNF-α, IL-1β, and IFN-γ, which effectively coerce the vast majority of pancreatic β-cells into programmed cell death (2, 11-13). Preventing β-cell death could reduce the burden on at-risk families and protection of the few remaining β-cells in type 1 diabetic patients has the potential to delay disease progression (12). Furthermore, massive β-cell death before, during and after clinical islet transplantation reduces the success of this promising therapy for type 1 diabetes (33-35). Type 2 diabetes results from the eventual loss of functional β-cell mass, which is in part due to increased β-cell death (9, 11). Thus, there is an urgent clinical need to develop or repurpose drugs that can enhance β-cell survival in both type 1 and type 2 diabetes.

Ion channels are a critical class of drug targets and significant effort has been devoted to understanding the ionic basis of glucose-stimulated insulin secretion (134). Particular attention has focused on K^+ and Ca^{2+} channels, while Na^+ channels are much less well understood despite their presence on β-cells (134). Moreover, the role of plasma membrane ion channels in cell fate decisions, such as apoptosis, remains to be fully elucidated. Unbiased screens are critical for the identification of new pathways involved in programmed β-cell death. We have recently developed rich multi-parameter screening platforms where multiple aspects of programmed cell death can be assessed simultaneously in the high-throughput manner (114).

Here, we report the results of a multi-parameter, image-based high-throughput screen to identify drugs that prevent β-cell death in the context of cytotoxic cytokines, designed to mimic conditions that precipitate type 1 diabetes (135). We identified several novel anti-apoptotic drugs, including carbamazepine, a use-dependent Na^+ channel inhibitor. The confirmation of these effects with another use-dependent Na^+ channel inhibitor strongly suggests a previously unappreciated role for Na^+ channels in pancreatic β-cells. These data will support therapeutic efforts to inhibit β-cell death in diabetes.

4.2 Results

4.2.1 A high-throughput screen for discovering drugs that protect β-cells

Image-based, high-throughput screening requires a high degree of reproducibility. For our screens, we chose the MIN6 β-cell line, which we and others have shown undergoes stereotypical apoptotic programmed cell death in response to pro-inflammatory cytokines (114). Apoptosis is the mode of cell death that is most commonly assessed in the fields of islet biology and diabetes research (2, 11), and guidelines on the measurement of apoptosis consistently state that multiple parameters should be assessed in order to distinguish it from other forms of cell death (40, 41). In the current study, we employed a 4-parameter live-cell imaging approach to assess the effects of drugs on cytokine-induced β-cell apoptosis. To assess cell number, MIN6 cells were continuously cultured in a low concentration of Hoechst 33342, which we have previously shown does not have significant effects on cell survival (114). To assess phosphatidylserine translocation to the plasma membrane outer surface, an early event in the classical apoptotic cascade (121, 122), cells were cultured in a low concentration of AlexaFluor647-conjugated annexinV, which we have also shown is non-toxic (114). Caspase-3 activation was assessed using a FRET sensor we recently modified to include eBFP2 and eGFP (114). The detection of late phase cell death was monitored with propidium iodide incorporation, which enters the cell only after the irreversible compromise of the plasma membrane. The combination of these fluorescent probes provided us with 4 distinct parameters for the analysis of β-cell death (Fig. 4-1).

4.2.2 Multiple anti-apoptotic drugs identified with a high-throughput, high-content assay

We screened the Prestwick library of 1120 drugs in an effort to identify chemicals, and also molecular mechanisms, that modulate apoptotic MIN6 cell death induced by a well-established toxic cocktail of cytokines. The results were automatically analyzed into self-organizing maps using the Acuity Express software program (Fig. 4-1A). This approach groups the treatments according to similarity, taking into account the four measured cell death-associated parameters. Using this method, 19 distinct drugs showed a pattern that was similar to the ‘no cytokine’ condition, meaning these were the closest to completely blocking the apoptosis-inducing effects of the cytokines (Fig. 4-1A). A variety of chemicals, from several

classes, populated this small hit list (Table 4-1). Notably, we identified 5 vitamins, 5 antibiotics or antifungals, 6 drugs that modulate plasma membrane ion channels and/or membrane receptors, and 3 miscellaneous drugs that had significant protective effects on β-cell survival. The identification of direct anti-apoptotic effects in a β-cell model was novel for most of the drugs. For 9 of these chemicals, we were unable to find evidence that they had been linked to apoptosis in any cell type. A literature search revealed that 4 of these chemicals had previously been shown to be anti-apoptotic in another cell type, while 3 had been shown to pro-apoptotic in other systems (Table 4-1). Two of these drugs, loperamide and carbamazepine, are known to either increase or decrease apoptosis, depending on the context. The possibility that these drugs might have specific effects on β-cells was intriguing.

The use of our multi-parameter screening approach was validated when we identified mitoxantrone dihydrochloride as a drug that could completely prevent propidium iodide incorporation in the presence of toxic cytokines (Fig. 4-1B). However, this was a false 'hit'. In fact, there was a very high percentage of dying cells in the presence of this compound as evidence by the dramatic cell loss, high annexinV fluorescence and high caspase-3 activity (Fig. 4-1B-D), but this topoisomerase inhibitor had apparently prevented the propidium iodide from binding to the DNA. Had we not employed a rich multi-parameter approach in our initial screen, valuable time and resources could have been wasted following up this false positive effect.

4.2.3 Use-dependent Na^+ channel blockers protect primary mouse β-cells from apoptosis

We chose a single drug for secondary validation. Out of the 19 unique hits, we chose to focus on carbamazepine, a Na^+ channel inhibitor, for four reasons. First, we were interested by the fact that carbamazepine has been found to have both pro-apoptotic and anti-apoptotic effects in other systems. Second, ion channels are a highly druggable class of membrane proteins. Third, little was known about the role of voltage-gated Na^+ channels in programmed cell death, in β-cells or in other cell types. Fourth, Na^+ channels are not thought to play a major role in normal β-cell physiology, raising the possibility that targeting these channels might be specific to a state of β-cell stress and/or β-cell death.

With the use of voltage clamp electrophysiology in the whole cell configuration, Na^+ currents were measured in β-cells from transgenic mice expressing GFP under the control of the *Ins1* promoter (a.k.a. MIP-GFP mice)(136, 137). Indeed, many MIP-GFP β-cells in our cultures expressed Na^+ currents (137), with voltage-gated Na^+ currents most frequently measured from GFP-positive β-cells, when compared to β-cells identified simply by their larger morphology, suggesting that these currents may be more prominent in 'mature' β-cells marked by activation of the mouse *Ins1* promoter (110, 138, 139), when compared to immature β-cells or in other islet cell types. Importantly, we confirmed the molecular mechanism of carbamazepine. As expected, carbamazepine treatment resulted in the use-dependent inhibition of β-cell Na^+ channels (137). The expression of voltage-gated Na^+ channels and associated β-subunits were detected in FACS purified β-cells (Fig. 4-2). Our results were consistent with other studies indicating the expression of $Na_v1.3$ and $Na_v1.7$ in mouse islet cells (140), and further indicated that $Na_v1.7$ was predominantly expressed in β-cells (Fig. 4-2). These data collectively demonstrated that many mature β-cells express voltage-gated Na^+ currents and validate that carbamazepine can block these channels, but they do not necessarily show that the anti-apoptotic effects of carbamazepine result from the use-dependent inhibition of Na^+ channels.

The use-dependent inhibition of Na^+ currents by carbamazepine was reminiscent of the effects of lidocaine and other classic local anaesthetics/anti-convulsants. In order to test the hypothesis that use-dependent inhibition of Na^+ channels protects β-cells from cytokine-induced apoptosis, we chose to compare the effects of carbamazepine with lidocaine, which is also a use-dependent Na^+ channel blocker. We compared these effects with tetrodotoxin, a Na^+ channel blocker that is not use-dependent. Remarkably, both carbamazepine and lidocaine prevented cytokine-induced death of primary islet cells, in a dose-dependent manner (Fig. 4-3A,B). On the other hand, tetrodotoxin was not protective (Fig. 4-3C). We further tested whether these drugs might suppress programmed cell death induced by ER-stress, which has been shown to share some mechanistic similarities with cytokine-induced apoptosis (141). Interestingly, all three drugs partially protected primary islet cells from death associated with the SERCA inhibitor, thapsigargin (Fig. 4-3D-F). Studies with MIP-GFP islet cells further determined that the protection against cytokine-induced islet cell death was β-cell specific (Fig. 4-4A-C). The non-β-cell population, indicated by the lack of GFP expression, did not display

any increase in cell death following cytokine treatment (Fig. 4-4C), which is in agreement with studies indicating that the cytokine treatment specifically promote β-cell death with no increase in α-cell death (142). These data establish previously unappreciated roles for Na^+ channels in β-cell death induced by cytokines and ER-stress.

4.2.4 Carbamazepine does not affect insulin secretion

It was not clear, what if any effects carbamazepine might have on insulin section. This is important because any β-cell protecting drug should not have deleterious effects on insulin secretion. Moreover, it was important to test if carbamazepine protected β-cells by modulating insulin secretion, which can have autocrine pro-survival effects (143, 144). Mouse islet cells treated with carbamazepine in the presence of cytokines did not display significant differences in insulin levels in the media collected 70 hours following treatment compared to islets treated with cytokines alone (Fig. 4-4D). Islet perifusion studies further showed that carbamazepine does not acutely modulate insulin secretion under both basal and glucose stimulated conditions (Fig. 4-5). Thus, carbamazepine can protect β-cells from toxicity without significant effects on insulin secretion. These data also imply that the pro-survival effects were independent of autocrine insulin signalling.

4.2.5 Carbamazepine modulates cytosolic, ER, and mitochondrial Ca^{2+}

We next assessed the molecular mechanisms associated with the protective effects of carbamazepine. Na^+ channel modulation could influence intracellular Ca^{2+} levels by altering the electrical activity of β-cells (145, 146) and disruption of Ca^{2+} homeostasis can induce cell death (68). Long-term cytosolic Ca^{2+} imaging with genetically-encoded Ca^{2+} biosensors revealed the elevation of intracellular Ca^{2+} in dying cells following treatment with a cocktail of pro-inflammatory cytokines and showed that this was reduced by CBZ (Fig. 4-6A *right*). The only cells that survived when treated with cytokines alone maintained a lower level of cytosolic Ca^{2+} (Fig. 4-6A *left).* These observations are consistent with the concept that carbamazepine protects β-cells by suppressing cytokine-induced Ca^{2+} excitotoxity via the use-dependent inhibition of Na^+ channels.

We also assessed Ca^{2+} levels under the same conditions within two key organelles, the ER and mitochondria. Interestingly, we also found that CBZ treatment could prevent the

decrease in the lethal depletion level of ER Ca^{2+} induced by cytokines and delay cell death following induction of Ca^{2+} depletion (Fig. 4-6B *right*). The prolonged depletion of ER Ca^{2+} was not associated with an increase in mitochondrial Ca^{2+} suggesting that CBZ treatment may not alter the Ca^{2+} mediated crosstalk between ER and mitochondria (Fig. 4-6C *right*). Overall, these experiments demonstrate that inhibition of voltage-gated Na^+ channel activity can modulate changes in Ca^{2+} disruptions induced by cytokines.

4.2.6 Carbamazepine decreases pro-apoptotic and ER-stress signalling

Pro-inflammatory cytokines can induce apoptotic and ER-stress signalling in β-cells (147, 148). Previous studies have also shown pro-inflammatory cytokines can induce p38 MAPK activation and that TNF-α can enhance Na^+ channel activity in mouse dorsal root ganglion neurons through a p38 MAPK-dependent mechanism (149). Thus, we considered the possibility that carbamazepine acts in part by blocking the activation of Na^+ channels induced by p38 MAPK. Indeed, in islet cells treated with cytokines, we observed increase in cleaved caspase-3 and CHOP protein levels and increase in activation of the p38 MAPK and JNK pathways (Fig. 4-7A-D). Use-dependent blockage of voltage-gated Na^+ channels by CBZ and lidocaine decreased the elevation in cleaved caspae-3, CHOP, and phosphorylated JNK induced by cytokines (Fig. 4-7A,B,D). Surprisingly, CBZ and lidocaine displayed differential effects on the phosphorylation of p38 MAPK (Fig. 4-7C). The pro-survival effects of CBZ were associated with the down-regulation of pro-apoptotic and ER-stress signalling, but not with changes in BAD phosphorylation at serine-112 (Fig. 4-7E,F). Together, these experiments describe mechanisms involved in the protection of β-cells from cytokine- and ER-stress-induced apoptosis by use-dependent Na^+ channel inhibitors.

4.3 Discussion

The goal of the present study was to identify small molecule drugs that protect pancreatic β-cells from programmed cell death induced by pro-inflammatory cytokines and to uncover their mechanisms of action. Our high-throughput screen identified a number of drugs as powerful pro-survival agents, including the use-dependent Na^+ channel blocker carbamazepine. This observation prompted us to investigate the roles of Na^+ channels in β-cells and pointed to an unexpected role of Na^+ channels in β-cell death.

The physiological and pathophysiological roles of Na^+ channels in β-cells remain poorly understood. Voltage-gated Na^+ channels have been identified on β-cells from mice, rats, dogs and humans (134, 150-155). It has been shown that Na^+ channels are more active in canine and human β-cells than in rodent cells (153). Heterogeneity of Na^+ currents and Na^+ channel expression has been observed between sub-populations of β-cells (156). In our hands, the use of MIP-GFP cells permitted the recording of Na^+ channels from many more cells, perhaps suggesting an enrichment of Na^+ channels in mature β-cells. We have previously shown that β-cells with *Ins1* promoter expression (i.e. MIP-GFP cells) represent a sub-group of β-cells in a mature state (110, 138, 139). Na^+ currents have been previously reported in MIP-GFP β-cells (136).

Insulin secretion from human β-cells is modulated by blockers of voltage-dependent Na^+ channel (157). However, in general, studies with chemical inhibitors have suggested that Na^+ channels have relatively modest effects on glucose-stimulated insulin secretion (134, 150, 152, 155). Our data suggest that use-dependent blockage of Na^+ channels does not influence insulin secretion. Glucose induces cytoplasmic Na^+ oscillations in pancreatic β-cells (158). Na^+ channel activation modulates the frequency of Ca^{2+} oscillations in β-cells (159). In β-cells, increased ATP can shift the current-voltage and the voltage-dependent inactivation curves to the right (160). On the other hand, life-long, complete knockout of the major regulatory Na^+ channel β1-subunit (Scn1b, a component of $Na_v1.7$) reduces insulin secretion (161). TTX blocks insulin secretion induced by carbachol (162). Na^+ channels have also been shown to play a role in glucagon release from α-cells (163). Beyond hormone secretion, virtually nothing has been reported on roles for Na^+ channels in β-cell fate decisions. To the best of our knowledge, our study is the first to report that Na^+ channels participate in programmed cell death in β-cells, or any endocrine cell type.

The role of Na^+ channels in neuronal apoptosis has been the focus of several studies. Overall, these studies paint a complex picture. The potent Na^+ channel blocker, tetrodotoxin has been shown to protect neurons from hypoxia (164). Similarly, 4-[4-fluorophenyl]-2-methyl-6- [5-piperidinopntyloxy] pyrimidine hydrochloride, an inhibitor that blocks both Ca^{2+} and Na^+ channels, protects neurons after ischemia (165). Moreover, Na^+ channel mutations correlate with increased survival and disease severity in glioblastoma multiforme (166). On the other hand, mice lacking the *Scn2a* sub-unit gene, a component of the $Na_v1.2$ channel,

exhibit significant neuronal apoptosis (167). Neurons in culture and *in vivo* show activity-dependent survival, where inhibition of Na^+ channels leads to apoptotic cell death (168-170) and selective activation of Na^+ channels promotes survival (171). Other mutations in Na^+ channels can have pro-apoptotic effects in the heart (172, 173). Together, these studies suggest that Na^+ currents may play a deleterious role in neurons subjected to hypoxic or ischemic stresses, whereas a certain level of Na^+ channel activity in basal conditions is essential for activity-dependent survival. This is similar to the well-established dual roles for Ca^{2+} channels in cellular survival. Collectively, these data support a model whereby plasma membrane excitability must be kept within a tight range to maintain optimal survival.

Prior to our study, very little was known about the effects of carbamazepine, or other use-dependent Na^+ channel inhibitors on pancreatic β-cells. Interestingly, it was recently shown that carbamazepine can rescue trafficking defects of mutant K_{ATP} channels involved in congenital hyperinsulinism (174). Whether these effects of carbamazepine are involved in its ability to protect β-cells from apoptosis remains to be elucidated, but with the lack of changes in insulin secretion upon carbamazepine exposure, we do not favor a major role for this pathway in the effects observed in our study. In our view, it is more likely that carbamazepine and lidocaine protect β-cells via direct actions on Na^+ channels and membrane excitability, similar to what may occur in neurons. Our studies suggest that inhibition of Na^+ channels could reduce excessive membrane depolarization, thereby preventing the cytokine-stimulated influx of Ca^{2+} through voltage-gated Ca^{2+} channels. Given the lack of β-cell protection from cytokines when cells were treated with tetrodotoxin, it is likely that the use-dependent mode of Na^+ channel inactivation is crucial for promoting cell survival. The difference between the effective concentrations of the inhibitors, which would dictate the extent of Na^+ channel inactivation may also influence the survival effects. Additionally, carbamazepine treatment extended the ER Ca^{2+} depletion time prior to cell death and improved the ER Ca^{2+} depletion threshold, which could have contributed to the observed down-regulation of ER-stress signalling. Recently, carbamazepine has also been used to protect human islets form palmitate-induced cell death through the upregulation of autophagy (175). Additional mechanistic studies into the pro-survival effects of carbamazepine are warranted.

In conclusion, we report the results of an unbiased high-throughput, high-content, multi-parameter screen that identified 19 drugs capable of protecting β-cells from cytokine-induced

apoptosis. The unexpected observation that carbamazepine and lidocaine protected primary β-cells from apoptosis afforded new insight into the role of Na^+ currents in apoptosis. Although, the current study focused on the validation of use-dependent Na^+ channel inhibitors as anti-apoptotic agents, additional insights are likely to come from the pursuit of other 'hits' from our screen. The therapeutic impact for diabetes is intriguing especially since carbamazepine and many of the 'hits' are already approved for the treatment of other conditions. Undoubtedly, these studies will continue to paint a complex picture of programmed cell death in the pancreatic β-cell.

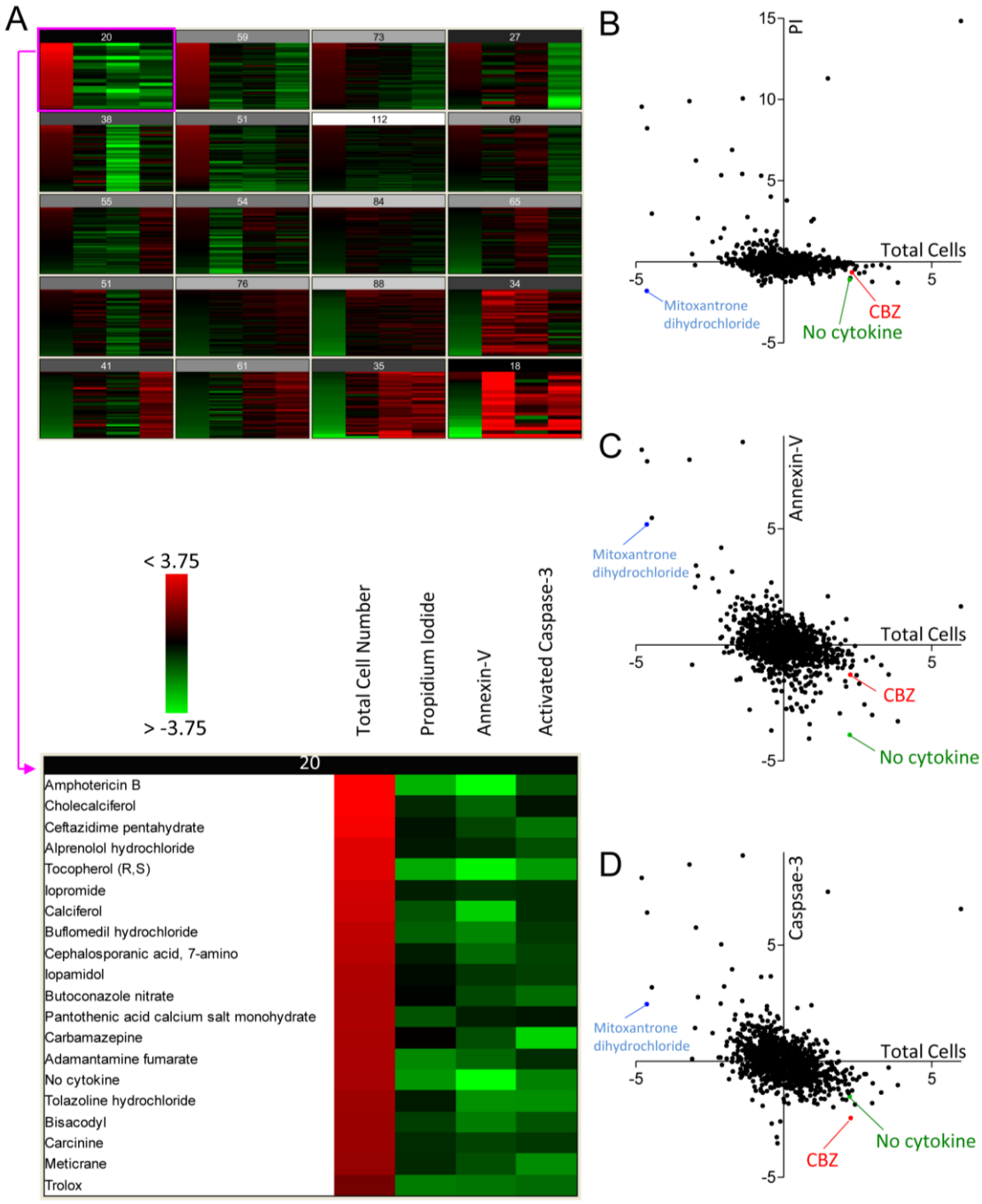

Figure 4-1. Multi-parameter, high-content screening for compounds that promote β-cell survival.
MIN6 cells stably expressing caspase-3 eBFP-devd-eGFP FRET sensor under the *Ins1* promoter were seeded into 96-well plates and stained with Hoechst 33342, propidium iodide, and AlexaFluor 647 conjugated annexin-V. Cell death was induced with a cytokine cocktail of 25 ng/mL TNF-α, 10 ng/mL IL-1β, and 10 ng/mL IFN-γ and cells were treated with 8.5 µM of each compound in the Prestwick library, which includes FDA approved drugs. Cells were imaged following 30 h of treatment with Molecular Devices ImageXpress^{MICRO} and images were analyzed using MetaXpress software. **A-D.** Z-score values calculated from number of total cells, propidium iodide (PI) positive cells, annexin-V positive cells, and activated caspase-3 positive cells were determined and displayed as a heatmap where red and green represents high and low numbers, respectively. The top hits that promoted β-cell survival were selected from automated clustering into 20 different self-organizing maps **(A)**. Scatter plots of PI **(B)**, annexin-V **(C)**, and caspase-3 **(D)** versus total cell were generated.

Table 4-1. Summary of 'hits' identified as similar to 'no cytokine' condition using self-organizing maps.

'Hit' Drug	Description	Known Effects on Apoptosis? anti- or pro-apoptotic	References
pantothenic acid	vitamin B5	anti: T-lymphocytes	(176)
calciferol	vitamin D (D2, D3)	pro: prostate cancer cells	(177)
cholecalciferol	vitamin D (D3)	unknown*	
tocopherol (R,S)	vitamin E	anti: neurons	(178, 179)
trolox	vitamin E	anti: thymocytes	(180)
amphotericin B	pore forming anti-biotic, anti-fungal	pro: cancer cells, erythrocytes, renal tubular cells	(181-185)
ceftazidime	antibiotic	pro: lympohcytes	(186)
cephalosporanic acid	antibiotic	unknown*	
butoconazole	anti-fungal	unknown*	
adamantanamine	anti-viral	unknown*	
alprenolol	non-selective β-blocker, 5-HT_{1A} antagonist	unknown*	
loperamide	μ-opioid agonist, calcium channel inhibitor	anti: neurons pro: cancer cells	(187-189)
buflomedil	vasodilator	unknown*	
tolazoline	adrenergic blocking agent, vasodilator	unknown*	
carbamazepine	Na^+ channel inhibitor, anticonvulsant	anti: neurons pro: neurons	(190-192)
carcinine	β-alanylhistamine, imidazole dipeptide	anti: photoreceptors	(193)
meticrane	diuretic	unknown*	
bisacodyl	laxative	unknown*	
iopamidol	contrast agent	unknown*	

* listed as unknown as a search for the drug name and "apoptosis" yielded no results in PubMed.

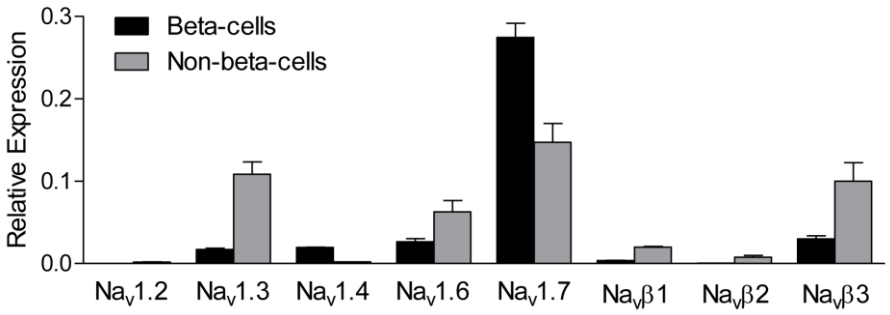

Figure 4-2. Expression of voltage-gated Na^+ channels in MIP-GFP dispersed islet cells.
Dispersed MIP-GFP islet cells were FACS sorted and the expression of voltage-gated Na^+ channels (Na_v) and beta subunits ($Na_v\beta$) were detected by quantitative RT-PCR with *Hprt1* as the reference gene ($2^{-\Delta Ct}$; n=3, mean ± SEM).

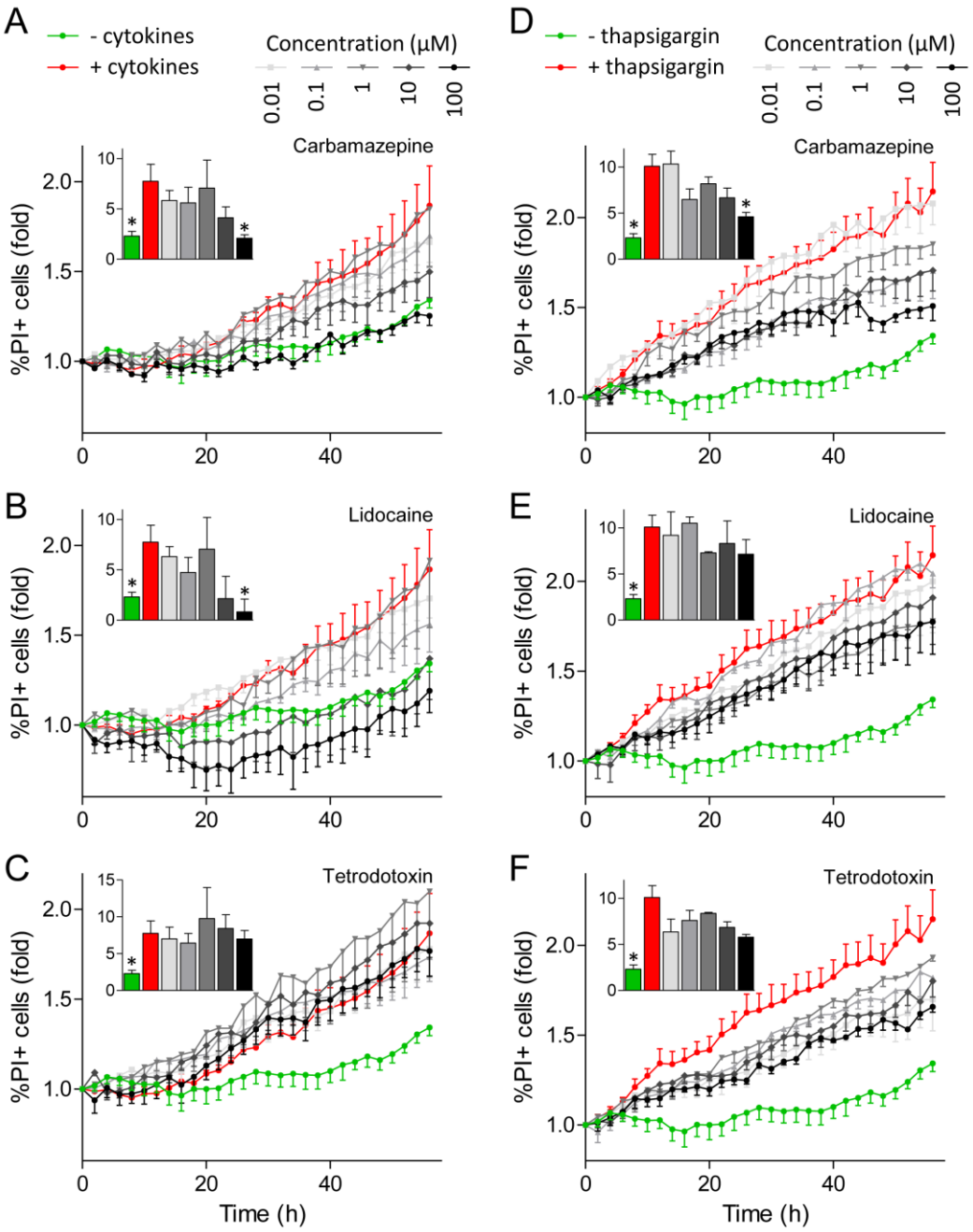

Figure 4-3. Na^+ channel inhibitors can reduce cytokine induced primary islet cell death.
Dispersed islet cells seeded into 96-well plate were stained with Hoechst and PI. Cells were treated with a cytokine cocktail (25 ng/ml TNF-α, 10 ng/ml IL-1β, and 100 ng/ml IFN-γ) **(A-C)** or 1 μM thapsigargin **(D-F)**, in combination with 0.01 to 100 μM of Na^+ channel inhibitors, carbamazepine (CBZ), lidocaine (LIDO), and tetrodotoxin (TTX). Cells were imaged with Molecular Devices ImageXpress^{MICRO} and percentage PI+ cells was calculated. *Insets*, area under the curve for the last 10 h was calculated (n=3-6, mean ± SEM, *, $p<0.05$ compared to cytokine treated cells).

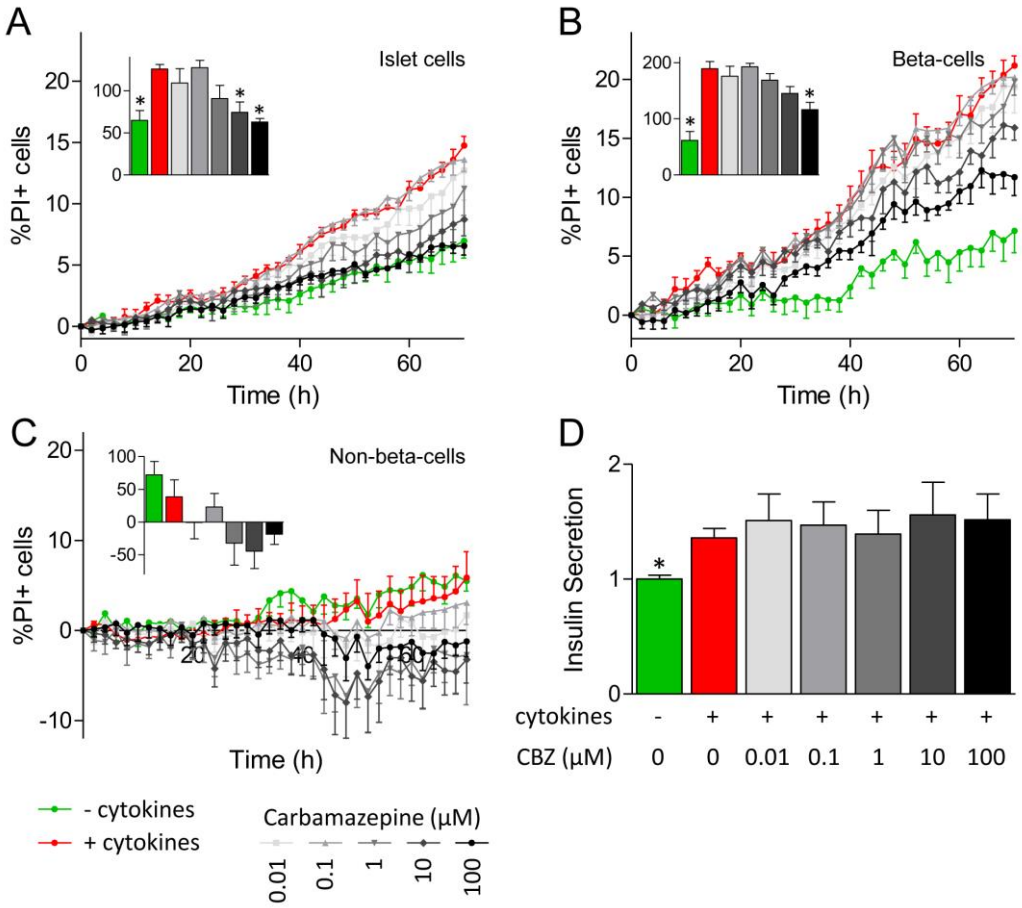

Figure 4-4. Na^+ channel inhibitors can reduce cytokine induced primary β-cell death.
A-C. Dispersed MIP-GFP islet cells seeded into 96-well plate were stained with Hoechst and PI. Cells were treated with a cytokine cocktail (25 ng/ml TNF-α, 10 ng/ml IL-1β, and 100 ng/ml IFN-γ), in combination with 0.01 to 100 μM of carbamazepine (CBZ). Cells were imaged with Molecular Devices ImageXpress^{MICRO} and percentage PI+ cells in the islet cell **(A)**, β-cell **(B)**, and non-β-cell **(C)** populations was calculated. *Insets*, area under the curve for the last 10 h was calculated (n=4-6, mean ± SEM, *, $p<0.05$ compared to cytokine treated cells). **D.** Insulin level in media collected 70 h following treatment of dispersed islet cells was measured (n=5).

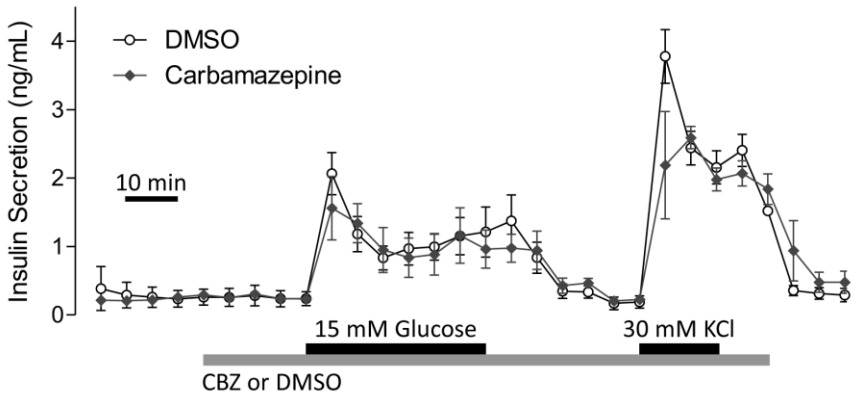

Figure 4-5. Insulin secretion is not modulated by acute carbamazepine treatment.
Mouse islets were perifused with KRB buffer containing 3 or 15 mM glucose in combination with 100 µM carbamazepine (n=3, mean ± SEM).

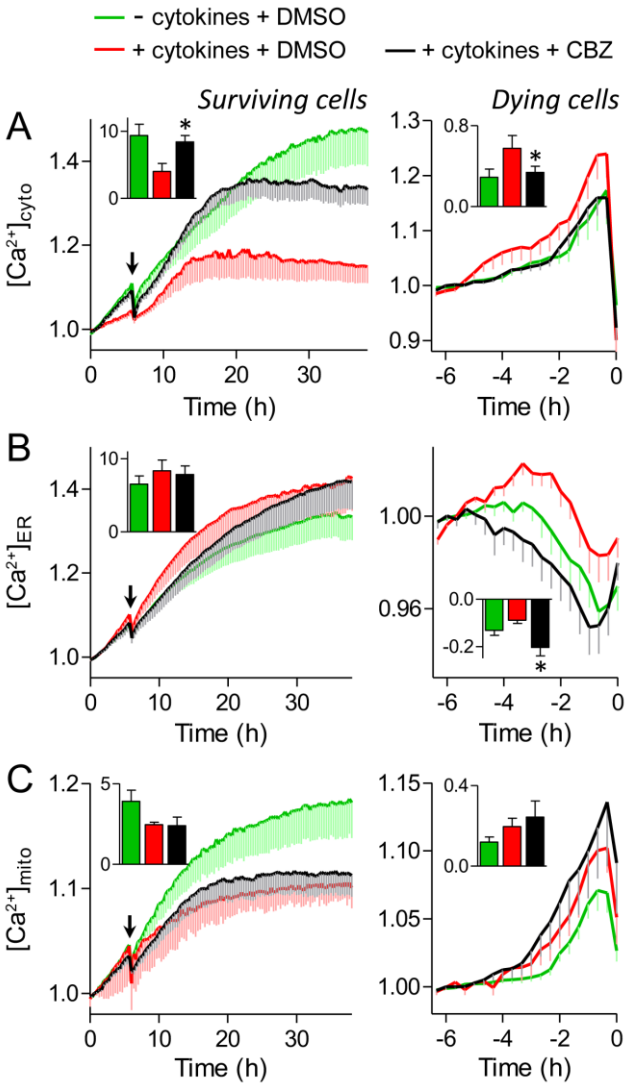

Figure 4-6. Carbamazepine modulates cytosolic, ER, and mitochondrial Ca^{2+} signalling.
Dispersed mouse islet cells were transfected with D3cpv **(A)**, D1ER **(B)**, or 4mtD3cpv **(C)** genetically-encoded Ca^{2+} biosensors to image cytosolic, ER, or mitochondrial Ca^{2+}, respectively. Cells were incubated in 20 mM glucose, serum-free RPMI medium prior to the treatments with cytokines (red), cytokines and 100 µM carbamazepine (black), or no cytokines (green) at the indicated time (arrow). *Left panel:* Ca^{2+} levels of cells that remained alive during the 38 h of imaging. Inset, area under the curve from the time of treatment to the end of the time course (n=6-28 cells, * $p<0.05$ compared to cytokine treated). *Right panel:* Ca^{2+} levels of cells that died during the 38 h of imaging. The FRET/CFP ratios were normalized to the average reading from 5-6 h prior to PI incorporation (0 h). Inset, area under the curve from the time of Ca^{2+} influx or depletion to the time of PI incorporation (n=11-26 cells, * $p<0.05$ compared to cytokine treated).

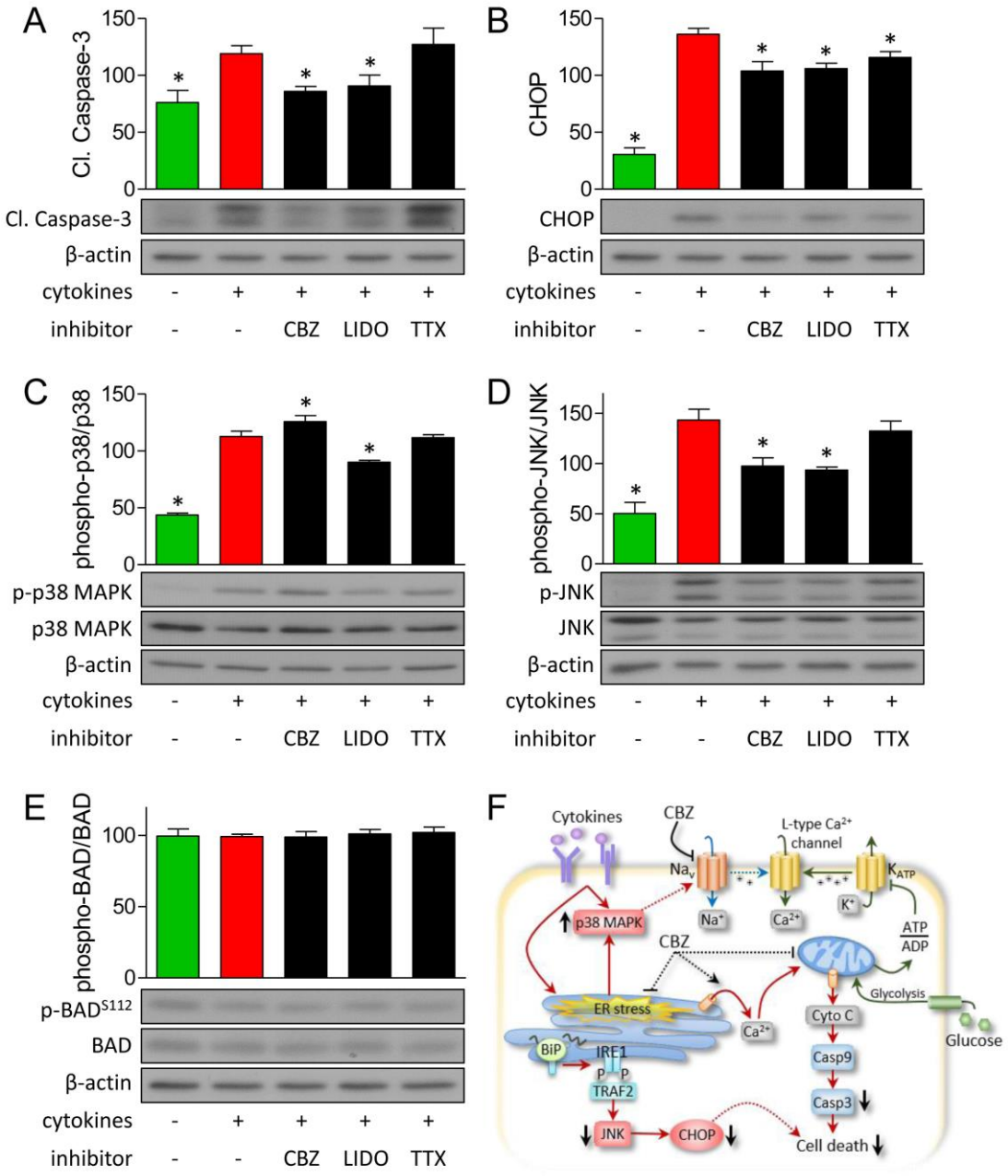

Figure 4-7. Carbamazepine down-regulates cytokine induced pro-apoptotic and ER-stress signalling. **A-E.** Mouse islet cells were treated with 100 µM carbamazepine, lidocaine, or tetrodotoxin under 20 mM glucose serum free condition for 24 h. Immunoblotting of cleaved caspase-3, CHOP, phosphorylated and total p38 MAPK, JNK, and BAD (n=4-6, * $p<0.05$ compared to cytokine treated). **F.** Model of effects of carbamazepine on cell death signalling in β-cells.

Chapter 5: Intra-islet signalling loops in adult pancreatic islets

5.1 Introduction

Pancreatic islets are micro-organs that contain mainly insulin-secreting β-cells, as well as glucagon-secreting α-cells, and somatostatin-secreting δ-cells. Rare cell types are also found, including multi-hormonal cells (194). The loss of functional β-cell mass results in diabetes, and thus factors that could increase β-cell growth, survival or function are urgently needed. In recent years, candidate gene studies have demonstrated that islets express and secrete factors in addition to the classical hormones, including multiple cytokines, neuropeptides, and growth factors (195, 196). In parallel, targeted studies have revealed growth factors that promote islet cell survival when over-expressed or added exogenously. For example, we and others have demonstrated potent anti-apoptotic and proliferative roles of insulin and IGF-1 (38, 144, 197). Increasing the production of islet GLP-1 is also protective (104). A novel isoform of the anti-apoptotic hormone GIP is also produced in islets (198, 199). Activation of the JAK-STAT signalling pathway with growth hormone, prolactin or placental lactogens can promote β-cell survival (200, 201). Similarly, over-expression of classical growth factors such as hepatocyte growth factor and fibroblast growth factor have been shown to exert positive effects on islets (98, 99), as has parathyroid hormone-related protein (202). Activation of the ErbB receptor pathway with betacellulin has been shown to protect β-cells and increase β-cell proliferation in a number of systems (203). Emerging evidence suggests important roles for locally produced members of the TGFβ family, such as activin, follistatin and bone morphogenic proteins (204, 205).

These studies demonstrate that islet survival can be modulated by soluble factors, although in many cases it is not yet clear whether administration of these factors at doses that can be tolerated clinically will increase β-cell mass. Endogenous autocrine/paracrine signalling factors could be ideal starting points for diabetes therapies, as they can display local action and self-limiting feedback. Insulin is a potent, self-limiting islet survival factor (144) and a useful tool for *in vitro* preservation of functional islet mass, but the risk of hypoglycaemia negates the utility of insulin therapy for preventing the loss of β-cell mass *in vivo*. Other candidate local islet survival pathways have been investigated, including pituitary adenylyl cyclase activating polypeptide (206), nerve growth factor (207), and Notch (37). Nonetheless, our knowledge of

the endogenous regulators of adult β-cell survival and proliferation remains insufficient. It is likely that many islet secreted factors and receptors remain to be uncovered using unbiased approaches. In the present study, we compiled a list of 233 secreted factors and 234 receptors that are expressed in mouse or human islets using gene expression databases, including those derived from FACS purified human and mouse β-cells. Together, our genome-level findings point to a large number of potentially important local paracrine growth factor loops in pancreatic islets.

5.2 Results

5.2.1 Database mining for islet secreted factors and their receptors

We used bioinformatics and genomics to search for secreted factors and their receptors employing up to ten independent lines of evidence for each gene. A list of 233 secreted factors and 234 receptors expressed in mouse or human islets was compiled from SAGE and Tag-Seq libraries, microarrays of FACS-purified human β-cells, and online databases (Fig. 5-1, 5-2). Secreted factors could be classified into four categories: axon guidance factors, growth factors, hormones, and cytokines. As expected, insulin, glucagon, somatostatin, and IAPP were ranked amongst the top 8 most abundantly expressed genes in islets. Some of the other highly expressed secreted factors were unexpected. In particular, islets and β-cells express very high levels of macrophage migration inhibitory factor. The analysis of receptors across multiple databases was also highly informative. A receptor for adiponectin was the top ranked gene. Commonly studied receptors, such as those for IGF1, glucagon and GLP-1 were abundant (i.e. found in the top third of expressed receptor genes; Fig. 5-2), but not in the top ten.

5.2.2 Potential intra-islet growth factor signalling loops

A total of 190 autocrine/paracrine signalling pairs, consisting of both the secreted factor and its known receptor, were identified in islets (Fig. 5-3A). We and others have investigated the roles of TGFβ family members in islet function, including the reciprocal effects of local activin and follistatin on β-cell maturation (204). We have also examined notch signalling (37). The Wnt-Fzd system has been under intense study since the implication of TFC7L2 in type 2 diabetes. Follow-up of each gene family was beyond the scope of the present study.

5.3 Discussion

The identification of factors that protect islets and increase functional β-cell mass is a major research goal. Here, we employed an unbiased approach to catalogue 233 secreted factors and 234 receptors found in islets, many of them previously unappreciated. Our results also confirmed the expression of several previously investigated candidate islet survival factors, such as HGF and its receptor c-met (99, 208, 209). Urocortin 3 and nerve growth factor, along with their receptors, are other examples of autocrine islet survival factors (207, 210). In summary, we determined that a large number of paracrine signalling loops are present in adult human and rodent islets. Examination of these genes is likely to reveal many more factors that influence islet survival and growth, both positively and negatively.

Color Code												
Tag-Seq (tpm)	nd	0	1	2	3	4	5	6	7	8	9	≥10
FACS purified cells & purified islets microarray (relative)	nd	0	1 - 100	101 - 200	201 - 300	301 - 400	401 - 500	501 - 600	601 - 700	701 - 800	801 - 900	≥901
T1DBase (relative) MPSS (TPM)	nd	0	1 - 10	11 - 20	21 - 30	31 - 40	41 - 50	51 - 60	61 - 70	71 - 80	81 - 90	≥91

Gene Symbol	Gene Name
INS (Ins2)	insulin
IAPP	islet amyloid polypeptide
GCG	glucagon
SCG5	secretogranin V (7B2 protein)
SCG2	secretogranin II (chromogranin C)
CHGB	chromogranin B (secretogranin 1)
CHGA	chromogranin A (parathyroid secretory protein 1)
SST	somatostatin
MIF	macrophage migration inhibitory factor
VEGFA	vascular endothelial growth factor A
GPI	glucose phosphate isomerase, autocrine motility factor
HDGF	hepatoma-derived growth factor
GRN	granulin
IK	IK cytokine, down-regulator of HLA II
SDF2	stromal cell-derived factor 2
OLFM1	olfactomedin 1
WNT4	wingless-type MMTV integration site family, member 4
PPY	pancreatic polypeptide
REG1A	regenerating islet-derived 1 alpha
NPY	neuropeptide Y
SCG3	secretogranin III
DLK1	delta-like 1 homolog (Drosophila)
SEMA4B	sema domain, (semaphorin) 4B
BMP1	bone morphogenetic protein 1
MDK	midkine (neurite growth-promoting factor 2)
ANGPTL2	angiopoietin-like 2
IL18	interleukin 18 (interferon-gamma-inducing factor)
ADM	adrenomedullin
NENF	neuron derived neurotrophic factor
CXCL12	chemokine (C-X-C motif) ligand 12
TFF3	trefoil factor 3 (intestinal)
CD55	CD55 molecule, decay accelerating factor for complement
JAG2	jagged 2
STC2	stanniocalcin 2
OLFM4	olfactomedin 4
CXCL10	chemokine (C-X-C motif) ligand 10
SEMA4F	sema domain, (semaphorin) 4F
SDF4	stromal cell derived factor 4
CCL5	chemokine (C-C motif) ligand 5
FRZB	frizzled-related protein
FSTL3	follistatin-like 3 (secreted glycoprotein)
IGF2	insulin-like growth factor 2 (somatomedin A)
FSTL1	follistatin-like 1
PYY	peptide YY
LTB	lymphotoxin beta (TNF superfamily, member 3)
GDF15	growth differentiation factor 15
NELF	nasal embryonic LHRH factor
EGF	epidermal growth factor (beta-urogastrone)
TGFB1I1	transforming growth factor beta 1 induced transcript 1
PDGFA	platelet-derived growth factor alpha polypeptide
VEGFB	vascular endothelial growth factor B
CXCL2	chemokine (C-X-C motif) ligand 2
DMKN	dermokine
SEMA5A	sema domain, (semaphorin) 5A
OLFML2B	olfactomedin-like 2B
VEGFC	vascular endothelial growth factor C
STC1	stanniocalcin 1

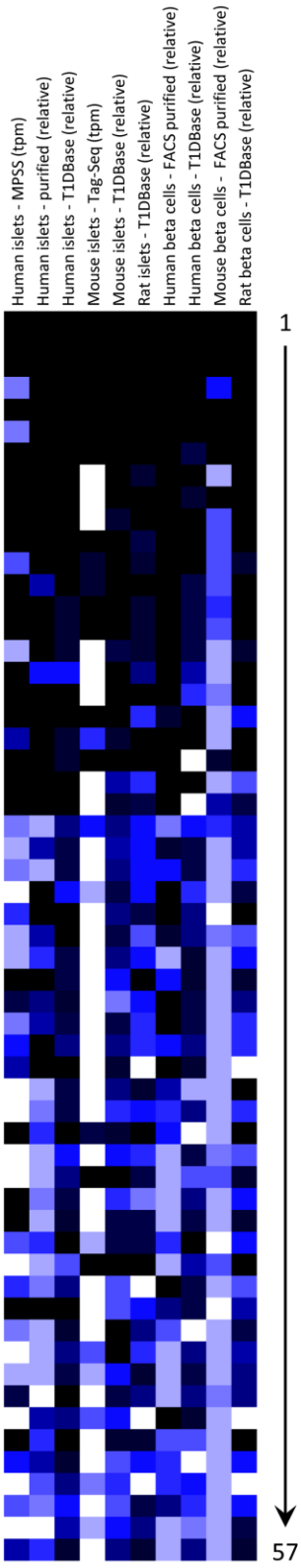

Color Code												
Tag-Seq (tpm)	nd	0	1	2	3	4	5	6	7	8	9	≥10
FACS purified cells & purified islets microarray (relative)	nd	0	1 - 100	101 - 200	201 - 300	301 - 400	401 - 500	501 - 600	601 - 700	701 - 800	801 - 900	≥901
T1DBase (relative) MPSS (TPM)	nd	0	1 - 10	11 - 20	21 - 30	31 - 40	41 - 50	51 - 60	61 - 70	71 - 80	81 - 90	≥91

Gene Symbol	Gene Name
ANGPTL6	angiopoietin-like 6
EFNB3	ephrin-B3
LIF	leukemia inhibitory factor
NPFF	neuropeptide FF-amide peptide precursor
CXCL11	chemokine (C-X-C motif) ligand 11
NGF	nerve growth factor (beta polypeptide)
EFNA1	ephrin-A1
CARTPT	CART prepropeptide
SEMA6A	sema domain, (semaphorin) 6A
INS1	insulin I
REG1B	regenerating islet-derived 1 beta
ANGPT1	angiopoietin 1
SDF2L1	stromal cell-derived factor 2-like 1
REG3A	regenerating islet-derived 3 alpha
SEMA3F	sema domain, (semaphorin) 3F
SLIT1	slit homolog 1 (Drosophila)
EDN3	endothelin 3
SEMA4D	sema domain, (semaphorin) 4D
CXCL1	chemokine (C-X-C motif) ligand 1
POMC	proopiomelanocortin
PBEF1	pre-B-cell colony enhancing factor 1
FAM3B	family with sequence similarity 3, member B
CCL20	chemokine (C-C motif) ligand 20
TGFBI	transforming growth factor, beta-induced, 68kDa
IL7	interleukin 7
SEMA4G	sema domain, (semaphorin) 4G
SEMA4A	sema domain, (semaphorin) 4A
SEMA3E	sema domain, (semaphorin) 3E
CCL2	chemokine (C-C motif) ligand 2
CRLF3	cytokine receptor-like factor 3
EFNB1	ephrin-B1
TGFA	transforming growth factor, alpha
CCL7	chemokine (C-C motif) ligand 7
CXCL16	chemokine (C-X-C motif) ligand 16
SEMA3B	sema domain, (semaphorin) 3B
UCN	urocortin
BMP5	bone morphogenetic protein 5
NTNG1	netrin G1
EFNA5	ephrin-A5
FGF1	fibroblast growth factor 1 (acidic)
SEMA6D	sema domain, (semaphorin) 6D
ANGPT2	angiopoietin 2
CCL4	chemokine (C-C motif) ligand 4
TNFSF4	tumor necrosis factor (ligand) superfamily, member 4
CKLF	chemokine-like factor
TNFSF10	tumor necrosis factor (ligand) superfamily, member 10
INHA	inhibin, alpha
WNT7A	wingless-type MMTV integration site family, member 7A
HDGF2	hepatoma-derived growth factor-related protein 2
VIP	vasoactive intestinal peptide
CCL11	chemokine (C-C motif) ligand 11
WNT2B	wingless-type MMTV integration site family, member 2B
SAA1	serum amyloid A1
CX3CL1	chemokine (C-X3-C motif) ligand 1
EFNA4	ephrin-A4
WNT5A	wingless-type MMTV integration site family, member 5A
EFNB2	ephrin-B2

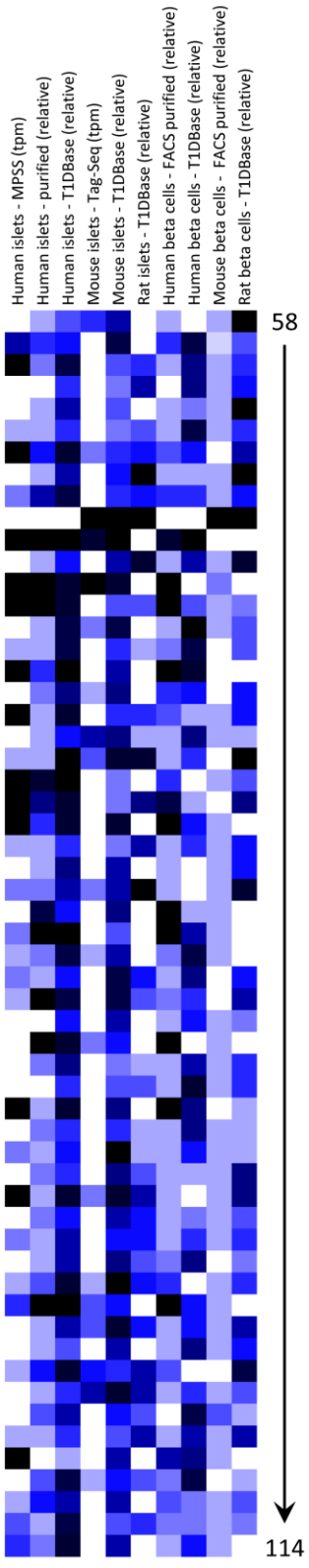

Color Code												
Tag-Seq (tpm)	nd	0	1	2	3	4	5	6	7	8	9	≥10
FACS purified cells & purified islets microarray (relative)	nd	0	1 - 100	101 - 200	201 - 300	301 - 400	401 - 500	501 - 600	601 - 700	701 - 800	801 - 900	≥901
T1DBase (relative) MPSS (TPM)	nd	0	1 - 10	11 - 20	21 - 30	31 - 40	41 - 50	51 - 60	61 - 70	71 - 80	81 - 90	≥91

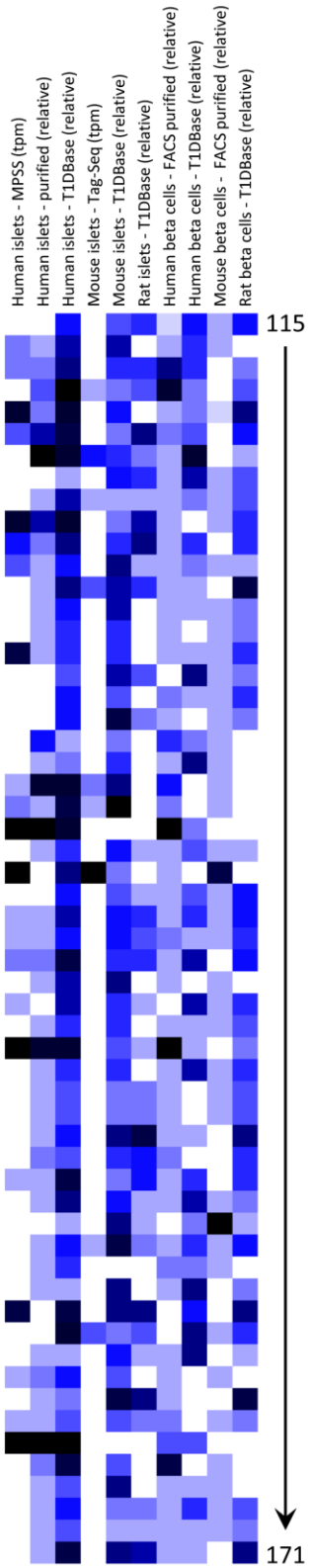

Gene Symbol	Gene Name
BMP6	bone morphogenetic protein 6
CCL27	chemokine (C-C motif) ligand 27
CALCB	calcitonin-related polypeptide beta
AGT	angiotensinogen
NMB	neuromedin B
BMP2	bone morphogenetic protein 2
CRH	corticotropin releasing hormone
BMP4	bone morphogenetic protein 4
GAST	gastrin
GHRL	ghrelin/obestatin preprohormone
CRLF1	cytokine receptor-like factor 1
BGLAP	bone gamma-carboxyglutamate (gla) protein (osteocalcin)
FGF9	fibroblast growth factor 9 (glia-activating factor)
TNFSF9	tumor necrosis factor (ligand) superfamily, member 9
WNT16	wingless-type MMTV integration site family, member 16
FSTL4	follistatin-like 4
PNOC	prepronociceptin
SAA4	serum amyloid A4, constitutive
DLK2	delta-like 2 homolog (Drosophila)
TNFSF14	tumor necrosis factor (ligand) superfamily, member 14
CCL25	chemokine (C-C motif) ligand 25
SAAL1	serum amyloid A-like 1
DNER	delta/notch-like EGF repeat containing
IL8	interleukin 8
SEMA3A	sema domain, (semaphorin) 3A
UCN3	urocortin 3 (stresscopin)
HGF	hepatocyte growth factor (hepapoietin A; scatter factor)
FGF13	fibroblast growth factor 13
FGF12	fibroblast growth factor 12
TGFB3	transforming growth factor, beta 3
WNT7B	wingless-type MMTV integration site family, member 7B
GDF11	growth differentiation factor 11
CCL19	chemokine (C-C motif) ligand 19
CXCL6	chemokine (C-X-C motif) ligand 6
WNT2	wingless-type MMTV integration site family member 2
FGF17	fibroblast growth factor 17
FGF21	fibroblast growth factor 21
PENK	proenkephalin
NTN1	netrin 1
FGF2	fibroblast growth factor 2 (basic)
SLIT2	slit homolog 2 (Drosophila)
PDYN	prodynorphin
TAC1	tachykinin, precursor 1 (neurokinin 1)
CALCA	calcitonin-related polypeptide alpha
WNT11	wingless-type MMTV integration site family, member 11
CXCL3	chemokine (C-X-C motif) ligand 3
PGF	placental growth factor
FGF3	fibroblast growth factor 3
ADM2	adrenomedullin 2
CRLF2	cytokine receptor-like factor 2
WNT5B	wingless-type MMTV integration site family, member 5B
IL32	interleukin 32
FSTL5	follistatin-like 5
OSM	oncostatin M
PRL	prolactin
FGF5	fibroblast growth factor 5
TGFB2	transforming growth factor, beta 2

Color Code												
Tag-Seq (tpm)	nd	0	1	2	3	4	5	6	7	8	9	≥10
FACS purified cells & purified islets microarray (relative)	nd	0	1 - 100	101 - 200	201 - 300	301 - 400	401 - 500	501 - 600	601 - 700	701 - 800	801 - 900	≥901
T1DBase (relative) MPSS (TPM)	nd	0	1 - 10	11 - 20	21 - 30	31 - 40	41 - 50	51 - 60	61 - 70	71 - 80	81 - 90	≥91

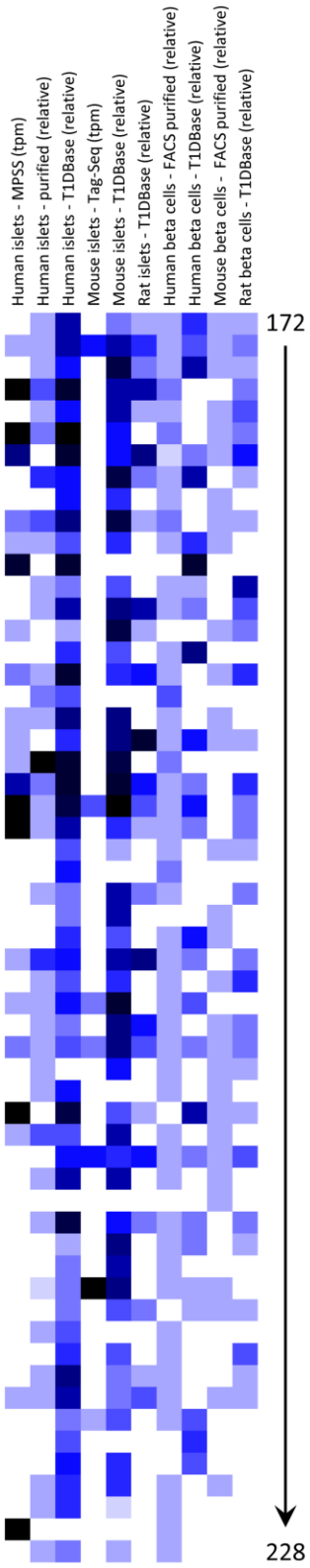

Gene Symbol	Gene Name
FGF18	fibroblast growth factor 18
BTC	betacellulin
IGF1	insulin-like growth factor 1 (somatomedin C)
ANGPTL4	angiopoietin-like 4
BMP15	bone morphogenetic protein 15
CFC1	cripto, FRL-1, cryptic family
INHBA	inhibin, beta A
GRP	gastrin-releasing peptide
NTNG2	netrin G2
DLL1	delta-like 1 (Drosophila
FLT3LG	fms-related tyrosine kinase 3 ligand
REGL	regenerating islet-derived-like
WNT1	wingless-type MMTV integration site family, member 1
INHBB	inhibin, beta B (activin AB beta polypeptide)
OLFM3	olfactomedin 3
WNT10B	wingless-type MMTV integration site family, member 10B
FGF14	fibroblast growth factor 14
TNFSF15	tumor necrosis factor (ligand) superfamily, member 15
TNFSF13B	tumor necrosis factor (ligand) superfamily, member 13b
PF4	platelet factor 4 (chemokine (C-X-C motif) ligand 4)
NTN4	netrin 4
TFF1	trefoil factor 1
TFF2	trefoil factor 2 (spasmolytic protein 1)
IL11	interleukin 11
ANGPTL3	angiopoietin-like 3
SAA2	serum amyloid A2
FGF23	fibroblast growth factor 23
WNT9B	wingless-type MMTV integration site family, member 9B
BMP10	bone morphogenetic protein 10
IL33	interleukin 33
ANGPT4	angiopoietin 4
SEMA3C	sema domain, (semaphorin) 3C
CXCL14	chemokine (C-X-C motif) ligand 14
PTHLH	parathyroid hormone-like hormone
WNT3A	wingless-type MMTV integration site family, member 3A
CCL26	chemokine (C-C motif) ligand 26
TGFB1	transforming growth factor, beta 1
NRG4	neuregulin 4
BMP7	bone morphogenetic protein 7 (osteogenic protein 1)
SEMA5B	sema domain, (semaphorin) 5B
Bglap2	bone gamma-carboxyglutamate protein 2
FGF7	fibroblast growth factor 7 (keratinocyte growth factor)
WNT8B	wingless-type MMTV integration site family, member 8B
WNT9A	wingless-type MMTV integration site family, member 9A
ANGPTL7	angiopoietin-like 7
CCL17	chemokine (C-C motif) ligand 17
PYY2	peptide YY, 2 (seminalplasmin)
WNT10A	wingless-type MMTV integration site family, member 10A
Tac2	tachykinin 3 (neuromedin K, neurokinin beta)
FGF11	fibroblast growth factor 11
NTN3	netrin 3
CCL16	chemokine (C-C motif) ligand 16
IHH	Indian hedgehog homolog (Drosophila)
WNT8A	wingless-type MMTV integration site family, member 8A
WNT3	wingless-type MMTV integration site family, member 3
INS-IGF2	insulin- insulin-like growth factor 2
IL25	interleukin 25

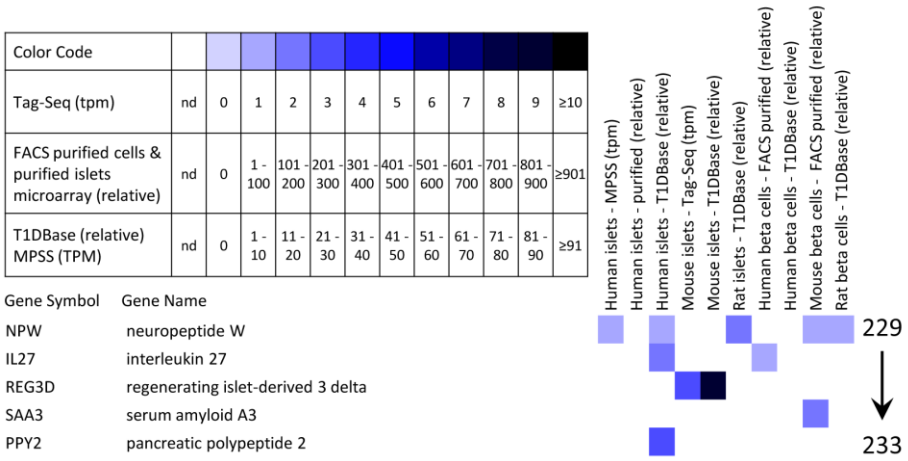

Figure 5-1. Identification of islet secreted factors.
Secreted factors expressed in human, mouse, and/or rat islets were extracted from 10 independent sources and ranked according to expression level. Expression levels for T1DBase (relative expression), FACS purified β-cells and purified islets microarray (relative expression), MPSS (tmp = transcripts per million), and Tag-Seq library (tpm = tags per million) are displayed by color (see look-up table; nd, data not determined).

Color Code												
Tag-Seq (tpm)	nd	0	1	2	3	4	5	6	7	8	9	≥10
FACS purified cells & purified islets microarray (relative)	nd	0	1 - 100	101 - 200	201 - 300	301 - 400	401 - 500	501 - 600	601 - 700	701 - 800	801 - 900	≥901
T1DBase (relative) MPSS (TPM)	nd	0	1 - 10	11 - 20	21 - 30	31 - 40	41 - 50	51 - 60	61 - 70	71 - 80	81 - 90	≥91

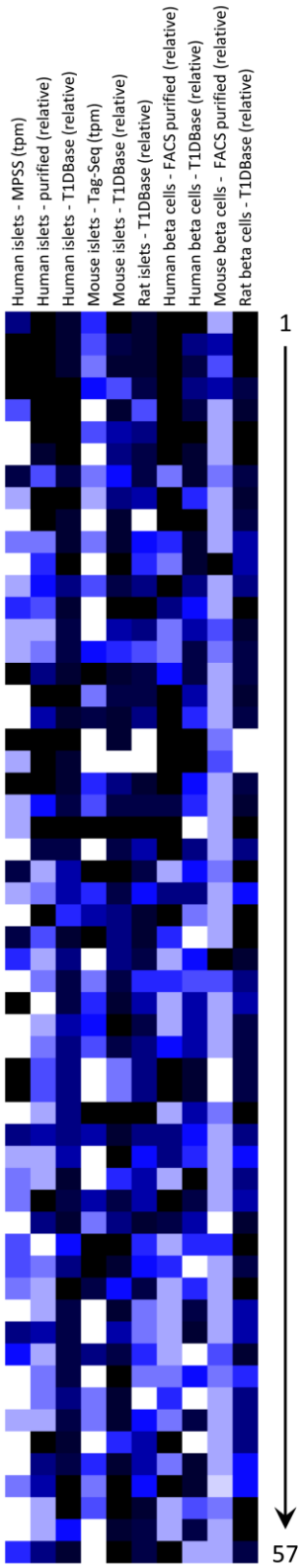

Gene Symbol	Gene Name
ADIPOR2	adiponectin receptor 2
IGF2R	insulin-like growth factor 2 receptor
TNFRSF1A	tumor necrosis factor receptor superfamily, member 1A
IFNGR2	interferon gamma receptor 2
ACVR1	activin A receptor, type I
GPR56	G protein-coupled receptor 56
PLXNB2	plexin B2
OGFR	opioid growth factor receptor
TNFRSF21	tumor necrosis factor receptor superfamily, member 21
IL10RB	interleukin 10 receptor, beta
PLXNA2	plexin A2
IL1R1	interleukin 1 receptor, type I
IGSF1	immunoglobulin superfamily, member 1
NEO1	neogenin homolog 1 (chicken)
IL17RA	interleukin 17 receptor A
OPRS1	opioid receptor, sigma 1
BAMBI	BMP and activin membrane-bound inhibitor homolog
IFNGR1	interferon gamma receptor 1
BMPR1A	bone morphogenetic protein receptor, type IA
ACVR1B	activin A receptor, type IB
TNFRSF10B	tumor necrosis factor receptor superfamily, member 10b
IL13RA1	interleukin 13 receptor, alpha 1
CRCP	calcitonin gene-related peptide-receptor component protein
ADIPOR1	adiponectin receptor 1
SSTR2	somatostatin receptor 2
GHR	growth hormone receptor
NPR2	natriuretic peptide receptor B
CSF2RA	colony stimulating factor 2 receptor, alpha, low-affinity
GPR108	G protein-coupled receptor 108
GLP1R	glucagon-like peptide 1 receptor
ROBO1	roundabout, axon guidance receptor, homolog 1 (Drosophila)
NRXN1	neurexin 1
RET	ret proto-oncogene
GPR19	G protein-coupled receptor 19
TNFRSF14	tumor necrosis factor receptor superfamily, member 14
TNFRSF14	tumor necrosis factor receptor superfamily, member 14
PRLR	prolactin receptor
PDGFRL	platelet-derived growth factor receptor-like
CSF1R	colony stimulating factor 1 receptor
FGFR1	fibroblast growth factor receptor 1
PLXNB1	plexin B1
LTBR	lymphotoxin beta receptor (TNFR superfamily, member 3)
NTRK2	neurotrophic tyrosine kinase, receptor, type 2
GPR180	G protein-coupled receptor 180
IGF1R	insulin-like growth factor 1 receptor
GPR107	G protein-coupled receptor 107
FGFR3	fibroblast growth factor receptor 3
ROBO2	roundabout, axon guidance receptor, homolog 2 (Drosophila)
PTCH1	patched homolog 1 (Drosophila)
FZD3	frizzled homolog 3 (Drosophila)
LPHN1	latrophilin 1
GPRC5C	G protein-coupled receptor, family C, group 5, member C
GPR116	G protein-coupled receptor 116
TGFBR3	transforming growth factor, beta receptor III
TGFBR1	transforming growth factor, beta receptor I
CCKAR	cholecystokinin A receptor
BMPR2	bone morphogenetic protein receptor, type II

Color Code												
Tag-Seq (tpm)	nd	0	1	2	3	4	5	6	7	8	9	≥10
FACS purified cells & purified islets microarray (relative)	nd	0	1 - 100	101 - 200	201 - 300	301 - 400	401 - 500	501 - 600	601 - 700	701 - 800	801 - 900	≥901
T1DBase (relative) MPSS (TPM)	nd	0	1 - 10	11 - 20	21 - 30	31 - 40	41 - 50	51 - 60	61 - 70	71 - 80	81 - 90	≥91

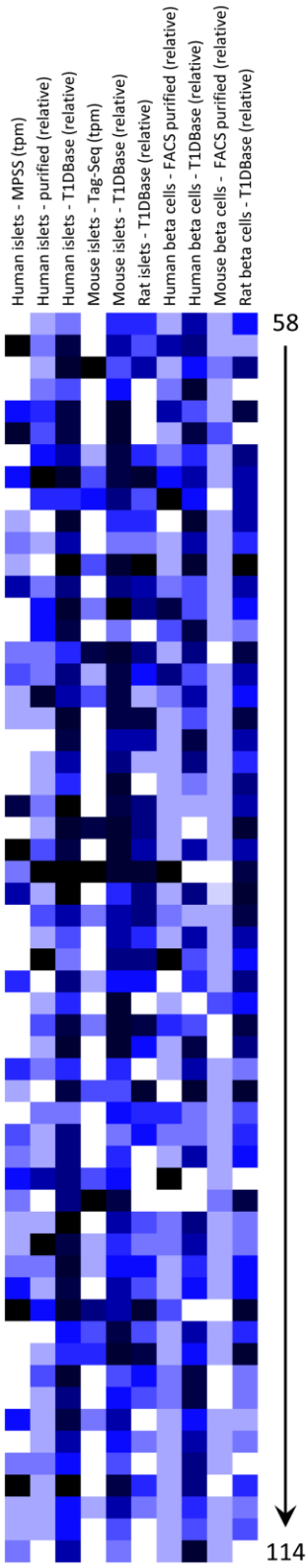

Gene Symbol	Gene Name
CXCR5	chemokine (C-X-C motif) receptor 5
SCTR	secretin receptor
IL6R	interleukin 6 receptor
ROR2	receptor tyrosine kinase-like orphan receptor 2
GPR137B	G protein-coupled receptor 137B
AMFR	autocrine motility factor receptor
FZD7	frizzled homolog 7 (Drosophila)
TGFBR2	transforming growth factor, beta receptor II (70/80kDa)
GCGR	glucagon receptor
PLXND1	plexin D1
IL10RA	interleukin 10 receptor, alpha
IL6ST	interleukin 6 signal transducer (gp130, oncostatin M receptor)
GPRC5A	G protein-coupled receptor, family C, group 5, member A
NRP1	neuropilin 1
GPR64	G protein-coupled receptor 64
RAMP2	receptor (G protein-coupled) activity modifying protein 2
PLXNA3	plexin A3
VIPR1	vasoactive intestinal peptide receptor 1
EGFR	epidermal growth factor receptor
FGFR2	fibroblast growth factor receptor 2
GPER	G protein-coupled estrogen receptor 1
UNC5C	unc-5 homolog C (C. elegans)
NOTCH2	Notch homolog 2 (Drosophila)
GPR89B	G protein-coupled receptor 89B
NOTCH3	Notch homolog 3 (Drosophila)
GPR177	G protein-coupled receptor 177
GPRC5B	G protein-coupled receptor, family C, group 5, member B
TNFRSF11B	tumor necrosis factor receptor superfamily, member 11b
NRXN2	neurexin 2
CCR6	chemokine (C-C motif) receptor 6
ACVR2B	activin A receptor, type IIB
FFAR2	free fatty acid receptor 2
ACVR2A	activin A receptor, type IIA
UNC5B	unc-5 homolog B (C. elegans)
FZD5	frizzled homolog 5 (Drosophila)
GIPR	gastric inhibitory polypeptide receptor
GPR162	G protein-coupled receptor 162
RARA	retinoic acid receptor, alpha
EPHB2	EPH receptor B2
GPR137	G protein-coupled receptor 137
GPR158	G protein-coupled receptor 158
LEPR	leptin receptor
IL4R	interleukin 4 receptor
RAMP1	receptor (G protein-coupled) activity modifying protein 1
BDKRB2	bradykinin receptor B2
TNFRSF12A	tumor necrosis factor receptor superfamily, member 12A
TBXA2R	thromboxane A2 receptor
SSTR3	somatostatin receptor 3
PDGFRA	platelet-derived growth factor receptor, alpha polypeptide
CCKBR	cholecystokinin B receptor
IL15RA	interleukin 15 receptor, alpha
NTRK3	neurotrophic tyrosine kinase, receptor, type 3
IL27RA	interleukin 27 receptor, alpha
ERBB3	v-erb-b2 erythroblastic leukemia viral oncogene homolog 3
SMO	smoothened homolog (Drosophila)
EPHB3	EPH receptor B3
GPR35	G protein-coupled receptor 35

Color Code												
Tag-Seq (tpm)	nd	0	1	2	3	4	5	6	7	8	9	≥10
FACS purified cells & purified islets microarray (relative)	nd	0	1 - 100	101 - 200	201 - 300	301 - 400	401 - 500	501 - 600	601 - 700	701 - 800	801 - 900	≥901
T1DBase (relative) MPSS (TPM)	nd	0	1 - 10	11 - 20	21 - 30	31 - 40	41 - 50	51 - 60	61 - 70	71 - 80	81 - 90	≥91

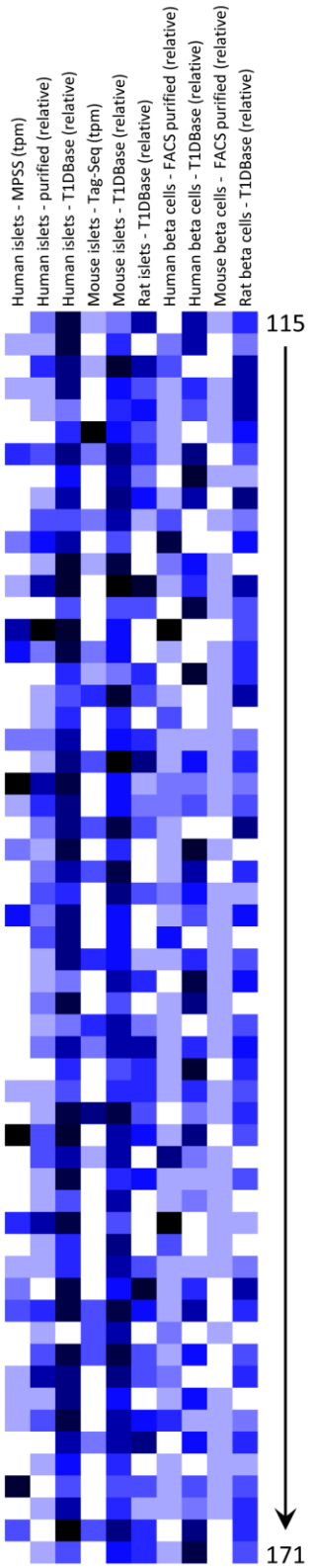

Gene Symbol	Gene Name
EDNRA	endothelin receptor type A
GPR68	G protein-coupled receptor 68
NOTCH1	Notch homolog 1, translocation-associated (Drosophila)
NRP2	neuropilin 2
AMHR2	anti-Mullerian hormone receptor, type II
INSRR	insulin receptor-related receptor
CD97	CD97 molecule
TNFRSF1B	tumor necrosis factor receptor superfamily, member 1B
FGFR4	fibroblast growth factor receptor 4
UNC5A	unc-5 homolog A (C. elegans)
RHBDF2	rhomboid 5 homolog 2 (Drosophila)
FZD6	frizzled homolog 6 (Drosophila)
EDNRB	endothelin receptor type B
NGFR	nerve growth factor receptor (TNFR superfamily, member 16)
IL17RB	interleukin 17 receptor B
IL17RC	interleukin 17 receptor C
AVPR1B	arginine vasopressin receptor 1B
GPR85	G protein-coupled receptor 85
GPR84	G protein-coupled receptor 84
BDKRB1	bradykinin receptor B1
KDR	kinase insert domain receptor
ERBB2	v-erb-b2 erythroblastic leukemia viral oncogene homolog 2
GPR37	G protein-coupled receptor 37 (endothelin receptor type B-like)
TPRA1	G protein-coupled receptor 175
PLXNC1	plexin C1
TEK	TEK tyrosine kinase, endothelial
CRHR1	corticotropin releasing hormone receptor 1
EPHB6	EPH receptor B6
IL17RD	interleukin 17 receptor D
NOTCH4	Notch homolog 4 (Drosophila)
SSTR5	somatostatin receptor 5
EPHB4	EPH receptor B4
GALR1	galanin receptor 1
IL1R2	interleukin 1 receptor, type II
CRHR2	corticotropin releasing hormone receptor 2
GPR39	G protein-coupled receptor 39
LIFR	leukemia inhibitory factor receptor alpha
PDGFRB	platelet-derived growth factor receptor, beta polypeptide
GPR98	G protein-coupled receptor 98
GPR176	G protein-coupled receptor 176
GPR65	G protein-coupled receptor 65
TNFRSF19	tumor necrosis factor receptor superfamily, member 19
CD300LF	CD300 molecule-like family member f
TNFRSF8	tumor necrosis factor receptor superfamily, member 8
CXCR4	chemokine (C-X-C motif) receptor 4
CXCR7	chemokine (C-X-C motif) receptor 7
GPR120	G protein-coupled receptor 120
MET	met proto-oncogene (hepatocyte growth factor receptor)
FZD4	frizzled homolog 4 (Drosophila)
OSMR	oncostatin M receptor
FZD1	frizzled homolog 1 (Drosophila)
S1PR1	sphingolipid G-protein-coupled receptor, 1
GPR75	G protein-coupled receptor 75
DCC	deleted in colorectal carcinoma
ADCYAP1R1	adenylate cyclase activating polypeptide 1 receptor type I
INSR	insulin receptor
SSTR4	somatostatin receptor 4

Color Code												
Tag-Seq (tpm)	nd	0	1	2	3	4	5	6	7	8	9	≥10
FACS purified cells & purified islets microarray (relative)	nd	0	1 - 100	101 - 200	201 - 300	301 - 400	401 - 500	501 - 600	601 - 700	701 - 800	801 - 900	≥901
T1DBase (relative) MPSS (TPM)	nd	0	1 - 10	11 - 20	21 - 30	31 - 40	41 - 50	51 - 60	61 - 70	71 - 80	81 - 90	≥91

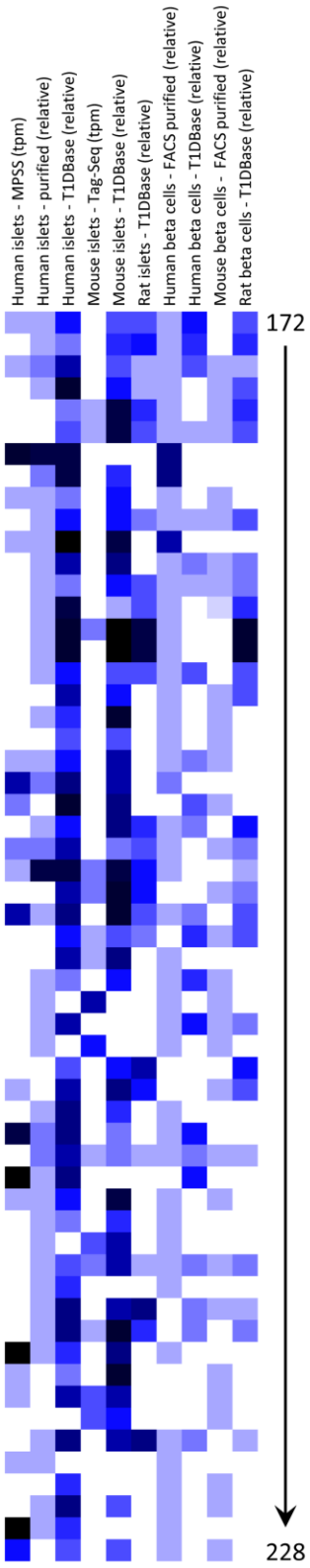

Gene Symbol	Gene Name
OPRM1	opioid receptor, mu 1
TACR1	tachykinin receptor 1
ERBB4	v-erb-a erythroblastic leukemia viral oncogene homolog 4
GPR125	G protein-coupled receptor 125, transcript variant 5
IL17RE	interleukin 17 receptor E
EPHA7	EPH receptor A7
GPR172A	G protein-coupled receptor 172A
KIAA1324L	KIAA1324-like
GPR132	G protein-coupled receptor 132
EPHA3	EPH receptor A3
UNC5CL	unc-5 homolog C (C. elegans)-like
EPHB1	EPH receptor B1
AVPR1A	arginine vasopressin receptor 1A
SSTR1	somatostatin receptor 1
LGR4	leucine-rich repeat-containing G protein-coupled receptor 4
LGR4	leucine-rich repeat-containing G protein-coupled receptor 4
FZD2	frizzled homolog 2 (Drosophila)
UNC5D	unc-5 homolog D (C. elegans)
GPR155	G protein-coupled receptor 155
GPRC6A	G protein-coupled receptor, family C, group 6, member A
ALK	anaplastic lymphoma receptor tyrosine kinase
PLXNA1	plexin A1
TNFRSF11A	tumor necrosis factor receptor superfamily, member 11a
EPHA4	EPH receptor A4
GPR110	G protein-coupled receptor 110
RHBDF1	rhomboid 5 homolog 1 (Drosophila)
ELTD1	EGF, latrophilin seven transmembrane domain containing 1
NRXN3	neurexin 3
NPR1	natriuretic peptide receptor A/guanylate cyclase A
GPR34	G protein-coupled receptor 34
FZD9	frizzled homolog 9 (Drosophila)
GPR142	G protein-coupled receptor 142
GPR126	G protein-coupled receptor 126
GPR119	G protein-coupled receptor 119
OR51E2	olfactory receptor 78
MCHR1	melanin-concentrating hormone receptor 1
FZD8	frizzled homolog 8 (Drosophila)
EPHA2	EPH receptor A2
GPR4	G protein-coupled receptor 4
TNFRSF10D	tumor necrosis factor receptor superfamily, member 10d
GPR146	G protein-coupled receptor 146
EPHA6	EPH receptor A6
MRGPRE	MAS-related GPR, member E
TACR2	tachykinin receptor 2
GPR82	G protein-coupled receptor 82
AT1	angiotensin II receptor, type 1
CALCRL	calcitonin receptor-like
GPRC5D	G protein-coupled receptor, family C, group 5, member D
PTCH2	patched homolog 2 (Drosophila)
ROBO4	roundabout homolog 4, magic roundabout (Drosophila)
Tnfrsf23	tumor necrosis factor receptor superfamily, member 23
AGTR1	angiotensin II receptor-like 1
OR5T2	olfactory receptor, family 5, subfamily T, member 2
VN1R1	vomeronasal 1 receptor 1
GPR124	G protein-coupled receptor 124
OR4F21	olfactory receptor, family 4, subfamily F, member 21
GPR133	G protein-coupled receptor 133

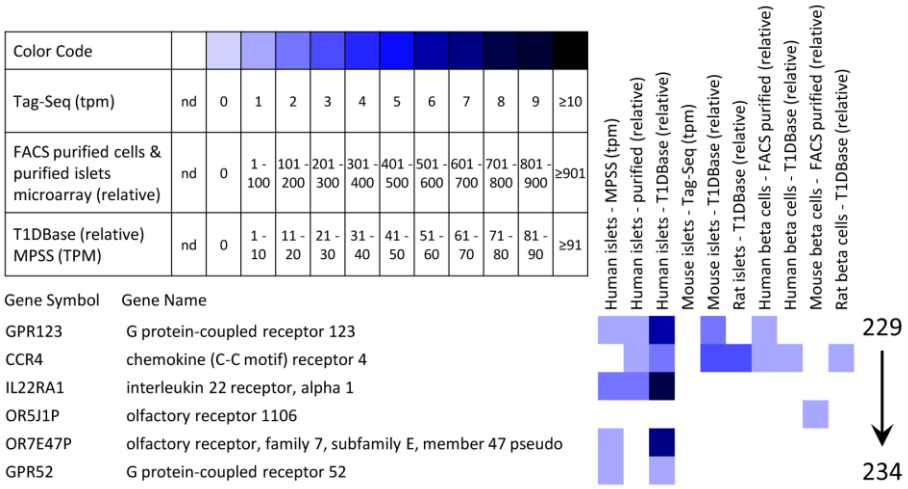

Figure 5-2. Identification of islet secreted factor receptors.
Secreted factor receptors expressed in human, mouse, and/or rat islets were extracted from 10 independent sources and ranked according to expression level. Expression levels for T1DBase (relative expression), FACS purified β-cells and purified islets microarray (relative expression), MPSS (tmp = transcripts per million), and Tag-Seq library (tpm = tags per million) are displayed by color (see look-up table; nd, data not determined).

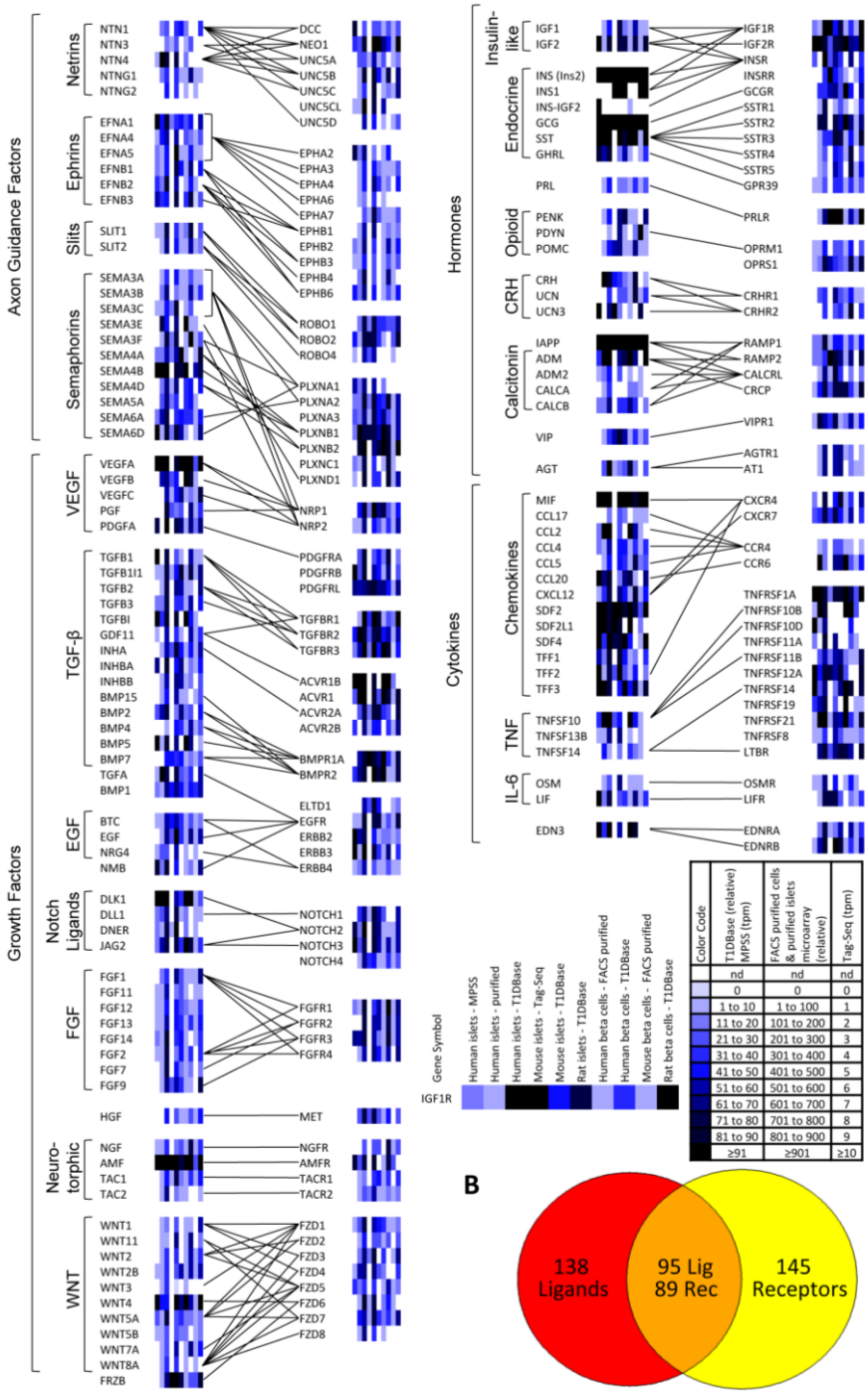

Figure 5-3. Identification of islet secreted factors and associated receptors.
A. Secreted factors and their associated receptors expressed in human, mouse, and/or rat islets were extracted from 10 independent sources. Expression levels for T1DBase (relative expression), FACS purified β-cells and purified islets microarray (relative expression), MPSS (tmp = transcripts per million), and Tag-Seq library (tpm = tags per million) are displayed by color (see look-up table; nd, data not determined) Known interactions between the factors and their receptors are represented by a connecting line. **B.** Venn diagram representing the 233 ligands and the 234 receptors found, as well as the 190 potential known interactions between 95 ligands and 89 receptors.

Chapter 6: Netrin-Unc5/Neo1 modulates apoptosis signalling in β-cells

6.1 Introduction

As we have demonstrated in Chapter 5, pancreatic islets have the potential to release and respond to more secreted factors than previously thought. Among these potential growth factors were a group known to provide cellular and axonal guidance cues during neuronal development, including members of the netrin, slit, semaphorin, and ephrin protein families (211, 212). Despite the fact that the neurons and the pancreatic endocrine cells are derived from different germ layers, the ectoderm and endoderm respectively, there are similarities between the transcription factor network and growth factors that mediate their development. Neurogenin 3, Nkx6.1, Nkx2.2, and Isl1 are key transcription factors regulating endocrine and neuronal cell fate (213). Modulation of fibroblast growth factor, sonic hedgehog, and notch signalling are also implicated in the development of both tissues (213). Given the many parallels between development and cell fate decisions in neurons and in the endocrine pancreas, we chose to examine the netrin family and their receptors in more detail.

The action of Netrins outside of neuronal development has been described in mammary gland, lung, and pancreatic development (211, 214-216). In the developing pancreas, netrins have been implicated as regulators of cell adhesion, migration, differentiation, and organ morphogenesis (211, 216, 217). Netrin-1 expression in the developing pancreatic ductal epithelium is thought to facilitate epithelial cell adhesion and migration via α6β4 and α3β1 integrin interactions (216). They regulate apoptosis via their dependence receptors (DCC, Neogenin, and UNC5) (218-220) and downstream signalling pathways involving Akt, Erk and ASK1 (211, 218, 219, 221). Netrin-1 may also play a role in fetal-islet cell and ductal cell migration during pancreatic morphogenesis and tissue remodelling following pancreatic duct ligation (217). Although it has been previously reported that Netrin-1 expression is undetectable in adult pancreatic islet cells and in the absence of tissue remodelling (216, 217), we show that multiple netrin proteins are expressed in adult β-cells, where they modulate caspase-3 activity in a context-dependent manner through the Neogenin and UNC5A dependence receptors. The aim of the present study was to determine whether Netrin can provide signals to promote β-cell survival and function.

6.2 Results

6.2.1 Netrins are expressed in adult mouse and human islets

Among the more interesting families of ligand/receptor pairs from our bioinformatics analysis (Fig. 5-3) were netrins and their receptors, best known for their roles in providing axonal guidance cues during neuronal development (211). Netrins have been ascribed a role in pancreatic development (211, 216, 217), but were previously undetected in adult islet cells in the absence of injury (216, 217). Three secreted netrins (Netrin-1, -3, -4) and the two glycosylphosphatidylinisotol-anchored sub-class (Netrin-G1, -G2) were identified via bioinformatics/genomics in mouse and human islets (Fig. 5-1). RT-PCR confirmed mRNA expression of the major netrin secreted factors in MIN6 cells and primary adult mouse islets isolated from 6 to 24-wk-old mice (Fig. 6-1A). However, in MIN6 cells Netrin-4 transcript was not detected. Quantitative RT-PCR of FACS purified human β-cells further confirmed the expression of Netrin-1 and Netrin-4 (Fig. 6-1B). Netrin-1 protein and Netrin-4 protein were confirmed by immunoblotting of human and mouse islets (Fig. 6-1C,D). Netrin expression was more prominent in mouse islets than in the exocrine tissue. Netrin-1 and Netrin-4 antibodies showed 2 bands in human islets, potentially representing the known netrin isoforms (222). Netrin-1 and Netrin-4 expression were most prominent in islets from older mice, which is perhaps why we did not see robust protein expression in the sub-differentiated MIN6 cells. Netrin-1 immunoreactivity was detected in mouse and human β-cells, but not α-cells (Fig. 6-1E,F). Netrin-4 immunoreactivity was detected in both mouse β- and α-cells, however it was only detected in human β-cells (Fig. 6-1E,F). Together with the bioinformatics described above, these data demonstrate unequivocally that netrins are in adult pancreatic β-cells. Netrins signal through the extracellular domain of their receptors and must be secreted to be functional. Netrin-1 was constitutively secreted from human islets, independent of high glucose or arginine (Fig. 6-1G). Indeed, insulin and Netrin-1 were stored in distinct secretory granules (Fig. 6-1H). Efforts to measure Netrin-4 by ELISA were unsuccessful, however we did observe distinct insulin and Netrin-4 secretory granules (Fig. 6-1H).

6.2.2 Netrin signalling regulates caspase-3 activity, but not insulin release or proliferation.

The expression of netrins in adult β-cells begs the question of their functional role. Netrin-1 and Netrin-4 each decreased caspase-3 cleavage under hyperglycemic conditions, suggesting a role in apoptosis (Fig. 6-2A,C). Interestingly, increased caspase-3 activation under basal glucose conditions was also observed upon treatment with Netrin-1 (Fig. 6-2A). A trend towards decreased cleaved caspase-3 was also observed when mouse islets were treated with Netrin-1 and 25 mmol/l glucose (109). Interestingly, under 5 mmol/l glucose conditions, Netrin-1 increased cleaved caspase-3 following 16-hour treatment (Fig. 6-2A), but not short term treatments (109), suggesting a temporal effect of Netrin-1. While netrins promote proliferation in some cell types (221, 223, 224), neither Netrin-1 nor Netrin-4 had significant effects on BrdU incorporation in MIN6 β-cells (Fig. 6-2B,D). Exogenous Netrin-1 and Netrin-4 did not have significant effects on glucose-stimulated insulin secretion from mature mouse β-cells (Fig. 6-2E).

6.2.3 Neogenin and UNC5A mediate the effects of Netrin-1 and Netrin-4

The axonal guidance by netrins is mediated through DCC and UNC5 dependence receptors (211). In adult mouse islets, mRNA for *Unc5A*, *Unc5B*, *Unc5C*, and Neogenin, but not *Unc5D* or *Dcc*, was detected by RT-PCR (Fig. 6-3A). Western blots confirmed the expression of UNC5A, UNC5C, and Neogenin proteins in mouse islets, where age-dependent differential expression patterns were observed (Fig. 6-3A,B). Neogenin, UNC5A, and UNC5C immunoreactivity was found in mouse and human α-cells and β-cells (Fig. 6-3C,D).

Neogenin and UNC5 dependence receptors induce apoptosis in the absence of netrin ligand and inhibit apoptosis when netrin is bound (225, 226). Netrin down-regulates these receptors in other cell types (227). Indeed, exogenous Netrin-1 significantly decreased Neogenin and UNC5A protein levels under high glucose (Fig. 6-4A,B). Transfection of MIN6 cells with Netrin-1 also decreased Neogenin levels, suggesting constitutive autocrine signalling (Fig. 6-4G). Netrin-1 also decreased Neogenin, but not UNC5A, in mouse islets (Fig. 6-4E,F). When MIN6 cells were treated with exogenous Netrin-4 under high glucose, a decrease in UNC5A levels was observed, while Neogenin remained unchanged (Fig. 6-4C,D). Together these data suggest that Netrin-1 and Netrin-4 decrease caspase-3 cleavage in adult β-

cells via down-regulation of distinct dependence receptors, specifically under high glucose conditions. Interestingly, glucose alone caused a significant increase in UNC5A protein levels (Fig. 6-4B,D).

To determine whether the observed decrease in Neogenin and UNC5A levels following netrin treatment was due to changes in gene transcription or protein degradation, we conducted quantitative RT-PCR on RNA from netrin-treated MIN6 cells. Netrin-1 or Netrin-4 treatment, in 5 or 25 mmol/l glucose, did not affect Neogenin or *Unc5A* mRNA (Fig. 6-4H,I), suggesting that netrins modulate receptor protein levels via degradation. This was consistent with the rapid decrease in Neogenin protein upon Netrin-1 treatment (109).

6.2.4 Netrin treatment acutely induces Akt and Erk pro-survival signalling

The mechanism by which netrin reduces caspase-3 activation was further investigated by immunoblot. Akt and Erk were phosphorylated after 5 minutes of 15 nmol/l Netrin-1 or Netrin-4 in 25 mmol/l glucose (Fig. 6-5A-C), but not 5 mmol/l glucose. Netrin-1 (0.15 nmol/l) activated the Akt and Erk pathways in the context of 5 mmol/l glucose. Following 60 minutes treatment with 15 nmol/l netrins, Akt phosphorylation remained significant and the stimulation of Erk phosphorylation was abolished (Fig. 6-6A-C). Netrin treatment did not change the phosphorylation level of JNK1 (Fig. 6-5D, Fig. 6-6D). However, under low glucose conditions Netrin-4 treatment significantly up-regulated ASK1-Thr845 phosphorylation, suggesting ASK1-dependent apoptosis (Fig. 6-5E).

Netrin-1 has previously been found to induce cAMP and RyR-dependent Ca^{2+} signals in neurons (228). To determine if cAMP is important for Netrin-1 signalling in β-cells, we conducted live cell imaging with a FRET-based cAMP probe (AKAR2). First, we validated AKAR2 function in MIN6 cells. Indeed, AKAR2 was diffusely cytoplasmic and exhibited rapid FRET changes upon perifusion with the cAMP-activating hormone GLP-1 or the adenylate-cyclase activating drug forskolin (Fig. 6-7A,B). Treatment with 15 nmol/l Netrin-1 for 30 minutes in a static bath resulted in only miniscule, delayed FRET signals (Fig. 6-7C). Thus, rapid cAMP signalling may not be critical for acute netrin signalling in β-cells. We also examined intracellular Ca^{2+} using Fura-2-AM and found that Netrin-1 had no effect in islet cells (Fig. 6-7D) and MIN6 cells. This suggests that Netrin-1 does not mediate its acute effects on MIN6 cells through the same pathways that it employs to control axon growth cone turning.

6.3 Discussion

The identification of axonal guidance factors in islets, including netrins, was a surprising finding of our unbiased analysis. In addition to neuronal development, netrins have been implicated in mammary, lung, and pancreas development (211, 214-216). In the developing pancreas, netrins act as regulators of cell adhesion, migration, and differentiation (211, 216, 217). Netrins were thought to be absent in adult pancreatic islets (216, 217). Our results show that all netrin genes are expressed in adult mouse islets. Netrin-1 in particular was more predominately expressed in the β-cells of the mouse and human islets. The predominant localization of Netrin-1 immunoreactivity in insulin containing cells has also been observed in adult rat islets following pancreatic duct ligations (217). In addition, human islet perifusion studies revealed that Netrin-1 was constitutively secreted from human islets at low levels and the secretion dynamics was independent of glucose levels. This suggests that the physiological role of Netrins act independently of glucose stimulated insulin secretion. Netrin receptors (Neogenin, UNC5A, UNC5B, and UNC5C) were also expressed in adult mouse and human islets. Consistent with previous reports, DCC was not found in adult islets (217). There appeared to be age-dependent changes in expression of both netrins and their receptors, which could implicate netrin signalling in the maintenance of islet survival throughout the aging process. Islet expression of netrins and their receptors suggests that local autocrine or paracrine netrin signalling exists in adult islets. Additionally, the down-regulation in Neogenin protein as a result of Netrin-1 overexpression further suggests existence of an autocrine signalling mechanism. Further studies will help determine if netrins and their receptors display differential regulation of the expression in the pancreatic islets under type 1 and type 2 diabetic states.

Hyperglycemia-induced apoptosis is a complication of diabetes, and likely plays a deleterious role in islet transplantation. In the present study, we demonstrated that netrins significantly reduced caspase-3 activity in high glucose. This is consistent with the pro-survival effects of netrins in other cell types, including neuronal, gastrointestinal epithelial, and mammary cells (215, 218, 220, 229, 230). The glucose-dependence of caspase-3 activation mirrors the effects of blocking Notch signalling in adult islets that we have described (37). Interestingly, netrins upregulated caspase-3 activation under basal glucose levels, without having any detrimental effects of overall cell death. Perhaps the concurrent activation of ERK

and AKT survival pathways was counter-balancing the caspase-3 induction. Our investigation of the mechanisms involved in β-cell netrin signalling implicated Neogenin and UNC5A. These receptors induce apoptosis in the absence of netrin and inhibit apoptosis when ligands are bound (225, 226). Ligand-bound netrin receptors sequester caspase-3, preventing its activation (219). The proteasome-ubiquitin system has been implicated in DCC down-regulation by Netrin-1 in embryonic neurons (227), and our results are consistent with degradation controlling β-cell netrin receptor levels. The residual amount of receptors may be sufficient for mediating the observed potentiation of ERK and AKT signalling. The proliferative effect of Netrin-1 in vascular smooth muscle cells during angiogenesis is mediated through Neogenin (224). Perhaps, the lack of proliferative response to Netrin-1 treatment could be due to the decrease in Neogenin upon treatment with Netrin-1. Future studies on the trafficking of the netrin receptors and the glucose-dependent regulation of netrin receptors could help elucidate the mechanism mediating the glucose-dependent survival effects of netrins.

Nerve growth cone guidance by Netrin-1 is dependent on cytoplasmic Ca^{2+} influxes via plasma membrane channels and ryanodine receptors (231). In our hands, exposing islet cells to Netrin-1 did not acutely induce intracellular Ca^{2+} signals. Whether Netrin-1 signalling in neurons requires cAMP is controversial (228). Some reports suggest that Netrin-1 can increase cAMP levels in neurons to induce guidance responses (228, 232, 233). While others suggest that cAMP acts as a modulator for Netrin-1 signalling by regulating the recruitment of the Netrin receptors to the plasma membrane (234-236). Under our experimental conditions, Netrin-1-treated MIN6 cells did not generate robust cAMP responses. The cAMP fluctuations observed in some β-cells following longer exposures to Netrin-1 could have been caused by other paracrine factors in this static milieu.

We focused on the detailed mechanisms and function of the netrins, which had not been described in normal adult islets. We demonstrate that netrins regulate caspase-3 activation in a glucose-dependent manner, via a mechanism involving their dependence receptors, Neogenin and UNC5A, and upregulation of Akt and Erk pro-survival signalling. Our results lay the ground-work to allow exploitation of local autocrine/paracrine survival signalling for therapeutic purposes.

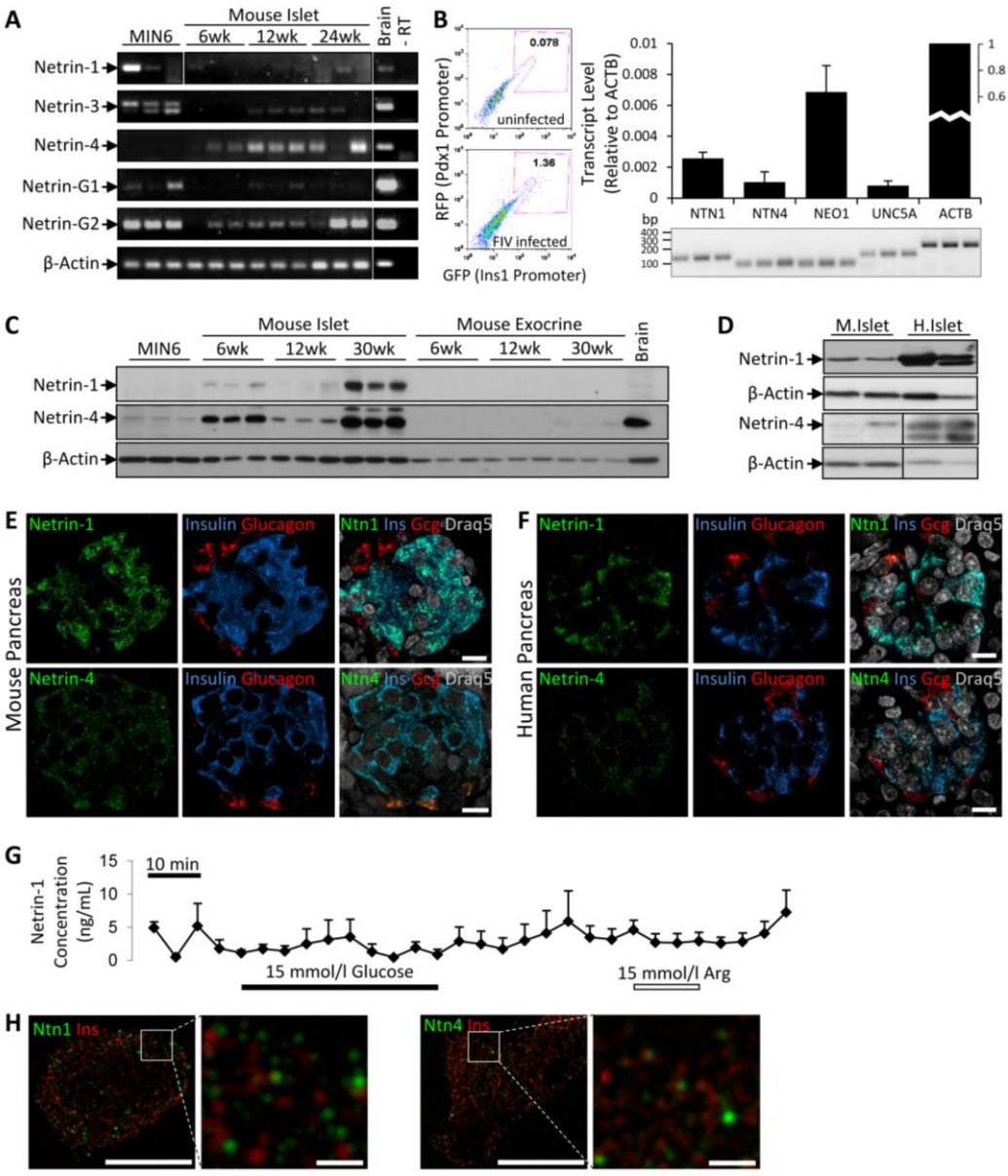

Figure 6-1. Expression of Netrins in adult mouse and human islet and exocrine cells.
A. Expression of netrins was assessed by RT-PCR of RNA isolated from MIN6 cells (passages 27, 38, 46), as well as islets from mice of different ages (n=3). Positive and negative controls were RT-PCR of RNA from mouse brain, with and without reverse transcriptase. **B.** FACS plot showing selection of β-cells that displayed both *Pdx1* and *Ins1* promoter activities. Quantitative RT-PCR of RNA isolated from FACS purified human β-cells. Relative differences in gene expression compared to β-actin (ACTB) were analyzed by $2^{-\Delta Ct}$ method. **C.** Western blotting of protein lysates from MIN6 cells (passages 18, 43, 46) and from 6, 12, and 30-week old mouse islet and exocrine cells. Positive control was lysate from mouse brain. **D.** Western blotting of protein lysates isolated from mouse and human islet cells. **E.** Immunofluorescence staining for Netrin-1 (Ntn1) and Netrin-4 (Ntn4) in 12-week-old mouse pancreas sections, co-stained with antibodies to insulin and glucagon. Nuclei were stained with Draq5. Scale bar is 10 µm. **F.** Immunofluorescence staining for Netrin-1 (Ntn1) and Netrin-4 (Ntn4) in human pancreas sections, co-stained with antibodies to insulin and glucagon. Nuclei were stained with Draq5. Scale bar is 10 µm. **G.** Netrin-1 release from human islets perifused in 3 mmol/l and 15 mmol/l glucose Kreb-Ringer's buffer (n=5). **H.** Immunofluorescence staining for Netrin-1, Netrin-4, and insulin in human β-cells. Scale bar is 10 µm for whole β-cell images and 1 µm for zoomed in images.

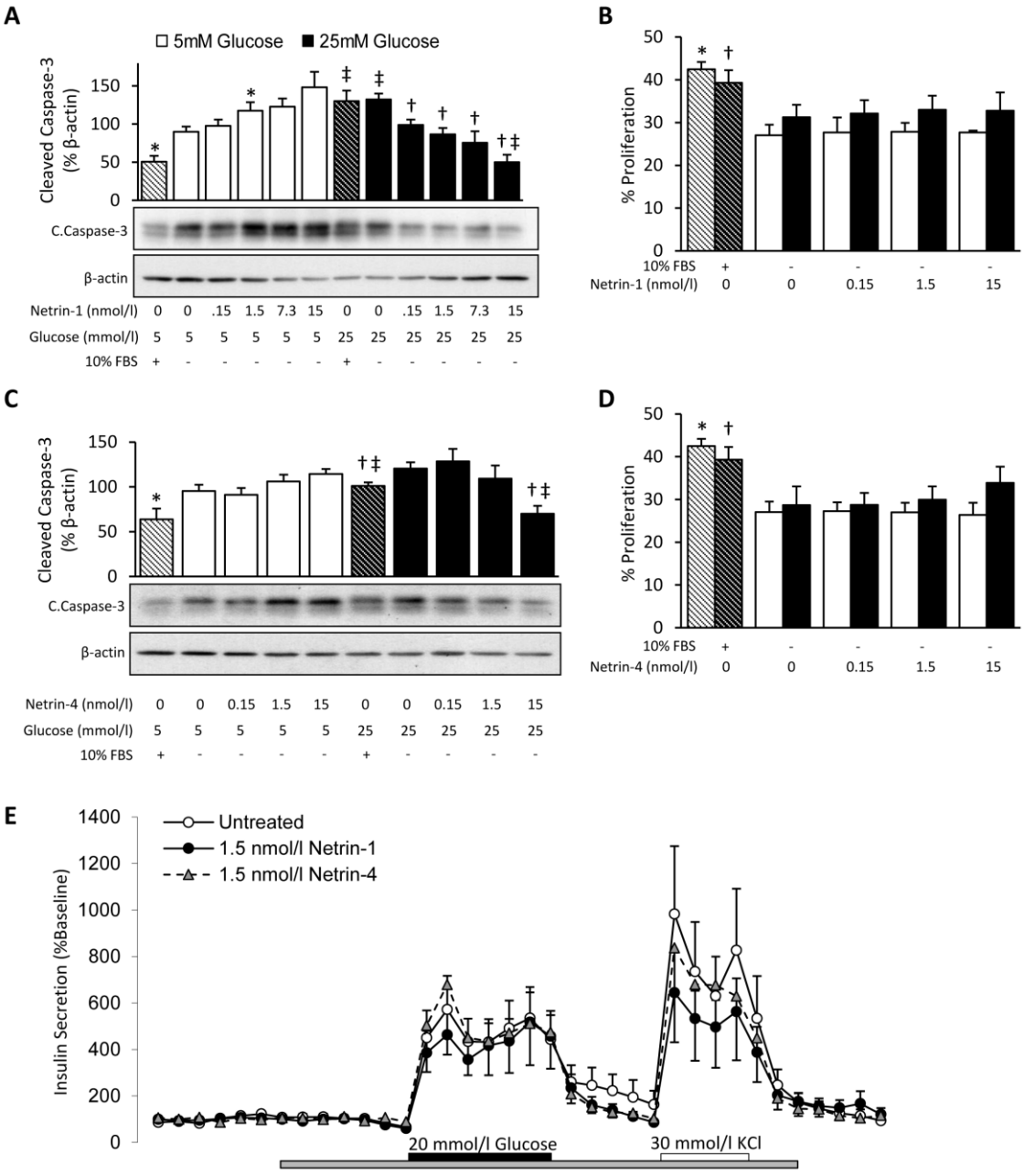

Figure 6-2. Effects of Netrin-1 and Netrin-4 on MIN6 cell viability, proliferation, and insulin secretion. **A,C.** Cleaved caspase-3 in MIN6 cells treated with Netrin-1 and Netrin-4 under 5 mmol/l or 25 mmol/l glucose for 16 hours was detected by western blotting and quantified by densitometry as percentage of β-actin levels (n=7). * P<0.05, compared to 5 mmol/l glucose control. † P<0.05, compared to 25 mmol/l glucose control. ‡ P<0.05, compared to 5 mmol/l glucose of the same treatment. **B,D.** Proliferation of MIN6 cells treated with various doses of recombinant mouse Netrin-1 or Netrin-4 for 6 hours under serum free conditions. Serum containing media was used as a positive control (n=4). **E.** Glucose and KCl stimulated insulin secretion from mouse islets perifused with 1.5 nmol/l Netrin-1 or Netrin-4 (n=6).

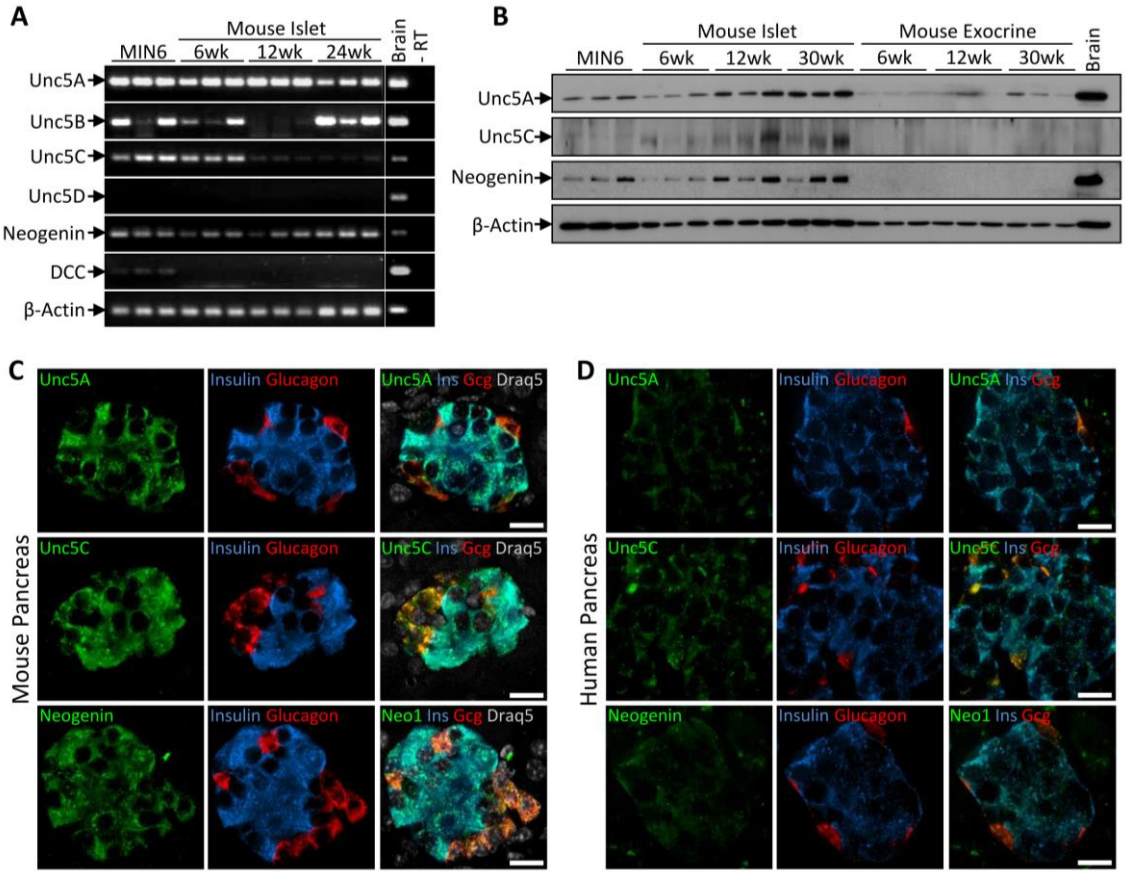

Figure 6-3. Expression of Neogenin, UNC5A, and UNC5C in adult mouse islet cells.
A. Expression of Neogenin, *Unc5A*, *Unc5B*, and *Unc5C* was detected by RT-PCR of RNA isolated from MIN6 cells and 6, 12, and 24-week old mouse islet cells (n=3). Positive and negative controls were RT-PCR of RNA from mouse brain, with and without reverse transcriptase. **B.** The expression of Netrin receptors detected by western blotting of lysates isolated from MIN6 cells and from 6, 12, and 30-week old mouse islet and exocrine cells. Positive control was lysate from mouse brain. **C.** Immunofluorescence staining of mouse pancreas sections was used to detect the expression of Neogenin, UNC5A, and UNC5C in mouse islets co-stained with antibodies to insulin and glucagon. Nucleus was stained with Draq5. Scale bar is 10µm. **D.** Immunofluorescence staining of human pancreas sections was used to detect the expression of Neogenin, UNC5A, and UNC5C in mouse islets co-stained with antibodies to insulin and glucagon. Nucleus was stained with Draq5. Scale bar is 10µm.

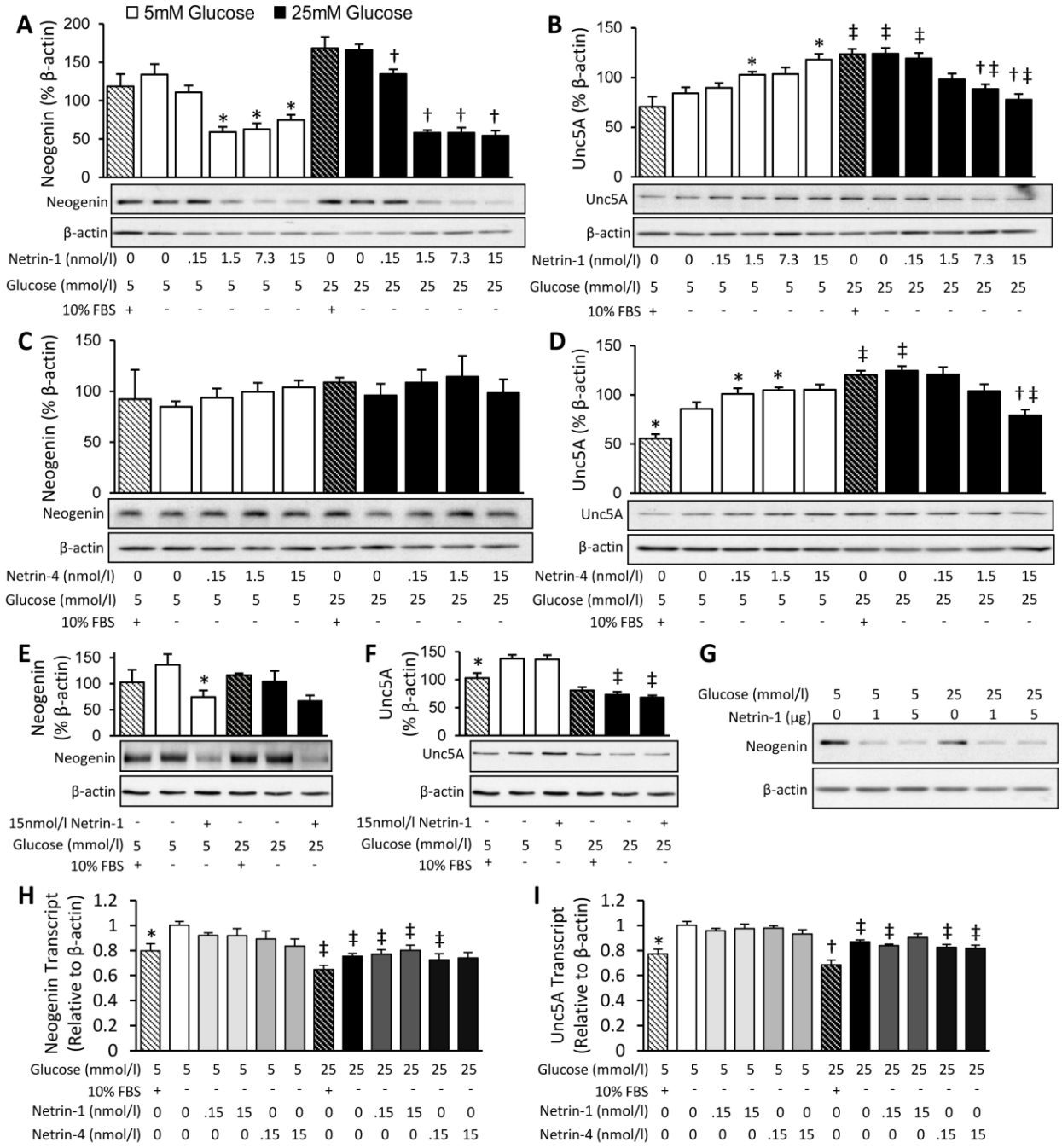

Figure 6-4. Effects of netrins on the expression level of associated receptors.
The protein levels of Neogenin and UNC5A, normalized to β-actin, were detected by western blotting in MIN6 cells treated with 0 to 15 nmol/l of Netrin-1 **(A,B)** or Netrin-4 **(C,D)** in DMEM medium supplemented with 5 mmol/l or 25 mmol/l glucose for 16 hours (n=6-7). * P<0.05, compared to 5 mmol/l glucose serum free control. † P<0.05, compared to 25 mmol/l glucose serum free control. ‡ P<0.05, compared to 5 mmol/l glucose of same treatment. The protein levels of Neogenin **(E)** and UNC5A **(F)**, normalized to β-actin, were detected by western blotting in mouse islets treated with RPMI media supplemented with 15 nmol/l of Netrin-1 for 72 hours (n=3). **(G)** The protein level of Neogenin was detected by western blotting in MIN6 cells 48 hours following transfection with a Netrin-1 construct. The expression level of Neogenin **(H)** and *Unc5A* **(I)** were detected by quantitative RT-PCR in MIN6 cells treated with Netrin-1 or Netrin-4 for 16 hours (n=3). Relative changes in gene expression were analyzed by $2^{-\Delta\Delta Ct}$ method.

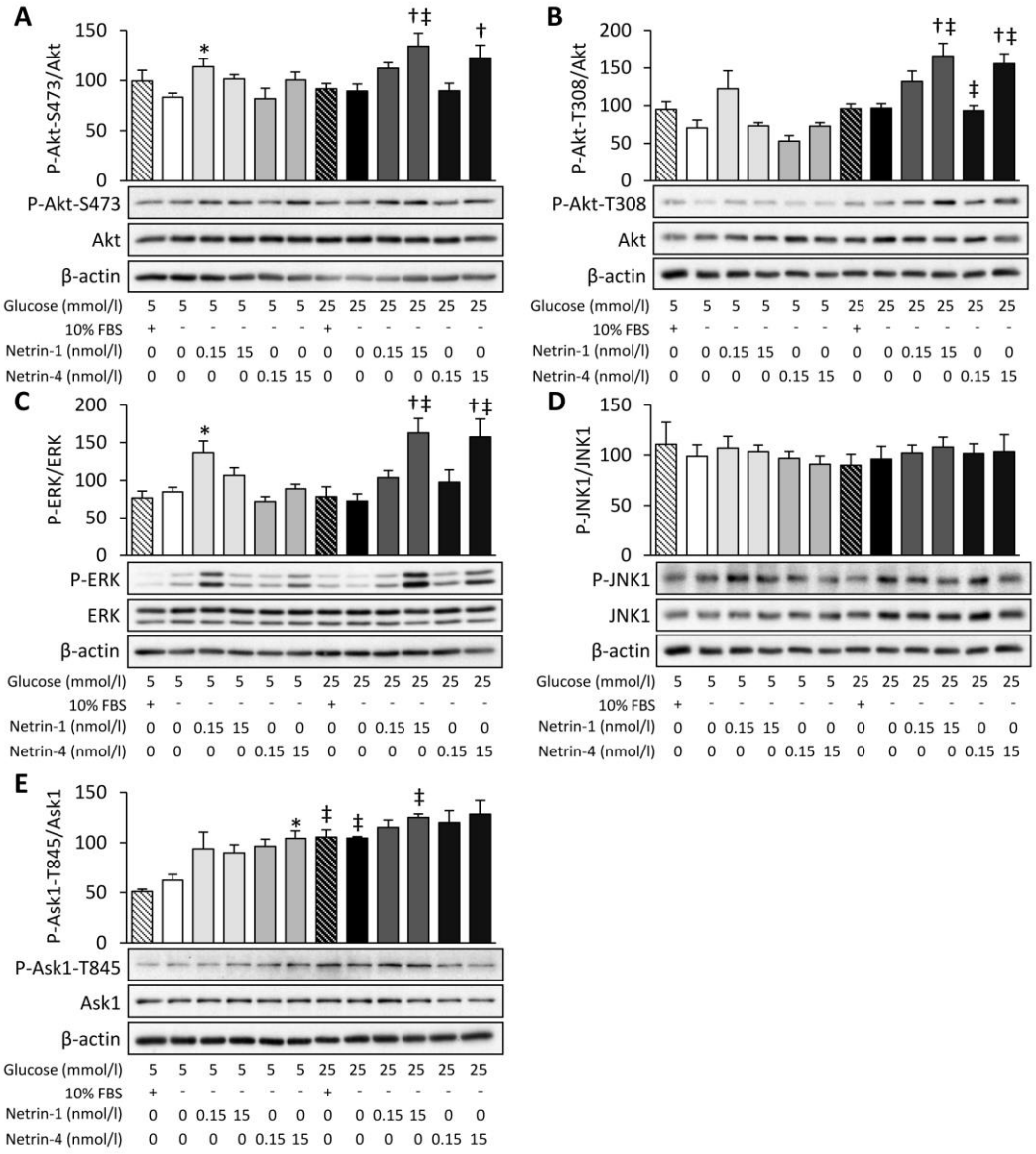

Figure 6-5. Netrins can activate Akt and Erk pro-survival signalling in MIN6 cells.
The phosphorylation level of Akt-Ser473 **(A)**, Akt-Thr308 **(B)**, Erk1/2-Thr202/Tyr204 **(C)**, JNK1-Thr183 **(D)**, and Ask1-Thr845 **(E)** were detected by western blotting in MIN6 cells treated with Netrin-1 or Netrin-4 for 5 minutes (n=7-12). * P<0.05, compared to 5 mmol/l glucose serum free control. † P<0.05, compared to 25 mmol/l glucose serum free control. ‡ P<0.05, compared to 5 mmol/l glucose of same treatment.

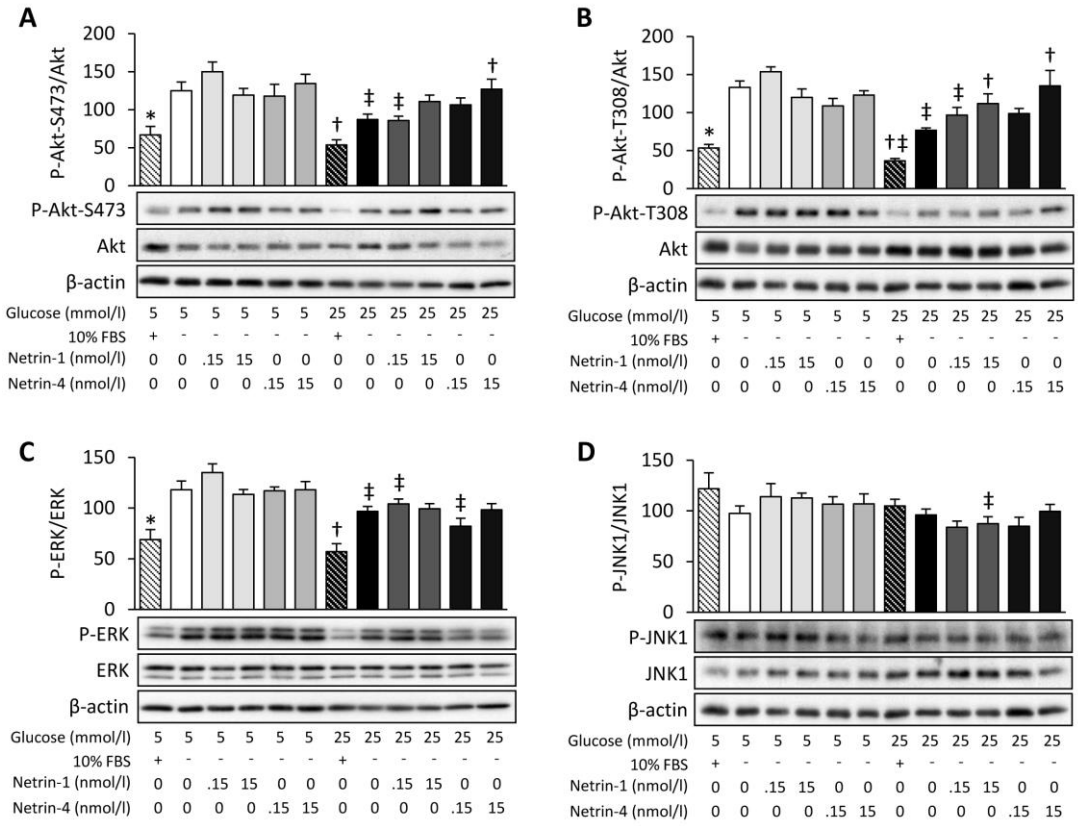

Figure 6-6. Prolonged netrin treatment shows differential Akt and Erk pro-survival signalling in MIN6 cells.

The phosphorylation level of Akt-Ser473 **(A)**, Akt-Thr308 **(B)**, Erk1/2-Thr202/Tyr204 **(C)**, and JNK1-Thr183 **(D)** were detected by western blotting in MIN6 cells treated with Netrin-1 or Netrin-4 for 60 minutes (n=7-12). * P<0.05, compared to 5 mmol/l glucose serum free control. † P<0.05, compared to 25 mmol/l glucose serum free control. ‡ P<0.05, compared to 5 mmol/l glucose of same treatment.

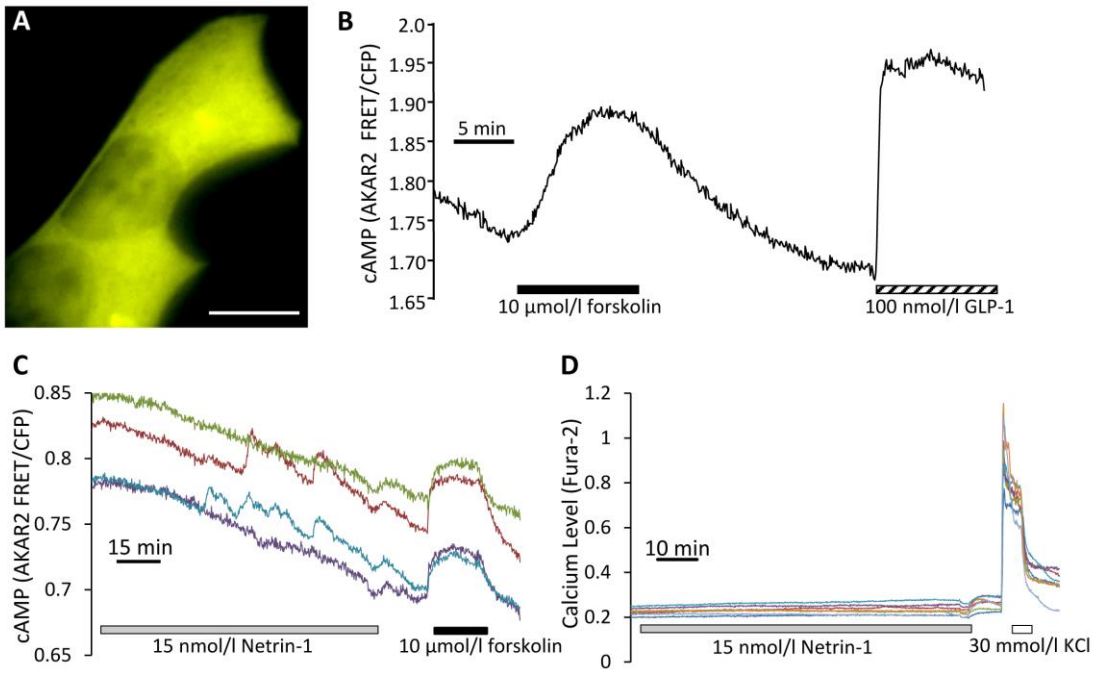

Figure 6-7. Netrin-1 does not induce large or consistent acute intracellular cAMP and Ca^{2+} signals in β-cells.

A. MIN6 cells transfected with AKAR2 cAMP FRET sensor. Scale bar is 10 µm. **B.** Representative trace of AKAR2 transfected MIN6 cell following perifusion with 3 mmol/l glucose Ringer's buffer containing cAMP-activating hormone GLP-1 or the adenylate-cyclase activating drug forskolin. **C.** MIN6 cells were exposed to a static bath of 3 mmol/l glucose Ringer's supplemented with 15 nmol/l Netrin-1 and the changes in intracellular cAMP levels were monitored using the AKAR2 FRET probe. Signal from four representative cells are displayed. 10 µmol/l forskolin was the positive control. **D.** Dispersed mouse islet cells were loaded with Fura-2-AM and exposed to a static bath of 3 mmol/l glucose Ringer's supplemented with 15 nmol/l Netrin-1 and the changes in intracellular Ca^{2+} levels were monitored. Signal from seven representative cells are displayed.

Chapter 7: Intra-islet SLIT-ROBO signalling is required for β-cell survival and potentiates insulin secretion

7.1 Introduction

Emerging evidence highlights the important role of locally released pancreatic islet peptide factors on β-cell mass growth, maintenance, and survival (38, 108, 109, 138, 195, 196, 198, 207, 237-240). In Chapter 5, we have presented a list of 233 ligands and 234 receptors expressed in islets and/or β-cells (109). While our list is undoubtedly not comprehensive, it provides a starting point for the investigation of factors in adult islets that had previously only been reported in other cell types or in fetal pancreas (109). We identified a group of molecules known to provide axonal guidance cues during neuronal development, comprising members of the netrin, slit, semaphorin, and ephrin families (212). In Chapter 6, the parallels between cell fate decisions in neurons and the endocrine pancreas prompted us to examine some factors in detail and discover that netrin treatment modulates β-cell survival signalling (109).

The Slit ligands and their Roundabout receptors (Robo) were discovered in *Drosophila* as regulators of axon guidance during development (241-244). Mammalian homologs of Slit and Robo with functions outside of axon guidance have since been identified (245, 246). Slit ligands have been implicated in liver, kidney, lung, and mammary development by modulating cell adhesion, migration, differentiation, and death (245, 247, 248). It was not known whether Slit-Robo signalling has any function in β-cells. Here, we found that Slit expression was regulated by stress and that local Slit production is required for β-cell survival and optimal function via a mechanism involving ER Ca^{2+} homeostasis and actin remodelling. Our work provides the first example of a 'guidance factor' that is required for β-cell survival and suggests new avenues for protecting functional β-cell mass.

7.2 Results

7.2.1 Slits are expressed in adult mouse and human islets

The mammalian genome contains 3 Slit ligands and 4 Robo receptors. Our bioinformatic studies identified the expression of several Slit and Robo family members in adult human and rodent pancreatic islet cells (109) and *Robo1* was identified by others as a transcript enriched in pancreatic endocrine cells during development (249). Nevertheless, no in-depth studies of

these proteins have been reported. We detected *Slit1*, *Slit2*, and *Slit3* transcripts in 6- and 30-week-old mouse islets, with higher expression of *Slit2* and *Slit3* (Fig. 7-1A). In human islets, *SLIT1*, *SLIT2*, and *SLIT3* expression was similar. *Robo1* and *Robo2* were expressed in MIN6 cells, mouse islets, and human islets (Fig. 7-1A). SLIT1, SLIT2, SLIT3, ROBO1, and ROBO2 were confirmed at the protein level (Fig. 7-1B-F). Secretion of SLIT2 and SLIT3 from mouse islets was detected following incubation under 3 mM and 15 mM glucose conditions (Fig. 7-1B). Although SLIT1 secretion from islets and SLIT1 protein content within islets fell below the detection threshold of the ELISA kit, the protein could be detected by immunoblotting and immunostaining (Fig 7-1B-F). It is possible that SLIT1 is expressed, but not secreted by islets. SLIT2 immunoreactivity was more predominant in β-cells, while SLIT1 and SLIT3 was detected in both β-cells and α-cells with the same intensity (Fig. 7-1E,F). Using deconvolution microscopy, SLIT2 immunoreactivity was found to co-localize with insulin-positive granules, whereas SLIT1 and SLIT3 were present in distinct granules (Fig. 7-1F). These data suggest that SLIT2 may act in an autocrine manner on β-cells, while SLIT1 and SLIT3 may play both autocrine and paracrine roles.

Next, we assessed the mechanism of local Slit signalling by investigating the expression and localization of Slit receptors. ROBO1 and ROBO2 staining was detected in both β-cells and α-cells (Fig. 7-1E). However, while ROBO1 could be found in the plasma membrane and cytosolic compartments typical for receptors of soluble ligands, ROBO2 displayed a prominent nuclear localization (Fig. 7-1F). Although ROBO1 has been reported to be nuclear in some cell types (250), we are unaware of reports of nuclear ROBO2. Our data suggest that SLIT ligands act via ROBO1 receptors on islet cell plasma membranes.

It is not well understood in any cell type whether the Slit-Robo system can be dynamically regulated, for example by stresses (76, 111). qRT-PCR revealed that cytokines, thapsigargin, and palmitate downregulated *Slit3*, and serum deprivation downregulated *Slit2* (Fig. 7-1G). *Slit1* expression could not be consistently detected under all the treatment conditions or upregulated under stress. In contrast to the situation in primary islets, thapsigargin and palmitate upregulated *Slit1* and *Slit2* in MIN6 cells (Fig. 7-2). *Slit3*, which is typically absent in MIN6 cells, was robustly induced under ER stress (Fig. 7-2). These data suggest that the production of Slit ligands can be regulated in response to specific cellular stresses, with differential effects observed between primary islet cells and MIN6 insulinoma

cells. We also examined the effects of stress on the Robo genes, and observed significant regulation by stress conditions (Fig. 7-1G).

7.2.2 Knockdown of endogenous Slits decreases β-cell survival

The regulation of Slit expression under stress suggests that Slit-Robo signalling play a role in β-cell survival. A loss-of-function approach was used to determine the role of endogenous Slit ligands in β-cell survival. In mouse islet cells, simultaneous siRNA targeting of all Slit ligands (to circumvent isoform compensation) resulted in a 48% knockdown of *Slit1*, 46% of *Slit2*, and 49% of *Slit3* mRNA (Fig. 7-3A). Remarkably, even modest reduction in endogenous Slit production significantly reduced β-cell survival in serum-free conditions (Fig. 7-3B). Similarly, knockdown of *Slit1/2/3* in MIN6 cells had significant negative effects on β-cell survival (Fig. 7-4). These studies clearly demonstrate that the local production of Slit ligands is required for optimal β-cell survival.

Next, we asked whether supplementing islet cell cultures with recombinant SLIT proteins would be sufficient to rescue the effects of *Slit1/2/3* knockdown. Indeed, while SLIT1 and SLIT2 alone could not rescue the elevated level of cell death observed under 5 mM glucose serum free condition (Fig. 7-3C), SLIT3 and a combination of all SLITs reversed the effects of SLIT knockdown on islet cell death (Fig. 7-3C). We did not observe significant differences in cell survival between control and Slit knockdown in primary islet cells and MIN6 treated with cytokines, thapsigargin, or palmitate (Fig. 7-3D; Fig. 7-4). Collectively, our data indicate that SLIT treatments have acute protective effects on islet cells.

7.2.3 Exogenous Slits increase β-cell survival during stress and hyperglycemia

Next, we tested whether exogenous SLIT1, SLIT2, and SLIT3 could protect β-cells from multiple forms of death. We first sought to determine whether the glucose milieu altered the protective effects of Slit treatment, as we have observed with Netrin and Notch signalling (37, 109). Indeed, treatment with SLIT1 and SLIT2 recombinant proteins significantly reduced thapsigargin-induced death in MIN6 cells under high, but not low glucose conditions (Fig. 7-5A,B). In mouse islet cells, SLIT1, SLIT2, and SLIT3 also reduced islet cell death in response to serum deprivation alone and in combination with cytokines (Fig. 7-6A,B). These effects were only seen in the context of high glucose and never in low glucose conditions, suggesting

a context-dependent switch. Cell death induced by exposure to thapsigargin under serum deprivation was rescued with combination treatment of SLIT1-3 (Fig. 7-6C). SLIT1 and SLIT2 also reduced the level of cell death induced by thapsigargin treatment alone (Fig. 7-5C). Palmitate induced cell death was not significantly reduced with SLITs (Fig. 7-6D). These data show that exogenous SLIT ligands, especially in combination, exert significant protection against several harsh stresses.

7.2.4 Slits protect β-cells by suppressing apoptosis and ER-stress

To assess the molecular mechanisms associated with Slit action in β-cells, we examined markers of ER-stress and apoptosis. Significant increases in annexinV positive cells were observed in *Slit1/2/3* knockdown cells compared to control (Fig. 7-7A-C), pointing to an effect on apoptotic cell death. Treatment of mouse islets with exogenous SLIT decreased expression of *Chop*, *Gadd34*, and s*Xbp1* mRNA, but only in high glucose conditions (Fig. 7-7D). In low glucose conditions, SLIT increased the expression of *Bip*, a protective chaperone (Fig. 7-7D). Consistent with the down-regulation of *Chop* observed in mouse islet cells, we also found a decrease in thapsigargin induced CHOP protein upon treatment with SLIT2 in high glucose (Fig. 7-8A). Treating mouse islets with SLITs reduced cleaved caspase-3 and cleaved PARP (Fig. 7-7E).

Upon induction of ER-stress, IRE1 activation can lead to the downstream activation of NF-κB and ASK1-p38 MAPK/JNK signalling cascades. Treatment with SLITs significantly reduced phospho-JNK and phospho-p38 MAPK, indicative of the down-regulation of these signalling cascades (Fig. 7-7E). Downstream mediators of p38 MAPK pathway, p53 and HSP27, were also down-regulated. Treatment of MIN6 cells with SLIT2 following ER-stress induction reduced ASK1 activation (Fig. 7-8B). Thapsigargin-induced cleaved caspase-3 and cleaved caspase-12 were also down-regulated by SLIT2 (Fig. 7-8C-E). Serum deprivation-induced cleaved caspase-3 levels were also down-regulated upon SLIT1 and SLIT2 treatments under high glucose, but not low glucose conditions (Fig. 7-8F,G). Cleaved caspase-7 and cleaved caspase-12 levels were also significantly decreased in cells treated with SLIT1 under hyperglycemic serum free conditions (Fig. 7-8H,I). Together, these experiments indicate that SLIT protects β-cells by broad suppression of the ER-stress-induced apoptosis pathway. Since, we have previously shown that the CHOP-caspase axis in β-cells can be controlled by luminal

Ca^{2+} (76, 111), we predicted that the effects on cell death signalling were downstream of the modulation of ER Ca^{2+} by SLIT-ROBO signalling.

7.2.5 Slits accelerate Ca^{2+}oscillations and modulate ER luminal Ca^{2+}

Ca^{2+} homeostasis, especially within the ER, plays a key role in both β-cell survival (76, 111, 147, 251) and glucose responsiveness (251-253). Given that SLIT2 signalling in neurons and olfactory cells involves Ca^{2+} release from the ER (254-256), we examined this mechanism in β-cells. Interestingly, SLIT treatment increased the frequency of glucose-stimulated cytosolic Ca^{2+} oscillations (Fig. 7-9A,B), a phenomenon that is known to be modulated by ER Ca^{2+} filling state and associated with increased insulin secretion (251-253, 257). At basal glucose, SLIT treatment had little or no effect on cytosolic Ca^{2+} (Fig. 7-9C). However, in cells transfected with luminal ER Ca^{2+} sensor, D1ER (76, 258), we observed that SLIT induced a gradual release of Ca^{2+} from the ER filled after exposure to high glucose (Fig. 7-9D; Fig. 7-10). These effects correlate well with the conditions under which SLIT proteins protect β-cells from ER-stress induced by cytokines and by thapsigargin, a drug that block ER Ca^{2+} refilling. This result fits with a model whereby ER stress-induced cell death is dependent on the rate at which Ca^{2+} is depleted and the level of depletion (76). SLITs only partially depleted ER Ca^{2+}, since thapsigargin treatment led to further depletion of ER Ca^{2+} (Fig. 7-9D; Fig. 7-10). The partial depletion of ER Ca^{2+} was maintained throughout a 6 h treatment with SLITs (Fig. 7-10 *bottom*). These experiments demonstrate that Slit signalling has direct effects on ER luminal Ca^{2+}, a parameter known to modulate ER stress and insulin secretion (76, 111, 147).

Ca^{2+}-dependent actin remodelling is induced by SLIT proteins during repulsive axon guidance (254, 255). Our collaborators demonstrated that treatment of dispersed mouse β-cells with recombinant SLIT1, SLIT2 or SLIT3 decreased cortical F-actin (Fig. 7-9E), an event expected to promote glucose stimulated insulin secretion (259-261). Temporal analysis of F-actin levels revealed a biphasic response following SLIT1 and SLIT3 treatments (Fig. 7-9E).

7.2.6 Slits potentiate glucose-stimulated insulin secretion

Given the roles of Ca^{2+} and actin on insulin secretion, we investigated whether SLITs affect insulin release. Static incubation showed that mouse islets cultured in 15 mM glucose secreted more insulin in the presence of SLIT (control: 9.6 ± 2.8 ng/ml, SLIT1: 21.6 ± 8.2

ng/ml, SLIT2: 19.1 ± 8.4 ng/ml). This preliminary observation led us to conduct more robust islet perifusions. Indeed, glucose stimulated insulin secretion was significantly potentiated in the presence of SLIT1, SLIT2, or SLIT3 (Fig. 7-11A). SLIT treatment did not potentiate insulin secretion when β-cells were directly depolarized with 30 mM KCl (Fig. 7-11A), ruling out effects distal to the opening of voltage-gated Ca^{2+} channels and pointing to effects on glucose sensing/signalling. SLITs did not affect *Ins1* and *Ins2* transcription (Fig. 7-11B). Thus, Slit proteins can both protect β-cells and increase insulin secretion, which itself is anti-apoptotic (108, 144, 240).

7.3 Discussion

The present study was conducted to determine the expression pattern, regulation, and roles of the Slit family of secreted factors and their Robo receptors in pancreatic islet cells. Slit and Robo transcripts and protein were detected in adult mouse and human islets and regulated in stress conditions. We identified an important role for this local autocrine/paracrine network in β-cell survival and function. We identified a novel anti-ER-stress and anti-apoptotic mechanism of action, involving the controlled release of Ca^{2+} from the ER lumen (Fig. 7-11C).

The roles of Slit-Robo signalling in cell survival remain poorly understood. Knockout mouse studies, along with the observed loss of expression of ROBO1 in some human cancers, provide evidence that the loss of ROBO is tumorigenic. *Slit1* and *Slit3* are candidate tumor suppressor genes due to their inactivation in various cancers via promoter hypermethylation and allelic loss (262). However, in human prostate tumors *SLIT1* expression is upregulated (263). In primary mouse islet and MIN6 cells, a modest knockdown of Slits significantly increased cell death, suggesting that endogenous secretion of SLITs plays an important role in cell survival. Conversely, SLIT1, SLIT2, and/or SLIT3 exogenous supplementation reduced stress induced cell death. When either mouse islet or MIN6 cells were treated with SLITs under hyperglycemic conditions, we observed significant decreases in both ER stress and serum starvation induced cell death. The mechanism by which SLITs increase cell survival was incompletely understood, but intracellular calcium was a strong candidate to mediate some of the effects of Slit-Robo signalling (76, 111, 147, 251, 254-256). Data from the current study suggests that Ca^{2+} dependent pathways are important for the reduction in cell death induced by

Slit. In particular, our results implicate a controlled depletion in ER Ca^{2+} and an increase in the frequency of cytosolic Ca^{2+} oscillations.

DCC, UNC5, and Neogenin are dependence receptors that can increase cell survival in the presence of netrins and induce cell death in the absence netrins (219, 220). Interaction between ROBO1 and DCC in a Slit-dependent manner can lead to a decrease in netrin-induced chemoattraction in neurons (264, 265). Perhaps Slit-Robo signalling regulates β-cell survival through down-regulation of netrin receptor-induced apoptosis. Additionally, since Slit-Robo signalling induces tumor angiogenesis by attracting endothelial cells, perhaps local production of SLITs could improve islet engraftment following transplantation (266). Validation of the *in vivo* application of SLITs for improving β-cell survival and function in diabetes will most likely require tissue-specific targeting due to its role in the regulation of other organs. The stress-induced upregulation of Slit expression, the survival effects of exogenous SLITs under high glucose conditions, and the protective effects of endogenous SLITs suggest an autocrine/paracrine compensatory survival network.

In addition to the protective effects on β-cells, our investigation also uncovered effects of SLIT ligands on proximal glucose sensing/signalling, an effect that was associated with an increase in Ca^{2+} oscillation frequency and the modulation of actin polymerization. It was not surprising to find that SLITs could potentiate glucose stimulated insulin secretion given that Rho GTPase Cdc42, Rac1, and RhoA play important roles in Slit induced cellular migration (256, 267, 268). The down-regulation of cortical F-actin staining observed upon SLIT treatment, is in agreement with the requirement for Cdc42 and RhoA inactivation via increasing Rho GTPase activating proteins for the repulsive effects of SLITs in neurons and olfactory ensheathing cells (256, 267). In addition to the release of anti-apoptotic insulin (108, 144, 240, 269-271), modulation of actin polymerization may also directly promote survival (272-275). In our current studies, we have not determined whether the survival effects of SLITs are due to direct down-regulation of apoptotic pathways or indirect effects through upregulation of insulin secretion (39, 144).

In conclusion, we provide the first detailed evidence that Slit ligands and their Robo receptors are present in pancreatic islet cells and define multiple roles for the Slit secreted factors in β-cell physiology. Our results reveal that Slit signalling depletes ER Ca^{2+} and protects β-cells from ER-stress. We identify a role for these paracrine regulators in glucose-

stimulated insulin secretion. Together, our results point to the Slit-Robo pathway and a new area for investigations around β-cell survival and function.

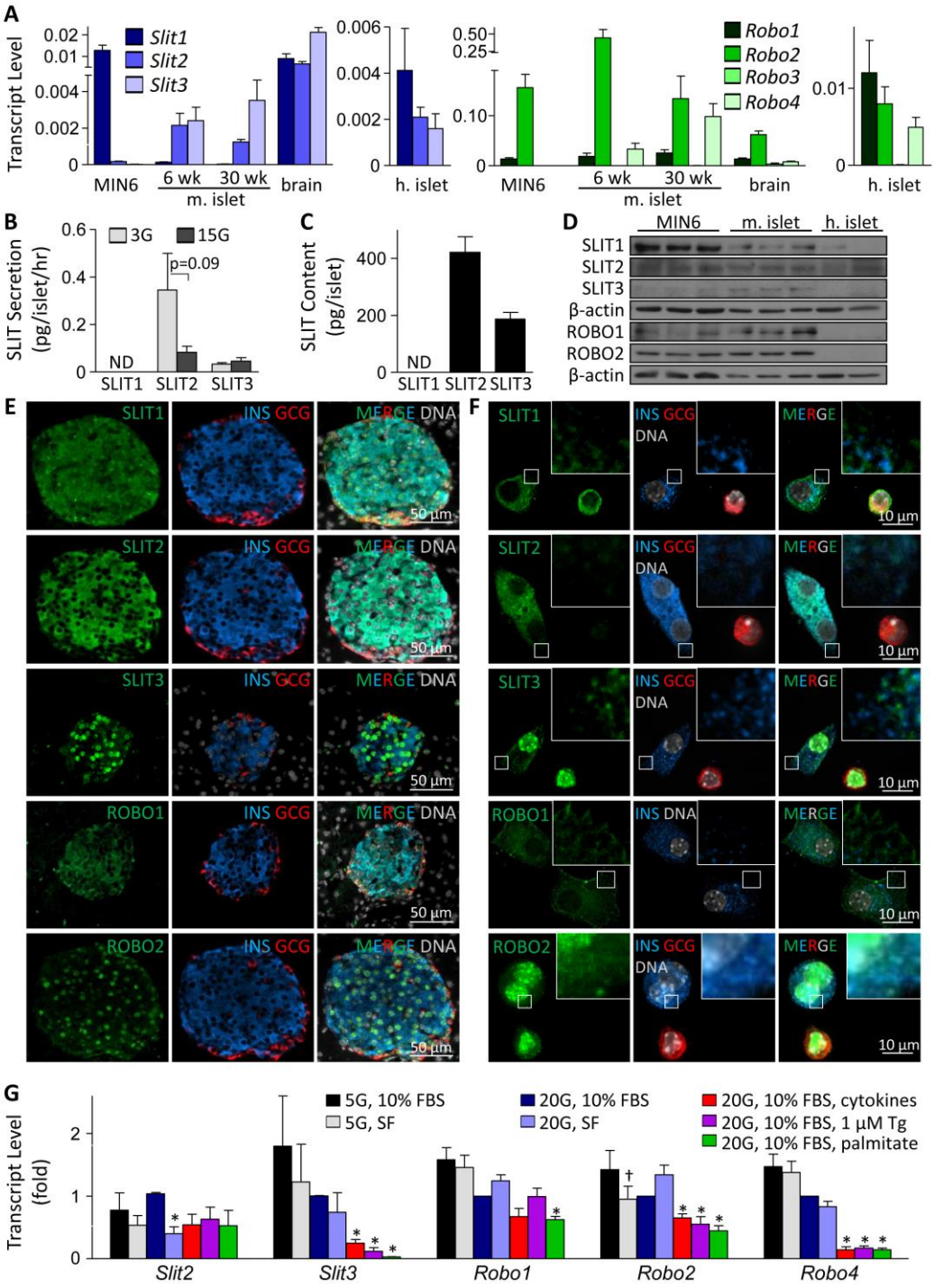

Figure 7-1. Slit-Robo autocrine/paracrine network in pancreatic islet cells.
A. qRT-PCR of Slit and Robo expression in mouse islets, human islets, and MIN6 cells ($2^{-\Delta Ct}$ relative to actin). **B.** SLIT1-3 secretion from mouse islets under 3 mM and 15 mM glucose (n=11) (ND, not detected). **C.** SLIT1-3 protein content in mouse islets (n=11). **D.** SLIT and ROBO immunoblot in MIN6, mouse islet, and human islet lysates. **E-F.** SLIT and ROBO staining in mouse pancreas sections and mouse islet cells. **G.** Slit and Robo expression in mouse islet cells treated with cytokine cocktail (25 ng/ml TNF-α, 10 ng/ml IL-1β, 10 ng/ml IFN-γ), 1 μM thapsigargin (Tg), 1.5 mM palmitate, or 5 mM or 20 mM glucose containing medium supplemented with 10% FBS or under serum free (SF) condition ($2^{-\Delta\Delta Ct}$; n=4, mean ± SEM, * $p<0.05$ compared to 20 mM glucose, 10% FBS; † $p<0.05$ compared to 5 mM glucose, 10% FBS).

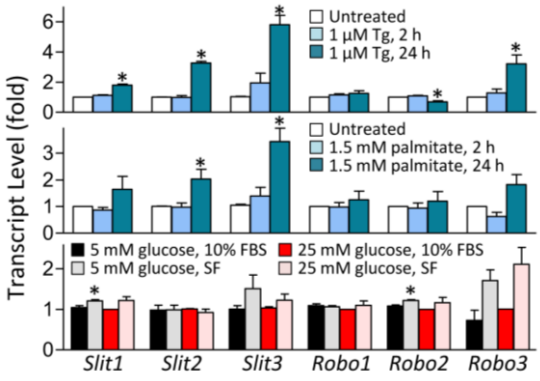

Figure 7-2. Expression of Slit and Robo in MIN6 cells under stress conditions.
Changes in Slit and Robo expression in MIN6 cells treated with 1 μM thapsigargin (Tg), 1.5 mM palmitate, or 5 mM or 25 mM glucose containing medium supplemented with 10% FBS or under serum free (SF) condition. Fold change in transcript level were calculated using $2^{-\Delta\Delta C_t}$ (n=3-4, mean ± SEM, * $p<0.05$ compared to untreated).

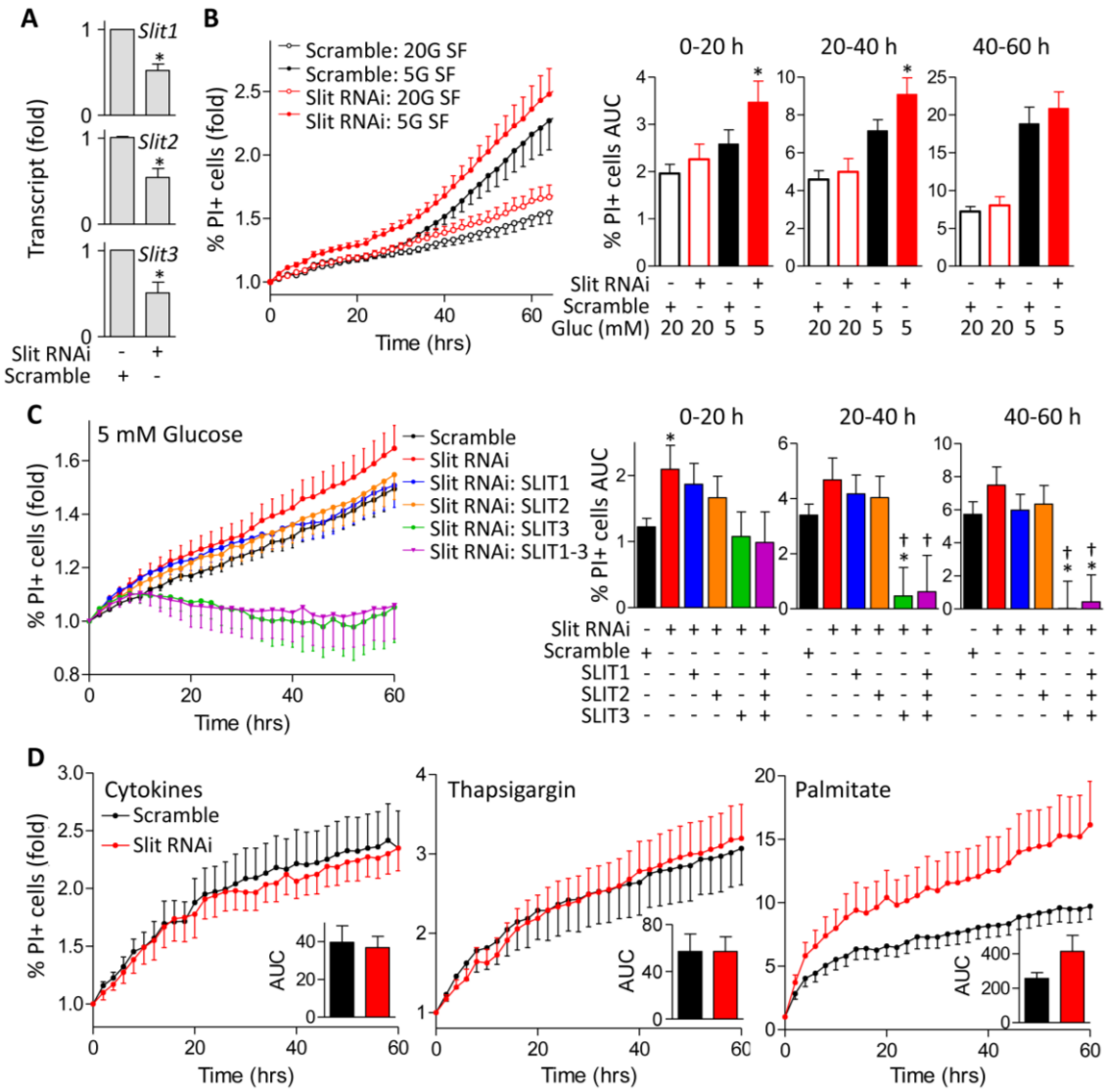

Figure 7-3. Knockdown of endogenous Slits increases cell death.
A. Dispersed mouse islet cells were transfected with siRNA for *Slit1*, *Slit2*, and *Slit3* or scramble siRNA as control, and examined by qRT-PCR after 72 h ($2^{-\Delta\Delta Ct}$; n=6, * p<0.05 compared to control). **B.** Mouse islet cells transfected with Slit siRNAs were stained with 0.05 µg/ml Hoechst and 0.5 µg/ml propidium iodide (PI) 48 h following transfection and imaged. Cells were in serum free (SF) conditions with 20 mM and 5 mM glucose. Percent PI positive cells and area under the curve (AUC) were calculated for indicated time intervals (n=12, * p<0.05 compared to control). **C.** Mouse islet cells transfected with Slit siRNAs were stained and incubated in 5 mM glucose SF conditions supplemented with 10 nM SLIT1-3 (n=10, * p<0.05 compared to scramble control, † p<0.05 compared to Slit knockdown without SLIT supplement). **D.** Mouse islet cells transfected with Slit siRNAs were stained and treated with cytokine cocktail (25 ng/ml TNF-α, 10 ng/ml IL-1β, 10 ng/ml IFN-γ), 1 µM thapsigargin, or 1.5 mM palmitate under 20 mM glucose (n=8-10).

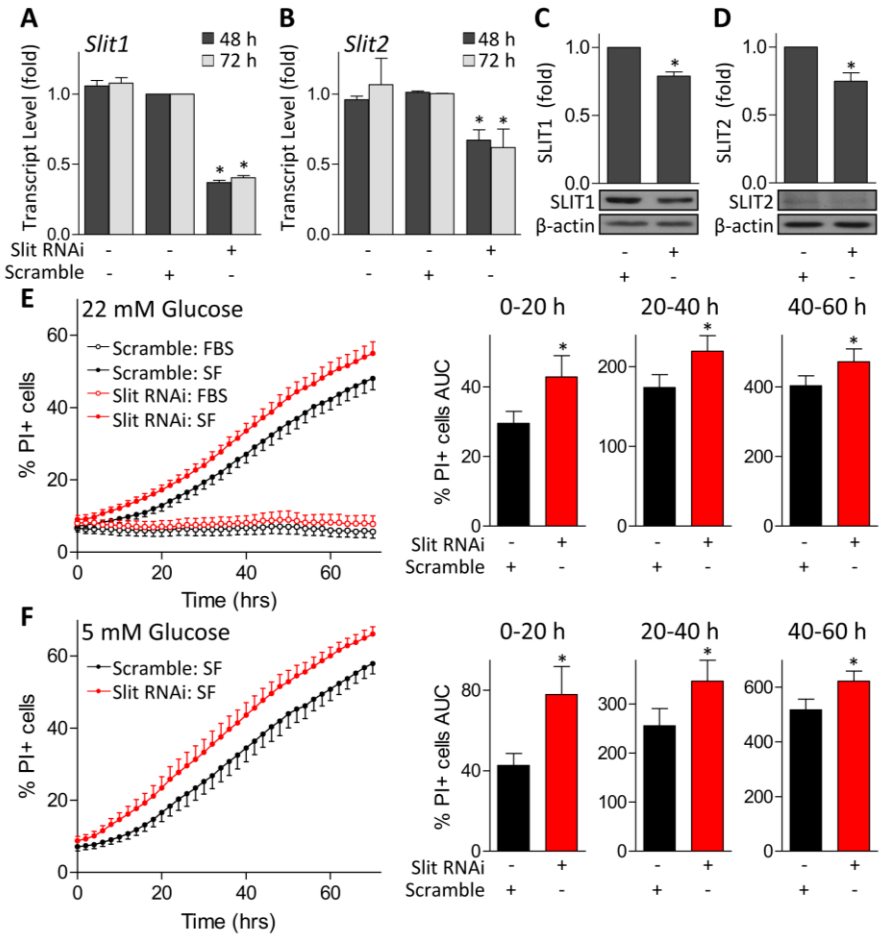

Figure 7-4. Knockdown of endogenous Slits increases MIN6 cell death following serum starvation.
A-B. MIN6 cells were transfected with siRNA for *Slit1*, *Slit2* and *Slit3* or scramble siRNA as control. 48 and 72 h following transfection, the fold change in transcript levels of *Slit1* and *Slit2* were analyzed by qRT-PCR using $2^{-\Delta\Delta C_t}$ (n=5, mean ± SEM, * p<0.05 compared to control at the same timepoint). **C-D.** The protein level of SLIT1 and SLIT2 knockdown was analyzed by immunoblotting 48 h following transfection (n=4-5, mean ± SEM, * p<0.05 compared to control). **E-F.** MIN6 cells transfected with Slit siRNAs were stained with 0.05 µg/ml Hoechst and 0.5 µg/ml propidium iodide (PI) 48 h following transfection. Cells were treated with 22 mM **(E)** and 5 mM **(F)** glucose serum free (SF) conditions and imaged at 37°C and 5% CO_2. The percentage of PI positive cells was determined and area under the curve (AUC) was calculated for the indicated time intervals (n=10, mean ± SEM, * p<0.05 compared to control).

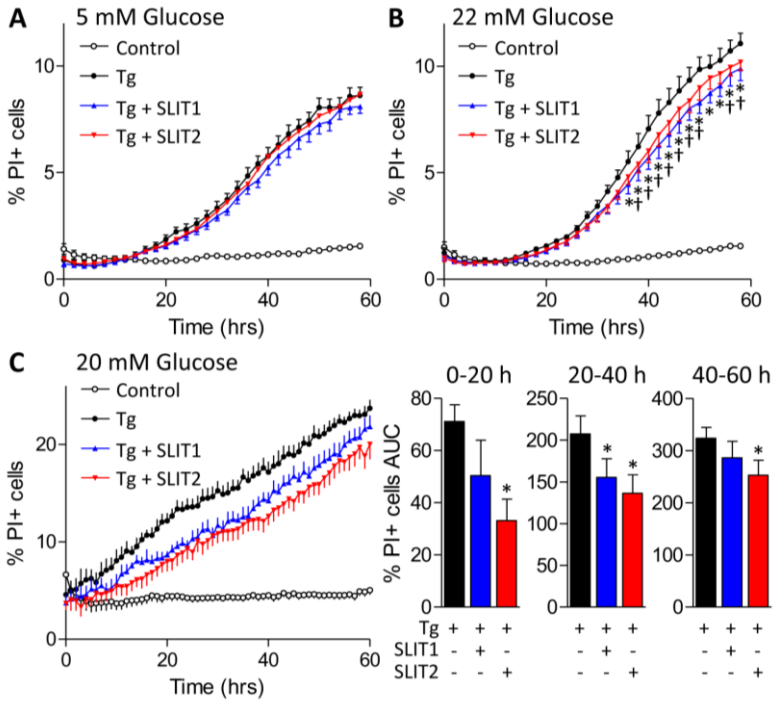

Figure 7-5. Slits reduce ER stress induced β-cell death under high glucose conditions.
A-B. MIN6 cells were stained with 0.05 µg/ml Hoechst and 0.5 µg/ml propidium iodide (PI). Cells were imaged under at 37°C and 5% CO_2. The percentage of PI positive cells was determined following 0.1 µM thapsigargin (Tg) treatments with 10 nM SLIT1 or SLIT2 under 5 mM **(A)** and 22 mM **(B)** glucose conditions with serum (n=14-15, mean ± SEM, * $p<0.05$ Tg + SLIT1 compared to Tg treatment, † $p<0.05$ Tg + SLIT2 compared to Tg treatment at the same timepoint). **C.** Dispersed mouse islet cells were stained with 0.05 µg/ml Hoechst and 0.5 µg/ml PI. Cells were imaged under at 37°C and 5% CO_2. The percentage of PI positive cells was determined following 1 µM Tg treatments with 10 nM SLIT1 or SLIT2 under 20 mM glucose conditions and area under the curve (AUC) was calculated for the indicated time intervals (n=6-8, mean ± SEM, * $p<0.05$ compared to 1 µM Tg or SF treatment).

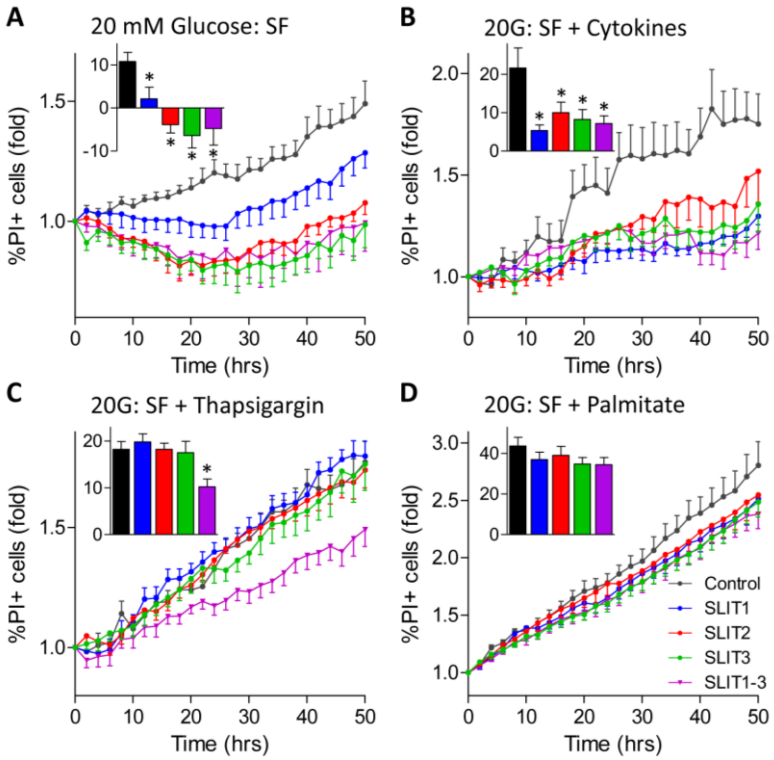

Figure 7-6. Slits reduce stress induced islet cell death under high glucose conditions.
A-D. Dispersed mouse islet cells were stained with 0.05 µg/ml Hoechst and 0.5 µg/ml propidium iodide (PI) and imaged. The percentage of PI positive cells was determined following treatments with 10 nM SLIT1, SLIT2, and/or SLIT3 under conditions of 20 mM glucose serum free **(A)**, 20 mM glucose SF with cytokine cocktail **(B)**, 20 mM glucose SF with 1 µM thapsigargin **(C)**, and 20 mM glucose SF with 1.5 mM palmitate **(D)**. *Inset*, area under the curve was calculated for the 50 h time course (n=8, * $p<0.05$ compared to untreated control).

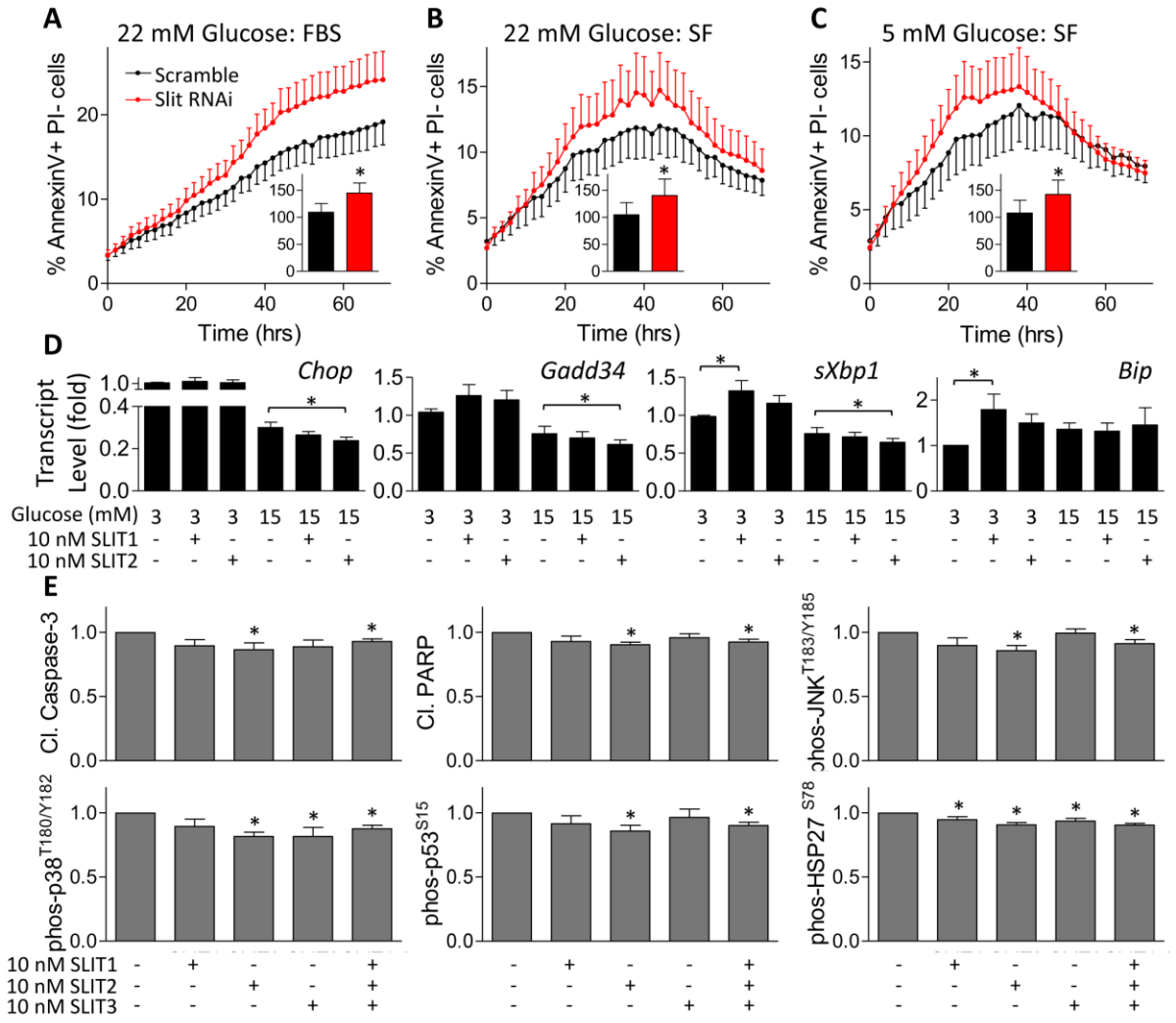

Figure 7-7. Slits down-regulate pro-apoptotic and ER-stress signalling.
A-C. MIN6 cells transfected with *Slit1*, *Slit2*, and *Slit3* siRNAs were stained with 0.05 µg/ml Hoechst, 0.5 µg/ml propidium iodide (PI), and AlexaFluor647 conjugated annexinV 48 h following transfection. Cells were cultured in 22 mM **(A,B)** and 5 mM **(C)** glucose conditions in the presence or absence of FBS and imaged. Area under the curve between 20 to 40 h is displayed in the insets. (n=10, * $p<0.05$ compared to scramble siRNA control). **D.** Mouse islet cells were treated with SLIT1 or SLIT2 for 4 h prior to RNA isolation and qRT-PCR analysis ($2^{-\Delta\Delta Ct}$; n=8, * $p<0.05$). **E.** Mouse islet cells were treated with SLIT1-3 under 20 mM glucose serum free condition. Immunoassay for protein levels of cleaved caspase-3, cleaved PARP, phospho-JNK, phospho-p38, phospho-p53, and phospho-HSP27 (n=6-8, * $p<0.05$).

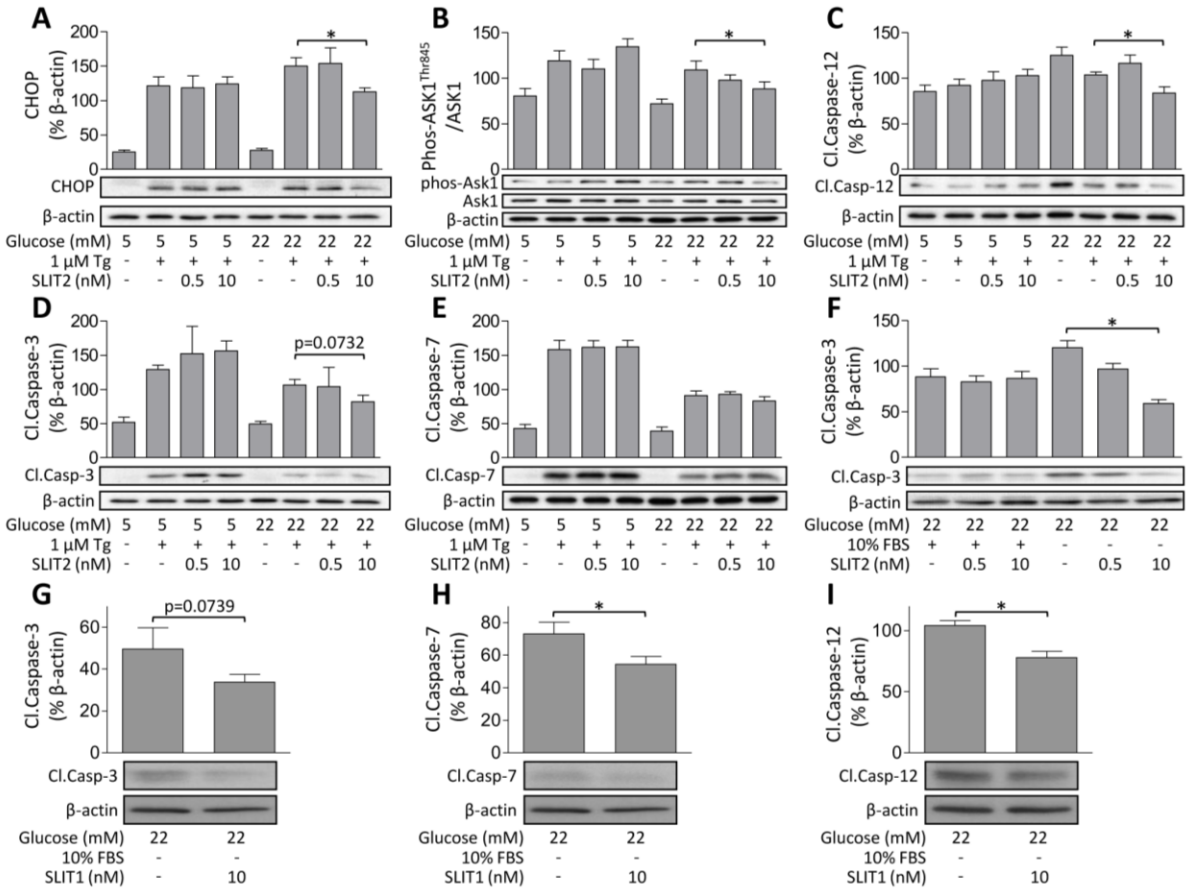

Figure 7-8. Slits can down-regulate pro-apoptotic and ER-stress signalling in MIN6 cells.
A-F. MIN6 cells were treated with 1 μM thapsigargin (Tg) in the presence or absence of SLIT2. Immunoblotting for protein levels of CHOP **(A)**, ASK1 **(B)**, Cl. Caspase-12 **(C)**, Cl. Caspase-3 **(D)**, and Cl. Caspase-7 **(E)** (n=7, mean ± SEM, * $p<0.05$). **F.** MIN6 cells were cultured in serum containing or serum free conditions in the presence or absence of SLIT2. Immunoblotting for Cl. Caspase-3 (n=4-7, mean ± SEM, * $p<0.05$). **G-I.** MIN6 cells were cultured in serum free conditions in the presence or absence of SLIT1. Immunoblotting for Cl. Caspase-3 **(G)**, Cl. Caspase-7 **(H)**, and Cl. Caspase-12 **(I)** (n=6-7, mean ± SEM, * $p<0.05$).

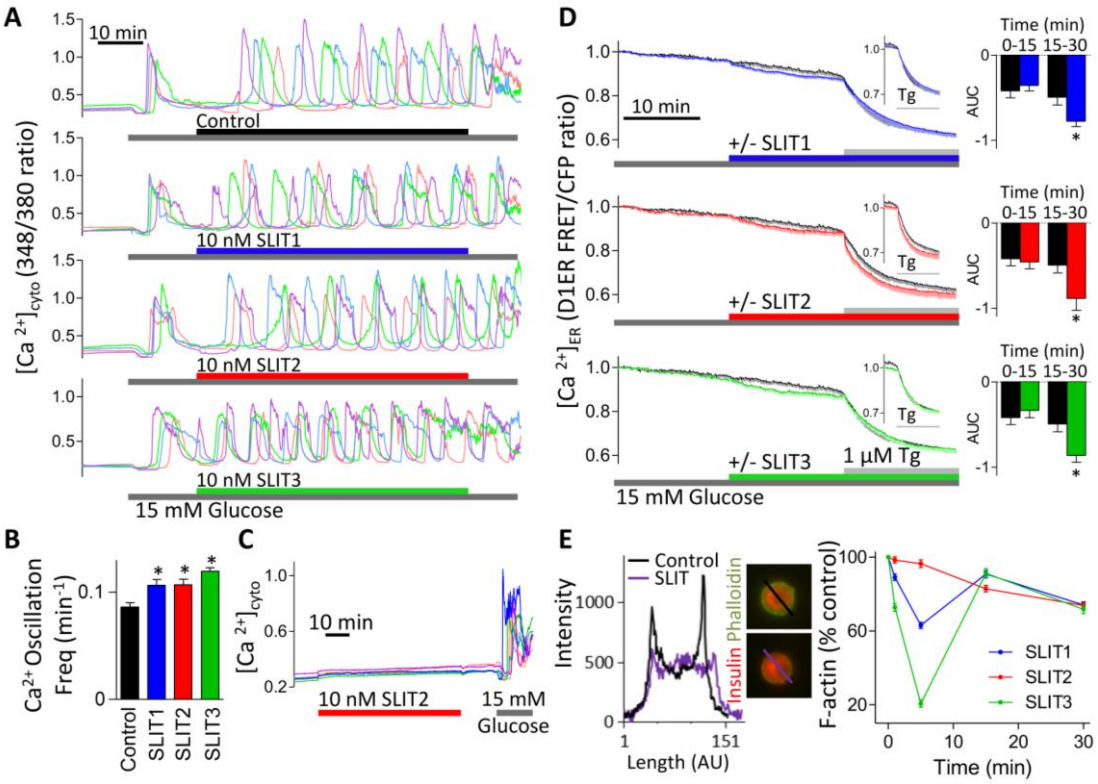

Figure 7-9. Slits modulate cytosolic Ca^{2+} and ER Ca^{2+} signalling and actin remodelling.
A-C. Dispersed mouse islet cells were loaded with Fura-2-AM. Representative single cell traces following exposure to 10 nM SLIT1, SLIT2, or SLIT3 under 15 mM glucose condition **(A)**. Single cell oscillation frequency of cytosolic Ca^{2+} level was calculated (n=91-104, * $p<0.05$) **(B)**. Representative single cell traces following exposure to 10 nM SLIT2 under 3 mM glucose condition **(C)**. **D.** Dispersed mouse islet cells were transfected with D1ER cameleon to image ER Ca^{2+}. Cells were exposed to 1 µM thapsigargin (Tg) 15 min following treatment with 10 nM SLIT1, SLIT2, or SLIT3 (colored lines) or untreated (black line) under 15 mM glucose (n=13-14). Inset, D1ER FRET/CFP ratios normalized to the timepoint following Tg addition. *Right panel:* Area under the curve (AUC) for the 15 min pre-incubation with 15 mM glucose and 15 min treatment with SLIT1-3 was determined (n=13-14, * $p<0.05$ compared to untreated). **E.** Mouse islet cells were treated with 10 nM SLIT1, SLIT2, or SLIT3 in 11 mM glucose containing RPMI. β-cells were stained for insulin and phalloidin and peak intensity of cortical F-actin staining was normalized to untreated cells at the same timepoint (n=39-60 cells).

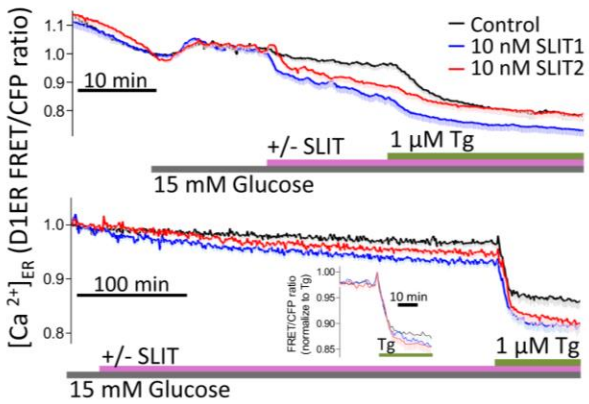

Figure 7-10. Slits can modulate ER Ca^{2+} signalling in MIN6 cells.
MIN6 cells were transfected with D1ER cameleon and ER Ca^{2+} level was imaged. *Top panel:* Cells were exposed to 1 µM thapsigargin (Tg) 15 min following treatment with 10 nM SLIT1 or SLIT2 under 15 mM glucose (n=24-28, mean ± SEM). *Bottom panel:* Cells were exposed to 1 µM Tg 6 h following treatment with 10 nM SLIT1 or SLIT2 under 15 mM glucose (D1ER FRET/CFP ratios were normalized to ratio at 1st timepoint; n=28-41, mean ± SEM).

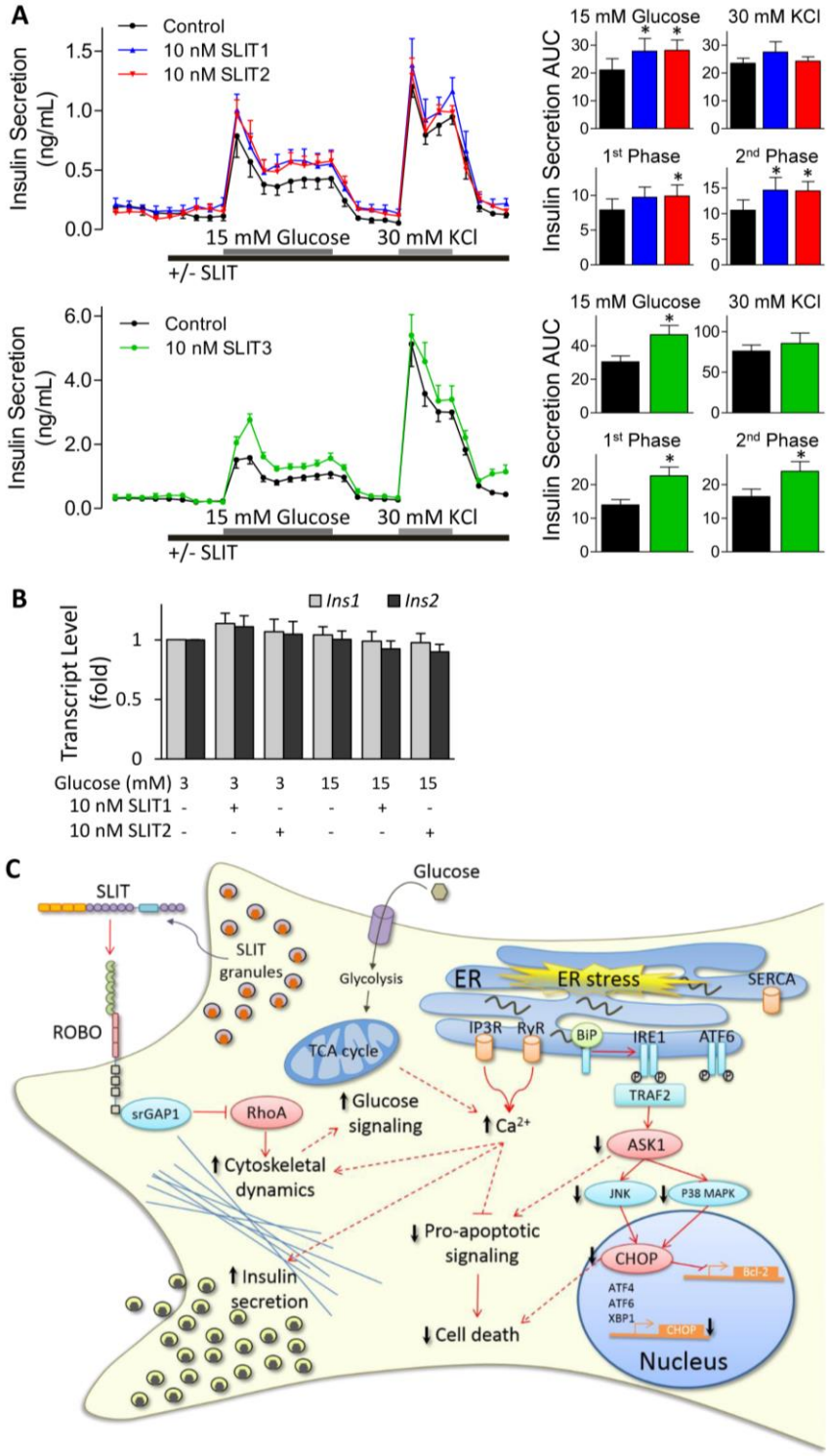

Figure 7-11. Slits modulate insulin secretion.
A. Mouse islets were perifused with KRB buffer containing 3 or 15 mM glucose in combination with 10 nM SLIT1, SLIT2, or SLIT3 (n=5-6). *Right panel:* Baseline subtracted area under the curve (AUC) for the 15 mM glucose stimulated and KCl stimulated insulin secretion, along with 1st phase and 2nd phase glucose stimulated insulin secretion are shown. (n=5-6, * $p<0.05$ compared to control). **B.** Mouse islet cells were treated with SLIT1 or SLIT2 for 4 h prior to RNA isolation. qRT-PCR analysis of *Ins1* and *Ins2* were expressed as fold change using $2^{-\Delta\Delta Ct}$ calculations (n=8, mean ± SEM). **C.** Model of Slit-Robo signalling in β-cells.

Chapter 8: High-throughput, live-cell imaging identifies stress-specific and general islet cell survival factors

8.1 Introduction

The loss of functional β-cell mass is a critical event in the pathogenesis of diabetes and it severely limits the success of therapies such as islet transplantation (276-278). The identification of new factors with direct protective effects on β-cells would represent an important breakthrough for diabetes cell therapy and represent a critical step towards *in vivo* β-cell protection and regeneration therapies. Significant research has been aimed at discovering β-cell survival factors, but this has typically been conducted one-at-a-time and limited by prior knowledge of β-cell survival pathways (100, 144, 279). Currently, glucagon-like peptide 1 (GLP-1) is widely considered to be the gold standard for β-cell protective factors (103), and it has been shown to activate the anti-apoptotic transcription factor Pdx1 (280). Although local transgenic over-expression of GLP-1 increases islet transplant success in an animal model (104), strong clinical evidence to support its efficacy to durably increase β-cell mass is lacking. Autocrine insulin signalling has also been shown to play protective roles *in vitro* and *in vivo* (143, 144, 270), but therapeutic approaches for its specific manipulation in the islet have not been validated. Clearly, there is an unmet need to identify more robust β-cell survival factors.

The *in vitro* and *in vivo* pro-survival effects of candidate growth factors supports the feasibility of harnessing pro-survival factor signalling pathways activated by endogenous hormones and growth factors for the prevention of β-cell death caused by stresses associated with isolation, culture, transplantation, and diabetes. In Chapter 5, our efforts to identify novel factors with sustained anti-apoptotic effects that exceed the current candidates led us to characterize and mine for locally acting pro-survival factors in the islet secretome, which includes at least 200 expressed soluble factors (109). In Chapters 6 and 7, our initial analyses of novel candidates revealed glucose-dependent protective roles for Netrin and Slit/Robo (109, 281). However, without an unbiased, side-by-side comparison, it is impossible to determine the relative merits of each candidate factor. In Chapter 3 and 4, we developed and validated high-throughput, live-cell imaging methods that allow the effects of hundreds of factors on multiple cell death parameters to be simultaneously evaluated in cultures of dispersed primary islet cells (114).

Here, we detail the identification of both stress-specific and general pro-survival factors from high-throughput studies, replicated under 5 distinct stress conditions employing a curated library of 206 endogenous soluble factors, the vast majority of which were recombinant proteins. Our high-content, automated live-cell imaging platform enabled the identification of dozens of factors with previously unreported, potent pro-survival effects that exceeded the protection observed with 'gold-standard' factors. Remarkably, each stress condition was associated with a unique set of protective factors, consistent with fundamental mechanistic differences in the cell death pathways associated with these 5 stresses. Our data represent the first systems-level evidence that specific factors are required to protect primary β-cells from specific cellular stresses associated with different types of diabetes and stages of the diseases. These findings have important implications for the development of β-cell protective and regenerative therapies.

8.2 Results

8.2.1 Identification of generalized and stress-specific islet cell survival factors

We set out to identify endogenous soluble factors that directly promote survival under 5 controlled stress conditions in dispersed mouse islet cells. Islet cells isolated from mice were chosen as a model because of their reproducibility and low baseline rates of apoptosis, relative to cultured human islet cells where the *in vitro* rates of cell death can more variable between batches. In the basal condition, dispersed mouse islet cells were cultured in the absence of serum and in 5 mM glucose. In the context of this serum-starved basal condition, we added a cytotoxic cytokine cocktail of IL-1β, TNF-α and IFN-γ meant to model the autoimmune attack in type 1 diabetes (282), thapsigargin to induce ER-stress that is a component of β-cell loss in both type 1 and type 2 diabetes (276, 283), palmitate to model lipotoxicity in type 2 diabetes (115, 283), or high glucose to model late-stage diabetes (277). The cells were concurrently treated with a library of 206 recombinant factors compiled using our previous bioinformatics analysis of islet cell ligands and receptors (109), along with candidates from the literature (Fig. 8-1A). We measured the accumulation of propidium iodide (PI) positive cells as an index of cell death. This captures multiple forms of cell death, including the 'partial apoptosis' that we recently demonstrated is the predominant mode of death in cultured primary β-cells (114). The results of these studies were visualized as heat maps of PI-positive cells over the 0-24 and 24-

48 hour time intervals and revealed both pro-survival and pro-death factors within our library of endogenous biologic factors. Overall, there was strong agreement between the replicate experiments (Fig. 8-2A-F). As expected, our positive control (10% FBS, presumably containing high concentrations of many factors) was ranked 1st under every condition, except ER-stress where it was ranked 2nd. Parallel assessment of the effect of 206 factors on PI incorporation in primary β-cells subjected to 5 stress conditions revealed factors with generalized survival effects, such as melanin-concentrating hormone (MCH), adiponectin (ACRP30), vasoactive intestinal peptide (VIP), semaphorin 3C (SEMA3C), secretin (SCT), indian hedgehog (IHH), β-melanocyte stimulating hormone (β-MSH), neuroligin 4 (NLGN4), neuroligin 1 (NLGN1), and angiopoietin 2 (ANGPT2) (Fig. 8-2A). This list of pan-protective 'hits' included factors that were ranked amongst the top 10 most potent survival factors under one or more conditions, along with those displaying moderate but consistent effects across all conditions. Resorting of these PI incorporation data revealed that each stress had a specific complement of pro-survival factors, with the top 3 protective factors being unique for each stress (Fig. 8-2B-F). Our analysis also revealed that some stress conditions were more resistant to protection than others (Fig. 8-2B-F). For example, only 18 factors provided any protection of islets cells from palmitate above the negative PBS control, with the rest of the factors being neutral or exacerbating lipotoxic cell death (Fig. 8-2F). On the other hand, more than half of the factors provided some protection in the context of ER-stress induced by a moderate dose of thapsigargin. The majority of the protective factors found across all stresses have not been previously characterized in the context of β-cell survival.

8.2.2 Multi-parameter analysis for improved identification of stress-specific survival factors

An advantage of high-content, image-based analysis is the ability to simultaneously assess multiple parameters for internal validation, which reduces the number of false positives and false negatives. Automated stages and environmental control permit cells to be continuously imaged for days, allowing for temporal analysis. When pro-survival effects were ranked based on the loss of Hoechst-positive cells and the accumulated PI positive cells in each time frame, pro-survival factors that were not originally ranked in the top 10 based on PI incorporation alone became evident (Fig. 8-1 to 8-6). There was generally good agreement

between the measurements of cell loss and PI incorporation (Fig. 8-1, 8-3 to 8-6), although some divergence would be expected if specific factors modified the adhesion of dead or dying cells. The number of early apoptotic, annexinV-positive and PI-negative cells was also analyzed, but as we have recently reported these are relatively rare and their analysis is less informative (114). Although the annexinV-positive and PI-negative cell measurements were not reliable in terms of identifying the overall protectiveness of the factors, they may be useful in identifying factors that can specifically modulate purely apoptotic cell death.

Multi-parameter analysis was performed for each of the 5 stress conditions (Fig. 8-1, 8-3 to 8-6). As noted above, this analysis also showed that there was little overlap between the top-ranked survival factors found for each of the 5 stress conditions (Fig. 8-1 to 8-6). For example, the Tie2-antagonist angiopoietin-2 (284) had strong protective effects in the low glucose serum-starved condition and in the presence of cytotoxic cytokines, but negligible protective effects under all other conditions tested (Fig. 8-1, 8-2). Oncostatin M (OSM), from the cytokine family that includes LIF, G-CSF and IL-6 (285), was protective in context of both thapsigargin and high glucose, but not in the context of low glucose serum withdrawal and the toxic cytokine cocktail. Members of the neuroligin family, including NLGN1 and NLGN4, displayed potent protection under all conditions except the toxic cytokine cocktail (Fig. 8-1, 8-3 to 8-6). Comparison across the different stress conditions also revealed factors that were pro-survival under one condition, but pro-death under other conditions. For example, semaphorin 4A (SEMA4A), known for its roles in axon guidance, morphogenesis, carcinogenesis, and immunomodulation (286), was the 2nd highest ranked protective factor in the context of palmitate lipotoxicity, but it promoted cell death under all other conditions tested, including the baseline serum-free condition where it was the most toxic factor (Fig. 8-1, 8-3 to 8-6). Through comparison across different stress conditions, we can eliminate factors with any adverse effects on cell survival, which may not be suitable targets for broad therapeutic development.

8.2.3 Time and concentration dependence of β-cell survival factors

We next compared the concentration dependent effects of each factor on cell survival under 5 mM serum free conditions (Fig. 8-7). We observed some factors that showed classical concentration-dependent effects. However, other factors exhibited bell-shaped survival curves,

a phenomenon we have previously observed with insulin (144, 240). Temporal analysis revealed that some factors showed protective effects throughout the entire time course, while others were highly protective only at the early time points and display rapid cell death at the later time points. This can be observed when the increase in the percentage of PI positive cell were displayed over time and when the same results were integrated for two time intervals, 0-24 and 24-48 h (Fig. 8-1, 8-3 to 8-7). For example, serotonin (5-HT) protected β-cells from serum starvation between 0-24 h, but not at the later time interval. It remains to be determined whether the factors were rapidly degraded following treatment or whether the cells displayed receptor desensitization in these cases.

When the survival effects of the factors were analyzed at both the 0.1 nM and 10 nM concentrations, some factors that were not originally seen as highly protective when given in moderate concentrations, were shown to have efficacy at the lower concentrations (Fig. 8-8). For example, cryptic family 1 (CFC1), γ-MSH, somatostatin (SST), ephrin-B2 (EFNB2), and insulin (INS) were ranked with higher protective effects when both the low and moderate concentrations were taken into consideration. Identifying factors with effective pro-survival effects under lower concentrations is important for therapeutic development because low effective concentrations can help reduce the incidence of off target effects.

8.2.4 Classification of survival factors by signal transduction pathways

Analysis of the canonical signalling pathways stimulated by the protective factors revealed that pro-survival signalling could be mediated by a number of known pathways, including JAK-STAT cytokine receptors, G-protein coupled receptors, tyrosine kinase receptors, serine/threonine kinase receptors, and axon guidance receptors (Fig. 8-9A,B). These analyses revealed that specific signalling pathways were more important in the context of certain stresses, relative to others. In the baseline serum withdrawal condition, factors that stimulate phospholipase C and/or the activation of adenylyl cyclase tended to be protective, whereas factors that inhibit adenylyl cyclase were less effective. In the context of programmed cell death induced by thapsigargin or palmitate, activation of adenylyl cyclase was identified as the predominant pro-survival G-protein-mediated pathway. We have previously implicated netrin-unc5/neogenin and slit-robo signalling in promoting β-cell survival (109, 281). Our current studies revealed that in addition to netrin and slit signalling, other factors involved in

axon guidance and synapse formation including semaphorins, neuroligins, and ephrins also promote survival. Some members of each axon guidance family also promoted cell death, indicating a bifurcation point in these signalling pathways, or perhaps a complex dose-response relationship. Further characterization of specific signalling cascades that are stimulated in the islet cells is necessary for deciphering the key pathways necessary for promoting survival.

8.2.5 Context-dependent effects on chronic insulin release

We also assessed insulin accumulation in the media, initially as an ancillary index of β-cell survival and function. We identified factors that promoted both survival and insulin release, including angiopoietin 2 in the 5 mM glucose serum-free condition (Fig. 8-1C). In such cases, our current data do not allow us to distinguish whether the survival effects were due to insulin independent survival signalling or pro-survival autocrine insulin signalling (143, 144). Other factors were protective, while at the same time inhibiting insulin secretion in the context of basal glucose (e.g. melanin concentrating hormone, Fig. 8-3B). It is known that inhibition of calcium fluxes can protect β-cells under specific conditions (74, 76), while these same manipulations block insulin secretion (150). We also detected factors, such as semaphorin 4A, that triggered cell death and increased insulin in media, likely secondary to the loss of cell integrity (Fig. 8-1C, 8-3B). The effects of soluble factors on insulin secretion were highly context dependent. Analysis of insulin secretion was not a primary endpoint in the present study, although these data nonetheless provide a starting point for additional detailed studies.

8.3 Discussion

The goal of the present study was to compare the effects of hundreds of putative β-cell survival factors, under multiple-stress conditions, using a newly developed multi-parameter, kinetic cell death imaging platform. We found dozens of previously unappreciated factors that can act directly to protect islet cells with improved efficacy when compared to previously reported factors. A principal observation of our study was that each cellular stressor examined requires its own unique set of protective factors. This observation has significant implications for the understanding of the molecular mechanisms controlling β-cell fate and for the

development of therapeutic approaches to prevent or treat type 1 diabetes or type 2 diabetes at various disease stages.

The activation or mimicking of local autocrine and/or paracrine survival factor signalling present within the islets may be the most ideal scenario for diabetes prevention strategies or therapies. The localized microenvironment of endogenous autocrine/paracrine signalling factors may eliminate or reduce effects on peripheral tissues. Many local factors act on self-limiting feedback mechanisms that prevent over-stimulation. Insulin, for example, has been shown to be a potent and self-limiting islet survival factor and physiological doses of insulin can increase β-cell proliferation (38, 143, 287). However, the search for other potent survival factors not involved in the regulation of metabolic pathways is needed. Several growth factors critical for pancreatic development can be found in the literature, including notch ligands, transforming growth factor-beta superfamily, fibroblast growth factors, bone morphogenic proteins and others (288-290); however, their functions in adult islets exposed to varying stress conditions are less well understood (37, 138). Nonetheless, we cannot overlook the potential importance of distally secreted endocrine factors acting to promote β-cell survival and function, including adipokines such as adiponectin.

The specific autoimmune destruction of pancreatic β-cells in type 1 diabetes by pro-inflammatory cytokines (TNF-α, IL-1β, IFN-γ) released from infiltrating T-cells (2, 11), leads to an almost complete ablation of functional β-cell mass (12, 13). Studies have also implicated ER-stress in β-cell death associated with type 1 diabetes (291). Thus, it is likely that factors showing protection in both of these conditions, such as vasoactive intestinal peptide, semaphorin 6A and urocortins may be of therapeutic value in type 1 diabetes. In type 2 diabetes, excessive fatty acid exposure associated with obesity and endoplasmic reticulum stress act through several common pathways to increase β-cell death following the initial compensation phase (11, 115, 292). These stresses had in common protection from the neuroligin family and the FGF family. Notably, the known anti-apoptotic incretin, glucose-dependent insulinotropic factor (279), was more protective in the context of lipotoxicity relative to the other stresses. Persistent hyperglycemia present in poorly controlled type 1 or type 2 diabetes induces further β-cell apoptosis (30-32) and factors such as oncostatin M and growth differentiation factor-15 may be candidates for adjunct or second-line treatments. Glial-derived neurotropic factor, which protected in the context of lipotoxicity and hyperglycemia,

would be predicted to protect islets cells against glucolipotoxity. Some factors promoted survival under only one condition and were actually strongly pro-death under all other conditions. The most striking of these were the palmitate-specific pro-survival effects of semaphorin 4A and olfactomedin-1, and we suggest that they would not make good therapeutic targets owing the presence of multiple β-cells stresses *in vivo*.

In addition to the discovery of stress-specific islet cell survival factors, our analysis also enabled the identification of factors with generalizable pro-survival effects across different diabetic stress conditions. In our hands, the most broadly effective protective factors were melanin-concentrating hormone, vasoactive intestinal peptide, and adiponectin. Melanin-concentrating hormone plays a role in obesity and has been previously implicated in islet growth (293). Vasoactive intestinal peptide is a member of the glucagon superfamily with known effects on the potentiation of insulin secretion (294). Adiponectin is an insulin sensitizing adipokine that protected β-cells against multiple stresses in our hands and in other studies (295-298). There is evidence that the anti-apoptotic effects of adiponectin do not extend to all cell types (299), suggesting a degree of β-cell specificity.

Virtually all of what is known about endogenous factors that can protect pancreatic β-cells is known from candidate studies. GLP-1 is often considered to be a 'gold standard' pro-survival factor for β-cells. However in our hands, there were dozens of factors that were more effective. It is notable, however, that a dual agonist for the GLP-1 and glucagon receptors, oxyntomodulin, displayed protective effects under multiple stresses, including the cytokine cocktail. Other factors modulating the G-protein-coupled receptor pathways also displayed protective effects under specific conditions, including proopiomelanocortin derived peptide hormones β-melanocyte-stimulating hormone, γ-melanocyte-stimulating hormone, and β-endorphin. Based on 24-48 hour PI incorporation, GIP provided strong protection in the context of palmitate and marginal protection from cytokines, but it was not effective in basal serum-free conditions (5 or 20 mM glucose) or in cells treated with thapsigargin. Additionally, factors that could modulate the JAK-STAT, tyrosine kinase, serine/threonine kinase, and axon guidance signalling pathways were also found to protect islet cells. Thus, our current data suggests that a large number of signalling pathways contribute to β-cell survival under specific stress conditions.

Our findings complement previous studies on the pro-survival signalling mediated by axon guidance factors, netrins and slits (109, 281), and emphasize the role of modulating actin dynamics on β-cell survival. In yeast, it has been demonstrated that increasing F-actin turnover leads to increased cell viability due to decreased ROS release from mitochondria (274). In Jurkat cells, overexpression of gelsolin, which mediates actin reorganization in response to changes in calcium and phosphoinositides, can inhibit apoptosis by blocking loss of mitochondrial membrane potential and inhibiting caspase activation (300, 301). Given that we observed strong protective effects of slits, neuroligins, and semaphorins, in our parallel comparisons, it is conceivable that modulating the actin cytoskeleton can have effects on both insulin secretion and cell survival, in addition to their known roles in β-cell development and pancreas morphogenesis (290).

Collectively, our unbiased, highly parallel analysis of endogenous soluble factors identified dozens of hormones/cytokines/growth factors with robust pro-survival effects on pancreatic β-cells under 5 specific stress conditions designed to model aspects of type 1 diabetes and type 2 diabetes. Perhaps the most important finding was that β-cells were best protected from each specific stress condition by a unique set of factors. This observation provides important mechanistic insight into the complexity of β-cell survival signalling pathways and guides therapeutic efforts to protect β-cells.

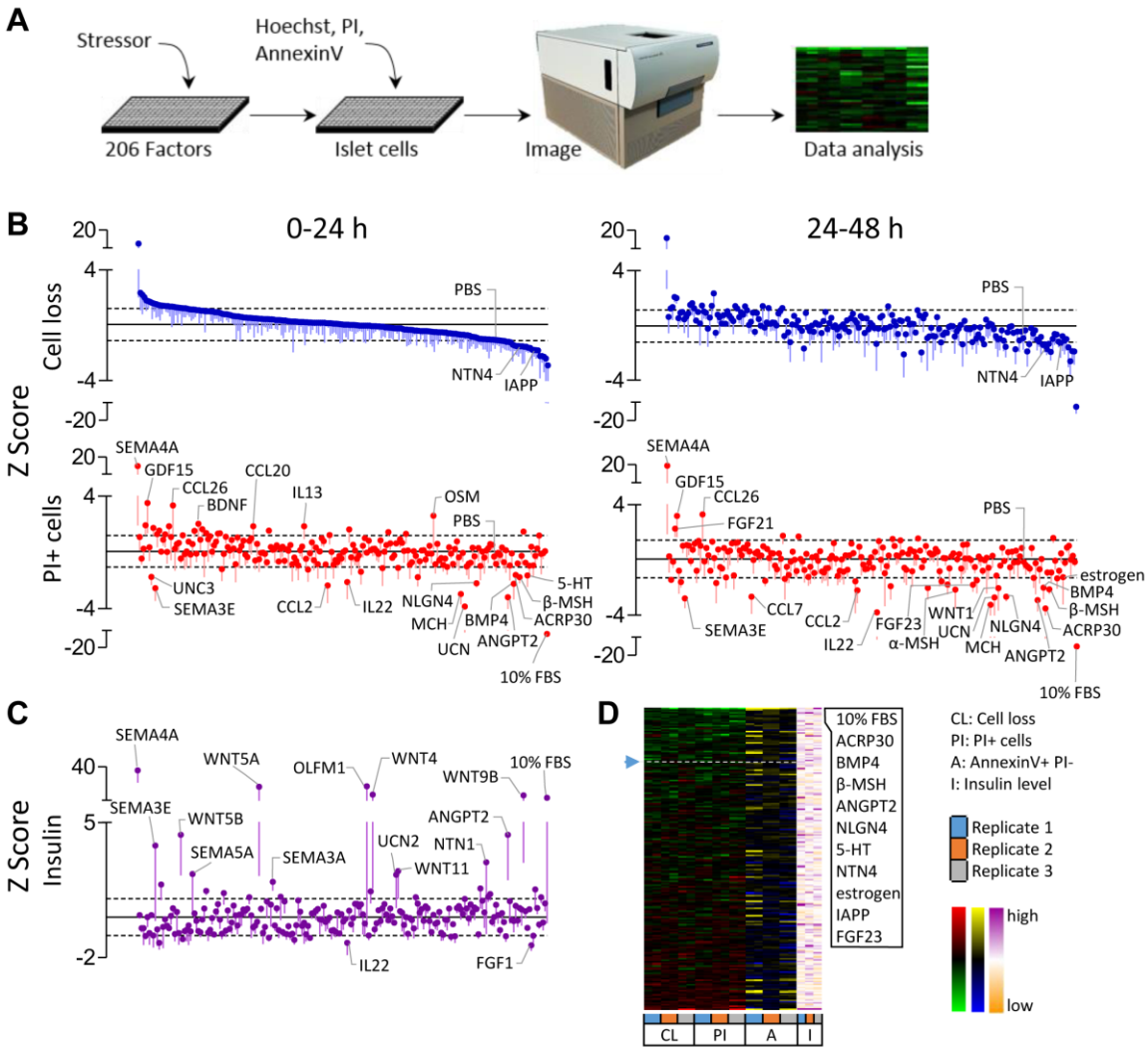

Figure 8-1. Factors protecting islet cells from death induced by serum starvation.
A. Schematic of high-content screening workflow. **B.** Dispersed mouse islet cells were imaged and the level of cell loss and percentage of PI positive cells were determined following treatments with a library of 206 factors (10 nM each) under 5 mM glucose serum-free conditions. 10% FBS was used as positive pro-survival control. Data are presented as robust z-scores for the 0-24 and 24-48 h time intervals after ordering based on the level of cell loss in the 0-24 h dataset (n=3, mean ± SEM). Solid lines represent the median and dotted lines represent ± (2*MAD). **C.** The level of insulin in the culture media collected 72 h following the treatments was determined (n=3, mean ± SEM). **D.** Factors were ranked based on low cell loss and low PI+ cell number (green-red heat maps). Here and elsewhere, AnnexinV+PI- cells are shown with blue-yellow heat maps, and insulin with orange-purple heat maps. The arrow and dotted line indicates the relative ranking of the PBS control. The top 10 most protective factors under each condition are listed in the callout.

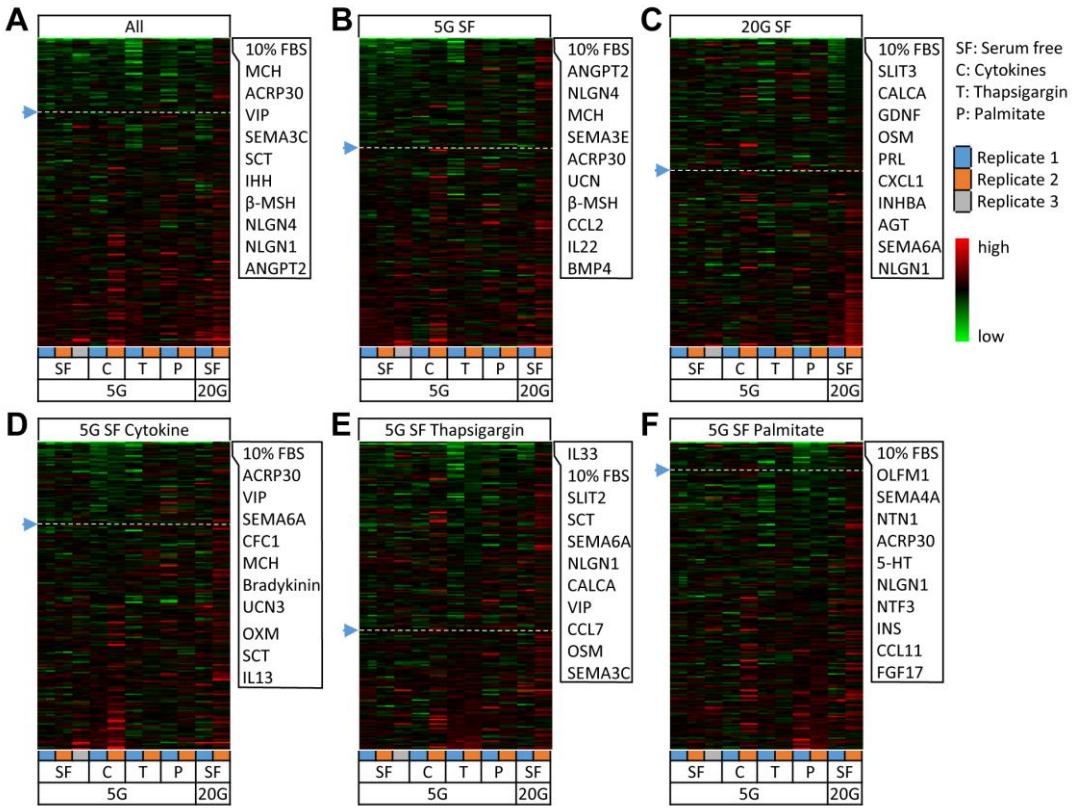

Figure 8-2. Multiple factors display stress specific protective effects.
A-F. Dispersed mouse islet cells were stained and imaged. The percentage of PI positive cells was determined following treatments with a library of 206 factors at 10 nM each. Cells were concurrently exposed to one of five stress conditions, including 20 mM glucose serum-free (SF), and 5 mM glucose SF only and in combination with a cytokine cocktail (25 ng/ml TNF-α, 10 ng/ml IL-1β, 10 ng/ml IFN-γ), 1 μM thapsigargin, and/or 1.5 mM palmitate. 10% FBS was used as positive control for unstressed cells. Data are presented as robust z-scores for the 0-24 hand 24-48 h time intervals for each replicate experiment. The factors were ranked for their protective effects (low levels of PI+ cells equates to high protection) based on the stress treatments indicated at the top of each heat map. The arrow and dotted line indicates the relative ranking of the PBS control. The top 10 most protective factors under each condition are listed in the callout.

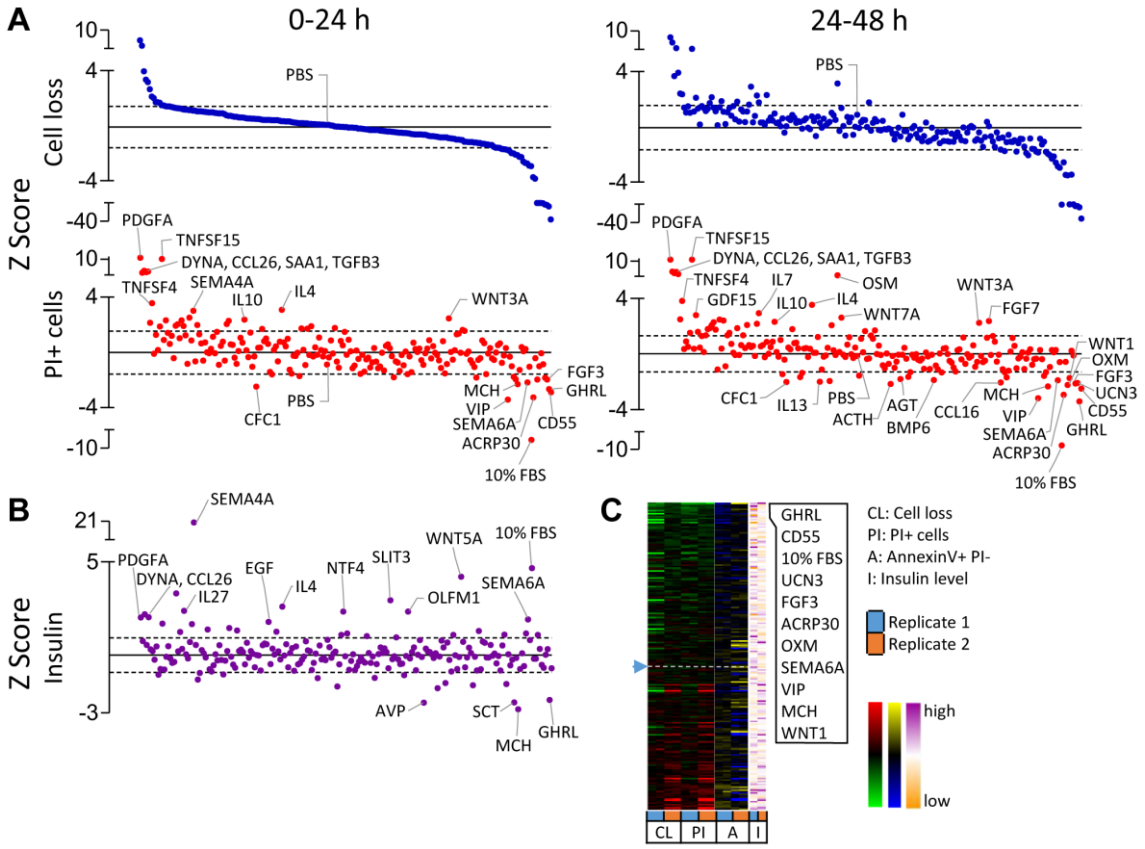

Figure 8-3. Factors protecting islet cells from death induced by toxic cytokines.
A. Dispersed mouse islet cells were imaged and the level of cell loss and percentage of PI positive cells were determined following treatments with a library of 206 factors (10 nM each) in the context of cytotoxic cytokine treatment in 5 mM glucose serum free conditions. Data are presented as robust z-scores for the 0-24 and 24-48 h time intervals after ordering based on the level of cell loss in the 0-24 h dataset (n=2, mean). Solid lines represent the median and dotted lines represent ± (2*MAD). **B.** The level of insulin in the culture media collected 72 h following the treatments was determined (n=2, mean). **C.** Factors were ranked based on low cell loss and low PI+ cell number.

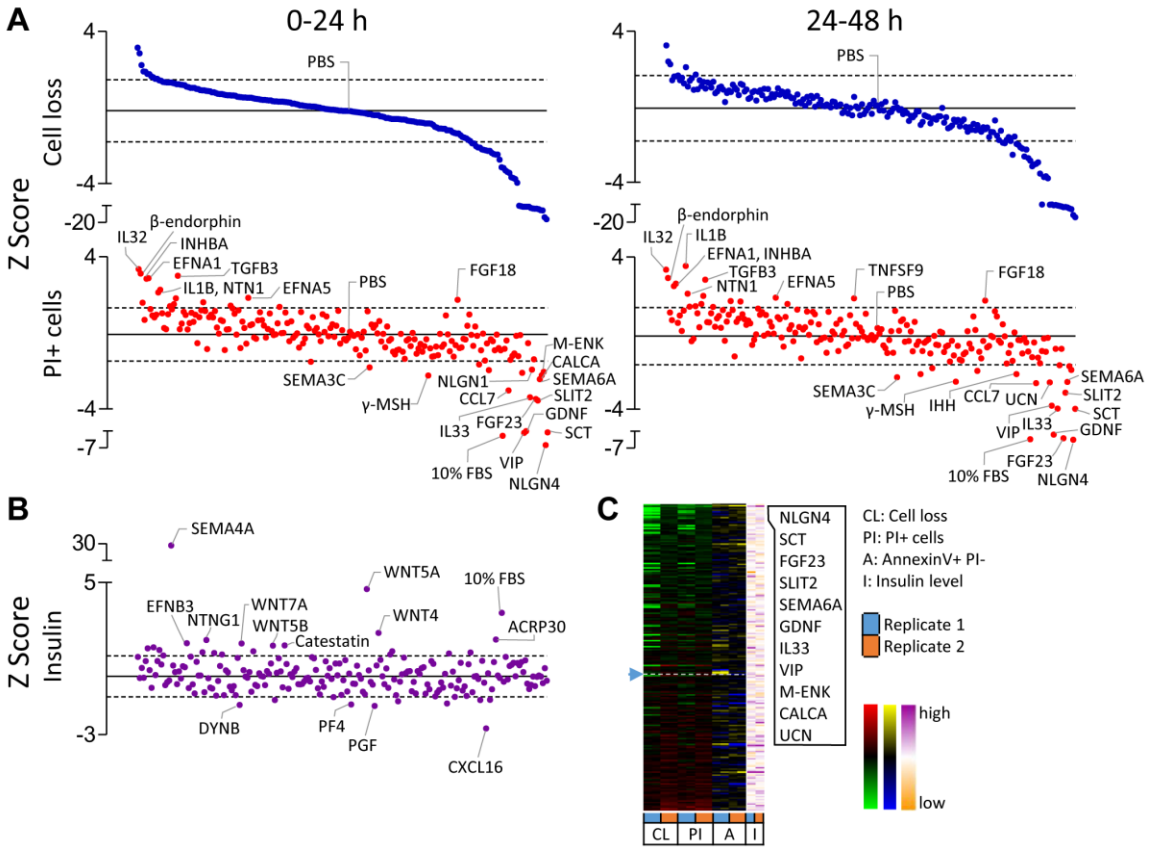

Figure 8-4. Factors protecting islet cells from ER-stress.
A. Dispersed mouse islet cells were imaged and the level of cell loss and percentage of PI positive cells were determined following treatments with a library of 206 factors (10 nM each) and thapsigargin in the context of 5 mM glucose and serum-free conditions. Data are presented as robust z-scores for the 0-24 and 24-48 h time intervals after ordering based on the level of cell loss in the 0-24 h dataset (n=2, mean). Solid lines represent the median and dotted lines represent ± (2*MAD). **B.** The level of insulin in the culture media collected 72 h following the treatments was determined (n=2, mean). **C.** Factors were ranked based on low cell loss and low PI+ cell number.

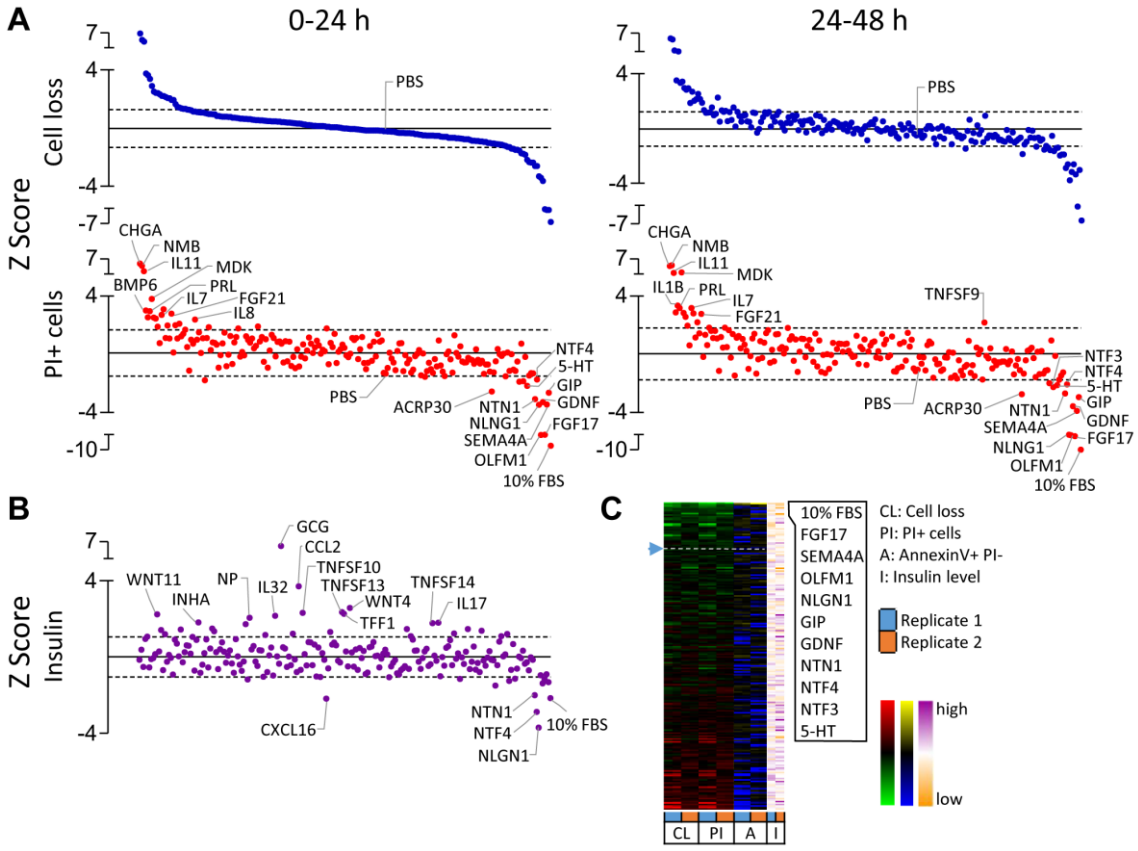

Figure 8-5. Factors protecting islet cells from lipotoxicity.
A. Dispersed mouse islet cells were imaged and the level of cell loss and percentage of PI positive cells were determined following treatments with a library of 206 factors at 10 nM each and palmitate in 5 mM glucose serum free conditions. Data are presented as robust z-scores for the 0-24 and 24-48 h time intervals after ordering based on the level of cell loss in the 0-24 h dataset (n=2, mean). Solid lines represent the median and dotted lines represent ± (2*MAD). **B.** The level of insulin in the culture media collected 72 h following the treatments was determined (n=2, mean). **C.** Factors were ranked based on low cell loss and low PI+ cell number.

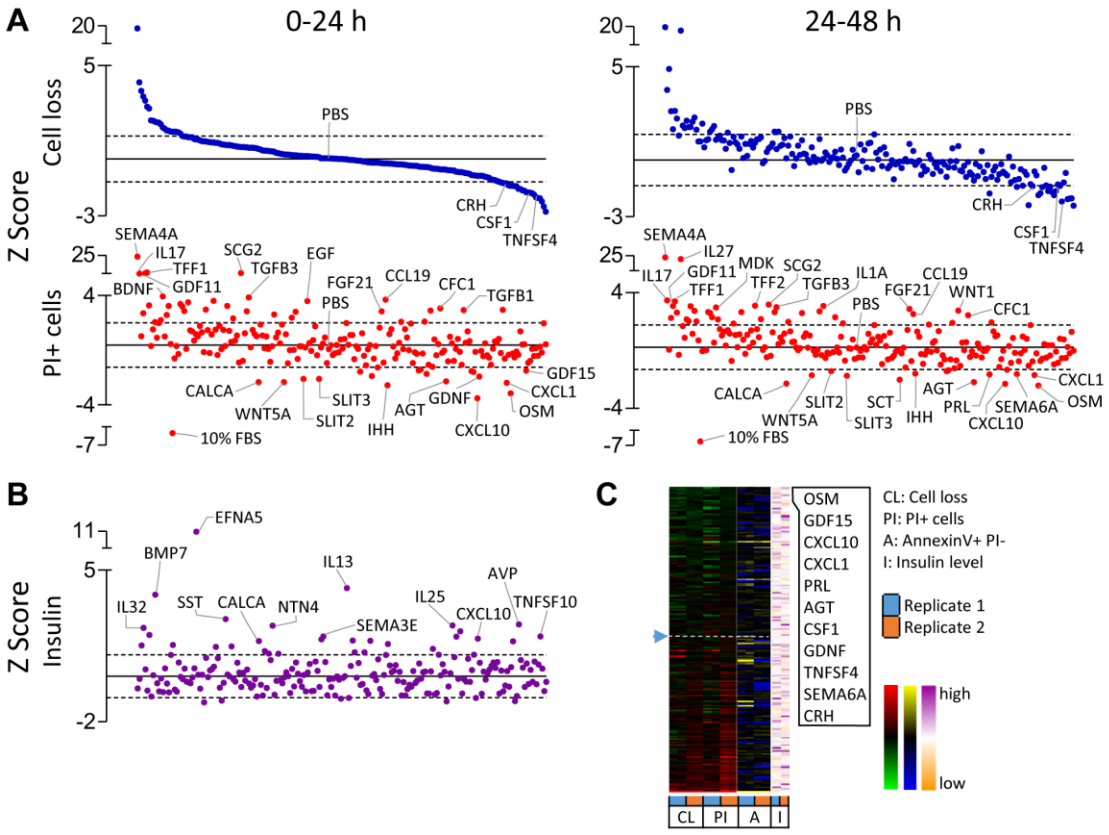

Figure 8-6. Factors protecting islet cells from death in the context of hyperglycemia.
A. Dispersed mouse islet cells were imaged and the level of cell loss and percentage of PI positive cells were determined following treatments with a library of 206 factors (10 nM for each) in 20 mM glucose and serum free conditions. Data are presented as robust z-scores for the 0-24 hand 24-48 h time intervals after ordering based on the level of cell loss in the 0-24 h dataset (n=2, mean). Solid lines represent the median and dotted lines represent ± (2*MAD). **B.** The level of insulin in the culture media collected 72 h following the treatments was determined (n=2, mean). **C.** Factors were ranked based on low cell loss and low PI+ cell number.

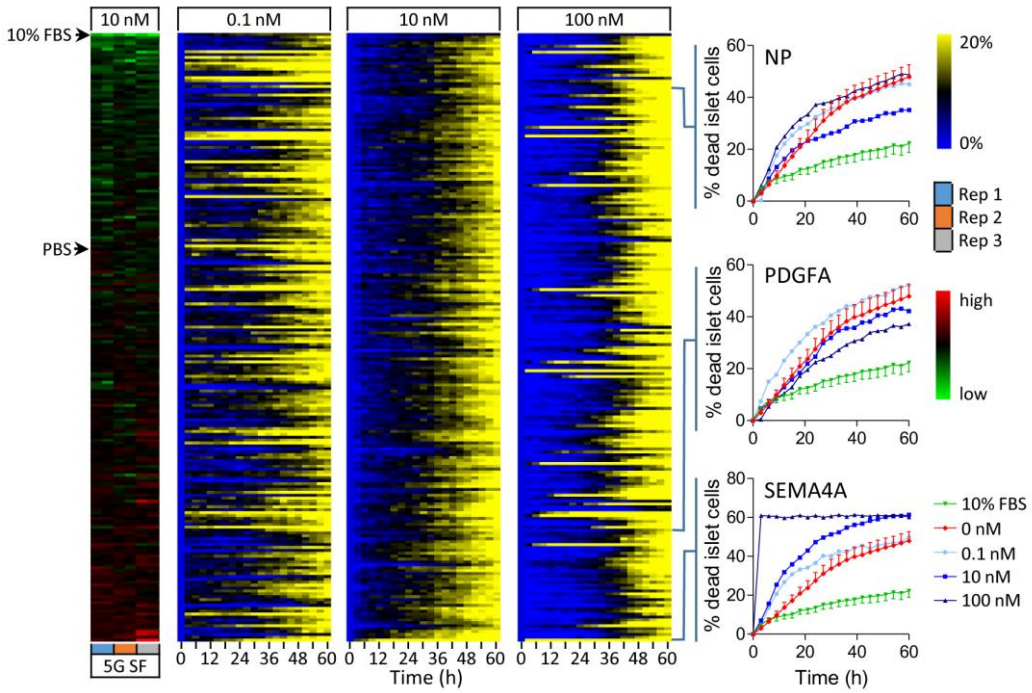

Figure 8-7. Multiple factors display concentration dependent transient or persistent protective effects. Dispersed mouse islet cells were stained and imaged. The percentage of PI positive cells was determined following treatments with a library of 206 factors at 0.1, 10, and 100 nM each. Cells were concurrently exposed 5 mM glucose serum free stress. 10% FBS was used as positive control for unstressed cells. *Left panel:* In the green to red heat map, data are presented as robust z-scores for the 0-24 hand 24-48 h time intervals for each replicate experiment and the factors were ranked for their protective effects (low levels of PI+ cells equates to high protection). *Middle panel:* In the blue to yellow heat map, data are presented as %PI positive cells at each timepoint. *Right panel:* Examples of factors showing concentration dependent effects on cell survival.

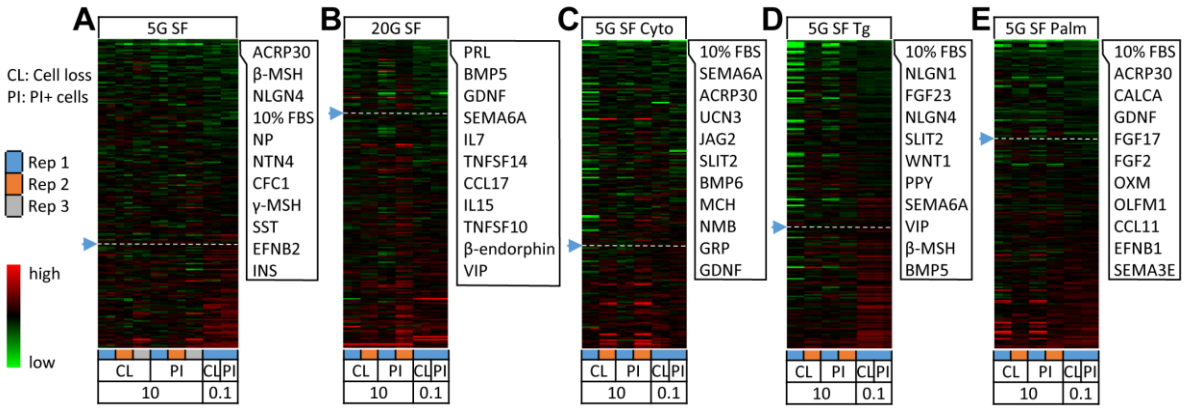

Figure 8-8. Multiple factors display concentration dependent stress specific protective effects.
A-E. Dispersed mouse islet cells were stained and imaged. The level of cell loss and percentage of PI positive cells was determined following treatments with a library of 206 factors at 10 nM each. Cells were concurrently exposed to one of five stress conditions, including 20 mM glucose serum-free (SF), and 5 mM glucose SF only and in combination with a cytokine cocktail (25 ng/ml TNF-α, 10 ng/ml IL-1β, 10 ng/ml IFN-γ), 1 μM thapsigargin, and/or 1.5 mM palmitate. 10% FBS was used as positive control for unstressed cells. Data are presented as robust z-scores for the 0-24 hand 24-48 h time intervals for each replicate experiment. The factors were ranked for their protective effects based on low levels of cell loss and low levels of PI+ cells under the stress treatments indicated at the top of each heat map. The top 10 most protective factors under each condition are listed in the callout.

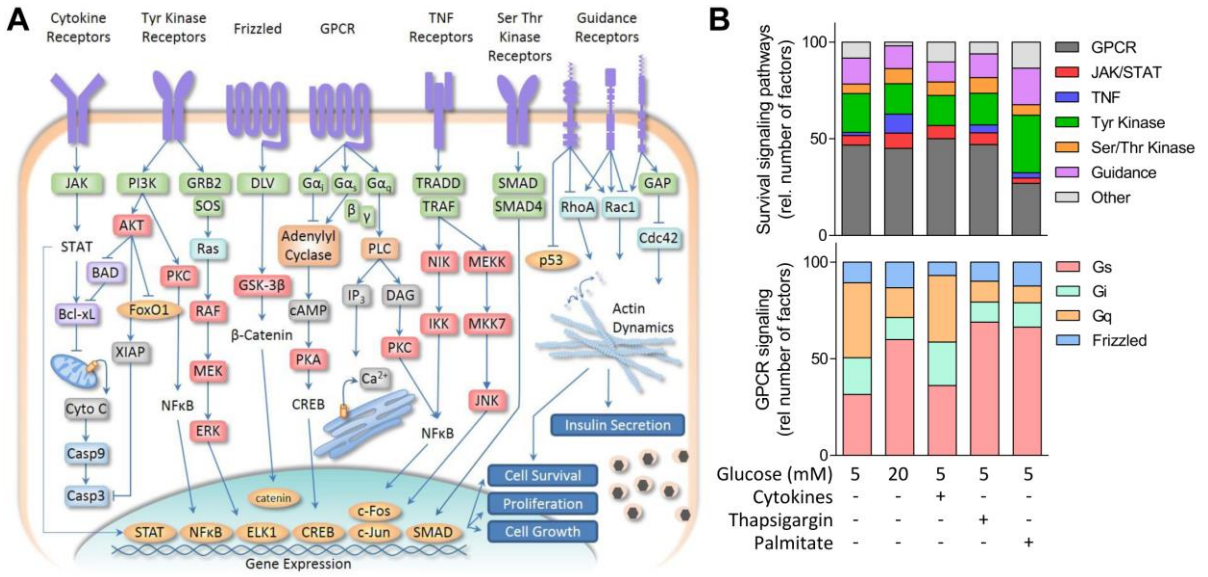

Figure 8-9. Signal transduction pathways of islet cell survival factors.
A. The major canonical signalling pathways that can be upregulated by the top-ranked pro-survival factors. **B.** *Top panel:* The proportion of factors that displayed protective effects with robust z-scores values below 2*MAD of each condition (for either the cell loss or PI+ measurements in the 0-24 or 24-48 time intervals) were further analyzed for the canonical signalling pathways that can be stimulated. *Bottom panel:* The proportion of factors signalling through G protein coupled receptor pathways were further analyzed for the specific downstream pathways.

Chapter 9: Conclusions and future directions

9.1 Averting β-cell death is crucial for diabetes prevention and treatment

Programmed β-cell death plays an important role in both type 1 and type 2 diabetes. In order to develop effective therapeutics to prevent β-cell death, it is important to first understand the molecular pathways regulating the process. Most of what is known about the mechanisms of β-cell death comes from single time-point, single parameter measurements of bulk populations of mixed cells. Such approaches are inadequate for determining the true extent of the heterogeneity in death mechanisms. In Chapter 3, we characterized the timing and order of molecular events associated with cell death in single β-cells under multiple diabetic stress conditions, including hyperglycemia, cytokine exposure, nutrient deprivation and ER stress (114). The kinetics of six distinct cell death mechanisms was simultaneously measured by using a caspase-3 sensor and three vital dyes, together with bright field imaging. We identified several cell death modes where the order of events that define apoptosis was not observed. This was termed 'partial apoptosis'. Remarkably, complete classical apoptosis, defined as cells with plasma membrane blebbing, caspase-3 activity, nuclear condensation and membrane annexinV labeling prior to loss of plasma membrane integrity, was found in only half of cytokine-treated primary β-cells and never in cells stressed by serum removal. On the other hand, MIN6 cell death was almost exclusively via complete classical apoptosis. Together, our data define the kinetic progression of β-cell death mechanisms under different conditions and illustrate the heterogeneity and plasticity of cell death modes in β-cells. *In vivo* and *in vitro* apoptotic β-cell death, based on single parameter measurements, is well described in the literature (2, 11). Whether other modalities of cell death play equally important roles requires further investigation.

Our data suggest that classical apoptosis is not the dominant mode of adult primary β-cell death *in vitro* under all of the diabetes-related stress conditions tested. To further investigate the mechanism controlling β-cell death, simultaneous detection of other cell death mechanisms on the single cell level is required. By coupling the temporal induction of multiple cell death morphological features with signalling, we will be able to characterize the involvement of different modes of cell death. Autophagy-related cell death can be monitored by tracking autophagosomes formation and autophagic flux with tandem monomeric RFP-

eGFP-tagged LC3 (95, 120). Upon fusion of the autophagosome with lysosome, the acidic environment quenches GFP fluorescence while mRFP fluorescence is retained, allowing for the detection of progression through autophagy (302). Alternatively, LC3 could be tagged with a pH sensitive red fluorescent protein pHRed that displays dual excitation at 440 and 585 nm (303) and emission peak at 610 nm. This allows for ratiometric imaging where acidification of the autophagosomes can be detected with an increase in the ratio of fluorescence detected following excitation at 585 nm and 440 nm (F585/F440 ratio) (303). Autophagy is recognized as a cell survival mechanism and by monitoring the induction of autophagosomes and their fusion with lysosomes, we can determine whether autophagy plays a role in pro-longing cell survival or promoting autophagic cell death. Necrotic cell death can be favoured when intracellular ATP levels required for caspase activation are depleted (59, 61, 62). The changes in ATP/ADP ratio can be simultaneously monitored using PercevalHR (82). Hoechst 33342, propidium iodide, and AlexaFluor 647-conjugated AnnexinV fluorescent dyes will allow us to simultaneously detect nuclear condensation, late phase cell death (PI incorporation), and early phase apoptotic cell death (AnnexinV incorporation) (114). Brightfield images will allow for the detection of plasma membrane blebbing. Monitoring apoptosis, autophagy, and necrosis with a combination of spectrally and spatially distinguishable indicators is crucial in determining the mechanism of death and the level of crosstalk between multiple modes of cell death.

Validation of our results *in vivo* will be crucial in determining the roles of different cell death modalities in diabetes pathophysiology. A noninvasive method of detecting *in vivo* cellular changes of pancreatic islets overtime is by transplanting them into the anterior chamber of the mouse eye (304-306). Different mouse models of diabetes could be used to access the effects on cell death. Non-obese diabetic (NOD) mice that spontaneously develop autoimmune diabetes or an accelerated system where NOD lymphocytes are transferred into immunodeficient NOD-SCID mice can be used as models for type 1 diabetes (304, 307). Prior to transplantation, the islets can be infected with adenoviruses to drive the expression of the fluorescent biosensors. The natural progression of β-cell death in autoimmune mediated diabetes can be imaged in anesthetized mice with a confocal microscope.

Given the propensity for cells to undergo cell death when chronically exposed to stress conditions, blocking specific cell death pathways may simply redirect cells to undergo death

through other pathways (59, 61-63). Therefore, upstream targets of cell death are more likely to show effective protection. It is becoming increasingly apparent that islets release and respond to more secreted factors than previously thought (109, 116, 308-310). In Chapter 5, we systematically analysed gene expression databases, islet specific Tag-Seq libraries, and microarray datasets of FACS purified β-cells to compile a list of secreted factors and receptors present in mouse or human islets (109). Potential autocrine/paracrine intra-islet growth factor loops were identified. A list of 233 secreted factors and 234 secreted factor receptors were found in islets. Advances in RNA-Seq technology has since led to the generation of numerous publically available islet and β-cell specific gene expression datasets (175, 311, 312). Bioinformatic analysis of these datasets is likely to increase the number of potential intra-islet signalling loops beyond the 190 that were found in our studies (109). Nonetheless, our results highlight the large number of potential islet growth factors and are important steps towards developing novel therapies to improve β-cell survival.

Informed by the genomics-derived list described above, a candidate approach led to our focus on the role of axon guidance factors in β-cells (109, 281). Netrin-Unc5/Neo1 and Slit-Robo signalling (in Chapters 6 and 7, respectively) were highlighted in our studies. Emerging evidence points to non-neuronal roles for these factors in cell growth, migration, and survival (211, 216-220, 245-248). Our studies revealed the expression of the netrin and slit family members along with their receptors in islet cells, some of which were β-cell specific. The observed glucose-dependent down-regulation of caspase-3 activation upon exposure to exogenous netrins was linked to the decrease in dependence receptors, Neogenin and UNC5A, and independent of insulin secretion. While the pro-survival signalling mediated by endogenous and exogenous SLITs upon serum deprivation, cytokine, and thapsigargin-induced cell death under hyperglycemic conditions was linked to the modulation of ER luminal Ca^{2+} levels. SLITs also potentiated glucose-stimulated insulin secretion and increased the frequency of glucose-induced Ca^{2+} oscillations. Although no changes in cytosolic Ca^{2+} levels were observed when β-cells were treated with netrins under basal glucose conditions, as observed in cells treated with SLITs, it is likely that netrins could be modulating glucose-induced Ca^{2+} signalling in a similar fashion as SLITs. Indeed, Ca^{2+} signalling in neuronal growth cones could be modulated by netrins (231, 313). Loss-of-function studies will also have to be conducted to determine if endogenous netrins could also protect β-cells from stress-

induced death. Overall, our observations point to unexpected roles for netrins and slits in the survival and function of pancreatic β-cells.

The signalling mechanism behind the context dependent survival effects of both netrins and SLITs remains elusive. How elevated glucose level is involved in the pro-survival signalling stimulated by these exogenous axon guidance factors may be dependent on the metabolic state of the cell. The increase in glucose stimulated insulin levels could also explain the prevention of cell death mediated by SLITs, but not by netrins. In neurons, axon attraction or repulsion requires ATP dependent cytoskeletal rearrangements. Perhaps insufficient levels of ATP under low glucose conditions prevent the activation of cytoskeletal-mediated pro-survival signalling pathways in β-cells. Given that we observed increases in cortical F-actin depolymerization upon SLIT treatment and modulation of actin polymerization may also directly promote survival (272-275), it would be interesting to see if disruptors or activators of actin polymerization could directly modulate the survival effects of SLITs. The mechanism described in yeast where mitochondrial ROS production decreases upon increase in F-actin turnover could explain the survival effects of SLITs and netrins (274). Cytoskeleton organization has been demonstrated to be required for Ca^{2+} signalling mediated by ATP release in astrocytes and neurons (314, 315) and cytoskeletal stabilizers can prolong Ca^{2+} channel activity even in the absence of ATP (315). Modulation of intracellular Ca^{2+} signalling is important for β-cell function and survival (67-72). The contribution of Ca^{2+} signalling towards cell survival is a reoccurring theme throughout the thesis and has been well studied in the literature (68). Cationic (Ca^{2+}, K^{+}, Na^{+}) and anionic (Cl^{-}) electrochemical gradients are maintained and modulated to support both β-cell function and survival (134, 145, 146, 316, 317). In Chapter 4, through our high-content, live-cell screening approach, we have uncovered the pro-survival effects of a Na^{+} channel inhibitor, carbamazepine, which led to our investigations of the effects of modulating Na^{+} channel activity on β-cell survival signalling. Our studies revealed that Na^{+} channel modulation could influence intracellular Ca^{2+} levels, perhaps by altering the electrical activity of β-cells (145, 146, 316). Ca^{2+} is a crucial second messenger for numerous biochemical pathways by directly or indirectly modulating the activities of kinases, phosphatases, transcription factors, and calcium-binding protein calmodulin (91). Cell motility, proliferation, and survival, gene transcription, and vesicle trafficking can all be regulated by Ca^{2+} signals.

9.2 Application of multi-parameter screening approaches in the discovery of potent β-cell pro-survival factors and small molecules

As presented in Chapters 4 and 8, we have developed live-cell imaging-based, high-throughput screening methods capable of identifying factors that modulate pancreatic β-cell death, with the hope of finding drugs that can intervene in this process. With an automated high-content, live-cell imaging platform, we screened the Prestwick library of small molecules to identify drugs that block cell death resulting from exposure to a cocktail of cytotoxic cytokines and conducted comparisons of 206 endogenous soluble factors for their pro-survival effects under 5 diabetes-relevant stress conditions. The Prestwick screen revealed 19 drugs that had profiles similar to the no cytokine condition, indicating protection. Carbamazepine, an anti-epileptic Na^+ channel inhibitor, was particularly interesting because Na^+ channels are not generally considered targets for anti-apoptotic therapy in diabetes and because function of these channels in β-cells has not been well studied. We analyzed the expression and characteristics of Na^+ currents in mature β-cells from MIP-GFP mice. We confirmed the dose-dependent protective effects of carbamazepine and another use-dependent Na^+ channel blocker in cytokine treated mouse islet cell. These pro-survival effects were associated with down-regulated pro-apoptotic and ER-stress signalling induced by cytokines. Cnop *et al* have recently demonstrated that carbamazepine can protect β-cells from lipotoxicity, through a pathway that increases autophagy (175). These studies point to Na^+ channels as a novel therapeutic target in diabetes, but their effectiveness *in vivo* warrants further studies.

Prevention of cell death from specific cellular stresses associated with type 1 or type 2 diabetes most likely requires specific β-cell survival factors. To date, analysis of candidate factors has yielded a few hormones and growth factors exhibiting modest β-cell protection against various stresses, but no systematic comparison of soluble factors in the context of multiple pro-apoptotic conditions has been published. We report the comparison of 206 endogenous soluble factors, predicted to act on islet cells, using multi-parameter, high-throughput, live-cell imaging to measure islet cell death under 5 diabetes-relevant stress conditions. Unique sets of protective survival factors for each stress and a cluster of survival factors exhibiting generalized protective effects were found. Collectively, our data reveal previously unidentified, stress-specific islet cell survival factors and point to their utility in individualized medicine.

Diabetes is a multi-factorial disease and β-cells are often exposed to more than one stress *in vivo*. Given that we discovered most of the factors that displayed prominent protection were unique to specific stresses, a combination of factors is probably necessary to prevent *in vivo* β-cell death. Additionally, some of the factors that displayed protection under specific stressors promoted cell death under other conditions, suggesting that they are not suitable for therapeutic use. The requirement of signalling from two or more survival factors to protect the islets under our distinct cell death inducing conditions and their potential interactions can be examined with the same high-content, live-cell imaging assay presented in Chapters 4 and 8. Factors promoting survival through redundant and/or parallel pathways can be uncovered. Knockdown studies can help us determine if endogenous production of specific factors is required for supporting β-cell survival. The results of our *in vitro* studies on the discovery of potent β-cell pro-survival factors can easily be applied to clinical islet transplantation settings by promoting β-cell survival during pre-transplantation culturing of human islets. Application of individual or combinations of pro-survival factors *in vivo* is crucial for translational research and will require animal studies. The therapeutic potential of the pro-survival factors or combinations can be determined through mouse models of type 1 diabetes (NOD mice or Streptozotocin-induced diabetes) (304, 307, 318). While the efficacy of factors that prevented cell death under lipotoxic conditions can be tested with mouse models of type 2 diabetes (high fat diet induced diabetes or db/db mice with impaired leptin signalling). Inducible transgenic overexpression of specific factors or intravenous administration of the factors both prior to or following diabetes onset could allow us to determine if the factors have the potential to prevent and/or reverse diabetes progression. The results presented in this thesis have contributed to our understanding of signals that control β-cell death in adult islets and to the therapeutic development for the prevention of diabetes initiation and progression.

References

1. Cho NH, *et al.* (2013) International Diabetes Federation Diabetes Atlas. eds Guariguata L, Nolan T, Beagley J, Linnenkamp U, & Jacqmain O (International Diabetes Federation, Brussels, Belgium).

2. Mathis D, Vence L, & Benoist C (2001) beta-Cell death during progression to diabetes. *Nature* 414(6865):792-798.

3. Prentki M & Nolan CJ (2006) Islet beta cell failure in type 2 diabetes. *J Clin Invest* 116(7):1802-1812.

4. Dor Y, Brown J, Martinez OI, & Melton DA (2004) Adult pancreatic beta-cells are formed by self-duplication rather than stem-cell differentiation. *Nature* 429(6987):41-46.

5. Bonner-Weir S (2000) Life and death of the pancreatic beta cells. *Trends Endocrinol Metab* 11(9):375-378.

6. Meier JJ, *et al.* (2008) Beta-cell replication is the primary mechanism subserving the postnatal expansion of beta-cell mass in humans. *Diabetes* 57(6):1584-1594.

7. Scaglia L, Cahill CJ, Finegood DT, & Bonner-Weir S (1997) Apoptosis participates in the remodeling of the endocrine pancreas in the neonatal rat. *Endocrinology* 138(4):1736-1741.

8. Finegood DT, Scaglia L, & Bonner-Weir S (1995) Dynamics of beta-cell mass in the growing rat pancreas. Estimation with a simple mathematical model. *Diabetes* 44(3):249-256.

9. Butler AE, *et al.* (2003) Beta-cell deficit and increased beta-cell apoptosis in humans with type 2 diabetes. *Diabetes* 52(1):102-110.

10. Kulkarni RN, Mizrachi EB, Ocana AG, & Stewart AF (2012) Human beta-cell proliferation and intracellular signaling: driving in the dark without a road map. *Diabetes* 61(9):2205-2213.

11. Cnop M, *et al.* (2005) Mechanisms of pancreatic beta-cell death in type 1 and type 2 diabetes: many differences, few similarities. *Diabetes* 54 Suppl 2:S97-107.

12. Meier JJ, Bhushan A, Butler AE, Rizza RA, & Butler PC (2005) Sustained beta cell apoptosis in patients with long-standing type 1 diabetes: indirect evidence for islet regeneration? *Diabetologia* 48(11):2221-2228.

13. Nakanishi K & Watanabe C (2008) Rate of beta-cell destruction in type 1 diabetes influences the development of diabetic retinopathy: protective effect of residual beta-cell function for more than 10 years. *J Clin Endocrinol Metab* 93(12):4759-4766.

14. Liadis N, *et al.* (2005) Caspase-3-dependent beta-cell apoptosis in the initiation of autoimmune diabetes mellitus. *Mol Cell Biol* 25(9):3620-3629.

15. Howson JM, Walker NM, Clayton D, Todd JA, & Type 1 Diabetes Genetics C (2009) Confirmation of HLA class II independent type 1 diabetes associations in the major histocompatibility complex including HLA-B and HLA-A. *Diabetes, obesity & metabolism* 11 Suppl 1:31-45.

16. Nejentsev S, *et al.* (2007) Localization of type 1 diabetes susceptibility to the MHC class I genes HLA-B and HLA-A. *Nature* 450(7171):887-892.

17. Pugliese A, *et al.* (1997) The insulin gene is transcribed in the human thymus and transcription levels correlated with allelic variation at the INS VNTR-IDDM2 susceptibility locus for type 1 diabetes. *Nat Genet* 15(3):293-297.

18. Weir GC & Bonner-Weir S (2004) Five stages of evolving beta-cell dysfunction during progression to diabetes. *Diabetes* 53 Suppl 3:S16-21.

19. Henquin JC & Rahier J (2011) Pancreatic alpha cell mass in European subjects with type 2 diabetes. *Diabetologia* 54(7):1720-1725.

20. Rahier J, Guiot Y, Goebbels RM, Sempoux C, & Henquin JC (2008) Pancreatic beta-cell mass in European subjects with type 2 diabetes. *Diabetes, obesity & metabolism* 10 Suppl 4:32-42.

21. Poitout V & Robertson RP (2002) Minireview: Secondary beta-cell failure in type 2 diabetes--a convergence of glucotoxicity and lipotoxicity. *Endocrinology* 143(2):339-342.

22. Robertson RP, Harmon J, Tran PO, & Poitout V (2004) Beta-cell glucose toxicity, lipotoxicity, and chronic oxidative stress in type 2 diabetes. *Diabetes* 53 Suppl 1:S119-124.

23. Haataja L, Gurlo T, Huang CJ, & Butler PC (2008) Islet amyloid in type 2 diabetes, and the toxic oligomer hypothesis. *Endocr Rev* 29(3):303-316.

24. Zraika S, *et al.* (2010) Toxic oligomers and islet beta cell death: guilty by association or convicted by circumstantial evidence? *Diabetologia* 53(6):1046-1056.

25. Eizirik DL, Cardozo AK, & Cnop M (2008) The role for endoplasmic reticulum stress in diabetes mellitus. *Endocr Rev* 29(1):42-61.

26. Westwell-Roper C & Ehses JA (2014) Is there a role for the adaptive immune system in pancreatic beta cell failure in type 2 diabetes? *Diabetologia* 57(3):447-450.

27. Donath MY & Shoelson SE (2011) Type 2 diabetes as an inflammatory disease. *Nature reviews. Immunology* 11(2):98-107.

28. Lyssenko V & Groop L (2009) Genome-wide association study for type 2 diabetes: clinical applications. *Current opinion in lipidology* 20(2):87-91.

29. Voight BF, *et al.* (2010) Twelve type 2 diabetes susceptibility loci identified through large-scale association analysis. *Nat Genet* 42(7):579-589.

30. Maedler K, *et al.* (2002) Glucose-induced beta cell production of IL-1beta contributes to glucotoxicity in human pancreatic islets. *J Clin Invest* 110(6):851-860.

31. Maedler K, *et al.* (2001) Glucose induces beta-cell apoptosis via upregulation of the Fas receptor in human islets. *Diabetes* 50(8):1683-1690.

32. Federici M, *et al.* (2001) High glucose causes apoptosis in cultured human pancreatic islets of Langerhans: a potential role for regulation of specific Bcl family genes toward an apoptotic cell death program. *Diabetes* 50(6):1290-1301.

33. Robertson RP (2004) Islet transplantation as a treatment for diabetes - a work in progress. *N Engl J Med* 350(7):694-705.

34. Robertson RP (2010) Islet transplantation a decade later and strategies for filling a half-full glass. *Diabetes* 59(6):1285-1291.

35. Shapiro AM, *et al.* (2000) Islet transplantation in seven patients with type 1 diabetes mellitus using a glucocorticoid-free immunosuppressive regimen. *N Engl J Med* 343(4):230-238.

36. Johnson JD, *et al.* (2009) Different effects of FK506, rapamycin, and mycophenolate mofetil on glucose-stimulated insulin release and apoptosis in human islets. *Cell Transplant* 18(8):833-845.

37. Dror V, *et al.* (2007) Notch signalling suppresses apoptosis in adult human and mouse pancreatic islet cells. *Diabetologia* 50(12):2504-2515.

38. Beith JL, Alejandro EU, & Johnson JD (2008) Insulin stimulates primary beta-cell proliferation via Raf-1 kinase. *Endocrinology* 149(5):2251-2260.

39. Alejandro EU & Johnson JD (2008) Inhibition of Raf-1 alters multiple downstream pathways to induce pancreatic beta-cell apoptosis. *J Biol Chem* 283(4):2407-2417.

40. Kroemer G, *et al.* (2009) Classification of cell death: recommendations of the Nomenclature Committee on Cell Death 2009. *Cell Death Differ* 16(1):3-11.

41. Galluzzi L, *et al.* (2009) Guidelines for the use and interpretation of assays for monitoring cell death in higher eukaryotes. *Cell Death Differ* 16(8):1093-1107.

42. Galluzzi L, *et al.* (2012) Molecular definitions of cell death subroutines: recommendations of the Nomenclature Committee on Cell Death 2012. *Cell death and differentiation* 19(1):107-120.

43. Spencer SL & Sorger PK (2011) Measuring and modeling apoptosis in single cells. *Cell* 144(6):926-939.

44. Mehlen P & Thibert C (2004) Dependence receptors: between life and death. *Cell Mol Life Sci* 61(15):1854-1866.

45. Mehlen P & Bredesen DE (2011) Dependence receptors: from basic research to drug development. *Sci Signal* 4(157):mr2.

46. Bao Q & Shi Y (2007) Apoptosome: a platform for the activation of initiator caspases. *Cell death and differentiation* 14(1):56-65.

47. Kroemer G, Galluzzi L, & Brenner C (2007) Mitochondrial membrane permeabilization in cell death. *Physiological reviews* 87(1):99-163.

48. Kroemer G, Marino G, & Levine B (2010) Autophagy and the integrated stress response. *Mol Cell* 40(2):280-293.

49. Fleming A, Noda T, Yoshimori T, & Rubinsztein DC (2011) Chemical modulators of autophagy as biological probes and potential therapeutics. *Nat Chem Biol* 7(1):9-17.

50. Levine B & Yuan J (2005) Autophagy in cell death: an innocent convict? *J Clin Invest* 115(10):2679-2688.

51. Ebato C, *et al.* (2008) Autophagy is important in islet homeostasis and compensatory increase of beta cell mass in response to high-fat diet. *Cell Metab* 8(4):325-332.

52. Jung HS, *et al.* (2008) Loss of autophagy diminishes pancreatic beta cell mass and function with resultant hyperglycemia. *Cell Metab* 8(4):318-324.

53. Levine B & Kroemer G (2008) Autophagy in the pathogenesis of disease. *Cell* 132(1):27-42.

54. Kang R, Zeh HJ, Lotze MT, & Tang D (2011) The Beclin 1 network regulates autophagy and apoptosis. *Cell Death Differ* 18(4):571-580.

55. Fujimoto K, *et al.* (2010) Loss of Nix in Pdx1-deficient mice prevents apoptotic and necrotic beta cell death and diabetes. *J Clin Invest* 120(11):4031-4039.

56. Steer SA, Scarim AL, Chambers KT, & Corbett JA (2006) Interleukin-1 stimulates beta-cell necrosis and release of the immunological adjuvant HMGB1. *PLoS Med* 3(2):e17.

57. Golstein P & Kroemer G (2007) Cell death by necrosis: towards a molecular definition. *Trends Biochem Sci* 32(1):37-43.

58. Fink SL & Cookson BT (2005) Apoptosis, pyroptosis, and necrosis: mechanistic description of dead and dying eukaryotic cells. *Infect Immun* 73(4):1907-1916.

59. Kim JS, He L, & Lemasters JJ (2003) Mitochondrial permeability transition: a common pathway to necrosis and apoptosis. *Biochem Biophys Res Commun* 304(3):463-470.

60. Vandenabeele P, Galluzzi L, Vanden Berghe T, & Kroemer G (2010) Molecular mechanisms of necroptosis: an ordered cellular explosion. *Nat Rev Mol Cell Biol* 11(10):700-714.

61. Leist M, Single B, Castoldi AF, Kuhnle S, & Nicotera P (1997) Intracellular adenosine triphosphate (ATP) concentration: a switch in the decision between apoptosis and necrosis. *J Exp Med* 185(8):1481-1486.

62. Eguchi Y, Shimizu S, & Tsujimoto Y (1997) Intracellular ATP levels determine cell death fate by apoptosis or necrosis. *Cancer Res* 57(10):1835-1840.

63. Silva MT (2010) Secondary necrosis: the natural outcome of the complete apoptotic program. *FEBS Lett* 584(22):4491-4499.

64. Frisch SM & Francis H (1994) Disruption of epithelial cell-matrix interactions induces apoptosis. *J Cell Biol* 124(4):619-626.

65. David KK, Andrabi SA, Dawson TM, & Dawson VL (2009) Parthanatos, a messenger of death. *Front Biosci (Landmark Ed)* 14:1116-1128.

66. Luo X & Kraus WL (2012) On PAR with PARP: cellular stress signaling through poly(ADP-ribose) and PARP-1. *Genes & development* 26(5):417-432.

67. Ramadan JW, Steiner SR, O'Neill CM, & Nunemaker CS (2011) The central role of calcium in the effects of cytokines on beta-cell function: implications for type 1 and type 2 diabetes. *Cell calcium* 50(6):481-490.

68. Harr MW & Distelhorst CW (2010) Apoptosis and autophagy: decoding calcium signals that mediate life or death. *Cold Spring Harbor perspectives in biology* 2(10):a005579.

69. Eizirik DL, Miani M, & Cardozo AK (2013) Signalling danger: endoplasmic reticulum stress and the unfolded protein response in pancreatic islet inflammation. *Diabetologia* 56(2):234-241.

70. Tengholm A, Hellman B, & Gylfe E (2001) The endoplasmic reticulum is a glucose-modulated high-affinity sink for Ca2+ in mouse pancreatic beta-cells. *J Physiol* 530(Pt 3):533-540.

71. Tengholm A, Hellman B, & Gylfe E (1999) Glucose regulation of free Ca(2+) in the endoplasmic reticulum of mouse pancreatic beta cells. *J Biol Chem* 274(52):36883-36890.

72. Wiederkehr A & Wollheim CB (2008) Impact of mitochondrial calcium on the coupling of metabolism to insulin secretion in the pancreatic beta-cell. *Cell calcium* 44(1):64-76.

73. Criddle DN, *et al.* (2007) Calcium signalling and pancreatic cell death: apoptosis or necrosis? *Cell Death Differ* 14(7):1285-1294.

74. Chang I, *et al.* (2004) Role of calcium in pancreatic islet cell death by IFN-gamma/TNF-alpha. *Journal of immunology* 172(11):7008-7014.

75. Gilon P, Arredouani A, Gailly P, Gromada J, & Henquin JC (1999) Uptake and release of Ca2+ by the endoplasmic reticulum contribute to the oscillations of the cytosolic Ca2+ concentration triggered by Ca2+ influx in the electrically excitable pancreatic B-cell. *J Biol Chem* 274(29):20197-20205.

76. Luciani DS, *et al.* (2009) Roles of IP3R and RyR Ca2+ channels in endoplasmic reticulum stress and beta-cell death. *Diabetes* 58(2):422-432.

77. Xu C, Bailly-Maitre B, & Reed JC (2005) Endoplasmic reticulum stress: cell life and death decisions. *J Clin Invest* 115(10):2656-2664.

78. Giacomello M, Drago I, Pizzo P, & Pozzan T (2007) Mitochondrial Ca2+ as a key regulator of cell life and death. *Cell Death Differ* 14(7):1267-1274.

79. Trenker M, Malli R, Fertschai I, Levak-Frank S, & Graier WF (2007) Uncoupling proteins 2 and 3 are fundamental for mitochondrial Ca2+ uniport. *Nat Cell Biol* 9(4):445-452.

80. Kepp O, Galluzzi L, Lipinski M, Yuan J, & Kroemer G (2011) Cell death assays for drug discovery. *Nat Rev Drug Discov* 10(3):221-237.

81. Berg J, Hung YP, & Yellen G (2009) A genetically encoded fluorescent reporter of ATP:ADP ratio. *Nat Methods* 6(2):161-166.

82. Tantama M, Martinez-Francois JR, Mongeon R, & Yellen G (2013) Imaging energy status in live cells with a fluorescent biosensor of the intracellular ATP-to-ADP ratio. *Nature communications* 4:2550.

83. Imamura H, *et al.* (2009) Visualization of ATP levels inside single living cells with fluorescence resonance energy transfer-based genetically encoded indicators. *Proc Natl Acad Sci U S A* 106(37):15651-15656.

84. D'Amelio M, Cavallucci V, & Cecconi F (2010) Neuronal caspase-3 signaling: not only cell death. *Cell death and differentiation* 17(7):1104-1114.

85. Karasawa S, Araki T, Nagai T, Mizuno H, & Miyawaki A (2004) Cyan-emitting and orange-emitting fluorescent proteins as a donor/acceptor pair for fluorescence resonance energy transfer. *Biochem J* 381(Pt 1):307-312.

86. Takemoto K, Nagai T, Miyawaki A, & Miura M (2003) Spatio-temporal activation of caspase revealed by indicator that is insensitive to environmental effects. *J Cell Biol* 160(2):235-243.

87. Zwaal RF, Comfurius P, & Bevers EM (2005) Surface exposure of phosphatidylserine in pathological cells. *Cellular and molecular life sciences : CMLS* 62(9):971-988.

88. Campalans A, Amouroux R, Bravard A, Epe B, & Radicella JP (2007) UVA irradiation induces relocalisation of the DNA repair protein hOGG1 to nuclear speckles. *Journal of cell science* 120(Pt 1):23-32.

89. Goldstein JC, Waterhouse NJ, Juin P, Evan GI, & Green DR (2000) The coordinate release of cytochrome c during apoptosis is rapid, complete and kinetically invariant. *Nature cell biology* 2(3):156-162.

90. Campello S & Scorrano L (2010) Mitochondrial shape changes: orchestrating cell pathophysiology. *EMBO Rep* 11(9):678-684.

91. Berridge MJ, Lipp P, & Bootman MD (2000) The versatility and universality of calcium signalling. *Nat Rev Mol Cell Biol* 1(1):11-21.

92. McCombs JE & Palmer AE (2008) Measuring calcium dynamics in living cells with genetically encodable calcium indicators. *Methods* 46(3):152-159.

93. Palmer AE, *et al.* (2006) Ca2+ indicators based on computationally redesigned calmodulin-peptide pairs. *Chemistry & biology* 13(5):521-530.

94. Zhao Y, *et al.* (2011) An expanded palette of genetically encoded Ca(2)(+) indicators. *Science* 333(6051):1888-1891.

95. Klionsky DJ, *et al.* (2012) Guidelines for the use and interpretation of assays for monitoring autophagy. *Autophagy* 8(4):445-544.

96. Scaffidi P, Misteli T, & Bianchi ME (2002) Release of chromatin protein HMGB1 by necrotic cells triggers inflammation. *Nature* 418(6894):191-195.

97. Christofferson DE & Yuan J (2010) Cyclophilin A release as a biomarker of necrotic cell death. *Cell death and differentiation* 17(12):1942-1943.

98. Vasavada RC, *et al.* (2006) Growth factors and beta cell replication. *Int J Biochem Cell Biol* 38(5-6):931-950.

99. Beattie GM, Rubin JS, Mally MI, Otonkoski T, & Hayek A (1996) Regulation of proliferation and differentiation of human fetal pancreatic islet cells by extracellular matrix, hepatocyte growth factor, and cell-cell contact. *Diabetes* 45(9):1223-1228.

100. Terra LF, Garay-Malpartida MH, Wailemann RA, Sogayar MC, & Labriola L (2011) Recombinant human prolactin promotes human beta cell survival via inhibition of extrinsic and intrinsic apoptosis pathways. *Diabetologia* 54(6):1388-1397.

101. Buteau J, Roduit R, Susini S, & Prentki M (1999) Glucagon-like peptide-1 promotes DNA synthesis, activates phosphatidylinositol 3-kinase and increases transcription factor pancreatic and duodenal homeobox gene 1 (PDX-1) DNA binding activity in beta (INS-1)-cells. *Diabetologia* 42(7):856-864.

102. Flamez D, *et al.* (1999) Altered cAMP and Ca2+ signaling in mouse pancreatic islets with glucagon-like peptide-1 receptor null phenotype. *Diabetes* 48(10):1979-1986.

103. Drucker DJ (2003) Glucagon-like peptides: regulators of cell proliferation, differentiation, and apoptosis. *Mol Endocrinol* 17(2):161-171.

104. Wideman RD, *et al.* (2006) Improving function and survival of pancreatic islets by endogenous production of glucagon-like peptide 1 (GLP-1). *Proc Natl Acad Sci U S A* 103(36):13468-13473.

105. Rickels MR, Mueller R, Markmann JF, & Naji A (2009) Effect of glucagon-like peptide-1 on beta- and alpha-cell function in isolated islet and whole pancreas transplant recipients. *J Clin Endocrinol Metab* 94(1):181-189.

106. Chen C, *et al.* (2003) An integrated functional genomics screening program reveals a role for BMP-9 in glucose homeostasis. *Nat Biotechnol* 21(3):294-301.

107. Chou DH, *et al.* (2010) Small-Molecule Suppressors of Cytokine-Induced beta-Cell Apoptosis. *ACS Chem Biol* 5(8):729-734.

108. Alejandro EU, *et al.* (2010) Acute insulin signaling in pancreatic beta-cells is mediated by multiple Raf-1 dependent pathways. *Endocrinology* 151(2):502-512.

109. Yang YH, *et al.* (2011) Paracrine signalling loops in adult human and mouse pancreatic islets: netrins modulate beta cell apoptosis signalling via dependence receptors. *Diabetologia* 54(4):828-842.

110. Szabat M, Luciani DS, Piret JM, & Johnson JD (2009) Maturation of adult beta-cells revealed using a Pdx1/insulin dual-reporter lentivirus. *Endocrinology* 150(4):1627-1635.

111. Gwiazda KS, Yang TL, Lin Y, & Johnson JD (2009) Effects of palmitate on ER and cytosolic Ca2+ homeostasis in beta-cells. *Am J Physiol Endocrinol Metab* 296(4):E690-701.

112. Zhang J, Hupfeld CJ, Taylor SS, Olefsky JM, & Tsien RY (2005) Insulin disrupts beta-adrenergic signalling to protein kinase A in adipocytes. *Nature* 437(7058):569-573.

113. Curran MA & Nolan GP (2002) Recombinant feline immunodeficiency virus vectors. Preparation and use. *Methods Mol Med* 69:335-350.

114. Yang YH & Johnson JD (2013) Multi-parameter single-cell kinetic analysis reveals multiple modes of cell death in primary pancreatic beta-cells. *J Cell Sci* 126(Pt 18):4286-4295.

115. Jeffrey KD, *et al.* (2008) Carboxypeptidase E mediates palmitate-induced beta-cell ER stress and apoptosis. *Proc Natl Acad Sci U S A* 105(24):8452-8457.

116. Kutlu B, *et al.* (2009) Detailed transcriptome atlas of the pancreatic beta cell. *BMC Med Genomics* 2:3.

117. Hoffman BG, *et al.* (2010) Locus co-occupancy, nucleosome positioning, and H3K4me1 regulate the functionality of FOXA2-, HNF4A-, and PDX1-bound loci in islets and liver. *Genome Res* 20(8):1037-1051.

118. Morrissy AS, *et al.* (2009) Next-generation tag sequencing for cancer gene expression profiling. *Genome Res* 19(10):1825-1835.

119. Hulbert EM, *et al.* (2007) T1DBase: integration and presentation of complex data for type 1 diabetes research. *Nucleic Acids Res* 35(Database issue):D742-746.

120. Klionsky DJ, *et al.* (2008) Guidelines for the use and interpretation of assays for monitoring autophagy in higher eukaryotes. *Autophagy* 4(2):151-175.

121. Koopman G, *et al.* (1994) Annexin V for flow cytometric detection of phosphatidylserine expression on B cells undergoing apoptosis. *Blood* 84(5):1415-1420.

122. Reutelingsperger CP & van Heerde WL (1997) Annexin V, the regulator of phosphatidylserine-catalyzed inflammation and coagulation during apoptosis. *Cell Mol Life Sci* 53(6):527-532.

123. Chu KY, *et al.* (2010) ATP-citrate lyase reduction mediates palmitate-induced apoptosis in pancreatic beta cells. *J Biol Chem* 285(42):32606-32615.

124. Cistola DP & Small DM (1991) Fatty acid distribution in systems modeling the normal and diabetic human circulation. A 13C nuclear magnetic resonance study. *J Clin Invest* 87(4):1431-1441.

125. Dror V, *et al.* (2008) Glucose and endoplasmic reticulum calcium channels regulate HIF-1beta via presenilin in pancreatic beta-cells. *J Biol Chem* 283(15):9909-9916.

126. Varadi A & Rutter GA (2002) Dynamic imaging of endoplasmic reticulum Ca2+ concentration in insulin-secreting MIN6 Cells using recombinant targeted cameleons: roles of sarco(endo)plasmic reticulum Ca2+-ATPase (SERCA)-2 and ryanodine receptors. *Diabetes* 51 Suppl 1:S190-201.

127. Johnson JD, *et al.* (2004) RyR2 and calpain-10 delineate a novel apoptosis pathway in pancreatic islets. *J Biol Chem* 279(23):24794-24802.

128. Chu KY, Li H, Wada K, & Johnson JD (2011) Ubiquitin C-terminal hydrolase L1 is required for pancreatic beta cell survival and function in lipotoxic conditions. *Diabetologia* 55(1):128-140.

129. Hoorens A, Van de Casteele M, Kloppel G, & Pipeleers D (1996) Glucose promotes survival of rat pancreatic beta cells by activating synthesis of proteins which suppress a constitutive apoptotic program. *The Journal of clinical investigation* 98(7):1568-1574.

130. Van de Casteele M, *et al.* (2003) Prolonged culture in low glucose induces apoptosis of rat pancreatic beta-cells through induction of c-myc. *Biochemical and biophysical research communications* 312(4):937-944.

131. Osborn SL, *et al.* (2010) Fas-associated death domain (FADD) is a negative regulator of T-cell receptor-mediated necroptosis. *Proc Natl Acad Sci U S A* 107(29):13034-13039.

132. Saisho Y, *et al.* (2009) Development of factors to convert frequency to rate for beta-cell replication and apoptosis quantified by time-lapse video microscopy and immunohistochemistry. *Am J Physiol Endocrinol Metab* 296(1):E89-96.

133. Kohler M, *et al.* (2003) On-line monitoring of apoptosis in insulin-secreting cells. *Diabetes* 52(12):2943-2950.

134. Misler S, Barnett DW, Gillis KD, & Pressel DM (1992) Electrophysiology of stimulus-secretion coupling in human beta-cells. *Diabetes* 41(10):1221-1228.

135. Eizirik DL, Colli ML, & Ortis F (2009) The role of inflammation in insulitis and beta-cell loss in type 1 diabetes. *Nat Rev Endocrinol* 5(4):219-226.

136. Leung YM, *et al.* (2005) Electrophysiological characterization of pancreatic islet cells in the mouse insulin promoter-green fluorescent protein mouse. *Endocrinology* 146(11):4766-4775.

137. Yang YH, Vilin YY, Roberge M, Kurata HT, & Johnson JD (2014) Multi-parameter screening reveals a role for Na+ channels in cytokine-induced beta-cell death. *Mol Endocrinol* 126(Pt 18):4286-4295.

138. Szabat M, *et al.* (2012) Maintenance of beta-Cell Maturity and Plasticity in the Adult Pancreas: Developmental Biology Concepts in Adult Physiology. *Diabetes* 61(6):1365-1371.

139. Szabat M, *et al.* (2011) Kinetics and genomic profiling of adult human and mouse beta-cell maturation. *Islets* 3(4):175-187.

140. Vignali S, Leiss V, Karl R, Hofmann F, & Welling A (2006) Characterization of voltage-dependent sodium and calcium channels in mouse pancreatic A- and B-cells. *J Physiol* 572(Pt 3):691-706.

141. Eizirik DL & Cnop M (2010) ER stress in pancreatic beta cells: the thin red line between adaptation and failure. *Sci Signal* 3(110):pe7.

142. Donath MY, Boni-Schnetzler M, Ellingsgaard H, Halban PA, & Ehses JA (2010) Cytokine production by islets in health and diabetes: cellular origin, regulation and function. *Trends Endocrinol Metab* In press.

143. Mehran AE, *et al.* (2012) Hyperinsulinemia drives diet-induced obesity independently of brain insulin production. *Cell metabolism* 16(6):723-737.

144. Johnson JD, *et al.* (2006) Insulin protects islets from apoptosis via Pdx1 and specific changes in the human islet proteome. *Proc Natl Acad Sci U S A* 103(51):19575-19580.

145. Goncalves AA, *et al.* (2003) Participation of Na(+) channels in the potentiation by Tityus serrulatus alpha-toxin TsTx-V of glucose-induced electrical activity and insulin secretion in rodent islet beta-cells. *Toxicon : official journal of the International Society on Toxinology* 41(8):1039-1045.

146. Eberhardson M & Grapengiesser E (1999) Role of voltage-dependent Na+ channels for rhythmic Ca2+ signalling in glucose-stimulated mouse pancreatic beta-cells. *Cellular signalling* 11(5):343-348.

147. Cardozo AK, *et al.* (2005) Cytokines downregulate the sarcoendoplasmic reticulum pump Ca2+ ATPase 2b and deplete endoplasmic reticulum Ca2+, leading to induction of endoplasmic reticulum stress in pancreatic beta-cells. *Diabetes* 54(2):452-461.

148. Cardozo AK, *et al.* (2001) A comprehensive analysis of cytokine-induced and nuclear factor-kappa B-dependent genes in primary rat pancreatic beta-cells. *J Biol Chem* 276(52):48879-48886.

149. Jin X & Gereau RWt (2006) Acute p38-mediated modulation of tetrodotoxin-resistant sodium channels in mouse sensory neurons by tumor necrosis factor-alpha. *J Neurosci* 26(1):246-255.

150. Barnett DW, Pressel DM, & Misler S (1995) Voltage-dependent Na+ and Ca2+ currents in human pancreatic islet beta-cells: evidence for roles in the generation of action potentials and insulin secretion. *Pflugers Arch* 431(2):272-282.

151. Philipson LH, Kusnetsov A, Larson T, Zeng Y, & Westermark G (1993) Human, rodent, and canine pancreatic beta-cells express a sodium channel alpha 1-subunit related to a fetal brain isoform. *Diabetes* 42(9):1372-1377.

152. Pressel DM & Misler S (1991) Role of voltage-dependent ionic currents in coupling glucose stimulation to insulin secretion in canine pancreatic islet B-cells. *J Membr Biol* 124(3):239-253.

153. Pressel DM & Misler S (1990) Sodium channels contribute to action potential generation in canine and human pancreatic islet B cells. *J Membr Biol* 116(3):273-280.

154. Plant TD (1988) Na+ currents in cultured mouse pancreatic B-cells. *Pflugers Arch* 411(4):429-435.

155. Hiriart M & Matteson DR (1988) Na channels and two types of Ca channels in rat pancreatic B cells identified with the reverse hemolytic plaque assay. *J Gen Physiol* 91(5):617-639.

156. Vignali S, Leiss V, Karl R, Hofmann F, & Welling A (2006) Characterization of voltage-dependent sodium and calcium channels in mouse pancreatic A- and B-cells. *The Journal of physiology* 572(Pt 3):691-706.

157. Misler S, Dickey A, & Barnett DW (2005) Maintenance of stimulus-secretion coupling and single beta-cell function in cryopreserved-thawed human islets of Langerhans. *Pflugers Arch* 450(6):395-404.

158. Grapengiesser E (1996) Glucose induces cytoplasmic Na+ oscillations in pancreatic beta-cells. *Biochemical and biophysical research communications* 226(3):830-835.

159. Eberhardson M & Grapengiesser E (1999) Role of voltage-dependent Na+ channels for rhythmic Ca2+ signalling in glucose-stimulated mouse pancreatic beta-cells. *Cell Signal* 11(5):343-348.

160. Zou N, *et al.* (2013) ATP regulates sodium channel kinetics in pancreatic islet beta cells. *J Membr Biol* 246(2):101-107.

161. Ernst SJ, Aguilar-Bryan L, & Noebels JL (2009) Sodium channel beta1 regulatory subunit deficiency reduces pancreatic islet glucose-stimulated insulin and glucagon secretion. *Endocrinology* 150(3):1132-1139.

162. Hiriart M & Ramirez-Medeles MC (1993) Muscarinic modulation of insulin secretion by single pancreatic beta-cells. *Molecular and Cellular Endocrinology* 93(1):63-69.

163. Olsen HL, *et al.* (2005) Glucose stimulates glucagon release in single rat alpha-cells by mechanisms that mirror the stimulus-secretion coupling in beta-cells. *Endocrinology* 146(11):4861-4870.

164. Banasiak KJ, Burenkova O, & Haddad GG (2004) Activation of voltage-sensitive sodium channels during oxygen deprivation leads to apoptotic neuronal death. *Neuroscience* 126(1):31-44.

165. Shi E, *et al.* (2005) NS-7, a novel Na+/Ca2+ channel blocker, prevents neurologic injury after spinal cord ischemia in rabbits. *J Thorac Cardiovasc Surg* 129(2):364-371.

166. Joshi AD, Parsons DW, Velculescu VE, & Riggins GJ (2011) Sodium ion channel mutations in glioblastoma patients correlate with shorter survival. *Mol Cancer* 10:17.

167. Planells-Cases R, *et al.* (2000) Neuronal death and perinatal lethality in voltage-gated sodium channel alpha(II)-deficient mice. *Biophys J* 78(6):2878-2891.

168. Schonfeld-Dado E & Segal M (2009) Activity-dependent survival of neurons in culture: a model of slow neurodegeneration. *J Neural Transm* 116(11):1363-1369.

169. Schonfeld-Dado E, Fishbein I, & Segal M (2009) Degeneration of cultured cortical neurons following prolonged inactivation: molecular mechanisms. *J Neurochem* 110(4):1203-1213.

170. Ikonomidou C (2009) Triggers of apoptosis in the immature brain. *Brain Dev* 31(7):488-492.

171. Salthun-Lassalle B, Hirsch EC, Wolfart J, Ruberg M, & Michel PP (2004) Rescue of mesencephalic dopaminergic neurons in culture by low-level stimulation of voltage-gated sodium channels. *J Neurosci* 24(26):5922-5930.

172. Zhang T, *et al.* (2011) LQTS mutation N1325S in cardiac sodium channel gene SCN5A causes cardiomyocyte apoptosis, cardiac fibrosis and contractile dysfunction in mice. *Int J Cardiol* 147(2):239-245.

173. Frustaci A, *et al.* (2005) Cardiac histological substrate in patients with clinical phenotype of Brugada syndrome. *Circulation* 112(24):3680-3687.

174. Chen PC, *et al.* (2013) Carbamazepine as a Novel Small Molecule Corrector of Trafficking-impaired ATP-sensitive Potassium Channels Identified in Congenital Hyperinsulinism. *J Biol Chem* 288(29):20942-20954.

175. Cnop M, *et al.* (2013) RNA-sequencing identifies dysregulation of the human pancreatic islet transcriptome by the saturated fatty acid palmitate. *Diabetes*.

176. Slyshenkov VS, Piwocka K, Sikora E, & Wojtczak L (2001) Pantothenic acid protects jurkat cells against ultraviolet light-induced apoptosis. *Free Radic Biol Med* 30(11):1303-1310.

177. Dunlap N, *et al.* (2003) 1alpha,25-dihydroxyvitamin D(3) (calcitriol) and its analogue, 19-nor-1alpha,25(OH)(2)D(2), potentiate the effects of ionising radiation on human prostate cancer cells. *Br J Cancer* 89(4):746-753.

178. Zakharova IO, *et al.* (2012) alpha-Tocopherol at Nanomolar Concentration Protects PC12 Cells from Hydrogen Peroxide-Induced Death and Modulates Protein Kinase Activities. *Int J Mol Sci* 13(9):11543-11568.

179. Ahlemeyer B & Krieglstein J (2000) Inhibition of glutathione depletion by retinoic acid and tocopherol protects cultured neurons from staurosporine-induced oxidative stress and apoptosis. *Neurochem Int* 36(1):1-5.

180. Forrest VJ, Kang YH, McClain DE, Robinson DH, & Ramakrishnan N (1994) Oxidative stress-induced apoptosis prevented by Trolox. *Free Radic Biol Med* 16(6):675-684.

181. Chen LY, *et al.* (2013) Taiwanofungus camphoratus (Syn Antrodia camphorata) extract and amphotericin B exert adjuvant effects via mitochondrial apoptotic pathway. *Integr Cancer Ther* 12(2):153-164.

182. Cohen BE (2010) Amphotericin B membrane action: role for two types of ion channels in eliciting cell survival and lethal effects. *J Membr Biol* 238(1-3):1-20.

183. Mahmud H, Mauro D, Qadri SM, Foller M, & Lang F (2009) Triggering of suicidal erythrocyte death by amphotericin B. *Cell Physiol Biochem* 24(3-4):263-270.

184. Odabasi Z, *et al.* (2009) Reduction of amphotericin B-induced renal tubular apoptosis by N-acetylcysteine. *Antimicrob Agents Chemother* 53(7):3100-3102.

185. Marklund L, *et al.* (2004) Cellular potassium ion deprivation enhances apoptosis induced by cisplatin. *Basic Clin Pharmacol Toxicol* 94(5):245-251.

186. Kadota J, *et al.* (2005) Antibiotic-induced apoptosis in human activated peripheral lymphocytes. *Int J Antimicrob Agents* 25(3):216-220.

187. Momeni HR & Jarahzadeh M (2012) Effects of a voltage sensitive calcium channel blocker and a sodium-calcium exchanger inhibitor on apoptosis of motor neurons in adult spinal cord slices. *Cell J* 14(3):171-176.

188. Gong XW, Xu YH, Chen XL, & Wang YX (2012) Loperamide, an antidiarrhea drug, has antitumor activity by inducing cell apoptosis. *Pharmacological research : the official journal of the Italian Pharmacological Society* 65(3):372-378.

189. Yoshida A, Tokuyama S, Iwamura T, & Ueda H (2000) Opioid analgesic-induced apoptosis and caspase-independent cell death in human lung carcinoma A549 cells. *Int J Mol Med* 6(3):329-335.

190. Park HJ, Kim SK, Chung JH, & Kim JW (2013) Protective effect of carbamazepine on kainic acid-induced neuronal cell death through activation of signal transducer and activator of transcription-3. *J Mol Neurosci* 49(1):172-181.

191. Gao XM, *et al.* (1995) Carbamazepine induction of apoptosis in cultured cerebellar neurons: effects of N-methyl-D-aspartate, aurintricarboxylic acid and cycloheximide. *Brain Res* 703(1-2):63-71.

192. Kim H, *et al.* (2012) Ionizing irradiation protection and mitigation of murine cells by carbamazepine is p53 and autophagy independent. *In Vivo* 26(3):341-354.

193. Gavin BA, Arruda SE, & Dolph PJ (2007) The role of carcinine in signaling at the Drosophila photoreceptor synapse. *PLoS genetics* 3(12):e206.

194. Chiang MK & Melton DA (2003) Single-cell transcript analysis of pancreas development. *Dev Cell* 4(3):383-393.

195. Yada T, *et al.* (1997) Pituitary adenylate cyclase-activating polypeptide (PACAP) is an islet substance serving as an intra-islet amplifier of glucose-induced insulin secretion in rats. *J Physiol* 505 (Pt 2):319-328.

196. Tsuda H, *et al.* (1992) Immunohistochemical localization of hepatocyte growth factor protein in pancreas islet A-cells of man and rats. *Jpn J Cancer Res* 83(12):1262-1266.

197. Okada T, *et al.* (2007) Insulin receptors in beta-cells are critical for islet compensatory growth response to insulin resistance. *Proc Natl Acad Sci U S A* 104(21):8977-8982.

198. Fujita Y, *et al.* (2010) Glucose-dependent insulinotropic polypeptide is expressed in pancreatic islet alpha-cells and promotes insulin secretion. *Gastroenterology* 138(5):1966-1975.

199. Widenmaier SB, *et al.* (A GIP receptor agonist exhibits beta-cell anti-apoptotic actions in rat models of diabetes resulting in improved beta-cell function and glycemic control. *PLoS One* 5(3):e9590.

200. Fujinaka Y, Takane K, Yamashita H, & Vasavada RC (2007) Lactogens promote beta cell survival through JAK2/STAT5 activation and Bcl-XL upregulation. *J Biol Chem* 282(42):30707-30717.

201. Sekine N, Wollheim CB, & Fujita T (1998) GH signalling in pancreatic beta-cells. *Endocr J* 45 Suppl:S33-40.

202. Cebrian A, *et al.* (2002) Overexpression of parathyroid hormone-related protein inhibits pancreatic beta-cell death in vivo and in vitro. *Diabetes* 51(10):3003-3013.

203. Yamamoto K, *et al.* (2000) Recombinant human betacellulin promotes the neogenesis of beta-cells and ameliorates glucose intolerance in mice with diabetes induced by selective alloxan perfusion. *Diabetes* 49(12):2021-2027.

204. Szabat M, Johnson JD, & Piret JM (2010) Reciprocal modulation of adult beta cell maturity by activin A and follistatin. *Diabetologia* 53(8):1680-1689.

205. Goulley J, Dahl U, Baeza N, Mishina Y, & Edlund H (2007) BMP4-BMPR1A signaling in beta cells is required for and augments glucose-stimulated insulin secretion. *Cell Metab* 5(3):207-219.

206. Yamamoto K, *et al.* (2003) Overexpression of PACAP in Transgenic Mouse Pancreatic beta-Cells Enhances Insulin Secretion and Ameliorates Streptozotocin-induced Diabetes. *Diabetes* 52(5):1155-1162.

207. Rosenbaum T, Vidaltamayo R, Sanchez-Soto MC, Zentella A, & Hiriart M (1998) Pancreatic beta cells synthesize and secrete nerve growth factor. *Proc Natl Acad Sci U S A* 95(13):7784-7788.

208. Garcia-Ocana A, *et al.* (2001) Transgenic overexpression of hepatocyte growth factor in the beta-cell markedly improves islet function and islet transplant outcomes in mice. *Diabetes* 50(12):2752-2762.

209. Otonkoski T, *et al.* (1996) A role for hepatocyte growth factor/scatter factor in fetal mesenchyme-induced pancreatic beta-cell growth. *Endocrinology* 137(7):3131-3139.

210. Li C, Chen P, Vaughan J, Lee KF, & Vale W (2007) Urocortin 3 regulates glucose-stimulated insulin secretion and energy homeostasis. *Proc Natl Acad Sci U S A* 104(10):4206-4211.

211. Cirulli V & Yebra M (2007) Netrins: beyond the brain. *Nat Rev Mol Cell Biol* 8(4):296-306.

212. Chilton JK (2006) Molecular mechanisms of axon guidance. *Dev Biol* 292(1):13-24.

213. Jorgensen MC, *et al.* (2007) An illustrated review of early pancreas development in the mouse. *Endocr Rev* 28(6):685-705.

214. Liu Y, *et al.* (2004) Novel role for Netrins in regulating epithelial behavior during lung branching morphogenesis. *Curr Biol* 14(10):897-905.

215. Srinivasan K, Strickland P, Valdes A, Shin GC, & Hinck L (2003) Netrin-1/neogenin interaction stabilizes multipotent progenitor cap cells during mammary gland morphogenesis. *Dev Cell* 4(3):371-382.

216. Yebra M, *et al.* (2003) Recognition of the neural chemoattractant Netrin-1 by integrins alpha6beta4 and alpha3beta1 regulates epithelial cell adhesion and migration. *Dev Cell* 5(5):695-707.

217. De Breuck S, Lardon J, Rooman I, & Bouwens L (2003) Netrin-1 expression in fetal and regenerating rat pancreas and its effect on the migration of human pancreatic duct and porcine islet precursor cells. *Diabetologia* 46(7):926-933.

218. Tang X, *et al.* (2008) Netrin-1 mediates neuronal survival through PIKE-L interaction with the dependence receptor UNC5B. *Nat Cell Biol* 10(6):698-706.

219. Forcet C, *et al.* (2001) The dependence receptor DCC (deleted in colorectal cancer) defines an alternative mechanism for caspase activation. *Proc Natl Acad Sci U S A* 98(6):3416-3421.

220. Llambi F, Causeret F, Bloch-Gallego E, & Mehlen P (2001) Netrin-1 acts as a survival factor via its receptors UNC5H and DCC. *EMBO J* 20(11):2715-2722.

221. Wang W, Reeves WB, & Ramesh G (2009) Netrin-1 increases proliferation and migration of renal proximal tubular epithelial cells via the UNC5B receptor. *Am J Physiol Renal Physiol* 296(4):F723-729.

222. Zhang C, *et al.* (2004) Identification of a novel alternative splicing form of human netrin-4 and analyzing the expression patterns in adult rat brain. *Brain Res Mol Brain Res* 130(1-2):68-80.

223. Lee HK, *et al.* (2007) Netrin-1 induces proliferation of Schwann cells through Unc5b receptor. *Biochem Biophys Res Commun* 362(4):1057-1062.

224. Park KW, *et al.* (2004) The axonal attractant Netrin-1 is an angiogenic factor. *Proc Natl Acad Sci U S A* 101(46):16210-16215.

225. Delloye-Bourgeois C, *et al.* (2009) Netrin-1 acts as a survival factor for aggressive neuroblastoma. *J Exp Med* 206(4):833-847.

226. Matsunaga E, *et al.* (2004) RGM and its receptor neogenin regulate neuronal survival. *Nat Cell Biol* 6(8):749-755.

227. Kim TH, *et al.* (2005) Netrin induces down-regulation of its receptor, Deleted in Colorectal Cancer, through the ubiquitin-proteasome pathway in the embryonic cortical neuron. *J Neurochem* 95(1):1-8.

228. Ming GL, *et al.* (1997) cAMP-dependent growth cone guidance by netrin-1. *Neuron* 19(6):1225-1235.

229. Mazelin L, *et al.* (2004) Netrin-1 controls colorectal tumorigenesis by regulating apoptosis. *Nature* 431(7004):80-84.

230. Furne C, Rama N, Corset V, Chedotal A, & Mehlen P (2008) Netrin-1 is a survival factor during commissural neuron navigation. *Proc Natl Acad Sci U S A* 105(38):14465-14470.

231. Hong K, Nishiyama M, Henley J, Tessier-Lavigne M, & Poo M (2000) Calcium signalling in the guidance of nerve growth by netrin-1. *Nature* 403(6765):93-98.

232. Wu KY, *et al.* (2006) Soluble adenylyl cyclase is required for netrin-1 signaling in nerve growth cones. *Nat Neurosci* 9(10):1257-1264.

233. Corset V, *et al.* (2000) Netrin-1-mediated axon outgrowth and cAMP production requires interaction with adenosine A2b receptor. *Nature* 407(6805):747-750.

234. Bouchard JF, *et al.* (2004) Protein kinase A activation promotes plasma membrane insertion of DCC from an intracellular pool: A novel mechanism regulating commissural axon extension. *J Neurosci* 24(12):3040-3050.

235. Moore SW & Kennedy TE (2006) Protein kinase A regulates the sensitivity of spinal commissural axon turning to netrin-1 but does not switch between chemoattraction and chemorepulsion. *J Neurosci* 26(9):2419-2423.

236. Moore SW, *et al.* (2008) Soluble adenylyl cyclase is not required for axon guidance to netrin-1. *J Neurosci* 28(15):3920-3924.

237. Dezaki K, Kageyama H, Seki M, Shioda S, & Yada T (2008) Neuropeptide W in the rat pancreas: potentiation of glucose-induced insulin release and Ca2+ influx through L-type Ca2+ channels in beta-cells and localization in islets. *Regul Pept* 145(1-3):153-158.

238. Yamamoto K, *et al.* (2003) Overexpression of PACAP in transgenic mouse pancreatic beta-cells enhances insulin secretion and ameliorates streptozotocin-induced diabetes. *Diabetes* 52(5):1155-1162.

239. Szabat M, Johnson JD, & Piret JM (2010) Reciprocal modulation of adult beta cell maturity by activin A and follistatin. *Diabetologia* 53(8):1680-1689.

240. Johnson JD & Alejandro EU (2008) Control of pancreatic beta-cell fate by insulin signaling: The sweet spot hypothesis. *Cell Cycle* 7(10):1343-1347.

241. Long H, *et al.* (2004) Conserved roles for Slit and Robo proteins in midline commissural axon guidance. *Neuron* 42(2):213-223.

242. Seeger M, Tear G, Ferres-Marco D, & Goodman CS (1993) Mutations affecting growth cone guidance in Drosophila: genes necessary for guidance toward or away from the midline. *Neuron* 10(3):409-426.

243. Kidd T, *et al.* (1998) Roundabout controls axon crossing of the CNS midline and defines a novel subfamily of evolutionarily conserved guidance receptors. *Cell* 92(2):205-215.

244. Kidd T, Bland KS, & Goodman CS (1999) Slit is the midline repellent for the robo receptor in Drosophila. *Cell* 96(6):785-794.

245. Ypsilanti AR, Zagar Y, & Chedotal A (2010) Moving away from the midline: new developments for Slit and Robo. *Development* 137(12):1939-1952.

246. Brose K, *et al.* (1999) Slit proteins bind Robo receptors and have an evolutionarily conserved role in repulsive axon guidance. *Cell* 96(6):795-806.

247. Fujiwara M, Ghazizadeh M, & Kawanami O (2006) Potential role of the Slit/Robo signal pathway in angiogenesis. *Vasc Med* 11(2):115-121.

248. Strickland P, Shin GC, Plump A, Tessier-Lavigne M, & Hinck L (2006) Slit2 and netrin 1 act synergistically as adhesive cues to generate tubular bi-layers during ductal morphogenesis. *Development* 133(5):823-832.

249. Juhl K, Sarkar SA, Wong R, Jensen J, & Hutton JC (2008) Mouse pancreatic endocrine cell transcriptome defined in the embryonic Ngn3-null mouse. *Diabetes* 57(10):2755-2761.

250. Seki M, *et al.* (2010) Human ROBO1 is cleaved by metalloproteinases and gamma-secretase and migrates to the nucleus in cancer cells. *FEBS Lett* 584(13):2909-2915.

251. Jahanshahi P, Wu R, Carter JD, & Nunemaker CS (2009) Evidence of diminished glucose stimulation and endoplasmic reticulum function in nonoscillatory pancreatic islets. *Endocrinology* 150(2):607-615.

252. Ravier MA, Sehlin J, & Henquin JC (2002) Disorganization of cytoplasmic Ca(2+) oscillations and pulsatile insulin secretion in islets from ob/ obmice. *Diabetologia* 45(8):1154-1163.

253. Ravier MA, *et al.* (2011) Mechanisms of control of the free Ca2+ concentration in the endoplasmic reticulum of mouse pancreatic beta-cells: interplay with cell metabolism and [Ca2+]c and role of SERCA2b and SERCA3. *Diabetes* 60(10):2533-2545.

254. Xu HT, *et al.* (2004) Calcium signaling in chemorepellant Slit2-dependent regulation of neuronal migration. *Proc Natl Acad Sci U S A* 101(12):4296-4301.

255. Guan CB, Xu HT, Jin M, Yuan XB, & Poo MM (2007) Long-range Ca2+ signaling from growth cone to soma mediates reversal of neuronal migration induced by slit-2. *Cell* 129(2):385-395.

256. Huang ZH, *et al.* (2011) Slit-2 repels the migration of olfactory ensheathing cells by triggering Ca2+-dependent cofilin activation and RhoA inhibition. *J Cell Sci* 124(Pt 2):186-197.

257. Beauvois MC, *et al.* (2006) Glucose-induced mixed [Ca2+]c oscillations in mouse beta-cells are controlled by the membrane potential and the SERCA3 Ca2+-ATPase of the endoplasmic reticulum. *Am J Physiol Cell Physiol* 290(6):C1503-1511.

258. Palmer AE, Jin C, Reed JC, & Tsien RY (2004) Bcl-2-mediated alterations in endoplasmic reticulum Ca2+ analyzed with an improved genetically encoded fluorescent sensor. *Proc Natl Acad Sci U S A* 101(50):17404-17409.

259. Thurmond DC, Gonelle-Gispert C, Furukawa M, Halban PA, & Pessin JE (2003) Glucose-stimulated insulin secretion is coupled to the interaction of actin with the t-SNARE (target membrane soluble N-ethylmaleimide-sensitive factor attachment protein receptor protein) complex. *Mol Endocrinol* 17(4):732-742.

260. Pigeau GM, *et al.* (2009) Insulin granule recruitment and exocytosis is dependent on p110gamma in insulinoma and human beta-cells. *Diabetes* 58(9):2084-2092.

261. Nevins AK & Thurmond DC (2003) Glucose regulates the cortical actin network through modulation of Cdc42 cycling to stimulate insulin secretion. *Am J Physiol Cell Physiol* 285(3):C698-710.

262. Mehlen P, Delloye-Bourgeois C, & Chedotal A (2011) Novel roles for Slits and netrins: axon guidance cues as anticancer targets? *Nat Rev Cancer* 11(3):188-197.

263. Latil A, *et al.* (2003) Quantification of expression of netrins, slits and their receptors in human prostate tumors. *Int J Cancer* 103(3):306-315.

264. Stein E & Tessier-Lavigne M (2001) Hierarchical organization of guidance receptors: silencing of netrin attraction by slit through a Robo/DCC receptor complex. *Science* 291(5510):1928-1938.

265. Bai G, *et al.* (2011) Presenilin-dependent receptor processing is required for axon guidance. *Cell* 144(1):106-118.

266. Wang B, *et al.* (2003) Induction of tumor angiogenesis by Slit-Robo signaling and inhibition of cancer growth by blocking Robo activity. *Cancer Cell* 4(1):19-29.

267. Wong K, *et al.* (2001) Signal transduction in neuronal migration: roles of GTPase activating proteins and the small GTPase Cdc42 in the Slit-Robo pathway. *Cell* 107(2):209-221.

268. Liu D, *et al.* (2006) Neuronal chemorepellent Slit2 inhibits vascular smooth muscle cell migration by suppressing small GTPase Rac1 activation. *Circ Res* 98(4):480-489.

269. Otani K, *et al.* (2003) Reduced beta-cell mass and altered glucose sensing impairs insulin secretory function in mice with pancreatic beta-cell knockout of the insulin receptor. *Am J Physiol Endocrinol Metab*.

270. Ueki K, *et al.* (2006) Total insulin and IGF-I resistance in pancreatic beta cells causes overt diabetes. *Nat Genet* 38(5):583-588.

271. Ueki K, Okada T, Ozcan U, & Kulkarni R (2003) Endogenous insulin-mediated signaling protects apoptosis induced by glucose in pancreatic beta-cells. *Diabetes* 52:A42-A42.

272. Xiao D, *et al.* (2011) Effect of actin cytoskeleton disruption on electric pulse-induced apoptosis and electroporation in tumour cells. *Cell Biol Int* 35(2):99-104.

273. Posey SC & Bierer BE (1999) Actin stabilization by jasplakinolide enhances apoptosis induced by cytokine deprivation. *J Biol Chem* 274(7):4259-4265.

274. Gourlay CW & Ayscough KR (2005) The actin cytoskeleton: a key regulator of apoptosis and ageing? *Nat Rev Mol Cell Biol* 6(7):583-589.

275. Yermen B, Tomas A, & Halban PA (2007) Pro-survival role of gelsolin in mouse beta-cells. *Diabetes* 56(1):80-87.

276. Laybutt DR, *et al.* (2007) Endoplasmic reticulum stress contributes to beta cell apoptosis in type 2 diabetes. *Diabetologia* 50(4):752-763.

277. Chang-Chen KJ, Mullur R, & Bernal-Mizrachi E (2008) Beta-cell failure as a complication of diabetes. *Rev Endocr Metab Disord* 9(4):329-343.

278. Johnson JD & Luciani DS (2010) Mechanisms of pancreatic beta-cell apoptosis in diabetes and its therapies. *Adv Exp Med Biol* 654:447-462.

279. Widenmaier SB, *et al.* (2010) A GIP receptor agonist exhibits beta-cell anti-apoptotic actions in rat models of diabetes resulting in improved beta-cell function and glycemic control. *PLoS One* 5(3):e9590.

280. Johnson JD, *et al.* (2003) Increased islet apoptosis in Pdx1+/- mice. *J Clin Invest* 111(8):1147-1160.

281. Yang YH, Manning Fox JE, Zhang KL, MacDonald PE, & Johnson JD (2013) Intraislet SLIT-ROBO signaling is required for beta-cell survival and potentiates insulin secretion. *Proc Natl Acad Sci U S A* 110(41):16480-16485.

282. Peakman M (2013) Immunological pathways to beta-cell damage in Type 1 diabetes. *Diabet Med* 30(2):147-154.

283. Cnop M, Ladriere L, Igoillo-Esteve M, Moura RF, & Cunha DA (2010) Causes and cures for endoplasmic reticulum stress in lipotoxic beta-cell dysfunction. *Diabetes Obes Metab* 12 Suppl 2:76-82.

284. Maisonpierre PC, *et al.* (1997) Angiopoietin-2, a natural antagonist for Tie2 that disrupts in vivo angiogenesis. *Science* 277(5322):55-60.

285. Tanaka M & Miyajima A (2003) Oncostatin M, a multifunctional cytokine. *Reviews of physiology, biochemistry and pharmacology* 149:39-52.

286. Nkyimbeng-Takwi E & Chapoval SP (2011) Biology and function of neuroimmune semaphorins 4A and 4D. *Immunologic research* 50(1):10-21.

287. Wang M, Li J, Lim GE, & Johnson JD (2013) Is dynamic autocrine insulin signaling possible? A mathematical model predicts picomolar concentrations of extracellular monomeric insulin within human pancreatic islets. *PLoS One* 8(6):e64860.

288. Wiater E & Vale W (2012) Roles of activin family in pancreatic development and homeostasis. *Mol Cell Endocrinol* 359(1-2):23-29.

289. Hiriart M, Vidaltamayo R, & Sanchez-Soto MC (2001) Nerve and fibroblast growth factors as modulators of pancreatic beta cell plasticity and insulin secretion. *The Israel Medical Association journal : IMAJ* 3(2):114-116.

290. Shih HP, Wang A, & Sander M (2013) Pancreas organogenesis: from lineage determination to morphogenesis. *Annu Rev Cell Dev Biol* 29:81-105.

291. Evans-Molina C, Hatanaka M, & Mirmira RG (2013) Lost in translation: endoplasmic reticulum stress and the decline of beta-cell health in diabetes mellitus. *Diabetes Obes Metab* 15 Suppl 3:159-169.

292. Cnop M, Foufelle F, & Velloso LA (2012) Endoplasmic reticulum stress, obesity and diabetes. *Trends Mol Med* 18(1):59-68.

293. Pissios P, *et al.* (2007) Melanin concentrating hormone is a novel regulator of islet function and growth. *Diabetes* 56(2):311-319.

294. Persson-Sjogren S, Forsgren S, & Lindstrom P (2006) Vasoactive intestinal polypeptide and pituitary adenylate cyclase activating polypeptide: effects on insulin release in isolated mouse islets in relation to metabolic status and age. *Neuropeptides* 40(4):283-290.

295. Jian L, Su YX, & Deng HC (2013) Adiponectin-induced inhibition of intrinsic and extrinsic apoptotic pathways protects pancreatic beta-cells against apoptosis. *Horm Metab Res* 45(8):561-566.

296. Wijesekara N, *et al.* (2010) Adiponectin-induced ERK and Akt phosphorylation protects against pancreatic beta cell apoptosis and increases insulin gene expression and secretion. *J Biol Chem* 285(44):33623-33631.

297. Rakatzi I, Mueller H, Ritzeler O, Tennagels N, & Eckel J (2004) Adiponectin counteracts cytokine- and fatty acid-induced apoptosis in the pancreatic beta-cell line INS-1. *Diabetologia* 47(2):249-258.

298. Holland WL, *et al.* (2011) Receptor-mediated activation of ceramidase activity initiates the pleiotropic actions of adiponectin. *Nat Med* 17(1):55-63.

299. Sun Y & Chen X (2010) Effect of adiponectin on apoptosis: proapoptosis or antiapoptosis? *BioFactors* 36(3):179-186.

300. Koya RC, *et al.* (2000) Gelsolin inhibits apoptosis by blocking mitochondrial membrane potential loss and cytochrome c release. *The Journal of biological chemistry* 275(20):15343-15349.

301. Harms C, *et al.* (2004) Neuronal gelsolin prevents apoptosis by enhancing actin depolymerization. *Molecular and cellular neurosciences* 25(1):69-82.

302. Kimura S, Noda T, & Yoshimori T (2007) Dissection of the autophagosome maturation process by a novel reporter protein, tandem fluorescent-tagged LC3. *Autophagy* 3(5):452-460.

303. Tantama M, Hung YP, & Yellen G (2011) Imaging intracellular pH in live cells with a genetically encoded red fluorescent protein sensor. *Journal of the American Chemical Society* 133(26):10034-10037.

304. Mojibian M, *et al.* (2013) Implanted islets in the anterior chamber of the eye are prone to autoimmune attack in a mouse model of diabetes. *Diabetologia* 56(10):2213-2221.

305. Speier S, *et al.* (2008) Noninvasive high-resolution in vivo imaging of cell biology in the anterior chamber of the mouse eye. *Nature protocols* 3(8):1278-1286.

306. Speier S, *et al.* (2008) Noninvasive in vivo imaging of pancreatic islet cell biology. *Nat Med* 14(5):574-578.

307. Anderson MS & Bluestone JA (2005) The NOD mouse: a model of immune dysregulation. *Annual review of immunology* 23:447-485.

308. Stutzer I, Esterhazy D, & Stoffel M (2012) The pancreatic beta cell surface proteome. *Diabetologia* 55(7):1877-1889.

309. Dorrell C, *et al.* (2011) Transcriptomes of the major human pancreatic cell types. *Diabetologia* 54(11):2832-2844.

310. Tattikota SG, *et al.* (2013) Argonaute2 regulates the pancreatic beta-cell secretome. *Molecular & cellular proteomics : MCP* 12(5):1214-1225.

311. Eizirik DL, *et al.* (2012) The human pancreatic islet transcriptome: expression of candidate genes for type 1 diabetes and the impact of pro-inflammatory cytokines. *PLoS genetics* 8(3):e1002552.

312. Nica AC, *et al.* (2013) Cell-type, allelic, and genetic signatures in the human pancreatic beta cell transcriptome. *Genome Res* 23(9):1554-1562.

313. Tang F & Kalil K (2005) Netrin-1 induces axon branching in developing cortical neurons by frequency-dependent calcium signaling pathways. *J Neurosci* 25(28):6702-6715.

314. Cotrina ML, Lin JH, & Nedergaard M (1998) Cytoskeletal assembly and ATP release regulate astrocytic calcium signaling. *J Neurosci* 18(21):8794-8804.

315. Johnson BD & Byerly L (1993) A cytoskeletal mechanism for Ca2+ channel metabolic dependence and inactivation by intracellular Ca2+. *Neuron* 10(5):797-804.

316. Fridlyand LE, Jacobson DA, & Philipson LH (2013) Ion channels and regulation of insulin secretion in human beta-cells: a computational systems analysis. *Islets* 5(1):1-15.

317. Best L (2005) Glucose-induced electrical activity in rat pancreatic beta-cells: dependence on intracellular chloride concentration. *J Physiol* 568(Pt 1):137-144.

318. Lenzen S (2008) The mechanisms of alloxan- and streptozotocin-induced diabetes. *Diabetologia* 51(2):216-226.